1975

Saturable Optical Behavior of Sulfur Hexafluoride.

William Hugh Thomason
Louisiana State University and Agricultural & Mechanical College

SATURABLE OPTICAL BEHAVIOR OF SULFUR HEXAFLUORIDE

A Dissertation

Submitted to the Graduate Faculty of the
Louisiana State University and
Agricultural and Mechanical College
in partial fulfillment of the
requirements for the degree of
Doctor of Philosophy

in

The Department of Chemistry

by
William H. Thomason
B.A., Hendrix College, 1967
December, 1975

ACKNOWLEDGEMENT

I wish to express my sincere appreciation to Professor James D. Macomber for his guidance and assistance throughout this research. His ability to make scientific research an exciting adventure has been particularly meaningful to me. I also wish to thank Don C. Elbers for his invaluable collaboration in portions of the experimental work and for his suggestions in the preparation of this dissertation. Further, I would like to thank the other members of my committee for their interest and suggestions in this work. The technical assistance of Leslie Edelen and Lloyd Young is also gratefully acknowledged.

My mother is due special thanks for her continued encouragement over my educational career. Most of all I recognize and appreciate the invaluable support, encouragement, and understanding of my wife, Jane, during the course of this work.

I am grateful for the financial assistance in the preparation of this Dissertation which was provided by the Charles E. Coates Memorial Fund of the Louisiana State University Foundation. NDEA Traineeships and a Texas-Eastman Research Fellowship are also gratefully appreciated.

TABLE OF CONTENTS

PAGE

LIST OF TABLES

LIST OF FIGURES

APPENDIX 1:

PAGE

APPENDIX 5: PAGE

ABSTRACT

The laws of optics have been generalized to describe the reflectance, absorptance, and transmittance of a saturable slab as a function of the irradiance under steady state conditions. The intensity distribution and divergence of the incident light beam, the optical properties of the sample container, the effects of sample heating due to absorbtion, and the molecular properties of the absorber have all been taken into account. The latter included the difference between the frequency of the radiation and the center of the absorption line, the transition dipole moment, and the relaxation rates, T_1 and T_2.

Experiments have been performed to test this theory at normal incidence, and the theory and experiments were found to agree within experimental error with no adjustment of the input parameters obtained from the literature. In addition, the precision of these experimental results was exceptionally high for laser induced saturation of gases. In the course of this work a goniometer and a dedicated analog computer for the routine measurement of reflectance was designed, built, and tested, an inexpensive, high quality frequency controller for a CO_2 laser was developed, a technique for the study of dynamic processes in gases irradiated with laser pulses was developed, and a sensitive new technique for resolving spectra consisting of many closely spaced and overlapping lines was developed. A method for studying the effects of collisions between identical molecules in gases was also explored.

The application of this new knowledge should be valuable to the design of goggles, lenses and filters designed to protect people and materials from harmful radiation.

CHAPTER I
INTRODUCTION

When an electromagnetic wave travels through an absorbing material, energy is transfered from the electromagnetic field associated with the wave to the atoms, molecules, or ions of the material. The rate of transfer of energy from the field to the matter depends upon the absorption coefficient. If the intensity of the wave is sufficiently great, the capacity of the atoms, molecules, or ions to absorb this energy will be exceeded and the absorption coefficient of the material will decrease without producing any permanent change in the material. This process is called optical saturation, and the material so affected is called a saturable absorber.

In the simplest case, optical saturation is associated with two nondegenerate quantum-mechanical levels in the absorbing atoms, molecules, or ions of the saturable absorber that are connected by an allowed dipole transition. If a low intensity light wave oscillating at the resonant frequency of this dipole transition strikes a saturable absorber, the intensity of the light, will be attenuated exponentially with increasing distance into the sample according to the relationship developed by Bouguer, Lambert, and Beer.[1] This relationship (Beer's law) is based upon the assumption that all of the absorbing species are in the lower of the two energy levels connected by the dipole transition. Of course, the

actual population of the excited state will not be zero at any temperature above absolute zero. It is further assumed that the excited species cannot contribute to the absorption and that multiple absorption and emission processes do not occur. If a molecule, for example, is struck by a photon and happens to be in the excited state, it may be forced to emit, thus contributing an extra photon to the light beam. In 1917, Einstein[2] showed that the cross-section or probability for this stimulated emission process is identical with that for the absorption. It follows that the net absorption coefficient of the material will be proportional to the population difference between the upper and lower states involved in the transition. Each time a photon is absorbed from the beam, this population difference diminishes by two from its equilibrium value. For a light beam of sufficiently low intensity, however, each excited molecule in the sample will have adequate time to relax to the lower state by stimulated emission or non-radiative processes before the next photon arrives. Thus the thermal equilibrium distribution can be maintained.

If the photon flux is very large, departures from equilibrium can occur, and the attenuation will no longer be strictly exponential: the absorption coefficient of the sample will decrease. In the limiting case the population of the upper state will equal that of the lower state; at this point optical saturation of the absorption is complete. The photons arrive so rapidly that spontaneous emission and non-radiative processes can be completely

neglected. A given photon will have a 50% chance of being annihilated (by absorption) and a 50% chance of being doubled (by stimulated emission). Thus for every photon entering the sample through its front face, one will exit through the rear face; the material will be, in effect, transparent. For an absorbing center that has many energy levels in which only the lowest level absorbs, saturation can be obtained without stimulated emission. If the energy from the upper state of the transition is transferred to other states not involved in the transition, the effective number of molecules interacting with the radiation will decrease.

Although the possibility of observing optical saturation had been known for many years, there were few observations of this effect before the discovery of the laser. These limited observations were caused by the unavailability of a convenient light source of sufficient intensity at the appropriate frequency. One of the earliest observations of optical saturation was reported by G. N. Lewis, D. Lipkin, and T. T. Magel[3] in 1941. Using a high pressure mercury arc lamp, they observed the saturation of the absorption of fluorescein in boric acid. Five years later C. H. Townes[4] observed the saturation of the absorption of ammonia gas with microwave radiation. The saturation of materials which absorb at optical frequencies was not <u>easily</u> observable until the development of the laser in 1960.

The ability of saturable absorbers to act as a very rapid shutter for intense light beams made them particularly useful in laser work. By placing the saturable absorber inside the

optical cavity of a pulsed laser, the threshold pump power for laser action is raised to a very high level. When the intensity of spontaneous emission for the pumped laser material eventually becomes sufficiently high to completely saturate the absorption, the laser fired a pulse of much higher intensity and shorter duration than would have been the case without the saturable absorber. This effect of the saturation process upon the laser output is called Q-switching. Because of this valuable application, saturable absorbers that could be used to Q-switch a laser were studied extensively by many workers.[5] In most of this work, the saturable absorbers were organic dyes in liquid solutions with organic solvents.

Shortly after the CO_2 laser was developed, Wood and Schwarz[6] reported that it could be Q-switched with a gaseous absorber at low pressure. This development led to the discovery of many saturable absorbers which could be used to Q-switch a CO_2 laser. Q-switching with gases involves the saturation of a rotational-vibrational type of electric-dipole transition since the CO_2 laser operates in the infrared somewhere in the wavelength region between 9.6 and 10.6-μm.

This interest in saturable absorber has continued beyond Q-switching applications because of the information which may be obtained from saturation phenomena. Since saturation is the result of a direct competition between excitation and relaxation processes, information about relaxation processes in absorbing atoms, molecules, and ions can be extracted from the results of

saturation experiments. This method could provide a powerful tool for the chemical physicists in obtaining such information. In the past most efforts in spectroscopy were devoted to finding the energies of the various stationary quantum states of the system rather than to the dynamic aspects of the interaction.

The interest in saturable absorbers was further heightened by recent developments which permitted a greater number of materials to undergo saturable absorption. In the past only materials that had a strong absorption band that overlapped one of a rather few laser transitions at fixed frequencies would exhibit saturable absorption. Tunable dye lasers, new frequency tuning techniques, and the development of many new material combinations which will sustain laser action have greatly increased the number of available laser transition. Further, Brewer[7] et al., showed that the Stark effect could be used to shift absorption bands into overlap with a laser transitions. Thus any gas which strongly absorbs in the vicinity of the many available laser transitions could become a saturable absorber if the molecules of the gas possessed a permanent electric-dipole moment.

Before information can be readily extracted from saturation experiments, however, the relationship between the degree of saturation achieved and the properties of the material and the laser radiation must be known. Quite recently researchers have sought to learn these relationships by measuring the optical properties of a saturable absorber under various levels of irradiance and developing a theoretical procedure which will predict these optical properties as a function of the properties

of the laser radiation and the saturable absorber. The theoretical treatments to date have not taken the reflectance of the sample into account and therefore to that extent they must be inaccurate. Thus a complete description of a material undergoing optical saturation must include reflectance phenomena as well as transmittance phenomena.

In this work, a theory was developed which describes the transmission, reflection, and refraction of light in a saturable absorber undergoing laser induced saturation. Experiments were performed to test the adequacy of the theory. The result is a generalization of the laws of Bouguer, Lambert, Beer, Snell, and Fresnel which have adequately described light propagation in non-saturable materials for over one hundred years. Thus this work must be considered as a fundamental contribution to the field of nonlinear optics. As a result chemical physicists who wish to add optical saturation as a powerful tool to their repertoire of spectroscopic techniques may do so with confidence that the results they extract from experimental data will be accurate.

This dissertation consists of five chapters. The theoretical procedures employed are discussed in Chapter II. Chapter III is devoted solely to describing the experimental apparatus and techniques required to perform the saturation experiments. The major effort of the author was the design and construction of the experimental apparatus. A study of the influence of temperature on optical saturation in SF_6 is

presented in Chapter IV. Sample heating caused difficulties in the interpretation of the saturation data which could not be overcome without this study. In Chapter V the experimental results are compared with the optical properties calculated from the theory. Techniques to improve the theory and optimize it for SF_6 will be discussed. A number of appendices present technical information such as descriptions of the design and operation of electronic equipment.

REFERENCES

1. The discovery that a light beam is attenuated exponentially with distance into an absorbing material was made by Pierre Bouguer in 1729 and independently by J. H. Lambert in 1760. In 1851, German A. Beer discovered that the argument of the exponential was proportional to the concentration of the absorbing species.
2. A. Einstein, Phys. Zeit., 18, 121 (1917).
3. G. N. Lewis, D.Lipkin, and T. T. Magel., J. Amer. Chem. Soc., 63, 3005 (1941).
4. C. H. Townes, Phys. Rev., 70, 667 (1946).
5. See references 48-87 in the bibliography given by J. D. Macomber, IEEE J. Quantum, Electron., 4, 1 (1968).
6. O. R. Wood and S. E. Schwarz, Appl. Phys. Lett., 11, 88 (1967).
7. R. G. Brewer, M. J. Kelly and A. Javan, Phys. Rev. Lett., 23, 559 (1970).

CHAPTER II
THEORY OF OPTICAL SATURATION

A. INTRODUCTION

Historically there have been two main theoretical approaches to describe optical saturation. In both approaches one needs one or more equations to describe the matter which is being struck by the light beam and one or more equations to describe the state of the electromagnetic field interacting with the matter.

The first method is called the rate-equation approach and was developed by Einstein to describe absorption and emission of radiation by matter. This approach derives one equation for the difference in population of the energy levels of the absorbing systems in the material by using the Einstein rate coefficients for spontaneous and stimulated emissions. The equation which describes the electromagnetic radiation is based simply on the conservation of energy; a change of two in the population difference is associated with the creation or annihilation of one photon. If the exciting light is coherent (a laser for instance), transient phenomena can be produced which are not calculable by means of this approach.

The second method uses time-dependent quantum-statistical mechanics (the density matrix formalism). Three equations are derived to describe the absorbing material. One of these equations describes the population difference in the manner of the rate-

equation approach. The other two are required to describe the dipole polarization of the sample because there are two components of the polarization: one in phase with the driving electromagnetic field and one in quadrature with it. The electromagnetic fields of the radiation are described by Maxwell's equations. While the rate-equation approach uses only one equation to describe the electric field (the square of the field amplitude), the density matrix approach gives one equation for the amplitude and one for the phase of the electric field. These equations permit the consideration of coherence effects. Arrecchi and Bonifacio[2] were responsible for the coupling of the three equations describing the material with the two equations describing the electromagnetic (em) waves which interact with the material. For this reason this approach is sometimes called the AB theory.

Although the rate-equation approach has had many successes, in principle it is incorrect because the quantum systems of the matter are not adequately described. The fields of the electromagnetic radiation act on the matter by exerting a torque on the dipoles of the quantum systems. To calculate the expectation value of the dipole moment a quantum mechanical treatment is required.

In a description of steady-state saturation (when the macroscopic properties do not change with time) these two methods are equivalent. The phase relationships of the matter become scrambled after a time T_2 which is called the transverse relaxation time. Coherence effects can no longer be observed and the phase equations of the AB theory are no longer meaningful; the rate-equation treatment

will be adequate. Although the theory required for this work treats steady-state saturation, the AB approach will be used to permit the treatment of non-steady-state systems at a later time.

There are many treatments of steady-state optical saturation in the literature. For the purpose of this discussion, only those which bear directly on saturable absorption will be referenced here. All of these suffer from one or more of the following deficiences:

1. Some[3-9] do not take into account both transmitted and reflected radiation. They assume that all of the light entering the sample was either transmitted or absorbed. Some of the attenuation attributed to absorption is in fact reflected from within the body of the absorber due to changes in the refractive index produced by the optical saturation. Thus the degree of saturation will be underestimated if the reflected radiation is not considered.

2. None[3-14] explicitly take into account the optical properties of the sample container. This is especially important in the case of gases because they must be confined. The windows of the container will reflect, refract, and sometimes absorb a portion of the exciting radiation. The radiation reflected by the rear window of the cell will pass back into the sample and interact with the sample and the forward-traveling wave. When the exciting radiation is coherent, the em wave reflected from the surfaces of each window can constructively or destructively interfer with each other depending upon

the properties of the window, the wavelength, and the angle of incidence of the radiation. Changing the angle of incidence and thus the optical thickness may change the transmittance of an individual window by as much as 14% because of these interference effects. If the incident radiation is normal to the sample cell and to both windows of the cell, interference phenomena can also occur between the reflected waves originating from the two windows. These interference effects are extremely sensitive to a change in the angle of incidence of the laser radiation. Finally, the amplitudes of the reflected waves depend upon the magnitude of the changes in the refractive index (n) which occur at all interfaces. These changes are also influenced by optical saturation.

3. Some[3-11] do not consider that the strength of the electric field at any given molecule or atom as the vector sum of the oscillating electric feilds of the forward and reverse em waves. When waves are traveling in opposing directions, they can interact through the bulk of the absorber.

4. None[3-14] takes into account the intensity profile of the em wave. Previous formulas use the infinite plane wave approximation. A laser usually exhibits a Gaussian intensity profile in the plane perpendicular to the beam axis.

The theoretical procedure employed in this work to describe steady-state optical saturation will not suffer from any of these four deficiencies.

B. CHARACTERISTIC MATRIX TECHNIQUE

A theoretical procedure which correctly describes optical saturation in an absorbing medium irradiated by two opposing electromagnetic waves is presented in this section. This procedure is much simplier to employ than the previous theoretical procedures[11-14] which treated opposing waves in an absorbing medium. The atoms, ions, or molecules of the absorbing material are assumed to possess two energy levels (ground and excited states) which are in exact resonance with the exciting radiation. For convenience, it will be assumed that the sample is a gas contained in a cell having flat, transparent, and parallel windows at each end . The origin of the backward-traveling wave is the reflection of the forward-traveling wave from the exit and entrance faces of the rear window of the sample container and possibly from within the body of the absorbing material.

When the radiation which is incident upon the sample has sufficient intensity to produce partial optical saturation, the degree of saturation will change with the depth into the sample material. The sample material at the very front of the cell will undergo the greatest saturation. As the radiation propagates through the sample it will be attentuated and saturate the saturable

absorber to a lesser extent. Thus the degree of saturation will be continuously varying throughout the sample material. When the forward-traveling radiation strikes the rear window of the sample container a small portion of the radiation will be reflected back into the sample. If the incident radiation is normal to the container windows this reflected radiation will be collinear with the forward-traveling wave. This reflected wave will encounter material the absorption coefficient of which is continuously decreasing as the front of the sample container is approached. A theoretical treatment of the effects produced by partial optical saturation will be very similar to the treatment of a system having many layers of material with each layer having different optical properties.

Several years ago a French graduate student named Abelés developed a very powerful technique for computing the optical properties of multi-layer dielectric coatings.[15] To employ this technique, a characteristic matrix (CM) is developed for each component of the optical system. Each matrix is square of order two, and therefore has only four elements. These elements depend upon the index of refraction, the absorption coefficient, and the thickness of the component being described. The reflectance, absorptance and transmittance of each component can be calculated directly from the values of the matrix elements. The characteristic matrices for all the components of the optical system are multiplied together in the same order that they are traversed by the wave. The resulting two-by-two product matrix characterizes the entire ensemble of optical components in the way that each individual CM in that product characterized the corresponding separate component. In particular, the elements

of this product matrix can be used to compute the reflectance (R) and the transmittance (T) of the entire optical system. Then using the law of the conservation of energy, the absorptance (A) can be computed by

$$A = 1 - T - R. \tag{1}$$

This characteristic matrix technique was derived by Abelés from the differential equations given by Maxwell to describe an em wave. The solution to these wave equations can be written in the form

$$\tilde{E}(x,y,z) = e^{i(Ky-\omega t)}[U^{TE}(z)\hat{y} - V^{TM}(z)\hat{x} - W^{TM}(z)\hat{z}] \qquad \text{and} \tag{2a}$$

$$\tilde{H}(x,y,z) = e^{i(Ky-\omega t)}[U^{TM}(z)\hat{y} + V^{TE}(z)\hat{x} + W^{TE}(z)\hat{z}] \qquad \text{where} \tag{2b}$$

$$\begin{pmatrix} U(z) \\ V(z) \end{pmatrix} = \begin{pmatrix} U_2(z) & U_1(z) \\ V_2(z) & V_1(z) \end{pmatrix} \begin{pmatrix} U(0) \\ V(0) \end{pmatrix} . \tag{3}$$

The two-by-two matrix in Eq. (3) is the transpose of the characteristic matrix defined by Abelés. For this work it was found that the transpose of Abelés CM was most convenient to use. Future references to the CM will in fact be the transpose of the CM defined by Abelés. In Eq. (3), U(0) and V(0) are the values of U and V at the entrance to the optical component where z=0 and must be supplied as a boundary condition. The z axis represents the direction of stratification

of the medium (the normal to the entrance and exit faces) which need not be the same as the direction of the propagation of the wave. In order to solve the differential equations associated with the elements of the CM it was necessary to transform the independent variable from z to ζ [to be defined in Eq. (13)]. The element of the characteristic matrix are now equal to

$$U_1(\zeta) = i \sin(\zeta)\, P(\zeta), \tag{4}$$

$$V_2(\zeta) = i \sin(\zeta)/P(\zeta), \tag{5}$$

$$V_1(\zeta) = \cos(\zeta-\alpha)/Q(\zeta), \tag{6}$$

and

$$U_2(\zeta) = \cos(\zeta+\alpha)Q(\zeta). \tag{7}$$

The variables P, Q, and α are defined for the transverse electric (TE) wave by

$$P_{TE}(\zeta) = [p(\zeta)\ p(0)], \tag{8}$$

$$Q_{TE}(\zeta) = [p(\zeta)/p(0)], \tag{9}$$

and

$$\alpha_{TE} = \partial\, \ell n \sqrt{p}/\partial\zeta\ . \tag{10}$$

The corresponding equations for the amplitude properties (U an V) of the transverse magnetic (TM) wave differ from Eqs.(8)-(10) only in the substitution of q for p. [The direction of propagation of the em wave and the z axis define a plane called the plane of incidence. The electric and magnetic wave vectors and the propagation direction form a mutually orthogonal set. Any em wave can be resolved into two independent components, one with the electric vector

perpendicular to the plane of incidence (TE wave) and one with the magnetic vector perpendicular to the plane of incidence (TM wave).] The quantities p and q are called the slant impedance and admittance of the sample, respectively, and are defined by

$$p = a/\Gamma \tag{11}$$

and

$$q = b/\Gamma \ . \tag{12}$$

Further

$$\zeta = \int_0^z \Gamma\,(w)dw \ , \tag{13}$$

and

$$\Gamma = (ab - K^2)^{\frac{1}{2}} \ , \tag{14}$$

where

$$K = \omega[\mu(0)\epsilon(0)]^{\frac{1}{2}}\sin\,\theta \ . \tag{15}$$

The angle θ is the angle between the z axis and the direction of propagation of the em wave. K is the propagation vector in the $\hat{y}$ direction and the symbols a and b are defined by

$$a(z) = \omega\mu(z) + i\sigma_m(z) \tag{16}$$

and

$$b(z) = \omega\epsilon(z) + i\sigma \ . \tag{17}$$

In the preceding equations ω is the angular frequency (presumed constant), μ is the magnetic permeability, ϵ is the electric permittivity, and σ is the electric conductivity. The parameter,

σ_m implies the existence of a magnetic conductivity associated with a current of magnetic monopoles induced by the field $\tilde{H}$. Because magnetic monopoles have never been observed there is no physical reason for retaining this term. It could be used, however, to represent physical effects not described by the other parameters. Finally,

$$W^{TE} = -KU^{TE}/a \ , \tag{18}$$

and

$$W^{TM} = KU^{TM}/b \ . \tag{19}$$

Equations (1)-(19) illustrate the procedure prescribed by Abelés and generalized by Macomber.[16] Equation (3) is particularly useful because it can be used to determine the changes in the amplitude and phase of the em wave as it propagates through a material. If U(z) and V(z) are known for a depth z into the material, U(z + d) and V(z + d) may be computed by means of Eq. (3) by using the z position as the initial boundary. Finally, ϵ and μ are the only parameters in this technique which describe the properties of the material interacting with the em wave. Thus any changes produced by the em wave in the properties of the material must be described by changes in ϵ and μ.

The CM technique does not automatically provide for the saturation of the absorption of the sample. Therefore, the effects of optical saturation upon the elements of the CM must be determined before this technique can be applied to a saturable

absorber. As previously mentioned the Abelés equations use only two parameters (aside from the thickness of the element) to characterize the electromagnetic properties of the medium through which an em wave is propagating. One of these (μ) may be treated as constant $\mu \cong \mu_o$ when only electric-dipole-allowed spectroscopic transitions occur. In this case, the absorptivity of the medium must be described by ϵ. The permittivity is complex and may be defined by the real and imaginary parts of the electric susceptibility (η). The susceptibility is a property of the absorbing material that determines the polarizability of the medium by the electromagnetic wave.

$$\hat{\epsilon} = \epsilon_o(1 + \eta' + i\eta'') , \tag{20}$$

where

$$\hat{n} = (1 + \eta' + i\eta'')^{\frac{1}{2}} . \tag{21}$$

The symbol $\hat{n}$ is the complex refractive index of the medium. The imaginary part of the electric susceptibility (η'') is related to the absorption coefficient (β) of the medium by

$$\eta'' = \frac{c_o\beta(1 + \eta')^{\frac{1}{2}}}{\omega} , \tag{22}$$

where c_o is the velocity of light is vacuum. In the absence of saturation η' and η'' are related by the Kramers-Kronig relations.

Since η characterizes the electromagnetic properties of the medium, a relationship between η and the intensity of the light is needed. Macomber[17,18] has reported a relationship which

describes the susceptibility as a tensor function of the electric field amplitude, the transition dipole moment of the absorber, and the relaxation times (T_1 and T_2) characteristic of the absorber.

$$\eta = \frac{m_e^2 T_2 \Omega N}{\Delta_e \epsilon_o \hbar (1-\Sigma_e)} \left[\begin{pmatrix} \delta T_2 & -\Sigma_e \\ \Sigma_e & \delta T_2 \end{pmatrix} + i \begin{pmatrix} 1 & \delta T_2 \Sigma_e \\ -\delta T_2 \Sigma_e & 1 \end{pmatrix} \right] \tag{23}$$

where

$$\Delta_e = 1 + \delta^2 T_2^2 + T_1 T_2 m_e^2 (|E_x|^2 + |E_y|^2)/\hbar^2 , \tag{24}$$

$$\Sigma_e = 2 T_1 T_2 m_e^2 |E_x| \; |E_y| \sin(\gamma)/\Delta_e \hbar^2 , \tag{25}$$

and

$$\Omega = \frac{\rho_g - \rho_{ex}}{\rho_g + \rho_{ex}} . \tag{26}$$

In Eq. (26) the ρ's refer to the populations of the ground and excited levels which are connected by a spectroscopic transition which has a transition dipole moment of m_e. The oscillating electric fields E_x and E_y differ in phase by γ, and δ is the angular frequency difference between the resonance frequency of the dipole transition and the frequency of these electric fields. The density of absorbing molecules per unit volume is N. Planck's constant

divided by two pi is represented by $\hbar$. The application of Eq. (23) is greatly simplified if the em waves of the radiation are polarized in the $\hat{y}$ direction. Then E_x and Σ_e will be zero and the $\hat{y}$ components of the tensor will give

$$\eta = \frac{N \; m_e^2 \; T_2 \; \Omega}{\epsilon_o \; \Delta_e \hbar} [\delta T_2 + i] . \tag{27}$$

With the susceptibility determined, the electric permittivity (ϵ) and the propagation of the em wave in the medium may be accurately described when optical saturation occurs. The CM technique may now be employed to saturable absorbers.

C. COMPUTATIONAL PROCEDURE

To apply the CM technique to a saturable absorber contained in a sample cell, an iterative procedure was used. In order to accurately describe the em wave interacting with the sample, the vector sum of the fields of the backward and forward-traveling waves had to be obtained. Since the properties of the backward-traveling wave are initially unknown, they had to be approximated. After performing this approximation, the optical properties of the sample system were computed and improved estimations of the fields of the backward-traveling wave were obtained and added vectorially to the fields of the incident wave. This improved description of the total em wave was used to determine the optical properties

of the system again, and a further improved description of the backward wave was obtained. This procedure was iterated until self-consistency was obtained within prescribed limits. For the initial approximation of the backward wave, the absorber was assumed to attenuate the radiation in accordance with Beer's law. The CM for the absorber was calculated with the use of the small-signal absorption coefficient with no consideration of optical saturation. The CM's for the two cell windows were calculated with the use of known optical properties of the window material. A product matrix was obtained by multipling the CM's of the front window, the absorber, and the rear window in that order. The elements of the product matrix (U' and V') were then used to compute the reflectance coefficient (r) and the transmittance coefficient (t) of the entire sample system by means of Eqs. (28)-(30).

$$\text{Denom}_{TE} = (U_1' - U_2' p) - (V_1' - V_2' p) p , \tag{28}$$

$$r_{TE} = [(U_1' + U_2' p) - (V_1' + V_2' p) p]/\text{Denom}_{TE}, \tag{29}$$

and

$$t_{TE} = -2p/\text{Denom}_{TE} . \tag{30}$$

As before, the coefficients for the TM wave were obtained by the substitution of q for p in Eqs. (28)- (30). The quantities p and q were evaluated for the medium in which the sample system is immersed. The medium was air in this case.

The approximate value of r was then used to compute U(0) and V(0) which describe the vector sum of the fields of the

reflected and incident em waves at the entrance to the sample system. The peak amplitude of the fields (E_p and H_p) of the incident laser radiation were computed from the intensity of the laser beam, Then

$$U_{TE}(0) = (1 + r)\, E_p \sin \phi \,, \tag{31}$$

$$V_{TE}(0) = (1 - r)\, H_p \sin \phi/p \,, \tag{32}$$

$$U_{TM}(0) = (1 + r)\, H_p \cos \phi \,, \tag{33}$$

and

$$V_{TM}(0) = (1 - r)\, E_p \cos \phi/p \,. \tag{34}$$

The symbol ϕ represents the polarization angle of the electric field associated with the em wave. The em wave at the entrance to the sample system is now defined by U(0) and V(0). The behavior of this wave upon propagating through the entrance window was calculated by means of Eq. (3). The em wave which exists this window was defined by $U(z_1)$ and $V(z_1)$. The absorber was imagined to be divided into M slabs of thickness dz. For this second approximation M=5 was used (i.e., 5 slices). The amplitude of the electric field present at the front of this stack of slabs was given by $U(z_1)$ and $V(z_1)$. The electric susceptibility was computed by means of Eq. (23), and the CM for the first slab was calculated by assuming a constant susceptibility through out the slab. The behavior of the em wave propagating through the first slab was again calculated by means of Eq. (3). The em wave striking the second slab was defined by $U(z_2)$ and $V(z_2)$. The electric field strength at

the front of this slab was used to compute a susceptibility. The CM of the second slab was calculated, and the em wave was allowed to propagate through the second slab. The same procedure was followed for the next three slabs. In this way the degree of saturation in each slab was taken into account by using the electric field strength at the front of each slab to compute the susceptibility. A product matrix was obtained by multipling the CM's of the front window, the five slabs of the absorber, and the rear window in that order. The r coefficient was computed from the elements of the product matrix as before by means of Eqs. (28) and (29). This latter r was compared with the previous r to see if self-consistency had been obtained. If self-consistency was not obtained, the latter r was used to recalculate U(0) and V(0) and the whole propagation procedure was repeated. On the third iteration the absorber was divided into 10 slabs, 15 slabs on the fourth, etc. As M became large, dz became very small and the smooth gradient of the changes in the optical properties of the saturable absorber could be accurately approximated. When the iteration procedure obtained self-consistency (<0.2% change), the r and t coefficients were calculated, and the radiant reflectance (R) and transmittance (T) of the entire sample system were calculated by

$$R(\theta,\phi) = |r_{TM}(\theta)|^2 \cos^2\phi + |r_{TE}(\theta)|^2 \sin^2\phi \qquad \text{and} \qquad (35)$$

$$T(\theta,\phi) = |t_{TM}(\theta)|^2 \cos^2\phi + |t_{TE}(\theta)|^2 \sin^2\phi \; . \qquad (36)$$

A computer program which is discussed later in this chapter was developed to execute this iterative procedure.

D. THEORETICAL TREATMENT OF A NON-SATURABLE SAMPLE

An experiment was performed to determine the feasibility of obtaining accurate experimental results in accord with existing theory on a non-saturable absorber. The "existing theory" was the characteristic matrix technique which was used for each ray of laser light to calculate μ and ϵ from the known properties of the sample material. A complete description of this experiment is given in Appendix 1. A mechanical device (theta two-theta goniometer) was designed and constructed to enable the measurement of the radiation reflected, absorbed, and transmitted by a sample at any angle of incidence. The goniometer was rotated by a synchronous motor so that the sample mounted upon the theta table rotated at a constant angular velocity of ω. The two-theta table rotated at a constant angular velocity of 2ω. A detector attached to this table therefore continuously tracked the radiation reflected from the sample. A helium-neon laser was used as the radiation source and photodetectors were used to detect the reflected, transmitted, and incident radiation. An analog computer, constructed for this research, converted these intensity measurements into reflectances, absorptances, and transmittances. When the goniometer was rotated at a constant velocity, the outputs from the analog computer were fed to a three-channel strip-chart recorder driven at a constant rate.

The resulting traces represented reflectance, absorptance, and transmittance of the sample as a function of the angle of incidence of the central ray of the laser beam upon the entrance face.

A computer program was developed to calculate the theoretical optical properties for these experimental conditions. The program employed the CM technique although this technique was not really necessary because there was only one component. The value of the absorption coefficient and refractive index of the sample and the angle of polarization of the incident radiation used in the program were adjusted for a simultaneous best fit with the data. The theoretical curves then differed by less than 0.4% from the experimental curves obtained. This excellent agreement between experiment and theory inspired confidence that these experimental and theoretical procedures were sound, and that the results of future work with a saturable system could be accepted with confidence.

E. COMPUTER PROGRAM

The computer program which was developed to execute the iterative procedure previously described had three features which further enhanced the accuracy of the procedure. A fourth feature enabled the convenient comparison of experimental data with the theory.

The first feature provided a better method for determining the electric susceptibility (η) within a particular slab of the absorber. When the saturable absorber was divided into M slabs

of thickness dz, the amplitude of the electric field associated with the em wave which struck the front of the slab was used to calculate η for that slab. The electric field amplitude, however, was oscillating and varied from $-E_p$ to $+E_p$ over a propagation distance of $\frac{1}{2}$ wavelength (λ). In the limit of an infinite number of slabs η would be correctly computed, but for slabs many λ thick, the phase and hence the amplitude of the electric field were greatly influenced by the precise choice of slab thickness. It is unlikely that the value of η which was calculated at the front face of the slab was the average of η within the slab. The slabs had to be many λ thick, however, or a tremendous computation time would have been required to execute the computer program. To obtain an average η for each slab, ten small slabs of thickness $\lambda/10$ were formed in between each major slab of thickness dz. The average of η for the ten small slabs was then used as the effective η for the slab of thickness dz. The amplitude of the electric field made one complete cycle while the em wave propagated through the ten slabs of thickness $\lambda/10$.

A second feature provided a technique to take into account the intensity profile and divergence of the incident light beam. The intensity profile is the relative intensity of the beam in the plane perpendicular to the axis of the beam. A light beam can be imagined as a bundle of many light rays having different directions and intensities so that the optical properties of the light beam is the sum of the optical properties of the many rays. The divergence of the laser beam has the effect of averaging the interference effects when the beam strikes a sample if a light

detector with an aperature larger than the beam is used. If a detector with a very small aperature is used, only one ray is observed, and this feature is not needed. This averaging routine used the experimentally measured divergence and intensity profile of the laser beam to determine the direction and intensity of a number of individual light rays. The reflectance and transmittance of each ray was computed. To compute the average reflectance for the complete beam, the reflectance of each ray was mathematically weighted according to the intensity of the ray. The average of the reflectances of the intensity-weighted rays was the reflectance of the beam. This same procedure was followed for the transmittance. A more complete explanation of this procedure and the trigonometry involved is given in section H of Appendix 1.

A third feature of the computer program was the option to vary the length of the sample cell over a range of $\lambda/2$ so that interference effects could be averaged. This feature was very useful when the interference effects were large. In the case of the reflected beam in saturation experiments in which the beam was at normal incidence to the sample cell the interference effects were large.

A final feature of the computer program enabled the convenient comparison of experimental data with the theory. With this feature the experimental data which consisted of laser intensities, transmittances and reflectances were read into the program. By means of the program the R and T for the laser intensities used in the experiments were calculated. A root-mean square deviation of the experimental data from the theoretical predictions was calculated for each set of experimental data.

A complete listing of this computer program is presented in Appendix 2. In Chapter 5 the employment of the program to calculate the optical properties of SF_6 is discussed.

F. EVALUATION OF THEORETICAL PROCEDURES

The theoretical procedure which has been described in this chapter has three weaknesses. One weakness arises from the model that was used to describe the absorbing species of the saturable absorber. It was assumed that molecules, ions, or atoms of the sample possessed only two energy levels which were connected by an electric-dipole transition. Most saturable absorbers have molecules that have several energy levels, and frequently more than one level will absorb the exciting radiation. Adapting this theory for a two-level system to a multi-level system could introduce inaccuracies into the theoretical procedures. A second weakness is that the theory assumes that the absorption line of the absorbing species is homogeneously broadened, For gases at moderately low pressures the Doppler broadening of the absorption line is frequently the order of the homogeneous broadening. Finally, a third weakness is that it was assumed that the relaxation mechanisms of the absorbing centers in the sample could be described by two relaxation times. In practice there are many relaxation mechanisms which require many relaxation times to fully describe them.

The strengths of this theoretical procedure are four. First, it takes into account the effects of the backward-traveling wave produced by the reflections at the interfaces of the sample cell windows and from gradients of optical properties within the absorber produced by partial optical saturation. Second, it explicitly calculates the optical properties of the total sample system which includes the sample cell windows. Third, it can explicitly treat a realistic laser beam without the infinite plane wave approximation. And fourth, it uses the vector sum of the fields of the forward and backward-traveling em wave to determine the effective field at an individual electric dipole.

Only a few workers[10,12-14] have reported a theoretical procedure to compute the reflectance of a sample undergoing partial optical saturation. The first of these, Macomber and Kestner[10] in 1969, treated a plane slab and reported a significant dependence of the reflectance upon the thickness of the slab. Their results predicted that the reflectance could increase by a factor of two or three as the incident intensity was varied from zero to infinity, or it could decrease to almost zero, depending on the initial slab thickness which was chosen. Three review articles[12-14] which develop the theory of saturation spectroscopy have recently been published. Two of these articles[12,14] suggested an experiment to study the effects of saturation upon the intensity of the radiation reflected from the sample system as a function of the incident intensity. Shirley[12] predicted

that the reflectance would increase monotonically with increasing intensity of the incident radiation. Haroche and Hartmann[13] predicted that the radiation reflected from the rear window of the sample cell would be amplified as it traversed the material which was saturated by the forward wave if the incident radiation had sufficient intensity. Although many workers have used a reflected wave to experimentally perform saturation spectroscopy, to the author's knowledge none has reported the influence of the intensity of the incident radiation upon the reflectance of a sample system containing a saturable absorber.

REFERENCES

1. J. D. Macomber, IEEE J. Quantum. Electron, 4, 1 (1968).
2. F. T. Arrecchi and R. Bonifacio, IEEE J. Quantum. Electron., 1, 196 (1965).
3. M. Hercher, Appl. Opt., 6, 947 (1967).
4. H. Brunet, IEEE J. Quantum. Electron., 6, 678 (1970).
5. L. Huff and L. G. DeShazer, J. Opt. Soc. Am., 60, 157 (1970).
6. J. J. Armstrong and O. L. Gaddy, IEEE J. Quantum. Electron., 8, 797 (1972).
7. I. Burak, J. I. Steinfeld and D. G. Sutton, J. Quant. Spectrosc. Radiat. Transfer, 9, 959 (1969).
8. U. P. Oppenheim and Y. J. Kaufman, IEEE J. Quantum, Electron., 5, 276 (1969).
9. O. R. Wood, P. L. Gordon, and S. E. Schwarz, IEEE J. Quantum. Electron., 5, 502 (1969).
10. J. D. Macomber and N. R. Kestner, J. Appl. Phys., 40, 3218 (1969).
11. N. G. Basov, O. N. Kompanets, V. S. Letokhov, and V. V. Nikitin, Sov. Phys. -JETP, 32, 214 (1971).
12. J. H. Shirley, Phys. Rev. A, 8, 347, (1973).
13. S. Haroche and F. Hartmann, Phys. Rev. A, 6, 1280 (1972).
14. E. V. Baklanov and V. P. Chebotaev, Sov. Phys. -JEPT, 33, 300 (1971).
15. M. Born and E. Wolf, Principles of Optics (Pergamon, Oxford, (1965), 3rd. ed., pp. 55-70.

16. J. D. Macomber, J. Opt. Soc. Am., 61, 308 (1971).

17. J. D. Macomber, Appl. Opt. 10, 2506 (1971).

18. J. D. Macomber, Dynamics of Spectroscopic Transitions, in press.

CHAPTER III
EXPERIMENTAL MEASUREMENT OF THE OPTICAL PROPERTIES OF SF_6 UNDER CONDITIONS OF PARTIAL OPTICAL SATURATION

A. INTRODUCTION

The experiments described in this chapter were performed to obtain data that could be used to test the adequacy of the theory presented in Chapter II. The phenomenon to be described is the optical behavior of a saturable absorber undergoing partial optical saturation. These measurements entail irradiating the saturable absorber with high intensity radiation and then detecting the amounts of that radiation which were reflected, absorbed, and transmitted by the saturable absorber. The intensity of the impinging radiation was systematically varied to produce various degrees of optical saturation. A careful selection of the necessary experimental components was made in order to enhance the accuracy of the results.

A continuous wave carbon dioxide laser was chosen for the intense radiation source for three reasons. First, it has a very stable power output of sufficient intensity to produce optical saturation. Second, the beam characteristics (single mode operation, narrow divergence, high coherence, small beam radius) are excellent and reproducible. And third, compared to the cost of detectors required for pulsed lasers, the cost of detectors required to detect the CO_2 radiation is not great.

The saturable absorber chosen for this work should have an intense absorption band near the output wavelength of the laser and relaxation times slow enough in relation to the incident photon flux to permit saturation to occur. There are several such materials suitable for saturation experiments with the CO_2 laser, and they are all gases at low pressure. The gas most commonly used is sulfur hexafluoride. It has a complicated energy level structure that may make a simple theoretical interpretation of the data rather difficult, but it is inexpensive, not very reactive, and easy to obtain. Also, because it has been studied expensively by other workers, comparison of the results of these experiments with those previously obtained in related studies would be possible. For these reasons sulfur hexafluoride was chosen to be the saturable absorber.

The detector chosen to detect the CO_2 laser radiation was a pyroelectric type. These detectors are very sensitive and can operate linearly over a wide range of input intensities. Furthermore, they operate at room temperature and have a moderately short risetime. The short risetime permits faster chopping of the incoming radiation than would be possible if thermocouple type infrared detectors were employed. This faster chopping produces a higher frequency output signal, and the higher frequency simplifies the electronics required to process the detector output.

The major criteria for the remaining experimental components were that they be compatible with the CO_2 laser, the pyroelectric detector, and SF_6 gas. Most of these additional components were designed and constructed in the laboratory because commericial

alternates were unavailable or too expensive. Each experimental component will be discussed in detail in section C of this chapter.

The characteristics of SF_6 which are pertinent to this work will be discussed in Section B. In Section D, the procedures and results of a transmittance experiment will be presented. In the last section of this chapter, the procedures and results of an experiment which simultaneously measured all the optical properties of the sample system will be presented. This latter experiment employed a Nova 1200 minicomputer to collect and treat the experimental data.

B. CHARACTERISTICS OF SF_6

Sulfur hexafluoride is very easy to handle because it is chemically inert and can be heated to 800 K without decomposition.[1] This ease of handling along with its intense infrared absorption at the 944.2 cm^{-1} (10.59-μm) CO_2 laser frequency has led to over a dozen different studies of the effects of CO_2 laser radiation on SF_6.[2] This absorption band is quite broad, and the center of the Q branch occurrs at 948 cm^{-1}. It has been shown that the separation between two rotational components of the vibrational lines is about 0.05 cm^{-1}, when the fine structure of the lines is neglected. Including the superposition of the fine structures, there are estimated to be about one thousand lines in a 1 cm^{-1} frequency interval. Since the Doppler width of a transition is 10^{-3} cm^{-1} (30 MHz), the absorption lines overlap each other within the Doppler width and the infrared

spectrum near 944 cm^{-1} is nearly continuous.[3] Further, it has been shown experimentally by means of Lamb-dip spectroscopy that several rotational sublevels from one or more vibrational manifolds are expected to absorb the 10.59-μm CO_2 laser line.[4]

Brunet studied the temperature dependence of the SF_6 absorption band contour and concluded that several "hot bands" overlap the fundamental band, and thus increase the complexity of the infrared spectrum.[3] He concluded that the absorption of the 10.59-μm laser radiation is mainly due to both transitions of the fundamental and of the hot band $(\nu_3 + \nu_6) - \nu_6$. The contributions to absorption of the laser radiation by the other hot bands were negligible because of the small populations of the lowest levels.

A three step mechanism which describes the various energy transfer processes between the laser radiation and the molecules and among the molecules is illustrated in Fig. 1. In step 1, molecules from a particular rotation energy sublevel of the ground vibrational manifold are excited by the laser radiation to a specified rotational energy sublevel of the ν_3=1 vibrational manifold. The initial population of this lower rotational sublevel is only about 0.3% of the molecules[5]; however, an equilibrium among the rotational sublevels occurs very rapidly (less than 300 nsec)[2]. Since this rotational equilibrium is so rapid compared to that of vibrational relaxations, the effects of saturation appear to be a result of absorption by the whole vibrational manifold. Also in step 1, a rotational sublevel in the ν_6=1 vibrational manifold is being pumped to the upper level of the $(\nu_3 + \nu_6) - \nu_6$ hot band. In step 2, the ν_3=1 level and the upper

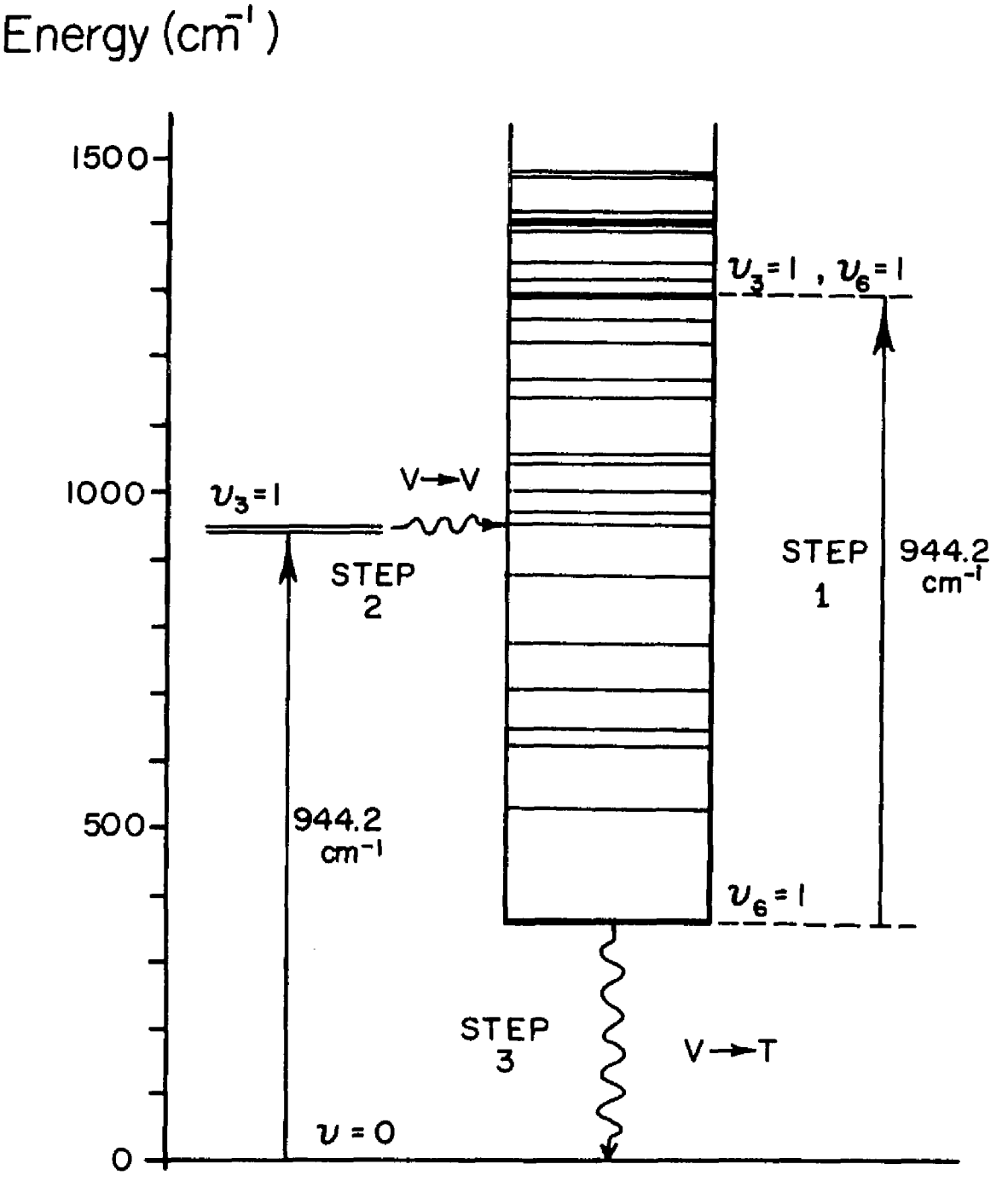

FIGURE 1. Vibrational excitation and relaxation model for SF_6.[3]

level of the hot band transfer vibrational energy by collisions to the complete set of excited vibrational levels in SF_6, among which an equilibrium is reached in a few microseconds. In step 3, the excess vibrational populations originating from the laser pumped ν_3=1 level and the upper hot band level relax to the ground vibrational level. The rate limiting process of this step is the vibrational-translation deactivation of the ν_6=1 level at 350 cm^{-1}.

This mechanism permits two nearly independent absorption processes. The ground to ν_3=1 process can be easily optically saturated due to the slow relaxation of the ν_6=1 level to the ground level. Thus T_1 will be characteristic of the ν_6=1 relaxation. The process in which the ν_6=1 level absorbs the laser radiation will be much harder to saturate because of the rapid equilibrium that occurs in the vibrational manifold beginning at ν_6=1. Thus a T_1 for the hot band transition will be very short. Treating two saturation processes simultaneously will further add to the complexity of the theoretical calculation of optical saturation in SF_6.

C. EXPERIMENTAL APPARATUS

This section will present a detailed description of the various experimental devices and apparatus used in this work. The techniques used to vary the laser power and the electronics which handle the output signals of the detectors will not be discussed here but will be discussed in the appropriate portion of the section on experimental procedure.

1. CO_2 Laser

The laser employed in this work was a Sylvania model 948 CO_2 laser which was warranted to produce a minimum of 6 watts of power. The intensity distribution in the plane perpendicular to the beam direction had a Gaussian shape with a radius (measured at the point where the intensity was 1/e of its peak) of 1.78 mm at the output of the laser and a full beam divergence of 1.58 milliradians. Special features of this laser was its very stable, electronically controlled power output and its operation in a single transverse mode. These features were major reasons for chosing this particular laser. One of several possible CO_2 laser lines (with correspondingly different output frequencies) was selected by changing the cavity length: the rear laser cavity reflector was mounted upon a piezo-electric transducer for that purpose.

Two modifications of the CO_2 laser were made to improve its performance. The first was the installation of a constant temperature control unit (stable to $\pm$ 0.01 K) which circulated an ethylene glycol-water mixture inside the cooling jacket of the laser plasma tube. The major purpose of this modification was to prevent the cavity length from changing because of thermal expansion due to small temperature fluctuations. Tap water was originally used as the cooling fluid. Another benefit of this modification was that it was possible to lower the laser temperature to 13 K by using a refrigation unit with the temperature controller. Bridges and Patel[6] have shown that the output and efficiency of a CO_2 laser are improved by cooling the plasma tube. The inside of the laser tube

housing was continuously flushed with dried air in order to prevent moisture collection.

The second modification of the CO_2 laser was the installation of an electronic servo system which stabilized the output frequency of the radiation. The manufacturer claimed a long term (hours) frequency deviation of less than 2 MHz after a $\frac{1}{2}$ hour warm-up when an auxiliary heat exchanger was used to obtain greater thermal stability. On some occasions the laser did acheive this frequency stability; however, in most cases the frequency drift was sufficient to cause a jump from one laser transition to another (i.e., from one CO_2 line to another) in less than 1 hour. Since the saturation experiments required a long term stability of the power and the frequency of the laser, this frequency drifting could not be tolerated. The modification was an electronic servo system which modulated the cavity length of the laser and used the effects of this modulation upon the impedance of the laser plasma tube to provide a frequency correction. Accurate tuning and locking of the frequency over the Doppler gain profile for each available laser transition was made possible by means of this modification. A complete description of this modification and the method of operation are presented in Appendix 3.

Identification of the CO_2 line producing the laser action was accomplished with the aid of silicon stopcock grease used as an infrared absorber. Although the CO_2 laser could be tuned to output several different frequencies, only the P(20) line at 10.59-μm (944.2 cm^{-1}) was desired for this study. A McPherson (Model 218, 0.3m) scanning monochromator which was borrowed temporarily from

Professor James Robinson's research group, was used to observe six output frequencies (lines) from this laser. Three of these lines were in the P branch of the 9.6-μm CO_2 transition and three were in the P branch of the 10.6-μm transition. Unfortunately, these lines could not be tuned reproducibly by calibrating the laser frequency adjustment representing the laser cavity length. Silicon stopcock

TABLE I

CO_2 LASER FREQUENCIES

Wavelength (μ)	Frequency (cm^{-1})	Transition
9.4884	1053.9	P(12)
9.5360	1048.7	P(18)
9.5524	1046.9	P(20)
10.5131	951.2	P(12)
10.5710	946.0	P(18)
10.5910	944.2	P(20)

grease (Dow-Corning Corp.) exhibits a very strong absorption from 9-μm to 10-μm and has a minimum absorption at 10.6-μm.[7] The silicon stopcock grease would be expected to have a very small transmittance for the 9.6-μm lines and to exhibit increasing transmittance in going from the P(12) to P(18) to P(20) of the 10.6-μm lines. This hypothesis was confirmed with the monochromator for a sand-blasted NaCl flat coated with the stopcock grease. To identify the 10.59-μm laser line without the monochromator, the coated flat was placed immediately in front of a Cintra (model 202) radiometer and irradiated with the laser radiation. The transmitted radiation was detected by

the radiometer as the laser was tuned over the six laser lines. The laser line which produced the maximum transmittance in the coated salt flat was the 10.59-μm line. This identification procedure was performed each time the CO_2 laser was brought into operation.

2. Sample Cell

The gas sample cell was constructed from a stainless steel right circular cylinder which had polished KCl windows at each end. Great care was taken in the construction of the cell to insure an accurate parallelism between the two end windows. When the laser beam was normal to the front window, the incident radiation and the radiation reflected from both windows were all collinear. The inside dimensions of the cell were a length of 10 cm and a diameter at 4.2 cm. The KCl windows were 6.5 mm thick and 49.5 mm in diameter, and a vacuum seal was obtained between them and the stainless steel cylinder with neoprene "O" rings. A Matheson brass stopcock was installed at the middle of the cell and connected to the gas-handling system.

In the Nova minicomputer experiments the sample cell was wrapped with an electrical heating element and was insulated with asbestos. A thermistor temperature probe was put into thermal contact with the cell using brass filings and silicon lubricant. A Sargent Thermoniter sensed the temperature of the cell with the thermistor and fed a variable current into the heating element to maintain the cell at a constant temperature ($\pm$0.05 K).

A second gas holding cell was used in the initial transmittance experiments. This cell was placed near the laser output so that the

laser beam traversed the axis of the cell. Filling this cell (25 cm long, 2.4 cm diameter) with ethylene and helium attentuated the laser radiation and permitted a convenient method to vary the intensity of the laser beam exiting this cell. The helium was added as a buffer gas to prevent optical saturation of the ethylene (ethylene, not helium was the absorber of the laser radiation). By slowly pumping the ethylene-helium mixture from the cell, the intensity of the transmitted laser beam would gradually increase. This cell was also attached to the gas-handling manifold. The cell was constructed from brass and had two NaCl end windows mounted at 45° to the cell axis. The transmittance of the empty cell was maximized by rotating the cell about its long axis until the cell windows were perpendicular to the plane of polarization of the incident laser radiation. The output of this CO_2 laser was plane polarized as a consequence of the discriminatory action of the laser tube windows, which by their orientation favored one polarization.

3. Gas-Handling System

The gas-handling system used in this work was capable of acheiving a vacuum of 0.005 Torr and had a leakage rate less than 0.0003 Torr per minute. The system was constructed with a brass manifold and flexible brass tubing which connected it to the sample cell and the gas storage cylinders. Each component of the vacuum system could be isolated by means of brass stopcocks. A copper line connected the manifold to a McLeod vacuum guage which was used to measure all the gas pressures. The gas pressures were sufficiently high to permit

the partial pressure of mercury to be ignored. (A thermocouple vacuum guage was also installed for rough pressure measurements.) The vacuum pump employed was a two stage Welch Scientific Duo-Seal.

4. Detectors

Two pyroelectric detectors were used to detect the chopped laser radiation in both the transmittance and Nova experiments. One of the pyroelectric detectors was a Harshaw model PY4 and the other was a Laser Precision model KT-1000. The heart of these detectors was the small permanently polarized pyroelectric crystal (1 mm by 1 mm) which changed its capacitance when heated. When the laser radiation strikes the pyroelectric element the temperature of the element increases and a small current flows in the circuit. This current is proportional to the rate of heating and hence, to the intensity of the impinging radiation. A load resistor was placed in parallel with the element to improve the response time of the detecting system. Because of the very high impedance of the pyroelectric element, the voltage created by the current flow is applied to the gate input of a field effect transistor. This transistor serves as an impedance converter and amplifier. This resulting voltage (millivolts or less in this work) was further amplified and passed to a synchronous detector (sometimes called a lock-in-amplifier) for processing. Because these detectors operate at room temperature and require no special housing, they were convenient to use. (More sensitive and faster infrared detectors must operate at liquid nitrogen temperatures or below.) Finally, pyroelectric detectors cost less than other infrared detectors of similar capabilities.

Another infrared detector used in this work was the Cintra model 202 thermal radiometer. This detector used a thermopile sensing element and was calibrated in watts/cm^2. The electronics were self contained and produced a digital display of the average irradiance striking the thermopile element. The radiometer was used as the absolute standard in determining the intensity of the laser beam in all of the experiments. The accuracy of the radiometer was determined to be $\pm$ 5% by the manufacturer.

A laser beam with a Gaussian intensity profile is conveniently characterized by its peak intensity and cross sectional diameter at the positions where the intensity has decreased to 1/e of the peak intensity. These two properties were determined from the average intensity (I_{av}) and a measurement of the beam profile. The average intensity over an area of 1 cm^2 at the beam center was given directly by the radiometer when the thermophile element was irradiated. Care was required to ensure that the beam and the detector aperatures were concentric. An intensity profile was obtained by slowly traversing one of the pyroelectric detectors across the laser beam. The 1/e diameter and 1/e radius ($R_{1/e}$) were directly determined from the profile and the peak intensity (I_{peak}) was calculated by means of Eq. (1). Measurements of I_{peak} when a 2 mm diameter pinhole was used

$$I_{peak} = I_{av}/[1 - \exp(-31.8/R_{1/e}^2)] \qquad (1)$$

gave similar results to the I_{peak} calculation when $R_{1/e}$ was 3.4 mm. The pinhole technique for determining I_{peak} was inconvenient for routine work.

The peak intensity of the laser beam was calculated in each experiment by means of Eq. (1). As a check, beam profiles were measured frequently, but they were quite reproducible. Since the pyroelectric detector saw only a 1 mm by 1 mm cross section of the laser radiation and a typical $R_{1/e}$ was 3.4 mm, the beam intensity was nearly constant over the small area of the detector element. Thus by aligning the detector to the very center (most intense) section of the laser beam, I_{peak} became an excellent approximation of the actual intensity seen by the detector.

5. Light Chopper

A mechanical device was constructed to chop the laser radiation and to provide the intermittent input required by the pyroelectric detectors. The chopper was driven by a synchronous electric motor which operated at 30 revolutions per second. Two outside spur gears reduced the chopper speed to 10 Hz for the transmittance experiments. Unfortunately, the pulses produced by this speed occurred at an exact multiple of the 60 Hz electronic noise produced by the ac power line. In the detection of very weak signals the 60 Hz noise was significant and could not be completely removed by synchronous detection. Two new outside spur gears were purchased to convert the final chopping frequency to 13.2 Hz, which was used in all later experiments. A synchronous output signal was obtained from the chopper by means of a small light and a photocell placed behind the slit openings in the chopping wheel. In the Nova minicomputer experiments, a second photocell was used to monitor the revolutions of the chopping wheel.

6. Optical System

Mirrors and salt optics were used to direct the laser radiation after it left the laser cavity. In order to save space on the laboratory table, two mirrors were used to fold the laser beam into a new path antiparallel to the original direction. These mirrors and all others used in this work were coated with aluminum on their front surfaces. The mirrors were made in our laboratory by vacuum deposition of aluminum onto 3" by 2" microscope slides. All of the optical components which were required to be transparent to the laser radiation were made from either NaCl or KCl (salt optics). Since these materials are highly hygroscopic, nichrome wire heaters were installed under each salt component. In spite of the heater, fogging eventually occurred over a period of time, and the salt component had to be restored by repolishing in most cases. A NaCl wedge was used instead of a flat to minimize interference phenomena.

The optical alignment of an infrared laser beam is difficult for two reasons. One, the CO_2 laser radiation is not directly visible to the eye. The laser beam could be observed only when it burned or melted something. The second difficulty is that the intense power of the laser beam is dangerous when its destination is unknown. For these reasons a low power helium-neon laser was installed so that its visible beam could be made collinear with the CO_2 laser output. Thus the initial alignment of all the components of the experiments was made by means of the visible He-Ne

laser output. Fine adjustments in the alignment could then be safely made with the CO_2 laser.

Other aids to optical alignment were the use of optical benches and adjustable mounts for components. These aids increased the mechanical stability of the system and permitted reproducible positioning of the components. Each infrared detector was mounted on special mounts which traversed in both directions (x and y) perpendicular to the laser beam (z). The sample cell was mounted on a modified sextant, which permitted roll, pitch, and yaw adjustments.

The table which contained all of the optical components was suspended upon six partially inflated boat-trailer inner tubes in order to damp out vibrations. The vibrational stability of the system was further enhanced by weighting down the optical benches and the laser with lead weights.

D. TRANSMITTANCE EXPERIMENT

The purpose of these initial transmittance experiments was to check the overall design of the experimental procedure. Since previous workers[3,8-10] had described transmittance studies on a similar SF_6 system, a comparison of the results of the present work with literature values was possible. Also, these initial experiments suggested refinements in the theoretical treatment of optical saturation.

1. Experimental

A schematic diagram of the experimental configuration employed in these transmittance experiments is presented in Fig. 2. Detector I was the Laser Precision pyroelectric detector. It monitored the intensity of the laser radiation that was reflected from the front surface of the NaCl wedge. This reflected intensity was proportional to the intensity of the radiation transmitted by the wedge; therefore, the signal from detector I was also proportional to the intensity of the radiation incident upon the sample cell. Detector II was the one manufactured by Harshaw, and it monitored the radiation which was transmitted through the sample. The chopping wheel had four slits which produced 6.25 msec pulses when the wheel was operated at 10 Hz. Two opposite slits were covered with a sheet of polystyrene 0.125 mm thick. The polystyrene sheet transmitted only 36% of the incident 944.2 cm^{-1} radiation. Thus the resulting radiation output after the chopper was a pulse of 100% intensity followed by one 36% of the intensity of the original laser beam. It was expected that optical saturation of the SF_6 would cause the intensity ratio of the two pulses to differ from 0.36 after they had passed through the sample.

The output voltage from detector I was fed to a preamplifier and its output was analyzed by an absolute value determining circuit (AVDC). This circuit outputs the time-average of the absolute value of any voltage signal input. Since the output of detector I was a series of pulses each of which was proportional to the

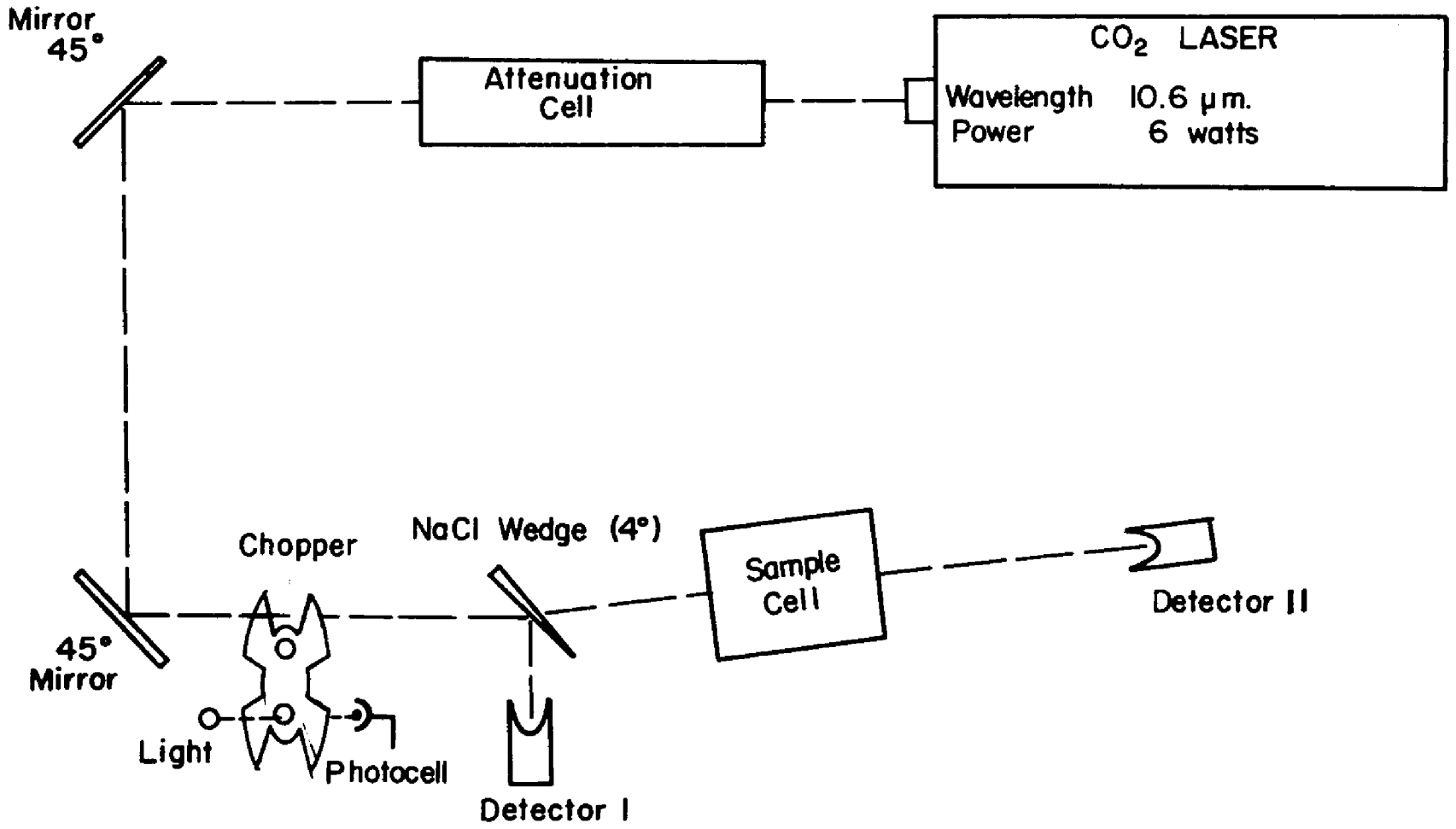

FIGURE 2. Experimental configuration used in the transmittance experiments.

incident power, the time-average of the magnitudes of these pulses produced a dc voltage proportional to the intensity of the radiation striking detector I. The AVDC was useful only so long as the voltage pulses from detector I were larger than the background electronic noise; in these experiments the pulses were appropriately large. The AVDC replaced a more expensive lock-in amplifier which is normally used to treat this type of voltage output.

The output of detector II was fed first to a preamplifier and then to a dual-channel lock-in amplifier. The lock-in provided dc output voltages proportional to the transmitted intensity of the 100% pulses and also of the 36% pulses. These dc outputs were fed to the R and T inputs of the dedicated analog computer described in Appendix 1. The AVDC output was fed to the analog input labeled I. With proper normalization, the analog computer then gave voltage outputs proportional to the transmittance of the 100% pulses (T_{100}) and to the transmittance of the 36% pulses (T_{36}). The analog computer was modified to permit taking the ratio of the radiances transmitted by the 36% pulses and the 100% pulses. The ratio (T_R) was independent of small fluctuations in the laser beam intensity and more importantly, independent of differences in detector characteristics since the same infrared detector was used to obtain both signals. The outputs representing T_{100} and T_R were fed to two channels of a Leeds and Northrup Speedomax M three-pen minirecorder. The voltage from the AVDC, which represented the incident intensity of the laser beam, was amplified by the analog computer and fed to the third channel of

the recorder. A schematic diagram and an explanation of the function and operation of the preamplifiers, the dual-channel lock-in amplifier, and the AVDC are given in Appendix 4.

The details of the exact procedure used to collect the transmittance data are also presented in Appendix 4. The general procedure involved tuning the laser to the 10.59-μm line, optimizing the alignment of the detectors to the beam center, and then zeroing and normalizing the outputs of the detectors. This zeroing and normalizing was accomplished for the evacuated sample cell with the adjustable gains of the preamplifiers and the zero offset adjustments available on the analog computer. The peak laser intensity (I_{peak}) was determined by the procedure which employed the radiometer and the measured beam profile. Since detector II was mounted on a motor driven traversing mount, the beam profile was conveniently obtained before each experimental run. The output of the AVDC was calibrated in W/cm^2 from I_{peak} and the simultaneous voltage of the AVDC. The attentuation cell was filled with a helium-ethylene mixture to attentuate the laser radiation by a factor of 1000. The sample cell was filled with the desired SF_6 pressure and sealed. Helium gas was added to the sample cell on occasions to observe the effects of a non-absorbing buffer gas upon optical saturation. The SF_6 gas used in this study was purchased from the Matheson Gas Products Co. which certified a purity of 99.99%. No further purification was performed. The temperature of the sample cell was 303 K. The data collection finally began when the gas mixture in the attentuation cell was slowly

pumped out to produce a gradual increase in the intensity of the laser radiation striking the sample cell. The large intensity range which covered three orders of magnitude was made possible by using attentuation filters (KBr disks containing SiO_2) in front of the detectors and changing the gain of the preamplifiers. In the 1-100 attentuation range the gains of the preamplifiers were reduced by 10 by means of a switch which exchanged two precision resistors that were used in the preamplifiers. In the 1-10 attentuation range the KBr disks were placed immediately in front of the detectors. A typical recorder output for a transmittance experiment is presented in Fig. 3.

2. Discussion of Results

To compare the results of these transmittance experiments with those predicted by the theory and with the results of other workers, sufficient data points were extracted from the recorder output to convert the data to a plot of T_{100} and T_R vs the logarithm of I_{peak}. The fact,that the average transmittance of the evacuated cell was 0.871, had to be considered when the results were compared with the theoretical predictions. Several of these plots of T_{100} vs $\log(I_{peak})$ are presented in Chapter V where they are compared with the theoretical predictions.

The results of the T_{100} data agreed reasonably well with the previous studies of Brunet[3] and Burak, Steinfeld and Sutton.[8] The shapes of the plots of T_{100} vs $\log(I_{peak})$ obtained in this work were the same as those in the literature,but exact values of

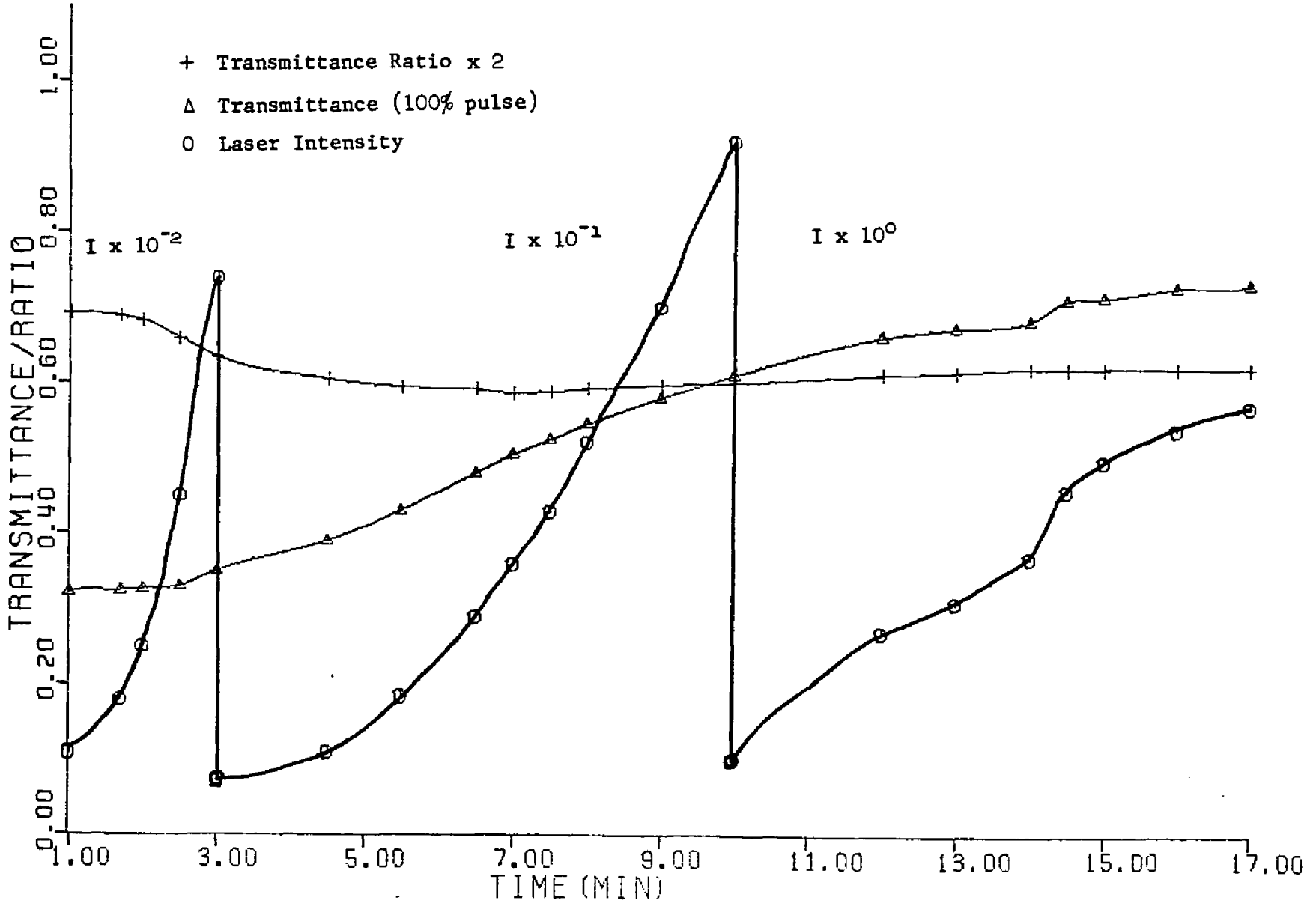

FIGURE 3. Typical recorder output for a transmittance experiment.

the transmittance differed by as much as 15% at high laser intensities. One criterion for the comparison of experimental data is the small signal absorption coefficient (β_o) which is obtained when the intensity of the laser radiation is too weak to produce saturation. A value of $0.46 \pm .02$ cm^{-1} was found for β_o in this work. This value was in good agreement with the 0.46 cm^{-1} reported by Brunet and Burak et al., Armstrong and Gaddy[9] reported a value of 0.47 cm^{-1} for β_o, while Wood[10] et al. reported a smaller value of 0.40 cm^{-1}. Another criterionfor the comparision of experimental data is the saturation intensity (I_s) which was used by Brunet to be an empirical parameter in his theoretical treatment of optical saturation. Roughly, I_s may be defined to be the intensity of the laser radiation which produces sufficient saturation of the absorption to decrease the effective absorption coefficient to $\beta_o/2$. Brunet reported that an I_s of 6 ± 2 $W/cm^2 \cdot Torr$ was consistent with his experimental data and also that of Burak[8] et al. Wood[10] et al. reported a value of 2.6 $W/cm^2 \cdot$ Torr for an I_s which was consistent with their experimental data. Although the theoretical treatment of Brunet was not employed in this work, a value of I_s was obtained in order to compare it with the literature values. The value of I_s determined from the results of these transmittance experiments was 5.5 ± 2 $W/cm^2 \cdot Torr$. Thus both I_s and β_o were in good agreement with the literature values reported by Brunet and Burak et al. The addition of helium as a buffer gas significantly decreased the observed effects of optical saturation, and this agreed with the results reported in previous

studies.[8] A more detailed comparison with the results of others would not be meaningful because of the variations in experimental conditions.

Three experimental improvements enhanced the accuracy of these transmittance experiments over that of previous experiments. First, in this work I_{peak} was determined by means of an accurate beam profile and the average beam intensity over an area of 1 cm^2. In two of the previous works[8,10] the beam diameter was determined by measuring the size of a spot burned by the laser beam. The procedure used to determine the diameter of the laser beam was not given by Brunet. Second, this work was the only one which employed a frequency stabilized laser. Two groups[3,10] used lasers from which the output laser line was selected by using a grating as the rear reflector of the laser. Selecting the output frequency of the laser with a grating alone does not permit fine tuning over the particular laser transition. Thus small changes in the cavity length will cause a small frequency drift within the 40 MHz bandwidth of the CO_2 transition. More importantly, operation at different frequencies within the particular CO_2 transition will cause significant variation in the gain and thus the intensity of the laser output. A third group[8] used a CO_2 laser which simultaneously produced laser action at several lines (P(18)-P(24)) in the vicinity of the desired P(20) line at 10.59-μm. Since there are variations in the absorptance of SF_6 for these different laser lines, the results obtained by means of the use of the average of the effects produced by several lines would not necessarily be the same

as those from the use of the P(20) line alone. And third, this work was also the only one which used a power-stabilized laser.

The T_R data clearly indicated the presence of optical saturation because this ratio would have been independent of varying laser intensity had there been no saturation affects. At low laser intensities neither pulse produced saturation and therefore, $T_R = 0.36$. At slightly greater laser intensities, the 100% pulses had sufficient power to partially saturate the SF_6 absorption but the 36% pulses did not; thus T_R began to decrease. On increasing the laser intensity still further, a point was reached at which the 100% pulses were almost producing complete saturation and the 36% pulses were beginning to produce partial saturation. At this time T_R had passed through a minimum and had begun to increase. If a sufficiently high laser intensity could be acheived, T_R would return to a value of 0.36. Unfortunately, no quantitative use for these T_R data has yet been found.

The major experimental problem encountered in this study was maintaining an accurate zero setting at the recorder when the laser radiation was blocked. One reason for this problem was the 10 Hz chopper speed which permitted 60 Hz noise to be picked up by the lock-in amplifier. Another reason was that the zero offset adjustments had to be reset when the preamplifier gains were switched during the course of an experiment. It was also difficult to maintain the initial calibrations when the offset adjustments were changed. The efficiencies of the two pyroelectric detectors and the

gains of the two preamplifiers were surprisingly well matched over the intensity ranges used in the experiments.

A second experimental problem was the alignment of the sample cell with respect to the laser beam. When the cell windows were exactly normal to the beam, the radiation reflected from the windows reversed its original path. This feedback of laser radiation into the plasma tube created tremendous oscillations in the impedance of the laser plasma tube. These oscillations occurred even when the intensity of the reflected radiation was only a few per cent of the initial laser output. Since the laser frequency stabilizing system must monitor the impedance of the laser plasma tube, these large oscillations severely taxed the frequency stabilizing system and reduced the frequency stability of the laser. To prevent these effects the sample cell was misaligned from the normal to the laser beam just enough to prevent the radiation feedback to the laser tube.

An attempt to conduct reflectance experiments with this procedure was made by placing detector II opposite detector I. In this position the radiation reflected from the sample struck the NaCl wedge and was reflected into detector II. This effort was discontinued after two discoveries. The first was that the high electronic gain required to produce a sufficient signal also produced too much noise when the laser radiation was attentuated by a factor of 100. The high noise level existed even after the chopper was converted to a 13.2 Hz frequency that significantly aided in eliminating 60 Hz noise which synchronous detection. The second

discovery was the great temperature dependence of the interference effects between the two end windows of the sample cell which were now aligned exactly perpendicular to the laser beam. Heating the cell by 1.5 K caused its length to change by 5.3-μm ($\lambda/2$). During this heating period, the reflectance went from 0.24 to 0.04 and back to 0.24. As a check these data were used to calculate the thermal expansion coefficient of the sample cell. The result (3.5×10^{-5} K^{-1}) fortunately agrees with the literature value for stainless steel. The difficulty of maintaining the sample cell at a sufficiently constant temperature and alignment to reproduce the interference effects eventually led to the decision to vary the cell length thermally during an experiment so that the optical properties would be averaged over several interference cycles (multiples of $\lambda/2$). This averaging eliminated interference effects.

E. SIMULTANEOUS MEASUREMENT OF REFLECTANCE AND TRANSMITTANCE BY USE OF THE NOVA MINICOMPUTER

1. Introduction

As previously mentioned, the purpose of this experiment was to obtain data which could provide a quantitative test of the theory presented in Chapter II. The transmittance experiments were successful and informative, but much of the information obtained had been presented previously by other authors. The major challenge of this work was the experimental measurement of the reflectance of the sample system. The effects of partial optical saturation upon the radiation reflected from a sample system had

not been reported by previous workers. As shown in Chapter II, the theoretical treatment of the reflected radiation was much more complex than the treatment of the transmitted radiation. The same increased complexity was also true for the experimental measurements of the reflectance. The principle source of this increased complexity was the interference phenomena which occurred when the sample cell was aligned exactly perpendicular to the laser radiation. (These same interference phenomena also affected the transmitted radiation, but relatively to a much lesser extent.)

Every time there is a change in the refractive index of the medium through which a light wave travels, there will be a reflected wave. The more abrupt is the refraction change, the greater will be the amplitude of the reflected wave. For this reason, the amplitude of waves reflected from the four surfaces of the two cell windows were larger than those originating from the smooth gradient in the refractive index of the sample produced by partial saturation of the absorption coefficient of SF_6. All the reflected waves interfered with one another by amounts which were determined by their phases and amplitudes. The amplitudes of the rays reflected by the surfaces of the exit window and the sample itself were affected by the absorption of the wave by unsaturated SF_6 molecules. The phases were affected by the spacing of all of the reflecting surfaces, measured in multiples of the wavelength (λ) of the light wave. The resultant amplitude (r) of all the individual reflected waves may be computed by means of Eq. (2) -- the intensity of the reflected radiation is proportional to r^2.

$$r = \sum_{i}^{n} A_i \sin(\omega t - \phi_i) \qquad (2)$$

n = total interfaces
A_i = amplitude of wave reflected from interface i
ϕ_i = phase angle of wave i
ω = angular frequency
t = time

It is normal to treat the refractive index as a complex number in which the real part is the ordinary refractive index (which determines the velocity of the wave) and the imaginary part is proportional to the absorption coefficient (which determines the damping of the amplitude of the wave in the medium). Because these two parts of the refractive index are connected (by the Kramers-Kronig equations), optical saturation changes the magnitudes of both parts. The magnitude of the changes of refractive indices at gradients and boundaries within the cell are therefore affected by the saturation process as are the amounts by which the waves are attentuated. Further, the relative phases responsible for the interference effects are also affected by the saturation process. A complete theoretical treatment of these interrelated properties can be quite complex.

To design an experiment in which the cell length, gas pressure, temperature, etc. could be controlled to the extent that these interference effects would be reproducible would be very difficult. To compare experimental results with the theory, however, such rigid experimental control would be necessary and the magnitude of these experimental parameters (cell length, gas pressure, etc.) would have to be known <u>exactly</u> in order to theoretically reproduce

the experimental interference effects. Fortunately, the need for this rigid control of the sample system can be eliminated by varying the cell length over a few interference cycles. The average optical properties of the sample system determined under such conditions are free of the influence of interference effects. This path length averaging can also be done in the theoretical treatment. Thus an accurate comparison between the theory and the experimental results is made possible by this technique. Because the thermal expansion of the salt windows was small, the optical path between the two surfaces of each window did not change when the cell length was changed by heating. Therefore interference effects between these two pairs of surfaces would not be averaged out. These effects had to be measured.

The large thermal expansion coefficient of stainless steel provided a convenient method to scan the cell length over a small range and thus became an asset to the experimental procedure instead of a liability. The scan distance had to be some exact multiple of $\frac{1}{2}$ the wavelength of the laser radiation (λ) to obtain an accurate average of the interference effects. The amount of heating necessary to produce two successive interference maximums was assumed to change the cell length by $\lambda/2$. Thus the proper scan distance was easy to determine.

Scanning the cell length during an experiment, however, required a very different type of data collection system than that described in the previous section. At each temperature (and therefore at each value of the cell length) data were collected

at several different incident intensities. The data had to be collected rapidly and stored (until time was available for analysis) before the temperature could change appreciably. Since a Nova 1200 minicomputer with a 12-bit analog to digital converter was available, an experiment was designed to utilize its data collection and storage capabilities. It was also desirable to design the experiment to simultaneously measure both the transmittance and reflectance of the sample system.

2. Experimental

The technique employed to vary the intensity of the laser beam striking the sample in this experiment was very different from that described in section D. A chopping wheel with eight slits was constructed. Seven of these slits were covered with polystyrene sheets ranging from one sheet to seven sheets on the final slit opening. By replacing the chopper used in previous experiments with this new wheel, a series of eight laser pulses could be obtained. The intensity of each successive pulse was half of that of the previous pulse when sheets of 0.76 mm thickness were used. This attentuation technique allowed eight logarithmically-varying laser beam intensities to strike the sample cell during one revolution of the chopping wheel. An example of the pyroelectric detector's response to the transmitted pulse trains for several SF_6 filling pressures is presented in Fig. 4.

If the intensity of the laser output remained constant, each of the eight pulses would also maintain a constant reproducible

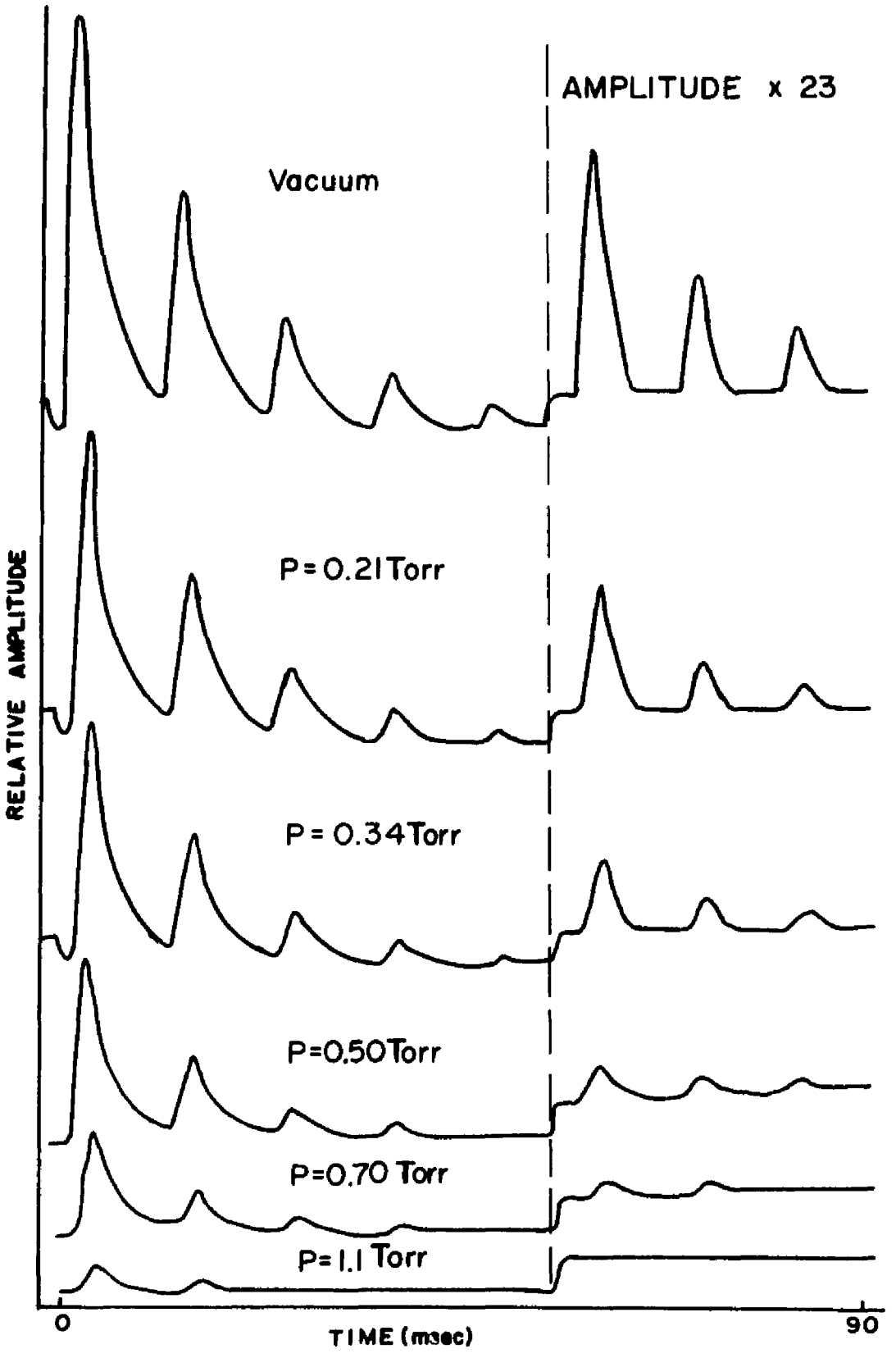

FIGURE 4. Typical signal waveform generated by the transmitted pulses.

intensity. As stated earlier the Sylvania model 948 CO_2 laser used in this work was especially designed for power stability, and a drift rate of less than 5%/hour was observed when the frequency stabilizing system was used. This good stability of the laser intensity made it possible to perform a normalization run with the sample cell evacuated. Then subsequent data runs could be normalized with respect to the evacuated cell. The normalization data could be stored in the computer memory and recalled when necessary. The need for a detector to monitor the incident intensity was eliminated since the incident intensities were constant. This extra detector could then be used to monitor the reflected radiation. The Cintra radiometer head was positioned to monitor a portion of the incident radiation so that any changes in the average laser intensity could be detected. A schematic diagram of the experimental configuration is presented in Fig. 5.

The "pinhole" shown in Fig. 5 was actually an adjustable iris diaphragm and was essential to accurate alignment of the reflected beam. The laser beam first was carefully aligned to strike the center of the pinhole. If the windows of the sample cell were exactly perpendicular to the laser beam, the radiation reflected from these windows would also strike the center of the pinhole but from the opposite direction of the laser beam. With the adjustable iris closed to a 2 mm diameter, the sample cell was positioned until a maximum reflected intensity was received by detector I. Detector I was then displaced slightly and sample cell realigned to maximize the output of detector I. These small

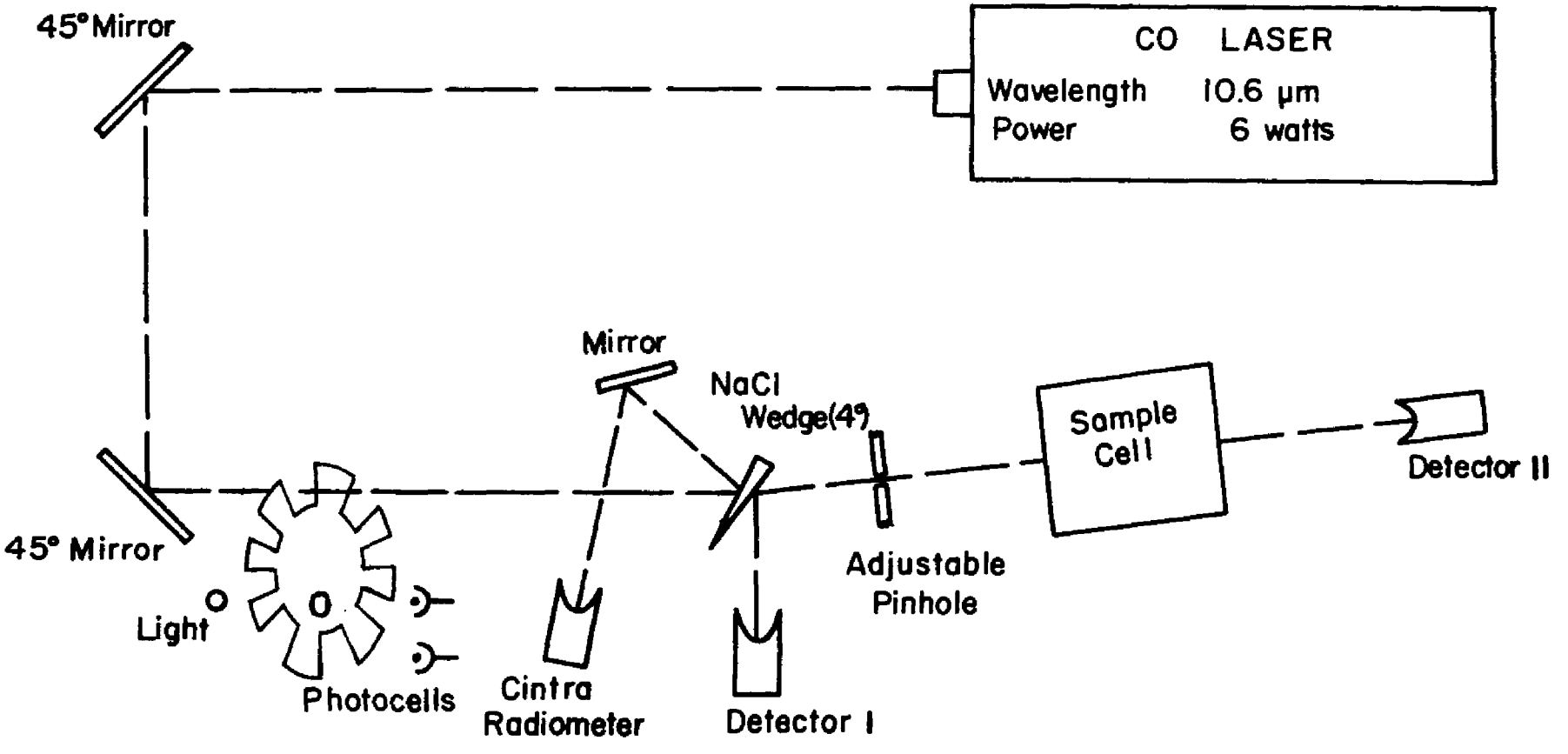

FIGURE 5. Experimental configuration used in simultaneous measurements of reflectance and transmittance.

alignment changes were systematically performed until a position of detector I and the sample cell produced a maximum output from detector I. This final position insured that the windows of the sample cell were perpendicular to the laser beam. The iris was then opened to its maximum position for the experimental runs.

The Data General Nova 1200 Minicomputer was equipped with 8K (16 bit words) of memory, a 12 bit analog to digital converter (resolution 2.5 mV), a 10 bit digital to analog converter, a Tektronix Model 611 storage oscilloscope, and a teletype machine which could read or punch perforated paper tape. An eight channel multiplexer enabled the analog to digital (A/D) converter to be switched from one to the other of eight different input channels. The A/D converter required 30 μsec to complete the conversion of an analog voltage signal. This fast response coupled with the fast execution time of the computer enabled a large amount of input data to be taken by the computer in a short time. Thus it was possible to spin the 8-slit chopping wheel at 13.2 Hz, to measure eight reflected signals and eight transmitted signals during each revolution, and concurrently to store the magnitudes of these measurements in the computer memory. On subsequent revolutions the new values measured were added to the previous measurements, and these sums were stored in the memory. In a few minutes these sums which symbolized the averages of the sixteen signals represented thousands of individual measurements, and the signal to noise ratio was greatly reduced thereby. Before the transmitted and reflected pulse trains could be monitored by the A/D converter, however, the voltages had

to be within a 0-10 volt range. Also, the computer program which controlled the A/D converter had to be synchronized with the two pulse trains in order to take measurements at the proper times.

A signal processor was used to prepare both the reflected and transmitted signals for the A/D converter. The outputs of the pyroelectric detectors receiving the pulsed radiation were amplified and passed through the signal processor. The signal processor further amplified the smaller pulses, and more importantly it automatically added the proper offset voltage to the signal so that the voltage corresponding to the baseline of each pulse train was slightly positive. This offset was necessary to insure that only positive voltages reached the A/D converter. Figures 6a and 6b show a typical pulse train reaching the signal processor and the resulting changes produced by the processor. Appendix 5 presents a schematic diagram of the electronics and an explanation of the signal processor.

Synchronization between the computer program and the pulse trains was provided by the chopper which was modified to output two synchronous signals. One was synchronous with the slit openings and other was synchronous with the revolutions of the chopper wheel. Before they were passed to the A/D converter, these two signals were processed in a pulse shaping and delay network (also described in Appendix 5) to provide the synchronous pulse outputs shown in Figs. 6c and 6d. The syn. I pulses were 0.7 msec in width and time delayed so that each corresponded to the time when the laser beam was passing through the center of

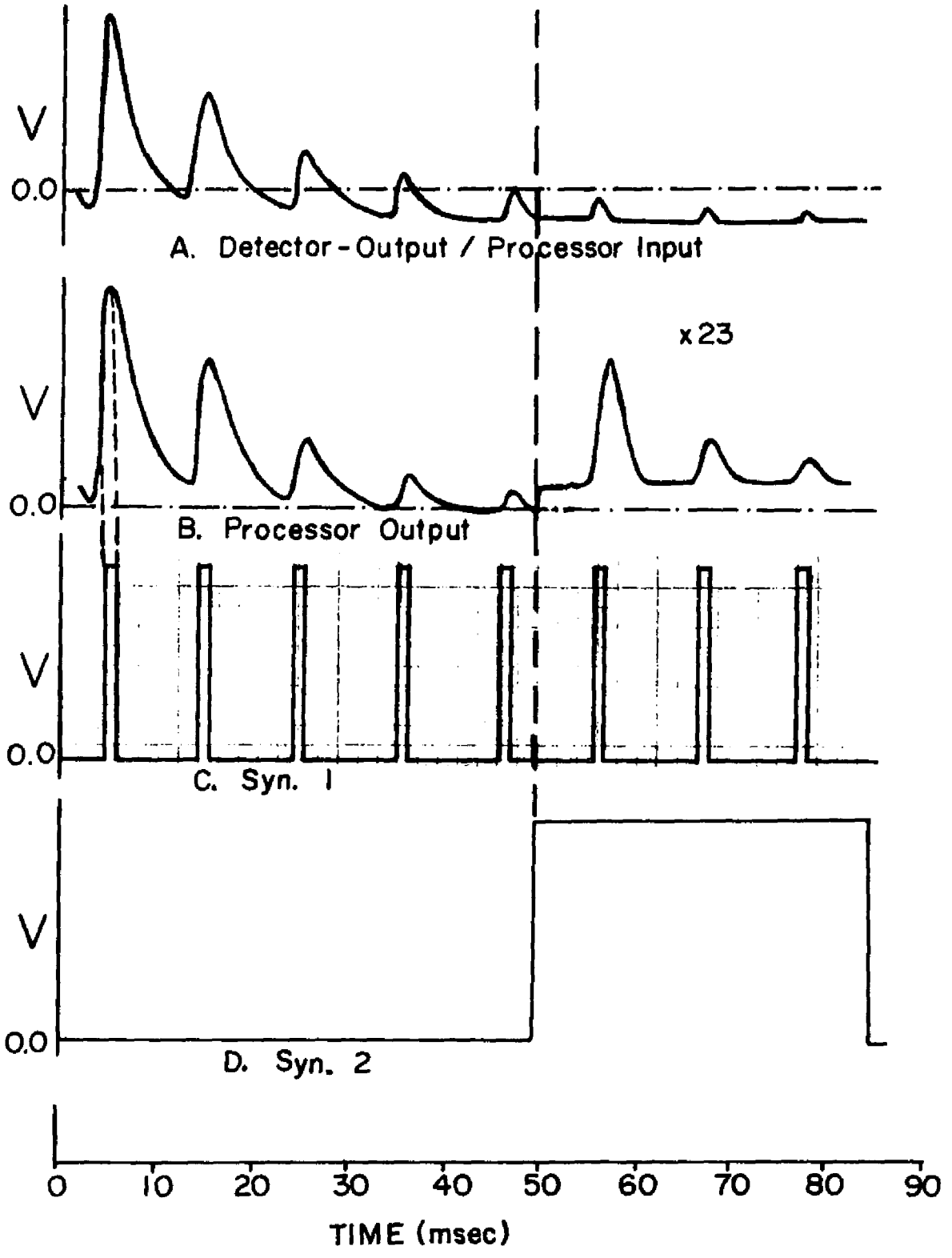

FIGURE 6. A,B. Voltage offset and small signal amplification by the signal processor. B,C,D. Time relationship among inputs to A/D converter.

the 1.8 msec slit opening. The end of the syn. II pulse indicated the beginning of one revolution of the chopping wheel. The syn. II pulses were also fed to the signal processor to trigger a gain increase for the small pulses throughout its duration.

The minicomputer was then programed to collect the data consisting of binary numbers, the magnitudes of which were proportional to the intensities of the reflected and transmitted radiation. It utilized the synchronization signals and the processed analog voltage outputs of the two pyroelectric detectors. The data collecting portion of the program first monitored the syn. II channel and waited until that pulse exhibited a negative slope. This signified the beginning of the pulse train with the 100% pulse coming first and the seven following pulses decreasing in intensity. The program next monitored the syn. I channel and waited until that signal exhibited a positive slope. As soon as the slope became positive the program instructed the A/D converter to read the current analog voltage occurring in the transmitted pulse train and convert it to a digital number. The same procedure was performed on the reflected pulse train. These digital numbers were stored temporarily as the baseline of the respective signals. The program again monitored the syn. I channel until that signal exhibited a negative slope. At this time the program again initiated the digital conversion of the voltages presently occurring in the transmitted and reflected pulse trains. These latter numbers corresponded closely to the peak values of their respective signals. Subtracting the baseline

numbers from the peak numbers gave digital numbers proportional to the intensity of the reflected and transmitted radiation for that particular pulse. These resulting numbers were stored for averaging with numbers from subsequent pulses passing through the "100% slot". The program again monitored the syn. I channel until a positive slope was detected and baseline numbers were obtained for the second pulse. As for the first pulse, peak numbers were obtained and the differences between peak and baseline numbers stored in the memory location reserved for data from radiation passing through the second slot. This procedure was repeated until pulses through all eight slots were handled. After the eight pulses were serviced, the program returned to monitor the syn II channel and seek a negative slope as before. In the second revolution the digital representations of the reflected and transmitted radiation intensities were added to those determined on the first revolution of the chopper wheel. This summing of the digital representations could be continued for as many revolutions as desired; 128 was commonly used in this work.

When the desired number of revolutions was reached, the accumulated sums were each divided by the number of revolutions and the sixteen resultants were stored in the computer memory. A second 128 revolutions produced sixteen other stored resultants, and, also, a current average over both resultants was taken. Thus, in a few minutes many resultants or data clusters were taken for each transmitted and reflected pulse. The current average of the data clusters for each pulse was updated as each data point

was taken. Six of these sixteen current averages were continuously outputed to the storage oscilloscope via the D/A converter as the experiment proceeded. Thus the progress of the experiment could be followed visually as these averages converged to their final values. The data clusters representing the reflected and transmitted radiation from the 100% pulses were also outputed to the oscilloscope concurrently with their measurement. In the actual experiment up to 50 data clusters (6400 points) could be taken for each of the sixteen measured pulses. At the end of the experiment the average of each of the sixteen sets of data clusters was printed by the teletype machine, and the operator had the option of having the individual data clusters printed also. A copy of the Nova computer programs and an explanation of their usages are presented in Appendix 6.

The Nova programs permitted the selection of several other options concerning the experiment to be conducted. The first option permitted the operator to select either a "calibration" run or a "data" run. In a calibration run, the data that were received were stored to be used for the normalization of subsequent data runs. This procedure produced reflectances and transmittances as outputs for the data runs. A second calibration option was available at the end of a data run. This option permitted a fine adjustment of the original calibration when a nonsaturable absorber was placed in front of the detectors. Other program options concerned the number of data points per data cluster, the maximum number of data clusters to be taken, and the use of the storage oscilloscope.

Two calibration runs were made at the beginning of each series of experiments. As long as the laser output power remained constant and the optical alignment was not changed, a new calibration was not required. Both runs were made with the sample cell evacuated. In the first run the calibration option was selected, and then the cell length was scanned over three interference cycles (multiplies of $\lambda/2$)--the cell length was changed by 2 or 3 half wavelengths during all runs. The number of cycles achieved at any given time could be seen visually on the screen of the storage oscilliscope. Each data cluster represented optical properties at a particular cell length. The final averages obtained represented the average intensity of the radiation transmitted by the evacuated cell and the average of the radiation reflected from the cell windows alone for each of the eight laser pulses. These two sets of averages [$T_{nc}(1\text{-}8)$ and $R_{nc}(1\text{-}8)$] were used as normalization constants for the data runs. In a previous experiment the average transmittance of the evacuated cell was found to be 0.871, and the average reflectance 0.128. If a subsequent data run measured the average intensity of the reflected radiation for the 4th pulse to be $\frac{1}{2} R_{nc}(4)$, the reflectance would be 0.064.

The second calibration run was made to minimize a slight nonlinearity in the detection system for the very weak pulses (6-8). Any normalization procedure will be most accurate when the magnitude of the reference is similar to that of the property being normalized. Hence a 0.25 attentuator was placed in front of

the transmittance detector (II) and a 0.5 attentuator was placed in front of the reflectance detector (I). After making a data run, the average transmittance (T_{avg}) and reflectances (R_{avg}) were obtained. At this point the second calibration option was selected, and the program executed the fine adjustments to T_{nc} (1-8) and R_{nc}(1-8).

The programming for this second calibration option assumed that all eight R_{avg}'s and all eight T_{avg}'s should have been the same since the attentuators did not saturate. In practice they were all nearly the same, but the last three of each set were frequently too high. These deviations were caused by a nonlinear response of either the detectors or the electronics for very small intensities or voltages as appropriate. The R_{avg}'s and T_{avg}'s for pulses 2-5 were consistently in agreement, so the averages of these two sets of four were assumed to be correct. The values of T_{nc}(1-8) and R_{nc}(1-8) which were used to normalize this second run were then changed so that all of the computed R_{avg}'s and T_{avg}'s would match the respective averages of the 2-5 pulses. This procedure effectively determined the transmittance normalizing constants when the transmittance was 0.25 and the reflectance normalizing constants when the reflectance was 0.5 that of the evacuated cell.

After the calibration runs were completed, the sample cell was filled with the desired gas pressure of SF_6 or SF_6-He mixture, and a data run was performed. The SF_6 gas was from the same container as the gas used in the "transmittance only" experiments.

The temperature of the sample cell was increased from 314 to 318.5 K. The computer program automatically normalized the magnitudes of all of the various averaged effects with $T_{nc}(1\text{-}8)$ and $R_{nc}(1\text{-}8)$ so that the outputs to the teletype and storage oscilliscope were given as transmittances and reflectances. Figure 7 is an example of the teletype output. Figure 8 is a plot of the changes in cell length vs the reflectance data clusters (each point on the plot represents the average of 128 measurements) which were printed after the data dump request.

3. Discussion of Experimental Results

The reflectance and transmittance averages obtained from these experiments exhibited an expected increase in magnitude with increasing intensity of the laser radiation. The transmittance data were in good agreement with the data obtained in the transmittance experiments of this work; however, the Nova experiments indicated a slightly greater degree of saturation. As in Section D a value of the small-signal absorption coefficient (β_o) and the saturation intensity (I_s) were obtained for the comparison with previous work. The same value was determined for β_o as in the transmittance experiments of this work, but a smaller value (5.1 ± 1 W/cm^2·Torr) was obtained for I_s. A possible explanation for this increased saturation at lower intensities is the contribution to the optical saturation by the radiation from the rear cell window. In the"transmittance only" experiments of this work the sample cell was not aligned exactly perpendicular to the

```
   DATE(1)= 4.30 1975
RUN TYPE(2)= 2 (CALIBRATION=1,DATA=2)
   RUN NUMBER(3)= 3
PSF6(4)= .30 TORR   PHE(5)= 0 TORR
LASER POWER(6)= 10.3 WATTS/SQCM
BEAM DIAMETER AT HALF HEIGHT(7)= .64 CM
TRAN. FACTOR(8)= .871  REF. FACTOR(9)= .128
WILL SCOPE BE USED(10)? 0 (YES=0,NO=1)
WILL TELETYPE BE USED CONCURRENTLY(11)? 1
MAX # POINTS(12)= 50   READINGS PER POINT(13)= 128
(MUST BE 2↑I)

ARE CURRENT  INPUTS CORRECT? YES-COLLECT DATA(1)
NO(2),  PRINT CURRENT PARAMETERS(3)
?1
                DATA ACQUISITION COMPLETE
      EACH AVERARE BASED ON 5888 MEASUREMENTS

AVERAGES FOR POWER 0 ARE R= 5.81901E-2     T= .633346
AVERAGES FOR POWER 1 ARE R= 5.21135E-2     T= .592266
AVERAGES FOR POWER 2 ARE R= 4.73431E-2     T= .529422
AVERAGES FOR POWER 3 ARE R= 4.42429E-2     T= .492218
AVERAGES FOR POWER 4 ARE R= 3.94716E-2     T= .390399
AVERAGES FOR POWER 5 ARE R= 3.83242E-2     T= .341374
AVERAGES FOR POWER 6 ARE R= 3.35466E-2     T= .299823
AVERAGES FOR POWER 7 ARE R= 3.54433E-2     T= .280221


IS DATA DUMP DESIRED (YES=0,N=1),CALIBRATION(5)
? 0
```

FIGURE 7. Typical teletype output for Nova experiment.

laser beam as it was in these Nova experiments. Thus the reflected radiation was not collinear with the transmitted radiation in the transmittance experiments and, therefore, made a smaller contribution to the saturation process. Several plots of the reflectance and transmittance vs the logarithm of the peak laser intensity for various pressures of SF_6 and SF_6-He mixtures are presented in Chapter V. These plots are compared with the theory of optical saturation in that chapter.

The changes in the optical properties due to interference that occurred as the length of the sample cell was varied produced modulations of equal amplitude in the reflectances (see Fig. 8) and transmittances. The modulations in the transmittances were 180° out of phase with respect to those in the reflectances. The relative phases of these modulations for the different laser intensities were progressively shifted on going from the lowest intensity to the highest. Since all of the experimental parameters were identical for each of the laser intensities, this interesting phase effect must have been produced by various degrees of saturation of the sample. These variations in saturation produced changes in the absorption coefficient and alsi in the real part of refractive index (n) of the sample (n is related to the absorption coefficient). The wavelength (λ) of an em wave in any medium is given by the ratio of the wavelength in vaccum to n. Thus variations in n would change λ and cause the length of the sample cell to be a different multiple of $\lambda/2$. When the distance (z) between two parallel optical interfaces which are normal to the em wave is

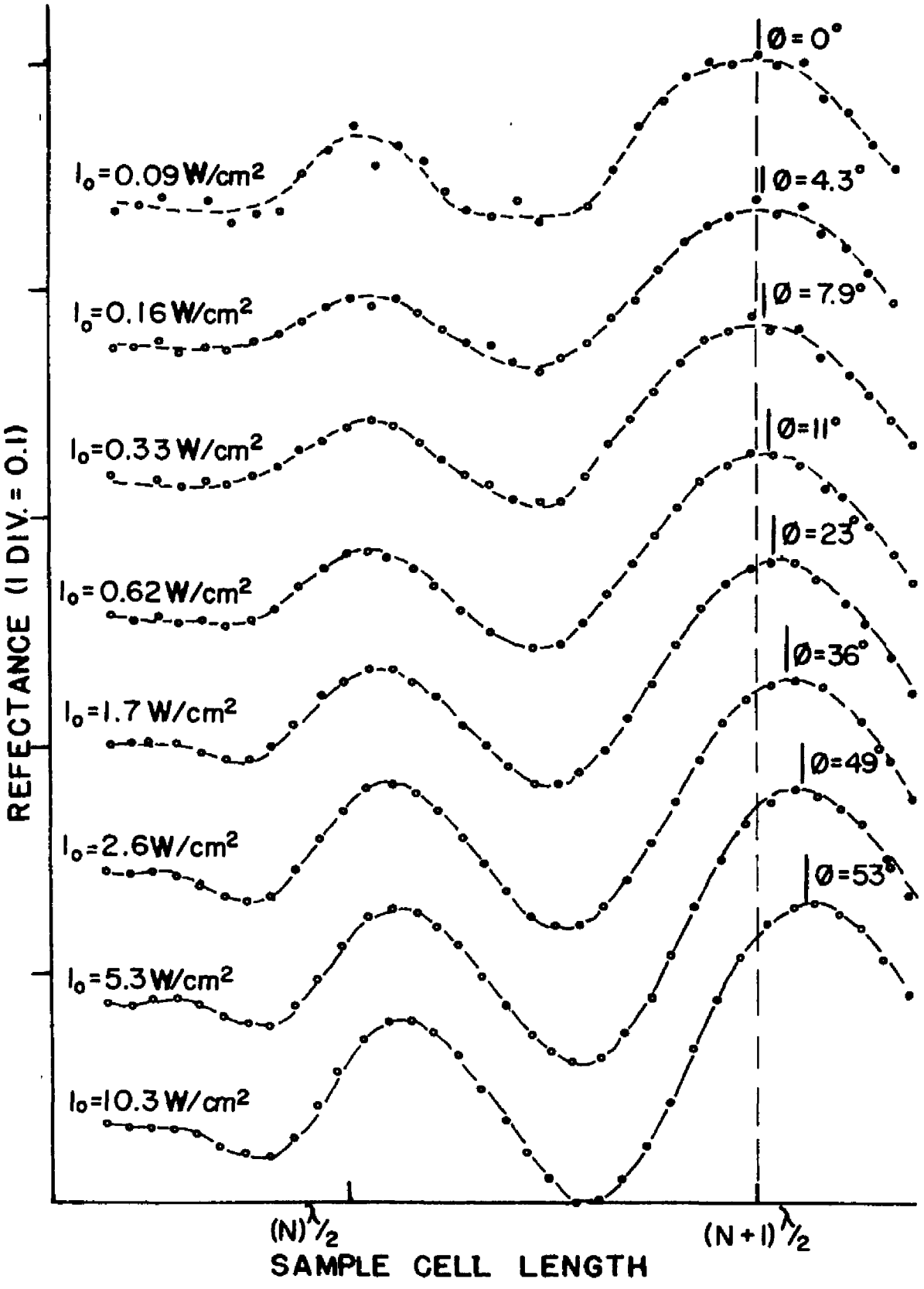

FIGURE 8. Phase relationship among reflected pulses.

$N\cdot(\lambda/2)$ (where N is a very large integer), the total amplitude of the two reflected waves is a maximum. When this distance is reduced to $(N - \frac{1}{2})\cdot(\lambda/2)$, this total is a minimum. Because N is large only a very small change in n and λ is required to change N by $\frac{1}{2}$.

It was possible to calculate a simple relationship between the magnitude of a relative phase difference and a change in the effective absorption coefficient. In Eq. (14) of Chapter II the propagation vector (Γ) for an em wave at normal incidence to a sample was given by

$$\Gamma = \omega(\hat{\mu}\hat{\epsilon})^{\frac{1}{2}} = \hat{n}(\mu_o\epsilon_o)^{\frac{1}{2}}, \tag{3}$$

where $\hat{\epsilon}$ and $\hat{\mu}$ are the complex permittivity and perameability, respectively. The symbol $\hat{n}$ represents the complex refractive index. If the cell length is z, the wave reflected from the rear of the sample cell must have traveled $2z$ before it returned to the front of the sample. Thus the difference in the phase (ϕ) of the weakest pulse (w) and that of any of the other seven pulses was

$$\phi_w - \phi_i = \int_o^{2z} \Gamma_w du - \int_o^{2z} \Gamma_i du , \tag{4}$$

where

$$\Delta\phi = \phi_w - \phi_i \simeq 2z(\bar{\Gamma}_w - \bar{\Gamma}_i) . \tag{5}$$

The bar indicates the average of the property over the optical path. Although $\bar{\Gamma}$ is complex only the real part can produce a phase

change - the imaginary part can only produce attenuation of the amplitude of the em wave. By use of Eq. (21) of Chapter II the real part of $\bar{\Gamma}$ may be computed in terms of the electric susceptibility by

$$\mathrm{Re}(\bar{\Gamma}) = \omega(\epsilon_o\mu_o)^{\frac{1}{2}}(1 + \eta')^{\frac{1}{2}}\left[1 + \tfrac{1}{8}\left(\frac{\eta''}{1 + \eta'}\right)^2\right] . \tag{6}$$

Since η''^2 is of the order of $\lambda^2\beta^2$, can be neglected in comparison to one. Thus only η' remains to be defined in measurable experimental quantities. From Eq. (27) of Chapter II the ratio of η' and η'' can be obtained and η'' was defined by Eq. (22) of that chapter. Then

$$\eta' = \delta T_2\eta'' = \frac{\delta T_2 c_o\beta(1 + \eta')^{\frac{1}{2}}}{\omega} \tag{7}$$

and

$$\eta' \simeq \frac{\delta T_2 c_o\beta}{\omega} , \quad \text{where } \eta' \ll 1 \tag{8}$$

The quantity $1/T_2$ is the half-width at half-height of the homogenous linewidth of the electric-dipole transition and δ is defined as the frequency difference between the resonance frequency of the transition and the frequency of the em wave. Further,

$$(1 + \eta')^{\frac{1}{2}} \simeq 1 + \eta'/2 \tag{9}$$

Then $\Delta\phi$ may be approximated by

$$\Delta\phi = 2z\omega(\mu_o\epsilon_o)^{\frac{1}{2}}\left[\frac{\delta T_2 c_o \beta_w}{2\omega} - \frac{\delta T_2 c_o \beta_i}{2\omega}\right], \tag{10}$$

which simplifies to

$$\Delta\phi = z\delta T_2(\beta_w - \beta_i), \tag{11}$$

where

$$c_o = (\mu_o\epsilon_o)^{-\frac{1}{2}} . \tag{12}$$

Equation (11) suggests a method to experimentally determine the frequency difference between the laser radiation and the center of the electric-dipole transition of a saturable absorber. The linear relationship which was predicted for $(\beta_w - \beta_i)$ and $\Delta\phi/z$ was confirmed by the experimental data. The effective absorption coefficients were calculated from the transmittances observed for each of the eight laser pulses. These calculations were accomplished by means of Eq. (13), a form of Beer's law.

$$\beta_i = \frac{\log_{10}(0.871/T_i)}{z} \tag{13}$$

T_i = transmittance of i_{th} pulse

0.871 = average transmittance of empty cell

The values of $(\beta_w - \beta_i)$ were computed for the seven more intense laser pulses and compared to the values of $\Delta\phi/z$ for the corresponding pulses. A comparison is presented in Table 2 for data taken with an SF_6 pressure of 0.30 Torr.

TABLE 2

COMPARISON OF $(\beta_w - \beta_i)$ AND ϕ/z FOR A SF_6 PRESSURE OF 0.30 TORR

LASER INTENSITY (w/cm^2)	$\Delta\phi^\circ$ ($\pm 5^\circ$)	$\Delta\phi$(rad.)/z	$\beta_w - \beta_i$
0.09	0	0.0	0.0
0.16	4	0.007	0.0068
0.33	8	0.014	0.0197
0.61	11	0.019	0.0332
1.70	23	0.040	0.0564
2.56	36	0.063	0.0636
5.25	49	0.085	0.0750
10.33	53	0.092	0.0813

The error range for ϕ was large ($\pm 5^\circ$) because there was a 21° interval between the data clusters that made interpolations necessary. This error range could be easily reduced by varying the cell length at a slower rate or by using a longer cell to increase the magnitude of ϕ and reduce the relative error range.

The magnitude of δT_2 was determined by the slope of $(\beta_w - \beta_i)$ vs $\Delta\phi/z$ and a value of 1 ± 0.1 was obtained. This value

of δT_2 indicates that the laser frequency is approximately $\frac{1}{2}$ of one homogeneous linewidth away from the effective resonance frequency of the electric-dipole transition which is being saturated. N. G. Basov[11] et al., experimentally measured the width of the homogeneously broadened absorption line of SF_6 by means of laser saturation spectroscopy. They reported a value of 17 ± 4 MHz/Torr. Rabinowitz[4] et al., employed saturation spectroscopy to locate the fine structure absorption lines of SF_6. They reported an SF_6 absorption line which was separated from the 10.6-μm P(20) CO_2 transition by + 4 MHz. The next closest line to the CO_2 transition was separated by + 10 MHz. These literature values for a SF_6 pressure of 0.30 Torr permit δT_2 to be calculated by

$$\delta T_2 = \frac{4}{0.3(8.5)} \approx 1.6 . \qquad (14)$$

This value of δT_2 is in general agreement with the value obtained by the phase technique of Eq. (11).

It should be possible to devise an experiment to measure $\Delta\phi$ which is more convenient and direct than those used to measure the reflectance and transmittance. It would be convenient because a normalization run would not be required and only one detector would be needed. The response of the detector need not be linear over a large range of input intensities. With an optimum experimental design a phase measurement can be obtained more accurately than the average of many relative intensity measurements, Both the phase measurement and intensity measurements use many

experimental points, but phase measurements are not subject to the systematic errors of the intensity measurements. Although the magnitude of $\Delta\phi$ for a particular laser intensity does not provide as much information about the optical behavior of the sample system as the reflectance and transmittance, the measurement of the relative phase of the reflectance or transmittance modulations could be a powerful method to employ in the study of optical saturation.

A second interesting feature of the reflectance data that is illustrated in Fig. 8 is the relatively large modulation depth in the reflectance of the less intense laser pulses. This modulation in the amplitude of the reflectance was produced by the optical interference between the radiation reflected from the front and rear windows. The radiation reflected from the rear window had to traverse the sample cell twice and therefore, be attentuated by the square of the transmittance. The ratio of the transmittances for the 10.3 W/cm^2 pulse and the 0.09 W/cm^2 pulse is about two. Interestingly, the ratio of the depths of the modulations for these two pulses is also about two, even though the intensities of the pulses reflected from the rear window and traversing the cell again vary by a factor of four. Of course, these ratios are to be expected since it is the amplitudes of the electric fields that are additive in optical interference and not the intensities of the reflected pulses. The intensity of the radiation is proportional to the square of the resultant electric field strength of the radiation. Thus the peak to peak (ptp) depth of the modulation of the reflectance (and transmittance)

will be the difference between the intensity of the reflected radiation when the two reflected pulses are in phase $(\frac{(E_f + E_r)^2}{Z_{fs}})$ and when they are 180° out of phase $(\frac{(E_f - E_r)^2}{Z_{fs}})$. If the impedance of free space is Z_{fs}, and at the entrance to the sample cell the electric field strengths of the pulses reflected from the front and rear windows are E_f and E_r, respectively, then the ptp depth of the modulation is

$$\frac{(E_f + E_r)^2}{Z_{fs}} - \frac{(E_f - E_r)^2}{Z_{fs}} = \frac{4E_rE_f}{Z_{fs}} . \qquad (15)$$

Because E_f is not affected significantly by saturation, E_r is the variable which determines the modulation depth of the reflected radiation. For each pass through the sample gas, E_r will be attentuated by the square root of the transmittance. For two passes through the cell E_r will be attentuated by a magnitude equal to the transmittance. Thus the ratio of the modulation depths for any two of the reflected (or transmitted) pulses should be the same as the ratio of their transmittances.

The original purpose of this experiment was to obtain accurate measurements of the reflectance and transmittance of a SF_6 sample system under conditions of optical saturation. This purpose has been accomplished by using signal averaging techniques and varying the length of the sample cell to average over the interference phenomena. As a consequence of these studies two useful characteristics of these interference phenomena were

discovered. The first is that the relative phase differences in the modulations of the reflectances and transmittances produced by the optical interference effects can be used to determine the frequency difference between the laser radiation and the center of the absorption band of the saturable absorber. A second characteristic of these modulations is that their ptp amplitudes are proportional to the transmittance of the sample gas.

4. Evaluation of Experimental Procedure

This experimental procedure which employed the Nova minicomputer measured two optical properties which were not considered in previous experiments involving optical saturation. The first property measured only in this work was the reflectance of a sample system undergoing partial optical saturation. The second property was the interference phenomena produced by the electromagnetic waves reflected from the two ends of the sample cell.

The employment of the Nova minicomputer offered several experimental advantages. Firstly, long term signal averaging was possible -- very weak, noisy electrical outputs from the detectors could be combined to improve the signal to noise ratio. Also this long term signal averaging capability permitted the length of the sample cell to be varied at a slow rate. Secondly, the A/D converter was very accurate and precise from 10 V to a few millivolts; the ratio of any two voltage inputs could be measured accurately over a wide range. Thirdly, the programing

of the minicomputer permitted convenient mathematical manipulation of the experimental results and flexibility in the operation of the experiments. Finally, the minicomputer permitted very rapid and nearly automatic collection of the experimental data.

The major experimental problem was maintaining the precise optical alignment of the sample cell and the pyroelectric detectors with respect to the laser beam. Another problem was the development of the electronic signal processor which selectively amplified three of the eight pulses and automatically maintained the electronic baseline at zero volts. Once this experimental system was operational, the collection of data was relatively simple and routine. The limiting time factor was, on many occasions, the need to wait for the teletype to finish typing the results of the previous experiment. Without the employment of the Nova minicomputer, the reflectance experiments at normal incidence would have been very difficult. For instance, the equivalent of sixteen lock-in amplifiers would have been required to conduct this same experiment without the minicomputer. It is the opinion of the author that this work has utilized the capability of a minicomputer to perform an experiment which would have been impractical by other means.

REFERENCES

1. P. J. Durrant and B. Durrant, Introduction to Advanced Inorganic Chemistry, (John Wiley, New York, 1962) p. 852.
2. J. I. Steinfeld, I. Burak, D. G. Sutton, and A. Nowak, J. Chem. Phys., 52, 5421 (1970).
3. H. Brunet, IEEE J. Quantum Electron., 6, 678 (1970).
4. P. Rabinowitz, R. Keller, and J. T. LaTourrette, Appl. Phys. Lett., 14, 376 (1969).
5. G. B. Hocker and C. L. Tang, Phys. Rev., 184, 356 (1969).
6. T. J. Bridges and C.K.N. Patel, Appl. Phys. Lett., 7, 244 (1965).
7. Standard Infrared Grating Spectra (Sadtler Research Laboratories Inc., Philadelphia, Pa.) p. 27.
8. I. Burak, J. I. Steinfeld, and D. G. Sutton, J. Quant. Spectrosc. Radiat. Transfer, 9, 959 (1969).
9. J. J. Armstrong and O. L. Gaddy, IEEE J. Quantum Electron., 8, 797 (1972).
10. O. R. Wood, P. L. Gordon, and S. E. Schwarz, IEEE J. Quantum Electrom., 5, 502 (1969).
11. N. G. Basov, O. N. Kompanets, V. S. Letokhov, and V. V. Nikitin, Sov. Phys.-JETP, 32, 214 (1971).

CHAPTER IV

THE EFFECTS OF HEATING UPON THE OPTICAL PROPERTIES OF GASEOUS SF_6

A. INTRODUCTION

When the intensity of infrared radiation impinging upon a sample cell containing SF_6 is increased, the absorbtance decreases. This is ordinarily taken to be experimental evidence that optical saturation of the gas molecules has occurred. When the power being absorbed by the gas becomes sufficiently great, however, the temperature of the gas will increase due to heating of the sample. This increase in the temperature will produce a number of changes in the characteristics of the gas system other than simple saturation that influence the ability of the gas to absorb the IR radiation. Three of these temperature-influenced characteristics will be discussed.

One of these characteristics is the abundance of low energy vibrational levels in gaseous SF_6. The populations of these levels are very sensitive to temperature changes because they obey the Boltzmann distribution law. At room temperature, a small increase in the temperature of gaseous SF_6 reduces the population of the ground and ν_6=1 levels. This is illustrated in Fig. 1 from a paper by Brunet.[1] Since the vibrational transitions involved in the present study originate from these two lowest vibrational levels, an increase in the temperature will reduce the number of molecules available to absorb the 10.6-μm radiation. The greater the intensity of the

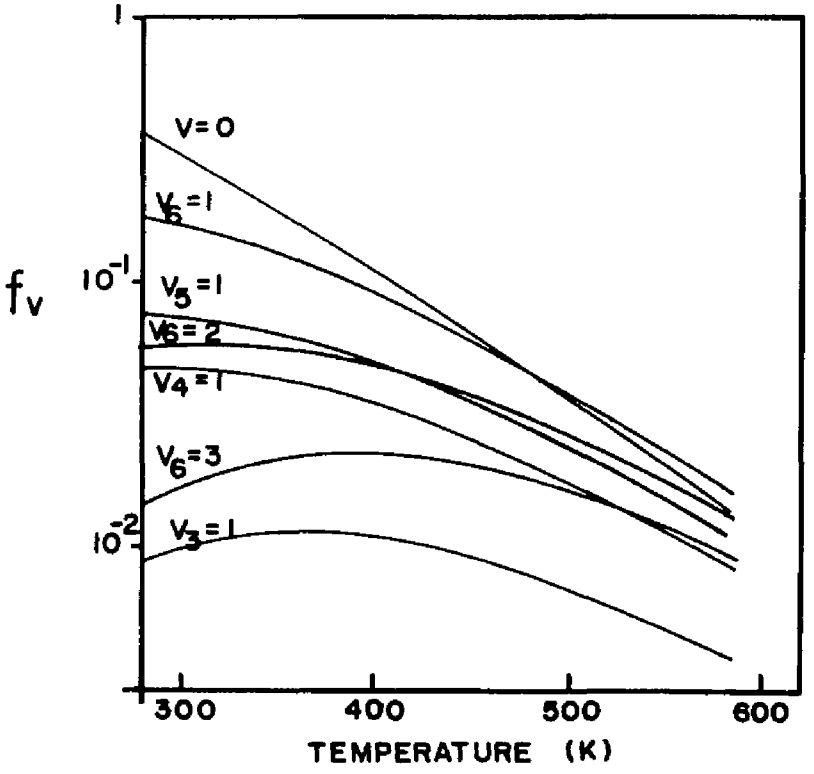

FIGURE 1. Fractional population in relevant SF_6 vibrational levels.[1]

incident infrared radiation, the greater this temperature rise will be. Therefore, the absorbtance will decrease with increasing intensity because of heating.

A second characteristic of SF_6 affected by temperature is the frequency of collisions between molecules. Since the vibrationally excited levels relax via a collision mechanism, the value of T_1 (vibrational relaxation time) will decrease with an increase in the molecular collision rate. Thus the excited levels will relax more rapidly at higher temperatures and a greater intensity of the impinging radiation will be required to produce the same amount of optical saturation acheived at a lower temperature.

The third characteristic of SF_6 influenced by the temperature is the density of the gas in the vicinity of the laser beam where the bulk heating occurs. A significant temperature increase would cause the density to decrease in that region of the sample cell. This density decrease would in effect remove potentially absorbing molecules from the path of the laser beam, thus decreasing the absorptance of the system.

In saturation experiments like those presented in this work it is common for the gaseous SF_6 to absorb 0.2 W/cm^3 of power. Significant heating of the gas would be expected due to the low heat capacity (92 joules/mole K)[2] and thermal conductivity (9.8mW/m·K)[1] of SF_6. In studies of SF_6 where even greater powers are absorbed by the gas, heating is the primary source of the observed decrease in the absorbtance rather than optical saturation.[1] Thus a

comparison of the theory which describes optical saturation in SF_6 with experimental results must consider the amount of bulk heating and its effects upon the optical characteristics of the gas.

If the temperature of the gaseous SF_6 at the center of the sample cell where the laser beam is passing is known, it is not difficult to calculate the influence of the three temperature characteristics upon the optical properties of the system. The density and T_1 may be calculated directly and the new values used in the theory. The population of the absorbing molecules may be calculated from the density and the relative population distribution obtained from the Boltzmann distribution law. A convenient form of the Boltzmann distribution law for vibrational levels is given by Herzberg,[3] if the relative populations of the i_{th} level is desired;

$$P_i = \frac{g_i\, e^{-\hbar\omega_i/kT}}{\prod_{j=1}^{n} \frac{1}{(1-e^{-\hbar\omega_j/kT})^{g_j}}} \qquad (1)$$

k = Boltzmann's constant
$\hbar$ = Plank's constant
T = temperature
g = degeneracy
ω = vibrational frequency
n = # of vibrational degrees of freedom in the molecules.

The new value of these properties influenced by the population changes may then be used directly in the theoretical calculations of optical saturation.

Determining the temperature change resulting from the absorption of power from the laser beam is not easy for four reasons. One, the power of the laser beam is not uniform in a direction transverse to the optic axis. At best, it has a Gaussian cross

section. Two, because the gas is such a poor conductor of heat, the wall of the sample cell may exhibit no detectable temperature rise while the temperature of the gas at the center of the cell may increase by several hundred Kelvins. This makes a direct measurement of the temperature rise in the gas very difficult. Three, in the experiments described in this work the laser beam was chopped before it struck the sample cell; therefore, the heating does not reach a steady state but will be changing with time. The fourth reason also involves the dynamic nature of the temperature effect, in that the heating is directly proportional to the power absorbed, but the absorbed power changes when the temperature changes.

B. PREVIOUS STUDIES OF BULK HEATING IN SF_6

Previous studies of the optical saturation of SF_6 have all recognized the problems associated with bulk heating of the SF_6. The incorporation of these temperature effects into their theory and the predicted changes in the optical properties of the sample system, however, have varied.

In the 1968 work of Burak, Steinfield and Sutton,[2] the laser radiation was chopped after it had passed through the sample cell, thus the heating in the sample was permitted to reach a steady state. These authors used an approximate solution of the following steady state heat flow equation to calculate the radial temperature distribution in their sample cell.

$$k\nabla^2 T + Q = 0 \qquad (2)$$

k = thermal conductivity
T = temperature change
Q = cross section of power absorbed per unit volume.

They used a cell 4 cm in diameter and 10 cm long filled with a pressure of SF_6 that absorbed 3 W/cm^3 of power in the region of the laser beam. Their solution of Eq. (2) for this system predicted a temperature rise of 500 K at the center of the sample cell in the region of the laser beam. They reported rough agreement between the calculated radial temperature distribution and measurements of the gas temperature at various depths into the cell. The temperature measurements were made with thermistors. To incorporate bulk heating into their theoretical calculations of optical saturation, they calculated temperature distributions for the various laser powers and SF_6 pressures used in their experiments. They then used those temperatures calculated for the region of the laser beam in their theoretical calculations of the saturation of the absorption of SF_6. Although they spoke of bulk heating greatly reducing the population of the absorbing vibration levels, they presented a figure which seems to indicate a theoretical increase in absorption when heating is considered. (In a later paper[4] they presented experimental evidence of heating decreasing the absorption.)

In 1970 Henri Brunet[1] used the same steady state heat flow equation and solved it exactly. He also found agreement between his predicted temperature rise and the temperature of gaseous SF_6

under intense laser radiation. He filled his sample cell with 10 Torr of SF_6 which resulted in 10 W/cm^3 of power being absorbed in the region of the laser beam. He measured the average temperature rise in the cell by noting the pressure change due to heating. He concluded, however, that his solution was invalid for a temperature rise exceeding 20 K "since the absorption coefficient, hence, the absorbed power decreases rapidly with increasing temperature". He further concludes that for large laser intensities striking SF_6 at pressures above 1 Torr, the saturation of the absorption is mainly due to SF_6 bulk heating. He did not incorporate temperature changes caused by bulk heating into his theoretical calculations.

The 1969 work of Wood, Gordon, and Schwarz[5] presented a convenient solution to the problem of bulk heating. They reasoned that for SF_6 at pressures below 1 Torr, molecular diffusion tends to delocalize the heat source, and since in many cases the diffusion length can be of the order of the radius of the sample cell, a large fraction of the vibrationally excited molecules reach the cell walls before being de-excited by collisions. These molecules would not contribute to the heating of the gas. They further add that since the temperature changes are small, a Boltzmann redistribution will not be important and temperature effects can, therefore, be neglected. They did not present experimental results to support their conclusions, nor were any experimental results for pressures below 1 Torr presented in the other two studies. Using 5.5 Å as the collision diameter[6] for SF_6, the product of the mean free path (λ) and the pressure was calculated to be 2.1×10^{-3} cm.·Torr.

By using λ and the result of the "random walk" problem, the distance which a vibrationally excited molecule can diffuse in a time of T_1 is $\lambda(2T_1/\tau)^{\frac{1}{2}}$, where τ is the mean time between molecular collisions. For SF_6 the diffusion length is then 0.103 cm·Torr, and for a sample cell with a 2.1 cm radius the SF_6 pressure would have to be less than 0.1 Torr before significant delocalization of the heating would occur. At pressures below 0.1 Torr molecular diffusion will actually interfere with optical saturation, because some of the vibrationally excited molecules will exit the region being pumped by the laser radiation before normal collision induced relaxation processes have had time to occur. Since the SF_6 studies of this work used pressures above 0.1 Torr and a sample cell with a 2.1 cm radius, the solution of Wood, Gordon, and Schwarz (which was to neglect bulk heating effects) will not be applicable to these studies.

To describe the bulk heating in the experiments of this work, the steady state heat flow equation is inadequate because of the use of the chopper between the laser and the cell. The dynamic nature of the heating may be treated by incorporating a time dependent term in the steady state equation.[7]

$$k\nabla^2 T + Q = dC\frac{\partial T}{\partial t} \qquad \begin{array}{l} t = \text{time} \\ d = \text{density} \\ C = \text{heat capacity} \end{array} \qquad (3)$$

Because Q is a Gaussian function, the above equation is very difficult to solve for the experiment conditions of this work. It was quite recently that Enrique[8] solved this equation for a laser calorimetry experiment using the method of finite Fourier transforms

to separate the variables. His solution is quite lengthy and is presented in Eqs. (4), (5), and (6). These equations were incorporated into a computer program which determined the temperature rise at the center of the sample cell as a function of time, using parameters appropriate to the experiments of this work. The results of the execution of this program by the IBM 360 computer will be compared with the results of experimental studies of heating effects vs time later in this chapter.

C. EXPERIMENTAL

It has been shown that the authors of previous works on this subject disagree as to the magnitude and importance of heating effects in determining the optical properties of SF_6 gas. Because the assumptions underlying the theoretical equations are not easy to verify, and the calculations themselves are not easy to perform, a series of experiments were performed in collaboration with Don Elbers to measure the effects of bulk heating upon the transmittance of gaseous SF_6. The samples were contained in the sample cell described in Chapter III.

The general procedure in these experiments was to irradiate the sample cell with a "rectangular pulse" of laser radiation having a peak intensity of 10 W/cm^2. A rectangular pulse is one which rises sharply in amplitude with time, persists at a constant amplitude for a certain interval, and then drops abruptly to zero amplitude. Then, the change in the temporal contour of the transmitted pulse that was caused by the dynamic heating of the gaseous SF_6

$$\Delta T(r,z,t) = \frac{I_o A_b a^2}{k\, b^2 \ell} \sum_{m=1}^{\infty} \frac{\alpha_m^2 \exp(-\frac{\alpha_m^2 a^2}{8})}{\alpha_m^2 + H^2} \frac{J_o(\alpha_m r)}{J_1^2(\alpha_m b)} \quad X$$

$$\sum_{n=1}^{\infty} \frac{(\lambda_n^2 + H^2)\ell}{(\lambda_n^2 + H^2)\ell + H} \frac{\sin(\lambda_n \ell)}{\lambda_n \ell} \cos(\lambda_n z) \quad X$$

$$\frac{1-\exp[-Kt(\alpha_m^2 + \lambda_n^2)]}{\alpha_m^2 + \lambda_n^2} \qquad (4)$$

α_m and λ_n are roots of the transcendental equations

$$\alpha_m J_1(\alpha_m b) = H J_o(\alpha_m b) \qquad (5)$$

$$\lambda_n \tan(\lambda_n \ell) = H \qquad (6)$$

Where,

h = heat transfer coefficient

k = thermal conductivity

H = h/k

K = k/C·d

d = density

C = specific heat capacity

A_b = absorptance

I_o = peak intensity of laser beam

a = radius of laser beam where the intensity has dropped to $1/e^2$ of I_o

b = radius of sample cell

ℓ = $\frac{1}{2}$ the length of the sample cell

r = radial distance from cell center

t = time

z = distance from cell center along the optical axis

was measured. Fortunately, the observed cooling time of SF_6 at the pressures used is so rapid (1/e in 1.22 msec for 1.15 Torr) that the temperature of the gas returns to that of the sample cell walls between pulses. The experimental configuration employed is presented in Fig. 2. One of two synchronous light choppers was used in the chopper I position. The first rotated at 60 Hz. The beam diameter was such that the rise time was 38 μsec. Slots cut in the chopper wheel provided 0.8 msec pulses with a 0.1 duty cycle. The second rotated at 13.2 Hz; the pulses had a 0.4 msec rise time, a 9 msec duration, and a 0.25 duty cycle. Two separate choppers were necessary to permit a fast rise time and also to obtain a long pulse. The pinhole was adjusted to a 2 mm diameter to permit a greater rise time for the chopper and to limit the power striking the detector. Chopper II was driven by a nonsynchronous air motor. The wheel rotated at approximately 200 Hz, and the pulses had a rise time of 24 μsec. The purpose of chopper II was to prevent pulse distortion by the detector; the distortion occurs for pulses longer than 0.5 msec. Thus one observes many short square pulses in a window defined by chopper I rather than one continuous pulse. Since the frequency of rotation of chopper II is incommensurate with chopper I, these short pulses appear to move randomly and rapidly within the observation window. The IR detector was a pyroelectric type made by Laser Precision (model SKT-1010-333) capable of an 11 μsec rise time in the configuration used for these experiments. The Tektronix Type 121 preamplifier was necessary to enable the output of the detector to be observed on the Fairchild 766H/F oscilloscope.

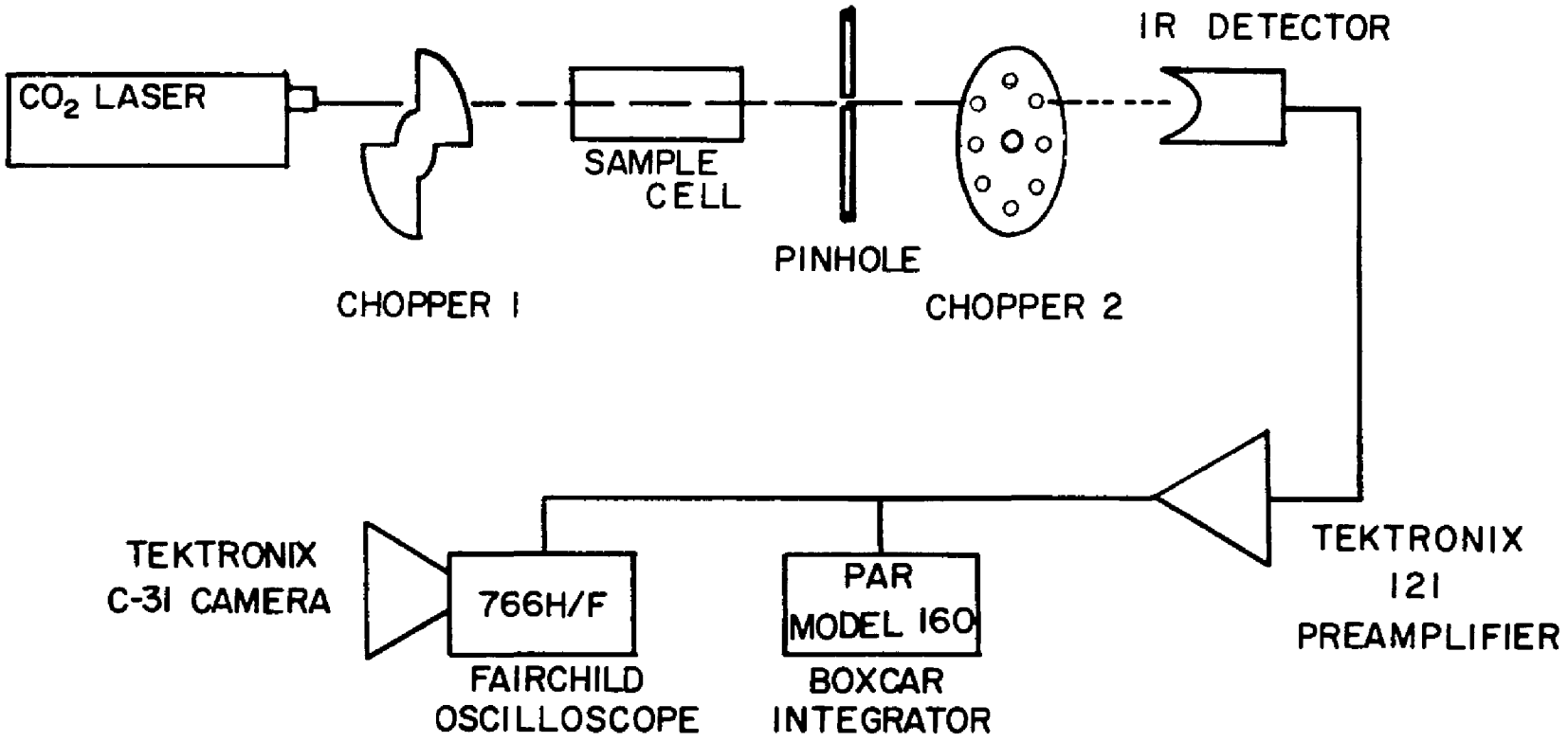

FIGURE 2. Experimental configuration employed for pulse shape detection.

This oscilloscope could be triggered for a single sweep so that the Tektronix C-31 camera could be used to photograph the oscilloscope trace. Making several exposures enabled the random short pulses created by chopper II to fill the observation window and present the true shape of the transmitted pulse. The PAR model 160 Boxcar Integrator was also used to obtain hard copy of the pulse shapes. The Boxcar Integrator slowly scans a narrow window over the synchronously detected pulse so that the random-relative-phase pulses of chopper II average out and a true profile of the transmitted pulse is obtained.

A reference pulse contour was obtained with the sample cell evacuated using both the long and the short pulse choppers in the chopper I position. The two resulting pulses were then fitted together (using the short pulse for the first 0.75 msec) to obtain a single pulse contour. This same procedure was used to obtain pulse contours when the sample cell was filled with various pressures of SF_6. There was good agreement between the results obtained using the Boxcar Integrator and the multi-exposed photographs of the oscilliscope traces. Since the signal to noise ratio was high in the photographic method, it proved to be the most convenient, since a scan with the Box car Integrator usually required 30 minutes. Transmittance vs time curves were obtained by dividing the amplitudes at various times of the pulses obtained at a particular pressure of SF_6 by the amplitude at the corresponding time of the pulse obtained for the evacuated sample cell. Fig. 3 presents the transmittance vs time curves for several pressures of SF_6.

The sharp spike in the transmittance curves at the onset of the pulse is explained by vibrational hole burning in the absorption of the SF_6 molecules. Measuring the healing time of the hole is a technique used to determine the relaxation times of excited vibrational levels.[4] The hole burning effect results from the intense laser pulses initially driving all of the molecules in an absorbing vibrational level to an upper vibrational level before relaxation processes begin returning the molecules to the absorbing vibrational level. Very quickly a steady state saturation is reached. The duration of these initial spikes in the transmittance is consistant with the 122 μsec·Torr value for T_1. The slow increase in the transmittance after the hole burning is attributable to bulk heating of the sample gas. When the intensity of the laser was reduced to 3 W/cm^2, the hole burning effect was not observed.

In many experiments where the transmittance of an IR absorbing gas is measured, the IR radiation is chopped in front of the sample cell and the signal from the IR detector is proportional to the area under the transmitted pulses.[1] Since the transmittance is changing with time, the frequency and duty cycle of the light chopper employed would influence the magnitude of the measured transmittance. For example, the results of this work predict an 11% increase in the transmittance of 0.7 Torr of SF_6 being irradiated with a peak laser intensity of 10 W/cm^2 when a chopper window of 8 msec is used instead of one 4 msec long. Thus workers in this field should always indicate the frequency and the duty cycle of the light choppers they used to obtain their experimental data.

D. DATA ANALYSIS

To better separate the hole burning and heating effects, the data points defining the transmittance curves were fitted to the sum of two exponential functions, the first function (A function)

$$T(t) = A \exp(-at) + B[1-\exp(-bt)] + C \qquad (7)$$

is appropriate for first order relaxation processes and describes the exponentially decreasing transmittance due to the healing of the hole in the absorption band. The second function (B function) describes the exponential increase in transmittance due to sample heating. A fifth constant (C) was necessary to define the transmittance at t=0. To obtain approximate values of the five coefficients, the curve fitting technique utilized the fact that the hole burning effect declines in amplitude very rapidly. Thus at some time past the minimum in the transmittance curve

$$T(t) \approx B[1 - \exp(-bt)] + C. \qquad (8)$$

Rearranging Eq. (8) and taking the logarithm of both sides gave

$$\log[B + C - T(t)] \approx \log(B) - bt. \qquad (9)$$

Various trial values of (B + C) were introduced and a least squares fit to the experimental data was used to determine B and b. The

trial value of (B + C) which gave the minimum standard deviation was saved along with the corresponding approximate values of B and b. These values of B, b, and C were returned to Eq. (7) and the logarithm of both sides was calculated.

$$\log[T(t) - B(1 - \exp(-bt)) - C] = \log(A) - at. \qquad (10)$$

By using experimental times and transmittances from the region where the slope of the T(t) was negative, approximate values of A and a were obtained by a least squares fit to this portion of the experimental data. These approximate values of the five coefficients were then used to find the local minimum of function F by employing the

$$F(A,a,B,b,C) = \sum_{i=1}^{n} [T(t_i) - T_{exp}(t_i)]^2 \qquad (11)$$

n = # experimental data points

computer routine of Fletcher and Powell.[9] This routine treated the coefficients of Eq. (7) as variables and determined the values of these coefficients which produced the minimum of F in the region of the initial approximate values. The values which produced the minimum of F, were then taken as the coefficients of Eq. (7) that enable this equation to best fit the experimental data. The values of these coefficients for each experimental pressure are presented in Table I. The solid lines in Fig. 3 represent the curves generated by Eq. (7) using these coefficients.

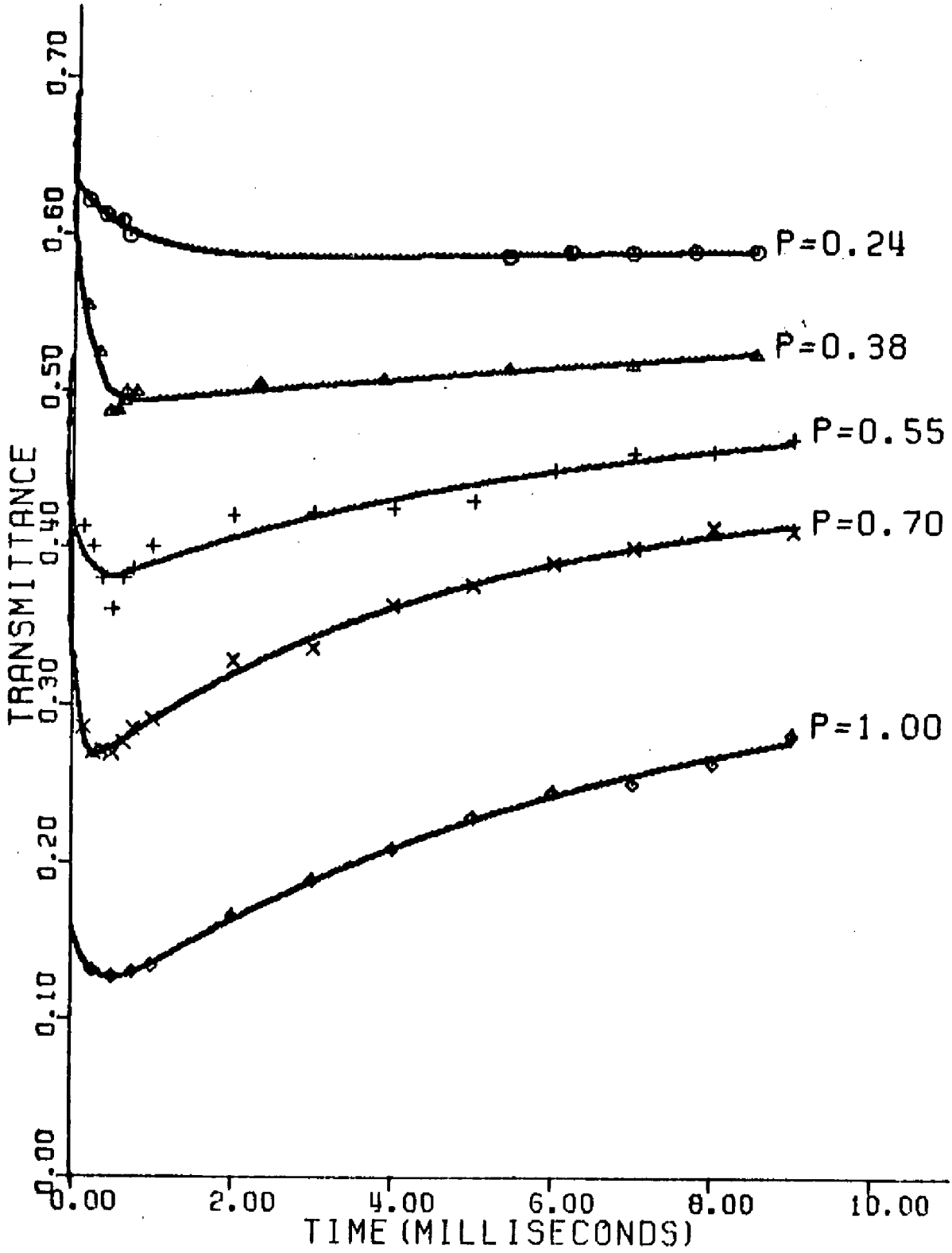

FIGURE 3. Transmittance vs time curves for several pressures of SF_6. The points represent experimental data. The solid lines represent a least squares fit to $T(t) = Aexp(-at) + B[1-exp(-bt)] + C$.

TABLE I

COEFFICIENTS OF EQ. (7) WHICH PRODUCED THE BEST FIT TO THE EXPERIMENTAL DATA

PRESSURE (TORR)	A	a($msec^{-1}$)	B	b($msec^{-1}$)	C
0.24	0.0488	1.344	0.1789	0.005549	0.5826
0.38	0.2008	7.146	0.1202	0.04090	0.4900
0.55	0.1512	10.10	0.1250	0.1667	0.3709
0.70	0.1818	15.43	0.1876	0.2114	0.2554
1.0	0.0565	4.114	0.2356	0.1522	0.1024

The B function in Eq. (7) gives the transmittance changes observed for bulk heating of the sample gas. Before these changes can be compared with the results obtained using the solution of the dynamic heat equation, the theoretical temperature curves must be converted to transmittance curves. The conversion of temperature changes to transmittance changes was accomplished by using the optical saturation computer program presented in Chapter II. The computer program was modified to contain the temperature dependence of the populations of the various vibrational levels, T_1, and the gas density in the vicinity of the laser beam. It was temporarily modified to calculate the reflectance, absorbtance, and transmittance of the sample system at various fixed temperatures with a peak laser beam intensity of 10 W/cm^2. These calculations provided a table of absorbtances and transmittances at various temperatures for each gas pressure used in the experiments. The theoretical temperature curves were computed for a position at the center of the sample cell assuming that 100% of a laser beam of 10 W/cm^2 peak intensity (standard) was absorbed by the gas. Since the temperature distribution is directly proportional to the power absorbed, the temperature distribution for any absorbed power will be proportional to the previous calculation by the ratio of that absorbed power to the standard power. The determination of the transmittance of the sample for a particular temperature change required finding the absorbtance in the table which was consistent with the temperature change predicted by both computer programs. For example, if the optical saturation program predicted a temperature rise of 50 K for

2 W/cm^2 of peak absorbed intensity and the dynamic heat equation predicted a temperature rise of 60 K for the same power absorption, a match was not acheived and a different absorbtance was considered until the temperatures matched. When a temperature match was acheived the transmittance corresponding to that absorbtance was characteristic of that particular temperature rise. The Nova minicomputer was programmed in "BASIC" to perform this matching technique with the necessary interpolations. Table II provides an example of this matching technique.

Figure 4 presents transmittance vs time curves generated by the B function that was obtained from the experimental data fit, and also curves resulting from the solution to the dynamic heat equation with the temperature-to-transmittance conversion. The second set of transmittance curves were offset at t = 0.5 msec to make both curves match at that time, so that a simple comparison was possible. The agreement between the curves predicted by the dynamic heat equation and the experimental data is excellent when the pressure of SF_6 is 1 Torr. However, the relative agreements between the predicted and observed changes in the transmittance become progressively worse as the pressures become smaller. A possible explanation for these deviations at low pressures will be presented later.

The original motivation for this study of temperature effects was to find a convenient method for calculating the temperature rise (produced by bulk heating of the gaseous SF_6 contained in the sample cell used in this work). With the experimental data obtained, it

TABLE II

A. OUTPUT FROM OPTICAL SATURATION PROGRAM

(PSF_6 = 0.7 TORR, PEAK INTENSITY = 10 W/cm^2)

TRANSMITTANCE	A_b (ABSORPTANCE)	TEMPERATURE RISE, K
0.137	0.796	0
0.154	0.778	10
0.174	0.757	20
0.194	0.737	30
0.213	0.718	40
0.231	0.699	50
0.248	0.680	60
0.265	0.663	70
0.281	0.646	80
0.296	0.630	90
0.310	0.615	100
0.323	0.601	110
0.336	0.588	120
0.348	0.575 x 225.3 ≈	130*

B. COMPUTER SOLUTION TO DYNAMIC HEAT EQUATION

(PSF_6 = 0.7 TORR, PEAK INTENSITY = 10 W/cm^2)

TIME (m sec)	TEMPERATURE, °C RISE(A_b=1)	TEMPERATURE, RISE(MATCHED)	TRANSMITTANCE (INTERPOLATED)
0.5	47.3	34.5	0.202
1.0	77.7	53.8	0.237
1.5	100.1	66.9	0.260
2.0	117.8	76.8	0.276
3.0	144.9	91.1	0.297
4.0	165.2	101.4	0.312
5.0	181.5	109.3	0.322
6.0	195.0	115.7	0.331
7.0	206.5	121.1	0.337
8.0	216.4	125.7	0.343
9.0	225.3	129.6*	0.348

*129.6 K is the Temperature Rise match for A_b=0.575 when the Temperature Rise predicted for A_b=1 is 225.3 K.

FIGURE 4. Transmittance vs time curves generated by the dynamic heat flow equation. The data points were generated by the emperically determined (B + C) function.

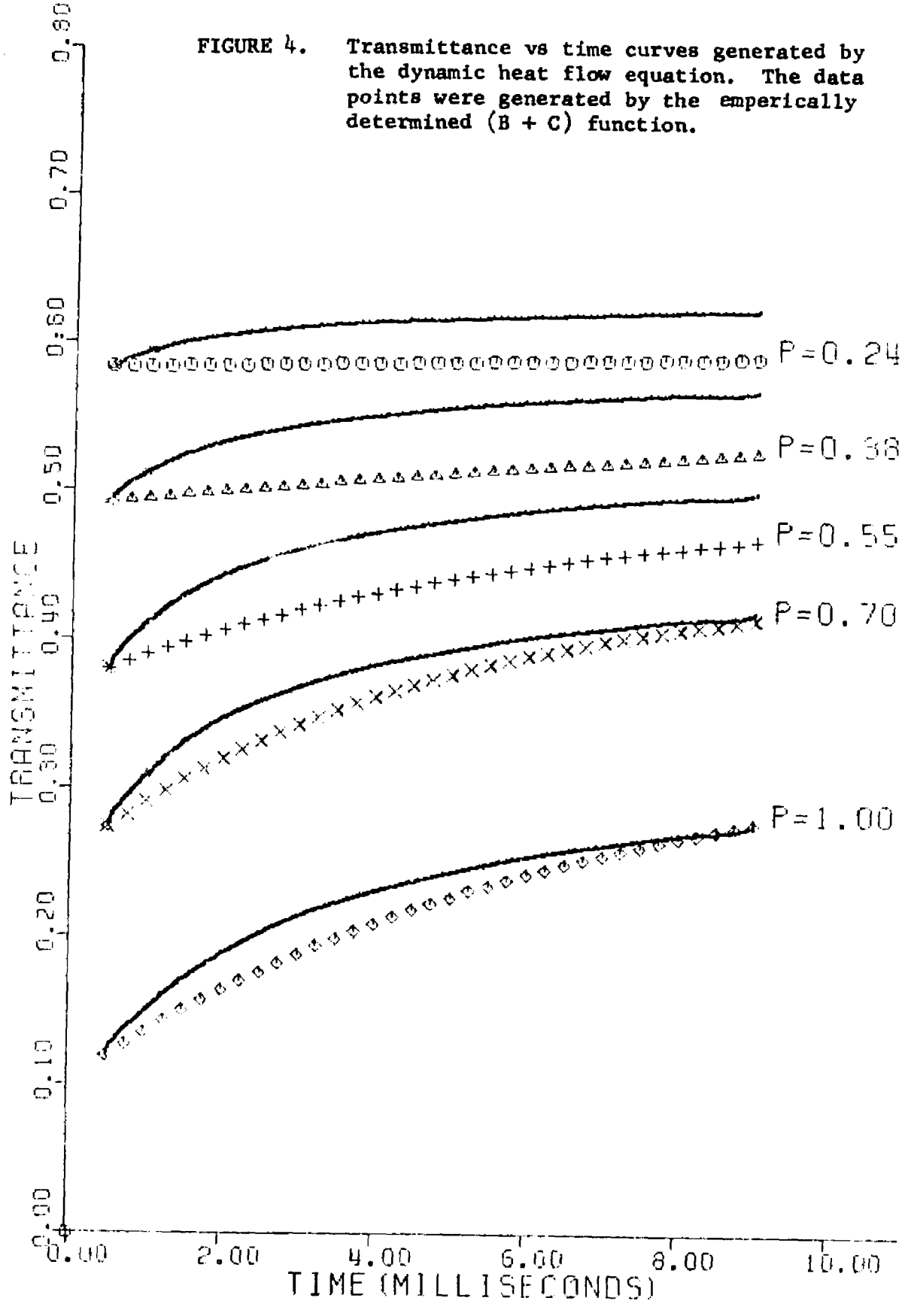

was possible to accomplish this goal by an empirical method. The theoretical technique had proved too involved and lacking in accuracy at low gas pressures. The empirical method involved a heating constant (K_h) which is a function of the gas pressure. This constant could be used in a simple equation to determine the temperature rise in the gas as a function of the absorptance, pressure, and peak laser beam intensity.

$$\text{Temperature rise} = K_h \times \text{Absorptance} \times \text{peak laser intensity} \quad (12)$$

The heating constant for a particular pressure was determined by evaluating the B function at the time when the midpoint of a slit in the chopper wheel crossed the optic axis. For the Nova experiments, this time was 0.9 msec. For the ratio experiments, a time of 3.1 msec was used. Using the absorptance, transmittance, temperature tables previously generated, a temperature rise was determined for each observed transmittance change predicted by the B function. Dividing these rises in temperature by the absorptance and peak laser intensity used in these experiments (10 W/cm^2) gave a value of K_h for each pressure. The shape of the plot of K_h vs pressure was reasonably well represented by Eq. (13), which also provided the proper values

$$K_h = a \exp(-b/p^2) \quad (13)$$

at the pressure extremes. The values of a and b were determined by a least squares fit to the experimental data. This function was then

incorporated into the optical saturation computer program to permit the calculation of a temperature rise appropriate to the experimental conditions.

The curves generated by Eq. (13) and the experimental values of K_h for each pressure are presented in Fig. 5. These curves indicate a decrease in the rate of bulk heating of the gas at lower pressures. Thus the thermal conductivity must increase at these lower pressures. This effect accounts for the inadequacies of the heat flow equations used to treat these experiments, since their derivations assumed that the thermal conductivity was independent of pressure. This assumption, however, is valid for heat transfer at pressures where the mean free path of the molecules is small compared to the dimensions of the container,[9] and therefore, should have been valid for these experiments.

A possible explanation for the influence of pressure upon the observed thermal conductivity of the gas is the occurrance of vibrational deactivation at the cell walls as suggested by Wood, Gordon, and Schwarz.[5] If a vibrationally excited molecule could reach the cell wall and transfer its excess vibrational energy directly to the wall, then that transferred energy would not produce any heating of the gas. As discussed in Chapter III, a SF_6 molecule excited by the absorption of a laser photon transfers its excess vibrational energy to the surrounding molecules via molecular collisions. In a single collision between two molecules, the probability of vibrational energy being converted to translational energy (V-T) decreases exponentially as the amount of energy being

FIGURE 5. Experimental values determined for the heating constant (K_h) and their approximation by $K_h = a \exp(-b/p^2)$.

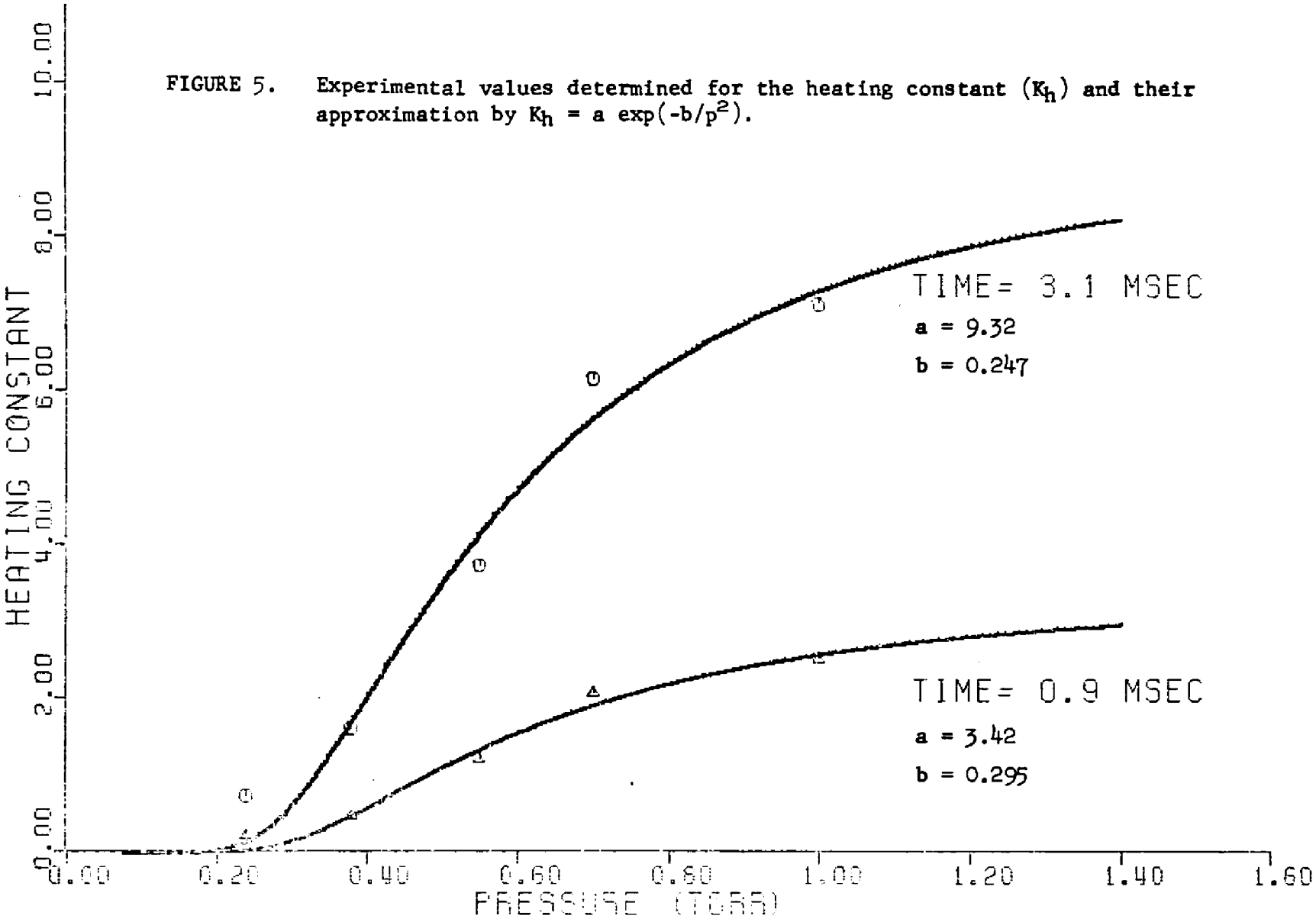

converted.[11] The probability, however, of resonance transfer of vibrational energy (V-V) between identical molecules involved in a collision is quite high.[12] For SF_6 the V-T energy transfer occurs primarily from the ν_6=1 vibration (350 cm^{-1}) and has a relatively small probability with each collision,[13] while the probability of the V-V energy transfer is high. Thus a great many V-V processes will occur before all of the excess vibrational energy of the laser (944.2 cm^{-1}) excited molecule is completely converted to translational energy (heating of the gas) by the V-T process. Although the particular molecule which was excited by the laser photon could not be expected to reach the cell wall and still possess excess vibrational energy, the collisional V-V energy transfer process could propagate this excess vibrational energy to molecules in the vicinity of the cell wall. These molecules near the wall could then strike the wall and be deactivated.

The feasibility of this propagation of vibrational energy by molecular collisions may be checked by calculating the average number of collisions which one molecule will undergo in a time period equal to T_1. This collision number will provide an indication of the maximum number of V-V energy transfers per molecule which can occur before the excess vibrational energy has been reduced to 1/e of its initial value by the V-T process. Using an average velocity (v) for SF_6 molecules at 300 K, the average number (Z) of collisions per molecule in a time T_1 is

$$Z = \frac{T_1 v}{\lambda} = 1200. \qquad \text{where } T_1 = 0.122 \text{ msec·Torr},\ \lambda = 2.1\times10^{-3} \text{cm·Torr},\ v = 2.1\times10^{4} \text{cm/sec} \qquad (14)$$

This seemingly large value of Z is consistent with the experimental results of several workers[14-16] who have studied the V-T transfer of energy in SF_6 by means of ultrasonic dispersion. The number of collisions per molecule is independent of pressure since the pressure dependence of T_1 and λ divide out. The collisional propagation length (PL) is a function of pressure and is given by

$$PL = \frac{Z\lambda}{\sqrt{2}} . \qquad (15)$$

Using Eq. (15), a SF_6 pressure of 0.81 Torr will produce a value of PL which is equal to the radius of the sample cell (2.1 cm). Lower pressures produce even greater values of PL. Interestingly, it is in the vicinity of 0.8 Torr that the heating constant K_h (see Fig. 5) begins to decrease markedly with decreasing pressure. At higher pressures K_h should become constant. Thus the sudden increase in the thermal conductivity of SF_6 at pressures below 0.8 Torr may be explained by collisional propagation of excess vibrational energy to the walls of the sample cell. Since the energy transfered in this manner does not contribute to the heating of the gas, the thermal conductivity appears to increase.

E. SUMMARY AND CONCLUSION

A major problem in studies of the optical saturation of gaseous SF_6 has been caused by bulk heating of the IR absorbing gas. Although it was not difficult to incorporate the influence of these

temperature changes into the present theory of optical saturation, determining the magnitude of the temperature change has not been easy. Theoretical methods using standard heat flow equations have proven inadequate for gas systems at pressures below 0.8 Torr. Experiments were performed to obtain the time rate of the heating in the sample cell used in this work. An experimental technique whereby the pulse distorting effects of an IR detector are eliminated was introduced. The results of these experiments provided the data necessary to develop an empirical method for determining the magnitude of the bulk heating. Unfortunately the constants determined by this empirical method apply only to the sample system of this work. The initial pulse shape experiments would have to be repeated for a sample cell of different geometry or composition.

The experimental data of transmittance vs time and its comparison with the solution of the dynamic heat equation permit three conclusions to be made. The first conclusion is that bulk heating of gaseous SF_6 by the power absorbed from the laser beam produces a decrease in the absorbtance of the sample system even at pressures below 1 Torr. A second conclusion for pressures below 0.8 Torr is that the molecular transfer of vibrational energy must play a major role in delocalizing the heating and permitting vibrational deactivation at cell walls. The conclusion is based upon the discrepancy between the observed heating effects and those predicted theoretically without considering deactivation at the cell walls. And thirdly,

although the heating effects are not large, they must be considered for an accurate comparison of a theoretical treatment of optical saturation and experimental observations.

The results of this study indicated three experimental procedures which may be utilized to minimize bulk heating in IR absorbing gases. One is to construct the sample cell with as small a radius as possible. A second is to work at low pressures (0.1-0.5 Torr) so that the molecular transfer of vibrational energy to the walls of the container is enhanced. At pressures below 0.1 Torr molecular diffusion would be so great that it would interfere with optical saturation. And the third is to chop the incoming radiation with narrow chopper slits to provide a short heating time and a small duty cycle. At least a 2 msec window should be used to prevent complications due to hole burning effects.

REFERENCES

1. H. Brunet, IEEE J. Quantum Electron. 6, 678 (1970).
2. I. Burak, J. I. Steinfeld, and D. G. Sutton, J. Quant. Spectrosc. Radiat. 9, 959 (1969).
3. G. Herzberg, Infrared and Raman Spectra (D. Van Nostrand Co., Princeton, 1945) p. 503.
4. J. I. Steinfeld, I. Burak, D. G. Sutton, and A. V. Nowak, J. Chem. Phys. 10, 5421 (1970).
5. O. R. Wood, P. L. Gordon, and S. E. Schwarz, IEEE J. Quantum Electron. 5, 502 (1969).
6. B. Stevens, Collisional Activation in Gases (Pergamon Press, Oxford, 1967) p. 221.
7. E. R. C. Eckert and R. M. Drake, Jr., Heat and Mass Transfer (McGraw-Hill Book Co., New York, 1959) p. 31.
8. B. G. Enrique, Appl. Opt. 14, 314 (1975).
9. R. Fletcher and M. J. D. Powell, Computer Journal 6, 163 (1963). Also see - System/360 Scientific Subroutine Package Version III Application Description, Form GH20-166 (IBM, Inc., White Plains, N. Y.).
10. R. D. Present, Kinetic Theory of Gases (McGraw-Hill Book Co., New York, 1958) p. 61.
11. Stevens, loc. cit., p. 36.
12. Ibid., p. 15.
13. A. B. Callear, Appl. Opt., Supplement 2, 145 (1965).
14. J. D. Lambert, D. G. Parks-Smith, and J. L. Stretton, Proc. Roy. Soc., A282, 380 (1964).

15. T. L. Cottrell and J. C. McCoubrey, Molecular Energy Transfer in Gases (Butterworths, London, 1961) p. 99.

16. C. L. O'Connor, J. Acoust. Soc. Amer., 26, 361 (1954).

CHAPTER V

COMPARISON OF THEORY AND EXPERIMENTAL RESULTS

A. OPTICAL SATURATION IN SF_6 - THEORY

The experimental portion of this work was performed in order to obtain quantitative measurements which could be used to test the adequacy of the theory presented in Chapter II. The saturable absorber studied was sulfur hexafluoride, which unfortunately is not a simple two-level system. Because the theory presented in Chapter II was designed only for an ensemble of two-level systems, it had to be modified to take into account the more complex energy level structure of SF_6. The presence of additional levels had two different effects upon the absorption characteristics of SF_6. The first effect was the change in the absorbtance due to redistribution of the SF_6 population among these levels which occurred when the temperature increased. The temperature increased because of the heating of the sample due to the absorption of energy from the incident radiation by the SF_6 molecules. The second effect was the presence of more than one energy level pair differing by just the right amount of energy to contribute to the absorption process. In addition to the multiple energy levels, another complication not envisioned in Chapter II was that each SF_6 absorption line was not only pressure-broadened (homogeneous broadening) but Doppler-broadened (inhomogeneous broadening) as well. The methods by which these effects were incorporated into the theory will be discussed in this section.

Recall that all of the optical properties of a sample undergoing electric-dipole-allowed transitions are determined by the electric susceptibilities (η). From Eq. (27) of Chapter II η is given by

$$\eta = \frac{N m_e^2 T_2 \Omega}{\Delta_e \hbar \varepsilon_0} [\delta T_2 + i], \tag{1}$$

where

$$\Delta_e = 1 + \delta^2 T_2^2 + T_1 T_2 m_e^2 \bar{E}_y^2 / \hbar^2 \tag{2}$$

and

$$\Omega = \frac{\rho_\ell - \rho_u}{\rho_\ell + \rho_u} \quad . \tag{3}$$

In Eq. (3) the ρ's refer to the populations of the lower and upper levels which are connected by a spectroscopic transition which has a transition dipole moment of m_e. The quantity δ is the frequency difference between the laser frequency and the effective center of the SF_6 absorption line produced by the transition.

The modification of the theory presented in Chapter II was necessitated by the fact that the temperature of the gaseous SF_6 was observed to rise with increased laser power due to bulk heating of the gas. This temperature rise produced changes in the population distribution among the many vibrational energy levels of SF_6, in T_1 and T_2, and in the density of the gas in the vicinity of the laser beam. All three of these changes must be taken into account by the theory.

The first problem, however, was to compute the rise in the translational temperature of the gas which resulted from the absorption of energy from the laser beam. The empirical method developed in Chapter IV was incorporated into the computer program and the temperature of the gas at the center of the laser beam was computed after each iteration of the theoretical procedure. This computed value for the temperature was then used in the calculations employed in the next iteration.

Temperature-induced changes in the relative population distributions of the vibrational energy levels of SF_6 affected the Ω term in Eq. (1). A subroutine called BOLTZ was added to the computer program to compute Ω as a function of temperature. This subroutine employed Eq. (1) of Chapter IV and used the vibrational frequencies of SF_6 that were reported by Brunet.[1] BOLTZ used, as input, the temperature calculated as described in the previous paragraph, and was called prior to each iteration.

The influence of a temperature change on T_1 and T_2 was easily calculated. The initial values of T_1 and T_2 were assumed to be valid for a temperature (T) of 300 K. These two relaxation times are both related to the time interval between molecular collisions of SF_6. The velocity of the molecules is proportional to $T^{\frac{1}{2}}$. The greater the velocity the shorter the time interval between molecular collisions. Thus T_1 and T_2 are proportional to $T^{-\frac{1}{2}}$. Thus

$$T_1(T) = (300/T)^{\frac{1}{2}} T_1(300), \qquad (4)$$

and a similar relation holds for T_2, where T is the absolute temperature computed as described previously. The relaxation times were recalculated before each iteration.

The influence of temperature on the density of the gas was also easily calculated. If the pressure of the gas was measured when the temperature of the gas was equal to the temperature of the sample cell (T_{sc}), then the density (N) for any temperature (T) is given by

$$N(T) = N(T_{sc})\, T_{sc}/T \qquad (5)$$

The second effect of the multiple energy level structure of SF_6 upon the absorptive process was the possibility of several transitions taking place simultaneously. As previously discussed in Chapter III, the vibrational hotband $(\nu_3 + \nu_6) - \nu_6$ makes a significant contribution to the absorption by SF_6 at 944.2 cm^{-1}. The longitudal relaxation time (T_1) for this hotband was reported to be only a few μsec, while the effective T_1 for the absorption by the vibrational ground level was reported[2] to be 122 μsec·Torr. When T_1 was very short, a very large intensity of the exciting radiation was required to saturate the absorption. The intensity required to saturate the absorption of the hotband, was well beyond the power capability of our laser.[3] Therefore, only those molecules in the vibrational ground level and $\nu_3 = 1$ level were permitted to undergo optical saturation in the theoretical procedure. This was accomplished in the computer program by calculating a

contribution to the susceptibility associated with the transition between the $\nu_3 = 0$ and $\nu_3 = 1$ state which was dependent upon the intensity of the laser radiation. Another contribution to η was calculated for the transition between the two levels of the $(\nu_6 + \nu_3) - \nu_6$ hotband which did not depend upon the intensity of the laser radiation. The total susceptibility was then the sum of these two contributions. The population figures required for these calculations were obtained from the subroutine BOLTZ as previously discussed.

Another effect that complicated the theoretical treatment of SF_6 was the Doppler (inhomogeneous) broadening of each of the absorption lines in the neighborhood of resonance with the laser. The theory presented in Chapter II assumed that absorption resulted from one homogeneously broadened line with a half-width at half-height of $1/T_2$. The Doppler broadening of the SF_6 absorption line was about 30 MHz at 300 K while the homogeneous broadening was about 8 MHz at the pressures used in these experiments. Rabinowitz[4] et al. has reported the observation of 4 absorption lines for SF_6 in the vicinity of the P(20) laser lines at 10.59-μm. These lines were displaced in frequency from the laser line by -13, -11, +4, and +10 MHz. If all of these lines were of equal intensity and the homogeneous width of each were 10 MHz, the total absorptance due to the sum of these broadened lines would be nearly independent of frequency in the vicinity of the laser line as illustrated in Fig. 1. If the locations of other SF_6 absorption lines which are located outside the 40 MHz width of the P(20) gain curve of the CO_2 laser were known, and the contributions of these lines to the total absorptance

FIG. 1. OVERLAP OF SF6 ABSORPTION LINES NEAR 10.6 LASER LINE

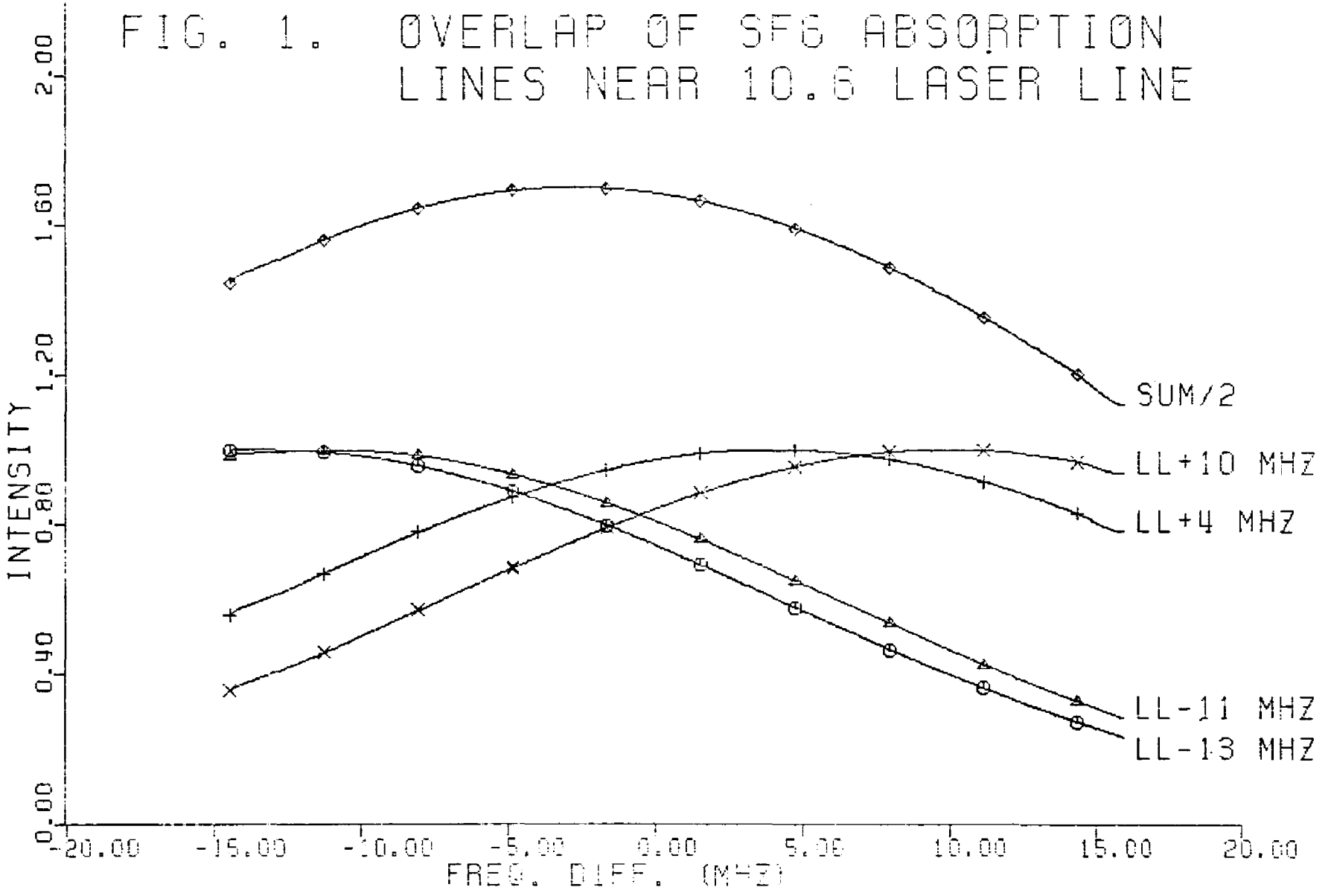

were also added to that of the four knowlines, the sum would appear even flatter. When the frequency of the laser used in this work was varied over the entire 40 MHz gain curve, no change in the absorption of SF_6 could be detected.[5] Goldberg and Yusek[6] used heterodyne methods to increase the sensitivity of saturation spectroscopy performed on SF_6 and reported that the abundance of absorption lines in SF_6 was greater than reported by Rabinowitz et al. Goldberg and Yusek observed many weaker lines among the same strong lines observed by Rabinowitz. Goldberg and Yusek only studied SF_6 in the vicinity of the P(16) and P(18) CO_2 laser lines at 10.59-μm, but the abundance of SF_6 lines in the vicinity of the P(20) laser line should be similar to that observed near P(16) and P(18). Since the absorption spectrum of SF_6 is nearly flat in the vicinity of the P(20) laser line, it was assumed (for the calculations involving absorption) that the laser frequency was at exact resonance with some transition so that the frequency difference (δ) between the center of the absorption line and the laser frequency was zero.

Since a phase shift in the reflectance could be produced by optical saturation in SF_6, there must be an "effective" $\delta \neq 0$. In fact, $\delta_{eff}\ T_2$ was observed to be about one. The true value of δ_{eff} depends upon all of the actual δ's associated with the various absorption lines which overlap the laser frequency. Absorption lines of SF_6 centered at a frequency greater than that of the laser, ω, where δ is positive tend to offset the dispersive effects produced by absorption lines centered at a frequency less than ω where δ is negative.

For example, if only two absorption lines of equal intensity and width were present, and ω was exactly half-way between their centers, δ_{eff} would equal zero. Mathematically speaking

$$\delta_{eff} = F(\delta_1, \delta_2, \delta_3, \cdots \delta_m) \ , \qquad (6)$$

where m is the total number of absorption lines that overlap ω. This explains why the experimental value of $\delta_{eff}T_2$ was less than the value calçulated by considering only the nearest absorption line. The lines located at -11 and -13 MHz with respect to the laser frequency tended to offset some of the changes in the velocity of the 10.6-μm wave that had been produced by the +4 and +10 lines. Because of this, the effective line center for determining phase shifts in the interference between reflected waves was located somewhere between the -11 and + 4 lines. If the frequency of the laser output were to be varied over a $\pm$ 10 MHz range and $\delta_{eff}T_2$ computed by means of Eq. (11) of Chapter III for each setting, the location and relative contributions to the absorption of these lines may be determined. Before accurate results could be extracted from the data, however, the theory presented in Chapter III would have to be generalized to allow for Doppler broadening (in addition to pressure broadening) of each of the absorption lines. Also, the formulas for the exact phase shift would have to take into account the presence of the several overlapping lines.

For all purposes except that of calculating the phase shift, exact resonance was assumed as stated previously. The problem

of what effective linewidth to use, in the presence of homogeneous and heterogeneous broadening, plus cross-relaxation between the various velocity groups in the Doppler curve was still not resolved. It was finally assumed that the laser radiation would "burn" a homogeneously broadened "hole" out of the featureless SF_6 absorption band. Therefore a value for T_2 was obtained from the experimentally measured homogeneous linewidth.

It is unfortunate that the saturable absorber that was chosen for study had such a complex interaction with the laser radiation. It is very likely that some inaccuracies were introduced into this treatment by the assumptions and approximations that were necessary to apply the theory to SF_6. A saturable absorber with a less complex energy level structure would have been easier to treat theoretically.

B. TRANSMITTANCE EXPERIMENTS

In Chapter III, a series of experiments were described in which the transmittance of CO_2 laser radiation by a sample cell containing SF_6 was measured. In this section, the results of these experiments will be presented, together with the results predicted by means of the theory presented in Chapter II (and modified as described in Section A). Before the calculations could be performed by the IBM 360/65 computer, the necessary parameters which describe the properties of the laser beam, the sample, and the sample cell had to be entered into the computer program as data. All of the

fundamental constants required by the computer program such as Planck's constant, Boltzman's constant, Avogadro's number, the velocity of light, ϵ_o, μ_o, and π were obtained from standard sources[7] and permanently stored in the computer program.

The properties of the laser beam which were required as input data were the peak intensity of the laser beam, the 1/e radius of the beam (3.4 mm), the divergence of the beam (0.79 mrad), the distance from the exit mirror of the laser to the sample cell (2.03 m), the angle of polarization of the laser output (90^o) and the wavelength of the laser radiation (10.59103-μm). The last named figure was obtained from the literature,[8] and the rest were obtained experimentally by the author.

The material parameters which describe the optical behavior of SF_6 were T_1 (122 μsec·Torr)[2], T_2 (20 nsec·Torr),[4,9,10] the absorption coefficient β(46 $m^{-1}Torr^{-1}$),[1] and the center frequency of the absorption line (10.591035-μm). In order to make $\delta = 0$, the wavelength at the center of SF_6 absorption line was set equal to the P(20) CO_2 laser line. The electrical conductivity (σ) and the magnetic conductivity (σ_m) were entered as zero. The contribution to the refractive index due to degrees of freedom in SF_6 molecules other than those responsible for the transmission were neglected. In other words, the host medium was taken to be a vacuum. The pressure of the gas was experimentally measured with a McLeod guage, and the initial temperature of the gas was assumed to be equal to the temperature of the sample cell (303.3 K). The transition dipole moment (m_e) was calculated by the program from the above parameters in accord with

$$m_e = \left(\frac{\epsilon_o c_o \beta n}{\omega_o T_2 N \Omega}\right)^{\frac{1}{2}} \qquad (7)$$

where ω_o is the angular frequency of the SF_6 absorption line, n is the refractive index of the host medium, and c_o is the speed of light in a vacuum.

The optical properties of the sample cell which were required by the theoretical procedure were the refractive index of the windows (n=1.454462),[11] the thickness of the windows (6.49809mm), the absorption coefficient of the windows (0), and the distance between the inside faces of the windows (100.0006mm). Since the average transmittance of the evacuated sample cell (averaged over all interference effects) was measured to be 0.871, the thickness of each window and the length of the sample cell used in the theoretical calculations were selected to give this experimental result. For example, each of the two cell windows was measured to be about 6.50mm thick. The computer was programmed to calculate the reflectance of the cell containing SF_6 at a pressure of 10 Torr. This pressure was used to insure that the contributions to the reflectance by the exit window would be negligible. The reflectance due only to the entrance window (presumed initially to be 6.5000mm thick) was obtained in this way, and then the thickness of the window was varied by a small amount until a theoretical reflectance of 0.064 was obtained. (The two windows were always presumed to be identical.) This same procedure was repeated assuming a SF_6 pressure of zero, this time, the cell length (presumed initially to be 100.0000mm long)

was varied by a small amount until the total reflectance of the cell became 0.128 (a 0.001 loss was assumed).

The input parameters having been determined, the computer was programed to calculate the optical properties of the sample using the data appropriate for the experiments actually performed. The results may be seen in Figs. 2A and 2B, where the transmittance of SF_6 as a function of the intensity of the laser radiation is presented. Runs using four different pressures of SF_6 and two different SF_6 - He mixtures are shown. The solid lines in Figs. 2A and 2B are the theoretical predictions and the points were obtained from the experimental data. The root-mean-square (rms) deviations (of the theoretical from the experimental transmittances) for the six curves ranged from a low of 2.3% [$P(SF_6) = 0.52$] to a high of 5.2% [$P(SF_6) = 0.475$, $P(He) = 0.41$]. The total rms deviation of all six curves was 3.6%. This agreement between the theory and experimental data was quite pleasing considering the approximations involved in the theory. The estimated uncertainty in the experimental measurements of the transmittance was $\pm$ 0.04 at the lowest laser intensities and $\pm$0.02 at the intensities greater than 0.2 W/cm^2. Another pleasing aspect of this agreement was that all of the parameters used to describe the properties of SF_6 were taken from the literature and no adjustment of variable parameters were required. Most other workers in this field have varied T_1 and β to obtain a theoretical fit to their experimental data.

When helium was added to the sample cell as a buffer gas, it tended to decrease the SF_6 relaxation times T_1 and T_2. Thus a

FIG. 2A. SATURABLE BEHAVIOR OF SF6 TRANSMITTANCE EXPERIMENTS

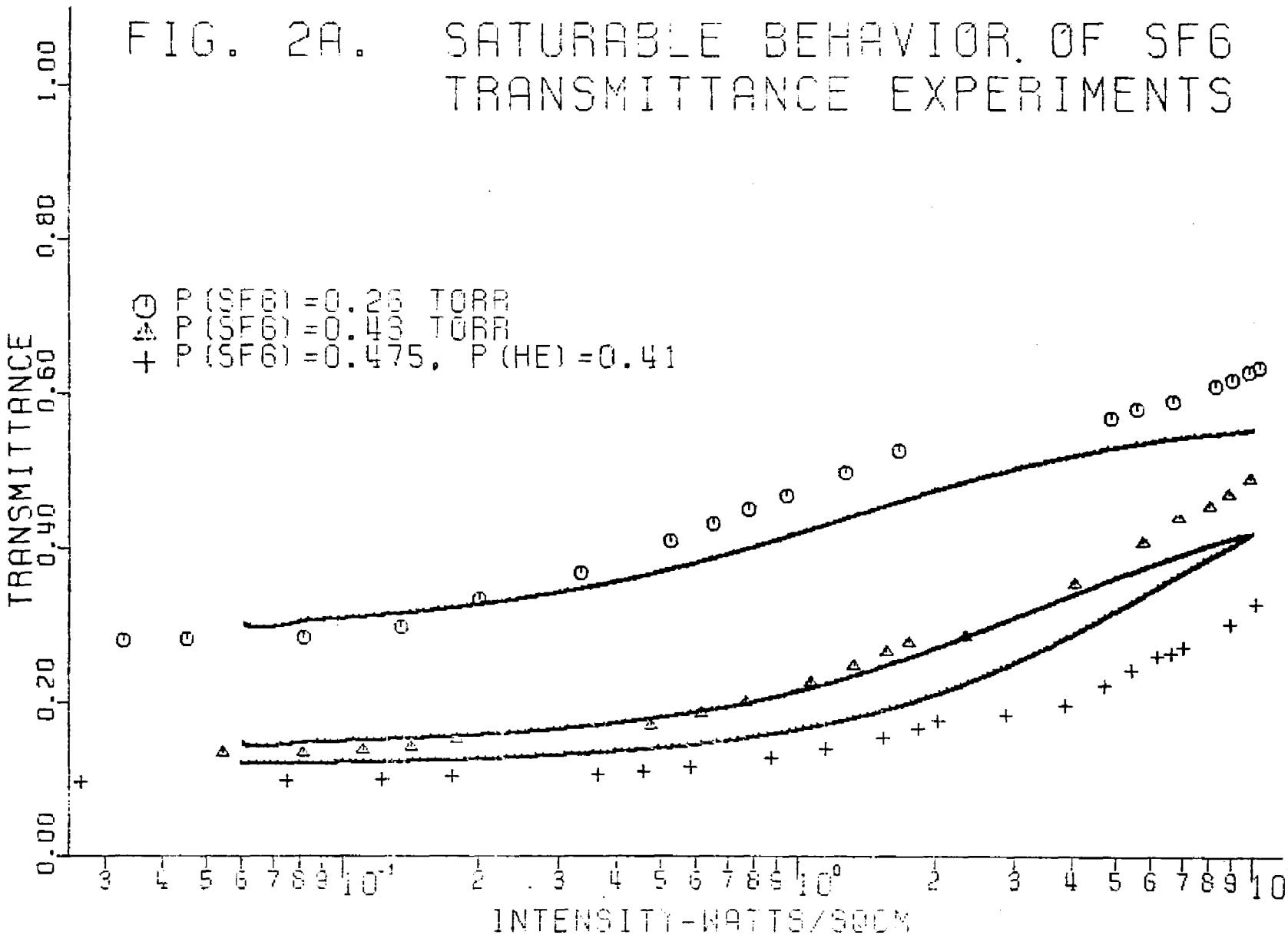

FIG. 2B. SATURABLE BEHAVIOR OF SF6 TRANSMITTANCE EXPERIMENTS

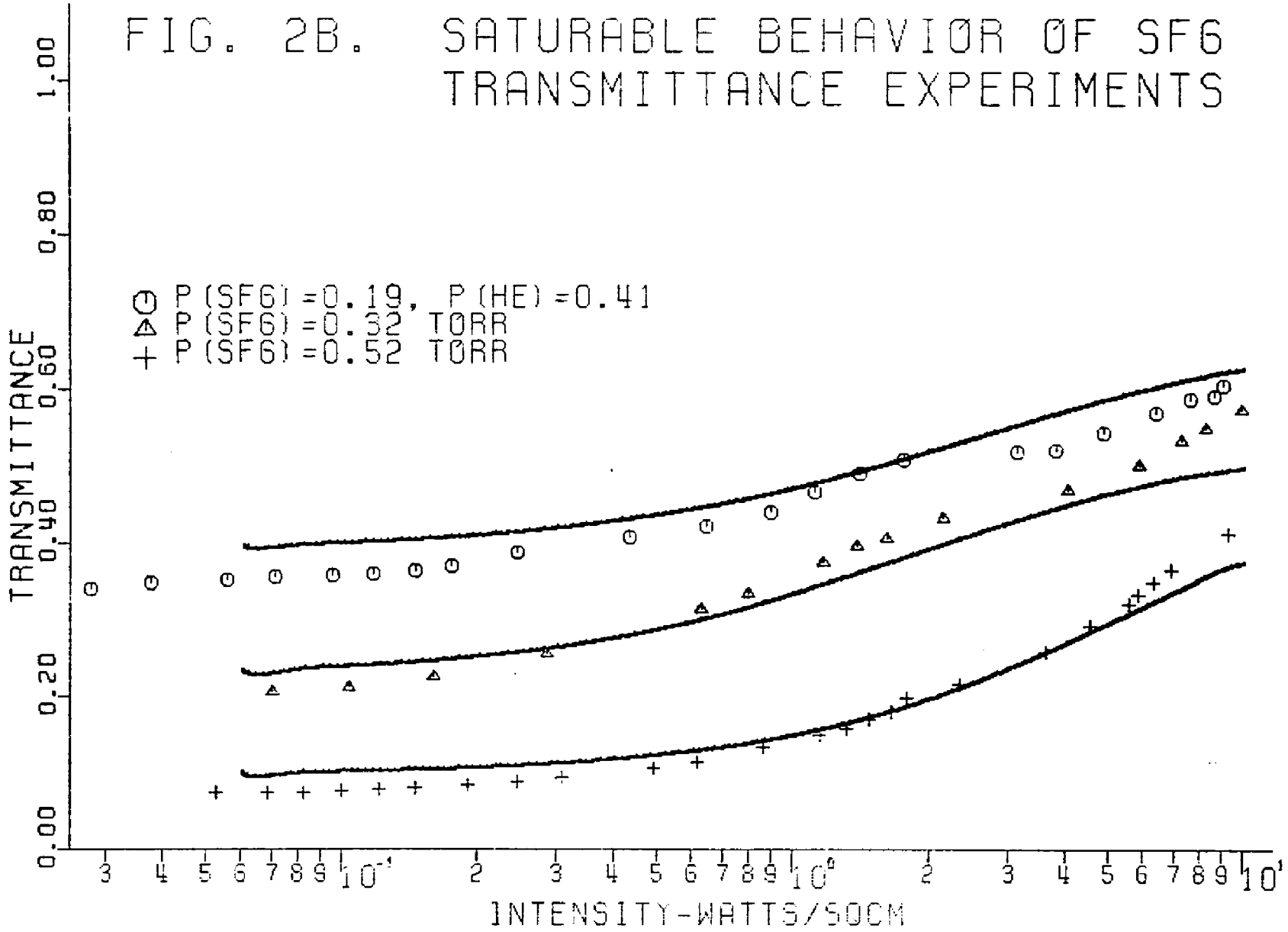

greater irradiance was required to produce the same degree of saturation when helium was present than was the case when helium was absent. The effects of helium upon saturation has been observed before by others.[2] In the application of the theory to the treatment of the SF_6-He mixtures it was assumed that the collisional cross-section of He was equal to that of SF_6. This assumption roughly agrees with the experimental collisional evidence from the literature.[2,10] Therefore, the total gas pressure in the cell was used in the calculations of T_1 and T_2, but only the partial pressure of SF_6 was used to calculate the absorption coefficient. The experimental results for the transmittance of the SF_6-He mixtures were not in as good agreement with the theoretical calculations as were the experimental results for the pure SF_6 samples.

C. REFLECTANCE AND TRANSMITTANCE EXPERIMENTS

The experiments in which the Nova minicomputer was employed were designed to obtain measurements of the reflectance of the sample cell as well as the transmittance. Thus the theoretical procedure used in section B to calculate the exact thicknesses of the cell windows could be checked experimentally. By good fortune, the theoretical reflectances associated with the chosen window thickness matched the measured reflectances within experimental error.

The same input parameters needed for the theoretical treatment of the transmittance only experiments were employed in the calculations discussed in this section. In these experiments (which

will be called Nova experiments) the length of the sample cell was varied, so the computer was programed to predict the effects of this variance upon the optical properties of the sample. Calculations were performed for eight different cell lengths over a $\lambda/2$ interval. The eight values obtained for each of the optical properties could be averaged if desired. The average temperature of the sample (and thus the initial gas temperature) in the Nova experiments was higher (313.3K) than that used in the"transmittance only"experiments. This temperature increase decreased the density of the gas and thus lowered the effective absorption coefficient. Finally the computer was programed to compare the experimental and theoretical reflectances of the sample cell system.

As in the "transmittance only" experiments, the experimental results obtained at four different SF_6 pressures and for two different SF_6-He mixtures were selected for presentation. The optical properties of SF_6 as a function of the intensity of the incident radiation are displayed in Figs. 3A-3F. The solid lines represent the theoretical calculations and the points were obtained from the experimental data. The rms deviation of the experimental points from the theoretical curves for the six sets of transmittance data ranged from 1.4% [$P(SF_6)$ = 0.30, P(He) = 1.17] to 3.9% [$P(SF_6)$ = 0.25] and the rms deviation for all six curves combined was 2.8%. The rms deviations for the six reflectance curves ranged from 0.20% [$P(SF_6)$ = 0.30, P(He) - 1.17] to 0.95% [$P(SF_6)$ = 0.25] and the rms deviation for all six curves combined was 0.58%. The uncertainties in the experimental measurements of the transmittance were estimated

FIG. 3A. SATURABLE BEHAVIOR OF SF6
P(SF6)=0.25 TORR

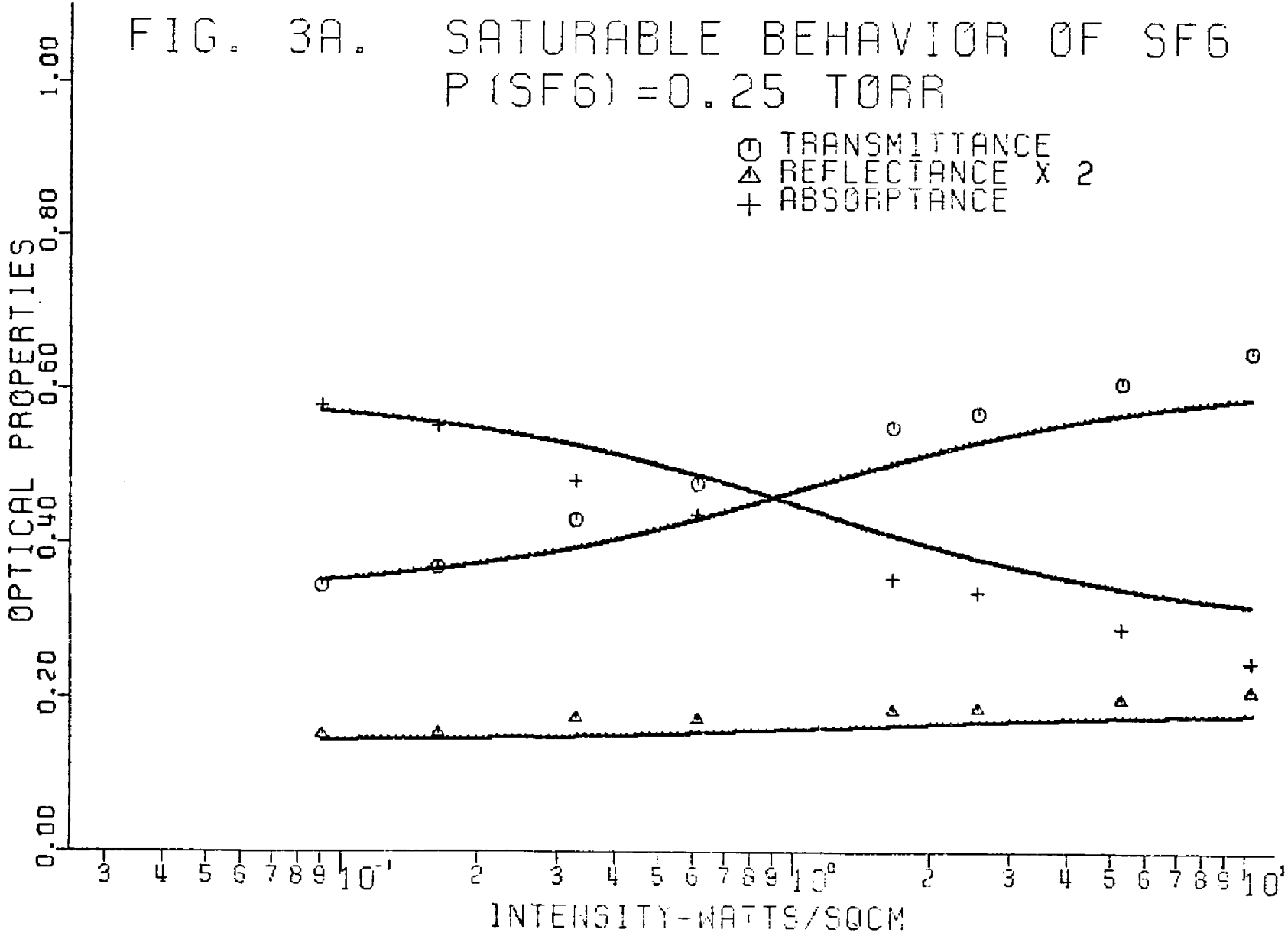

FIG. 3B. SATURABLE BEHAVIOR OF SF6
P(SF6) = 0.34 TORR

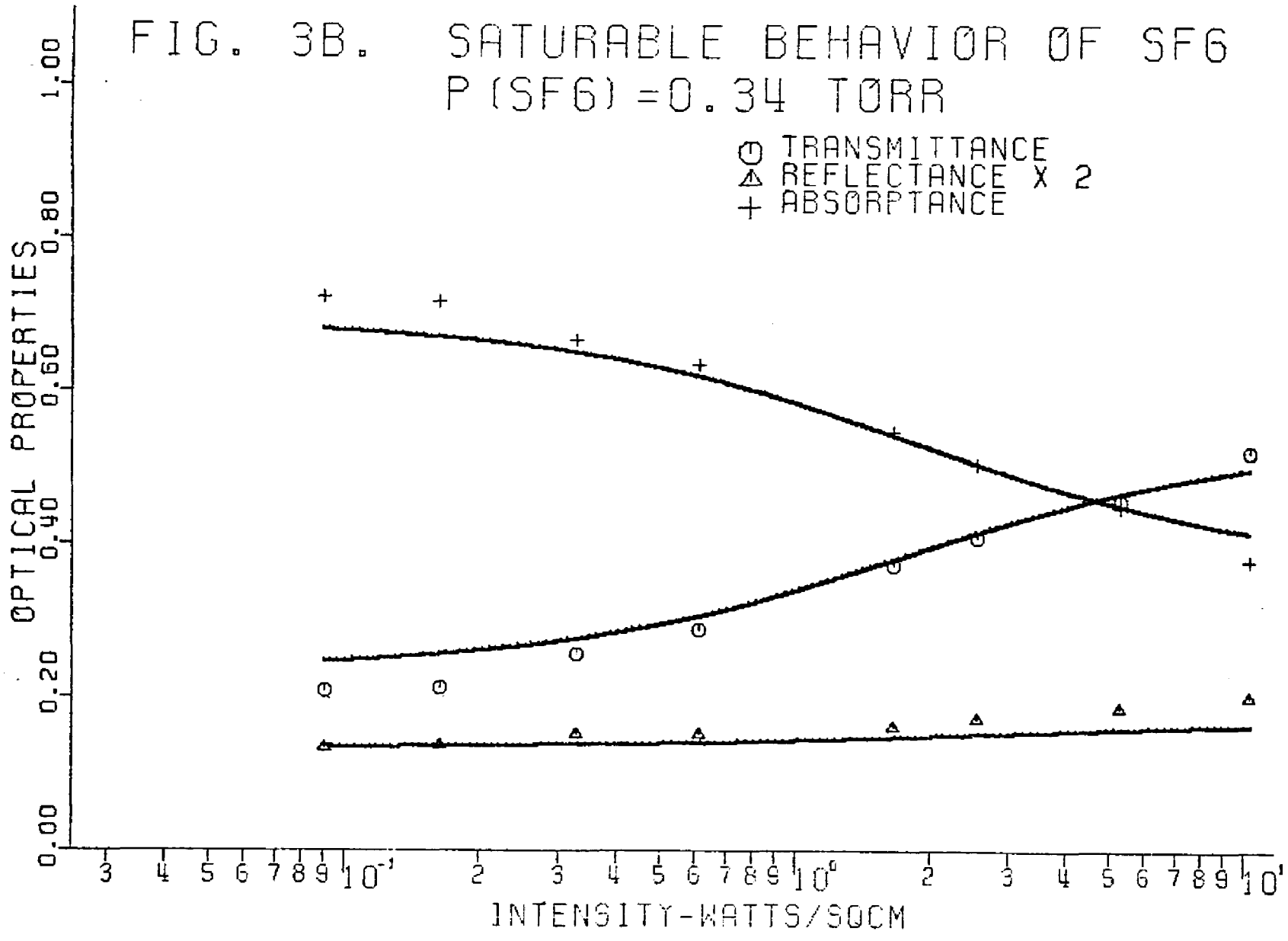

FIG. 3C. SATURABLE BEHAVIOR OF SF6
P(SF6) = 0.43 TORR

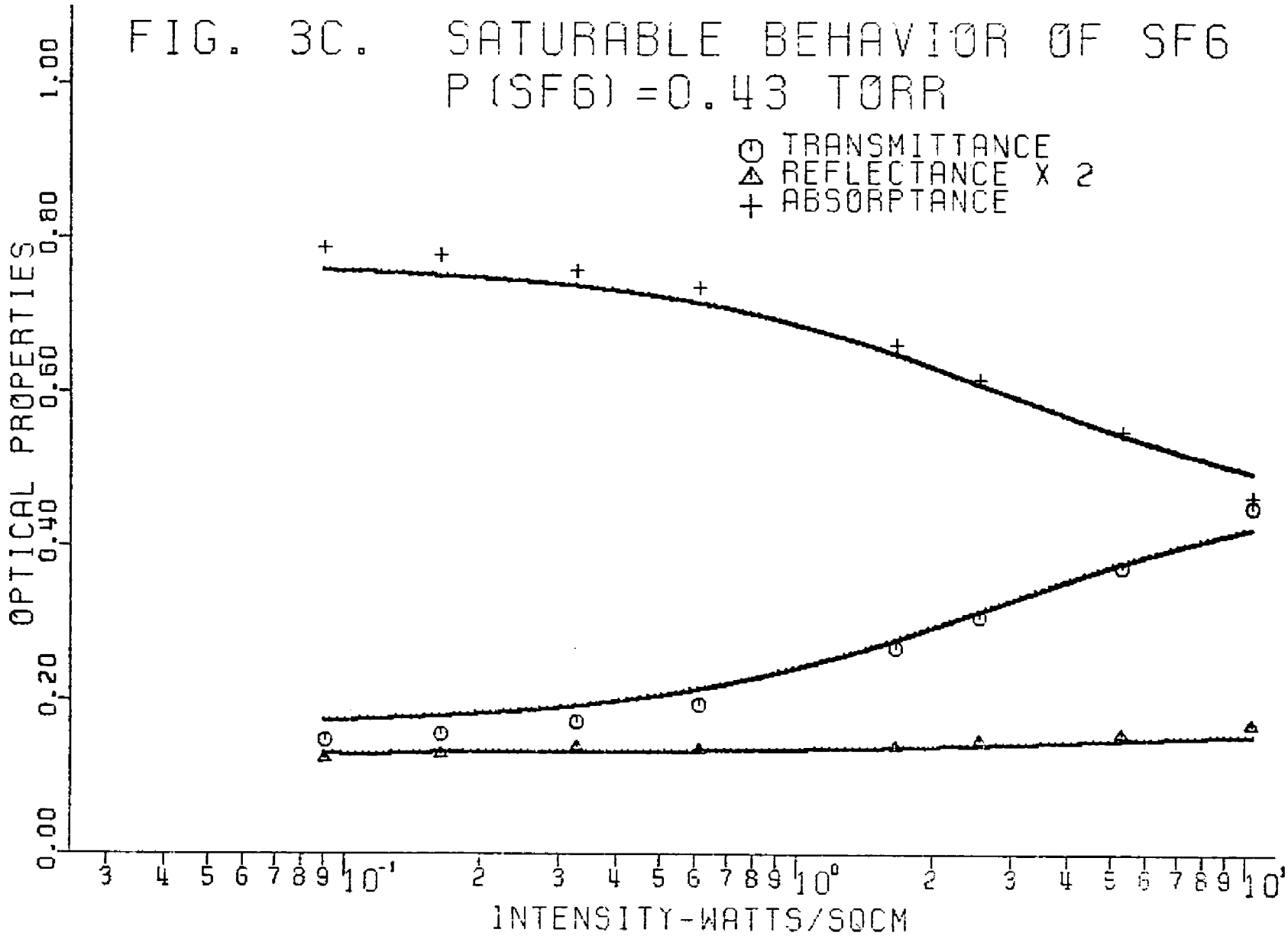

FIG. 3D. SATURABLE BEHAVIOR OF SF6
P(SF6) = 0.61 TORR

FIG. 3E. SATURABLE BEHAVIOR OF SF6
P(SF6) = 0.30, P(HE) = 1.17

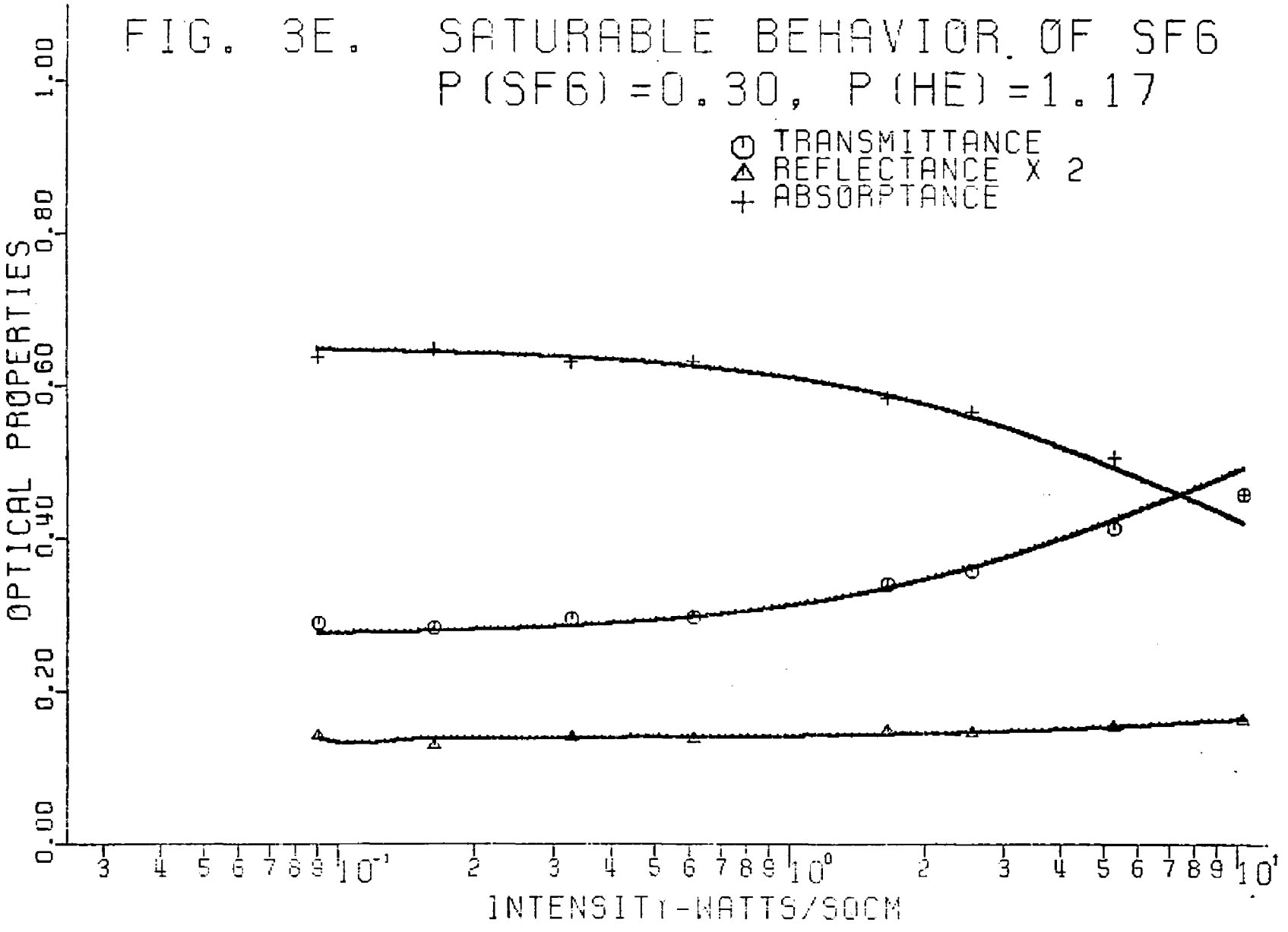

FIG. 3F. SATURABLE BEHAVIOR OF SF6
P(SF6) = 0.56, P(HE) = 0.48

to be less than $\pm$ 0.01, in the measurement of reflectance, the uncertainties were estimated to be less than $\pm$ 0.005.

The agreement between theory and experiment was excellent for the transmittance and satisfactory for the reflectance curves. The same material parameters were used for these calculations as were used for the theoretical calculations of the "transmittance only" experiments. No adjustments in the values of any physical parameters taken from the literature were made. These adjustments were not necessary because the rms deviations were of-the-order of the estimated experimental uncertainties. Since the average value of the reflectance ranged between 0.06 and 0.10, the rms deviation of 0.58% indicated a 5 to 10% disagreement between the theory and the experimental data. The major source of this disagreement in the reflectance data was caused by small changes in the reflectance of the front cell window that were not taken into account by the theory. The nature of these changes varied from one run to the next. (A run consists of a measurement of the reflectance and transmittances associated with eight different irradiances for various cell lengths.) In some runs, the reflectances would be systematically high (i.e. greater than the theoretical values for all irradiances), and in other runs, low. A possible source of this error was that the thickness of the entrance window changed by a small amount due to thermal expansion. Since the greatest heating of the sample gas occurred just inside the entrance window of the cell, this window would absorb heat from the gas. A change in thickness of 0.15λ would produce a 10% change in the reflectance and the salt from

which the window was made has a thermal expansion coefficient[12] of $33 \times 10^{-6}\ K^{-1}$. A temperature change of only 7.4 K would be sufficient to produce this large change in the reflectance.

$$\Delta T = \frac{(0.15)(10.59\times10^{-8})}{(33\times10^{-6})(6.5\times10^{-3})} = 7.4\ K \qquad (8)$$

It is reasonable to expect heating of this magnitude to occur since the temperature of the gas rose in a typical case several times 7.4 K

The deliberate changes in the length of the sample cell in these experiments produced oscillatory changes (modulations) in the reflectance and transmittance of the sample system. An example of this modulation of the reflectance was presented by Fig. 8 in Chapter III. If the transmittance and reflectance of the sample system were measured as a function of the intensity of the incident radiation with the cell length fixed, the results would vary significantly depending upon the length of the sample that was chosen. If the length of the cell were an even integral multiple of $\lambda/4$, the reflectance would exhibit a greater increase with increasing irradiance than would the reflectance averaged over all cell lengths. Under the same conditions, the transmittance would exhibit a smaller increase than would the average transmittance. If the cell length were an odd integral multiple of $\lambda/4$ the dependence of the optical properties upon irradiance (again, relative to the averaged values of these properties) would be opposite to those which occurred for an even multiple. In this case, the reflectance would actually decrease with increasing laser intensity. These predicted effects are

presented in Fig. 4. These effects were also observed experimentally. These same predictions were made earlier by Macomber and Kestner.[13] In previous experimental work reported in the literature, and in the "transmittance only" experiments described previously in this work, a sample cell of fixed but unknown length was used. Therefore, there was no way of telling which curve, T(max), T(min), or T(avg), was to be expected. The simultaneous effects of cell length and irradiance upon the reflectance or transmittance can be seen most easily in a three-dimensional graph of the type presented in Fig. 5.

The contribution to the total reflectance of the sample system produced by the gradient of the refractive index within the bulk of the absorber was theoretically predicted to be quite small. In order to determine the reflectance produced from within the bulk of the absorbing gas, the compouter program was executed with the refractive index of the entrance and exit windows of the sample cell set equal to the refractive index of the vacuum. The refractive indices of air and of the matrix surrounding the absorbing centers of the gas were also set equal to the refractive index of the vacuum. This procedure insured that the only change in refractive index encountered by the laser radiation would be within the bulk of the SF_6 gas. The results of this calculation predicted a reflectance of 1.2×10^{-11} for an SF_6 pressure of 0.43 Torr.

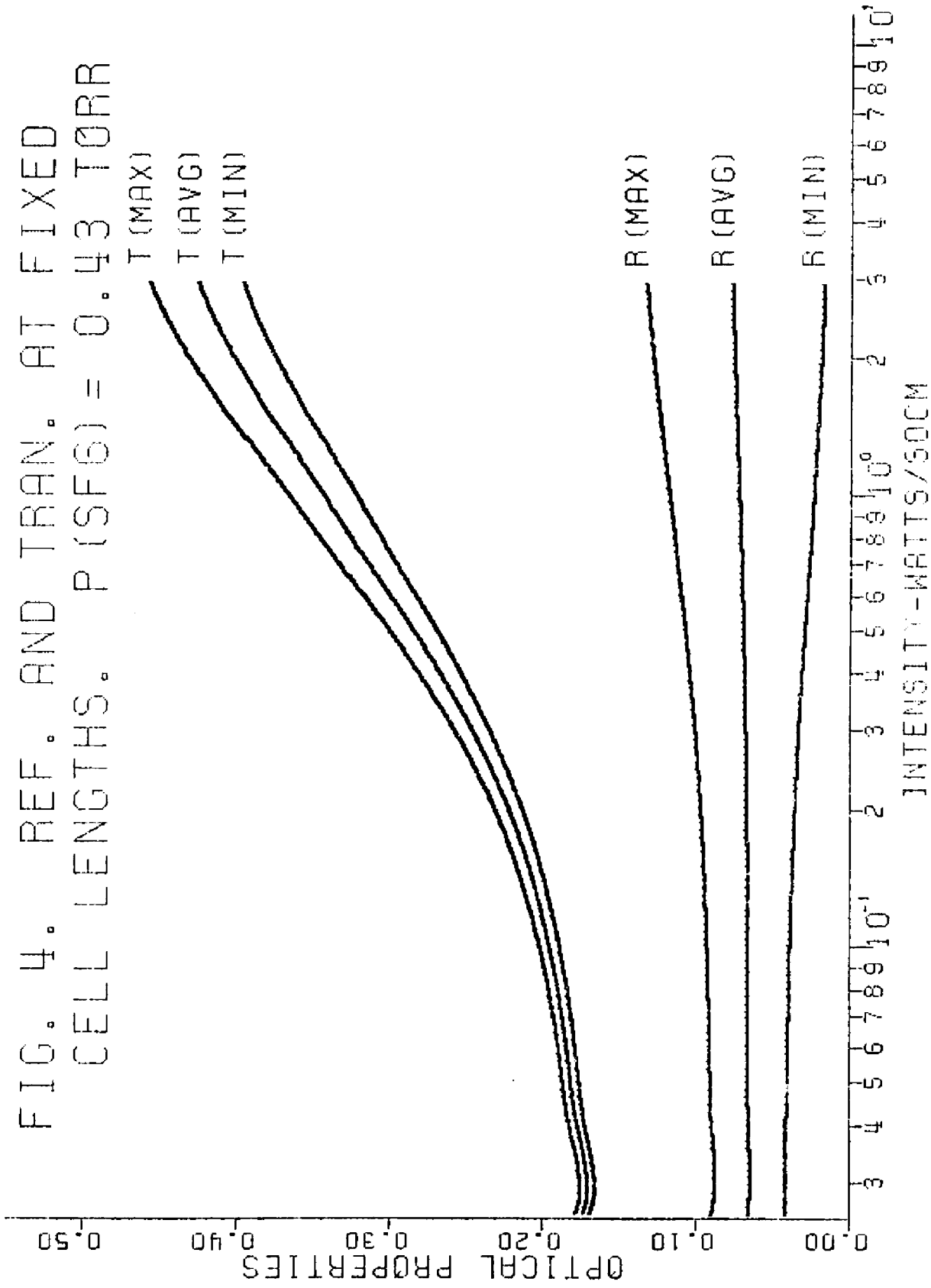
FIG. 4. REF. AND TRAN. AT FIXED CELL LENGTHS. P(SF6) = 0.43 TORR
T(MAX)
T(AVG)
T(MIN)
R(MAX)
R(AVG)
R(MIN)
OPTICAL PROPERTIES
0.00
0.10
0.20
0.30
0.40
0.50
INTENSITY-WATTS/SQCM
3 4 5 6 7 8 9 10⁻¹ 2 3 4 5 6 7 8 9 10⁰ 2 3 4 5 6 7 8 9 10¹

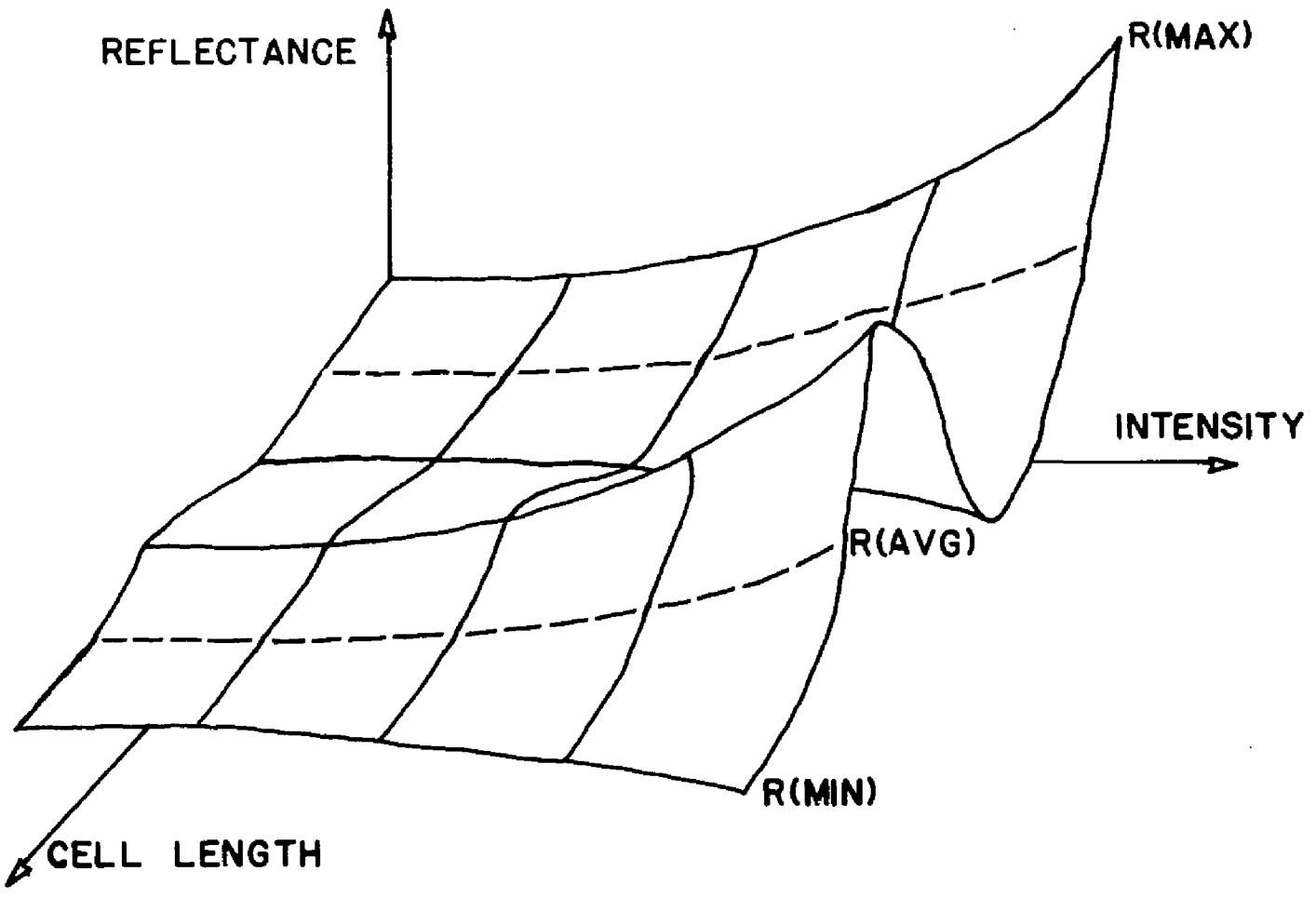

FIGURE 5. Saturable behavior of SF_6 as a function of irradiance and length of the sample cell.

D. SUMMARY AND CONCLUSIONS

In this work, the theory of the steady state optical behavior of a saturable slab was developed. The theory takes into account the optical properties of the windows of the sample cell and the interactions of the transmitted and reflected waves (whether originating at the window faces or within the body of the sample) at the sites of the molecular chromophores. Experiments were performed to test this theory. Sulfur hexafluoride gas at low pressures was confined in a cell with salt windows and irradiated by a CO_2 laser beam. The average reflectance, absorptance, and transmittance of the entire sample system was measured as the length of the sample cell was continuously varied over several $\lambda/2$. It was necessary to determine the effects produced by bulk heating of SF_6 upon the optical properties of the absorber in order to correctly interpret the experimental data on optical saturation. The empirically determined heating effects were incorporated into the theoretical procedure and the corresponding optical properties of SF_6 were computed by means of the theory. The agreement between the theoretical calculations and the experimental results were excellent even without optimization of the parameters obtained from the literature.

The experimental portion of this work measured two properties of a sample system undergoing partial optical saturation that have not been reported in the literature. One was the reflectance of the sample system and the other was the interference effects produced by varying the length of the sample cell. It was suggested that the

phase relationship of these interference effects as a function of the degree of saturation could be used to compute the location of the center of various absorption lines in SF_6 and other gases.

This work was a preliminary study in that only one saturable absorber was studied. A continuation of this work would require the theoretical and experimental study of several other saturable absorbers. A continuation of the thermal conductivity experiments presented in Chapter IV might produce information about vibrational energy transfer between identical molecules. Finally, a most interesting continuation of this effort would involve the study of phase changes in the interference between the waves reflected from the entrance and exit windows produced by optical saturation. Techniques which employ this effect might be used to determine effective homogeneous linewidths and to resolve closely-spaced absorption lines which overlap due to Doppler broadening. This method would complete with the current techniques in saturation spectroscopy.

In conclusion, the theoretical procedure described in this work generalizes the laws of Bouguer, Lambert, Beer, Snell, and Fresnel so that they may describe reflectance, absorptance, and transmittance of saturable optical materials.

REFERENCES

1. H. Brunet, IEEE J. Quantum. Electron., 6, 678 (1970).
2. J. I. Steinfeld, I. Burak, D. G. Sutton, and A. V. Nowak, J. Chem. Phys., 52, 5421 (1970).
3. J. J. Armstrong and O. L. Gaddy, IEEE J. Quantum. Electron., 8, 797 (1972).
4. P. Rabinowitz, R. Keller, J. T. LaTourrett, Appl. Phys. Lett., 14, 376 (1969).
5. F. Shimizu [Appl. Phys. Lett. 14, 378 (1969)] reported a factor-of-two variation in the absorptance of SF_6 when the frequency of the exciting P(20) CO_2 laser line was varied over a $40MH_z$ range.
6. M. W. Goldberg and R. Yusek, Appl. Phys. Lett., 17, 349 (1970).
7. E. R. Cohen and B. N. Taylor, J. Phys. Chem. Ref. Data, 2, 663 (1973).
8. R. C. Weast, Ed., Handbook of Lasers, (The Chemical Rubber Co., Cleveland, Ohio, 1971) p 331.
9. N. G. Basov, O. N. Kompanets, V. S. Letokhov, and V. V. Nikitin, Soviet Physics-JETP, 32, 214 (1971).
10. C. K. N. Patel and R. E Slusher, Phys. Rev. Lett., 20, 1087 (1968).
11. M. J. Dodge and I. H. Malitson, Annual Meeting of the Optical Society of America, Houston, Oct. 1974, ThD12.
12. E. Pietsch, ed., Gmelins Handuch der Anorganischen Chemie (Verlag Chemie, G.M.B.H., Berlin, 1938) vol. 22, p 363.
13. J. D. Macomber and N. R. Kestner, J. Appl. Phys., 40, 3218 (1969).

APPENDIX 1

AN APPARATUS FOR THE SIMULTANEOUS MEASUREMENT OF REFLECTANCE, ABSORPTANCE, AND TRANSMITTANCE[1]

A. INTRODUCTION

This appendix describes a simple, inexpensive apparatus for the accurate measurement of the angular dependence of the reflectance, R, absorptance, A, and transmittance, T, of small objects illuminated by a laser having a continuous output. The angle of polarization is preset from 0° to 90° for a given run; during the run, RAT data are continuously and automatically recorded at angles of incidence between 3° and 75°. The root-mean-square difference between the RAT data and numbers obtained from theory is less than 0.4%.

We were motivated to produce this apparatus by our desire to study the laser-induced nonlinear optical properties of materials, especially reflectance. Our data in these studies consists of the difference between measured values of the reflectance of samples illuminated by the laser and the corresponding theoretical values calculated from the standard formulae for linear optical behavior. Prior to the construction of the device described in this paper, we found ourselves unable to distinguish between those departures from theoretical linear behavior produced by genuine nonlinearities and those due to experimental error. While we have yet to detect the nonlinearities which we had hoped to find under conditions

of intense laser irradiation, we now feel confident that we can accurately measure the optical properties of our sample. This confidence is inspired by the gratifying agreement between data obtained by means of the RAT measurement assembly, under conditions of low-level laser illumination, and the results expected from the theory of linear optics. We have also found that this apparatus is very convenient for measuring the beam profile and divergence of the laser output, and for refractive indices of samples and also to study diffuse reflectors and transmitters of light, in order to ascertain how closely the latter follow Lambert's Law. Finally, we should like to point out that this apparatus is a potentially useful tool for teaching the laws of elementary optics (e.g., for a lecture demonstration of Fresnel's Law).

The RAT measurement assembly has three basic components: a light source, a goniometer, and a detection system (Fig. 1). Each component is compact, light-weight, inexpensive, and constructed of easily assembled parts. The light source, L, produces a beam of light, polarized by the polarizer, P, which is then incident upon the sample, S. The sample is mounted on the goniometer, G, which is constructed in such a way that the sample is continuously rotated about an axis passing through the center of its entrance face. In this way, all angles of incidence from 0° to 90° are generated. The detection system consists of several parts. First there are three photoelectric transducers, V. One of these V_R, is mounted on the goniometer in such a way that it moves about the rotation axis continually monitoring that portion of the incident beam that is

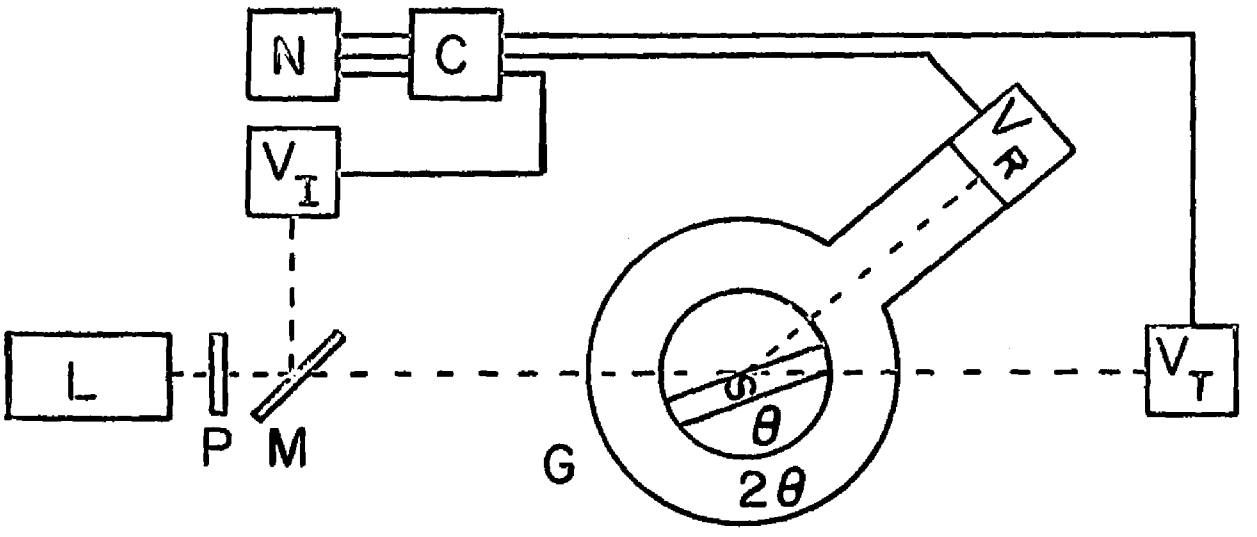

FIGURE 1. Block diagram of the reflectance, absorptance, and transmittance (RAT) measurement assembly, with light source, L, polarizer, P, beam splitter, M, sample, S, goniometer, G, detector, V_I, V_R, V_T, analog computer, C, and output device, N.

reflected by the sample. Another transducer, V_T, is mounted permanently on the side of the sample directly opposite the light source. This intercepts that fraction of the light beam that is transmitted by the sample. The last transducer, V_I, is also fixed in position, slightly off the optic axis, between the light source and the sample. A beam splitter, M, mounted on the axis between the light source and the sample, reflects a fixed fraction of the incident beam into this detector. The electrical signals from V_R, V_T, and V_I are continuously fed to an electronic signal processor, C, which computes the reflectance, absorbance, and transmittance of the sample and delivers electrical signals proportional to these properties to one of several possible output devices, N, for permanent recording.

B. DESIGN AND CONSTRUCTION

1. Light Source

The light source is a Spectra Physics Model 133 He-Ne laser with output beam intensity of about 13 mW (measured by means of a Cintra Model 202 thermal radiometer). The beam profile is nearly Gaussian in shape. The beam diameter (distance between the points at which the intensity had dropped to $1/e^2$ of its peak value) was 0.70mm at the exit aperature and the divergence (full angle between $1/e^2$ points) was 5.76 milliradians. This laser operates continuously at a wavelength of 632.8nm. The beam intensity is quite stable (less than 1% drift per minute), although we did not investigate the possibility of fluctuations faster than about 1 Hz. Because the output of this device is not polarized, we placed a Polaroid

polarizing sheet between it and the sample. The polarizer was attached to an Ealing Scientific Corporation rotatable mount (Model No. 22-8767) in a plane perpendicular to the beam axis. The error in perpendicularity is small and has a negligible effect. The engraved scale and vernier fastened thereupon enabled us to set and read the angle of polarization to $\pm$ 0.3°. The polarizer transmits about 54.5% of the desired beam and about 0.02% of the unwanted polarization.

2. Goniometer

The goniometer was designed so that it could be constructed from standard precision components (purchased from Precision Instrument Corporation), with a minimum of machining. See Figs. 2-4. Some of the parts keyed in these figures are described below: their numbers appear in square brackets. A complete list of parts and their PIC catalog numbers can be obtained by writing the Authors.

The V_R platform is mounted upon a 6.35 mm diameter shaft, [19], hollowed out so that the 3.175 mm diameter shaft [1] which supports the S platform may pass through. The 3.175 mm shaft is supported by two ball bearings, [10] and [26], at the opposite ends of the 6.35 mm shaft. The 6.35 mm shaft in turn is supported by bearings [17] and [21] mounted on a turret [18] (bearing adapter) bolted, through slightly oversize holes, to the upper bearing plate [20]. A fine toothed (120 pitch) gear [25] is fastened to the bottom of the 6.35 mm shaft and serves as the V_R drive gear. The 3.175 mm shaft protrudes below the 6.35 mm shaft and is driven by a gear [29] having twice

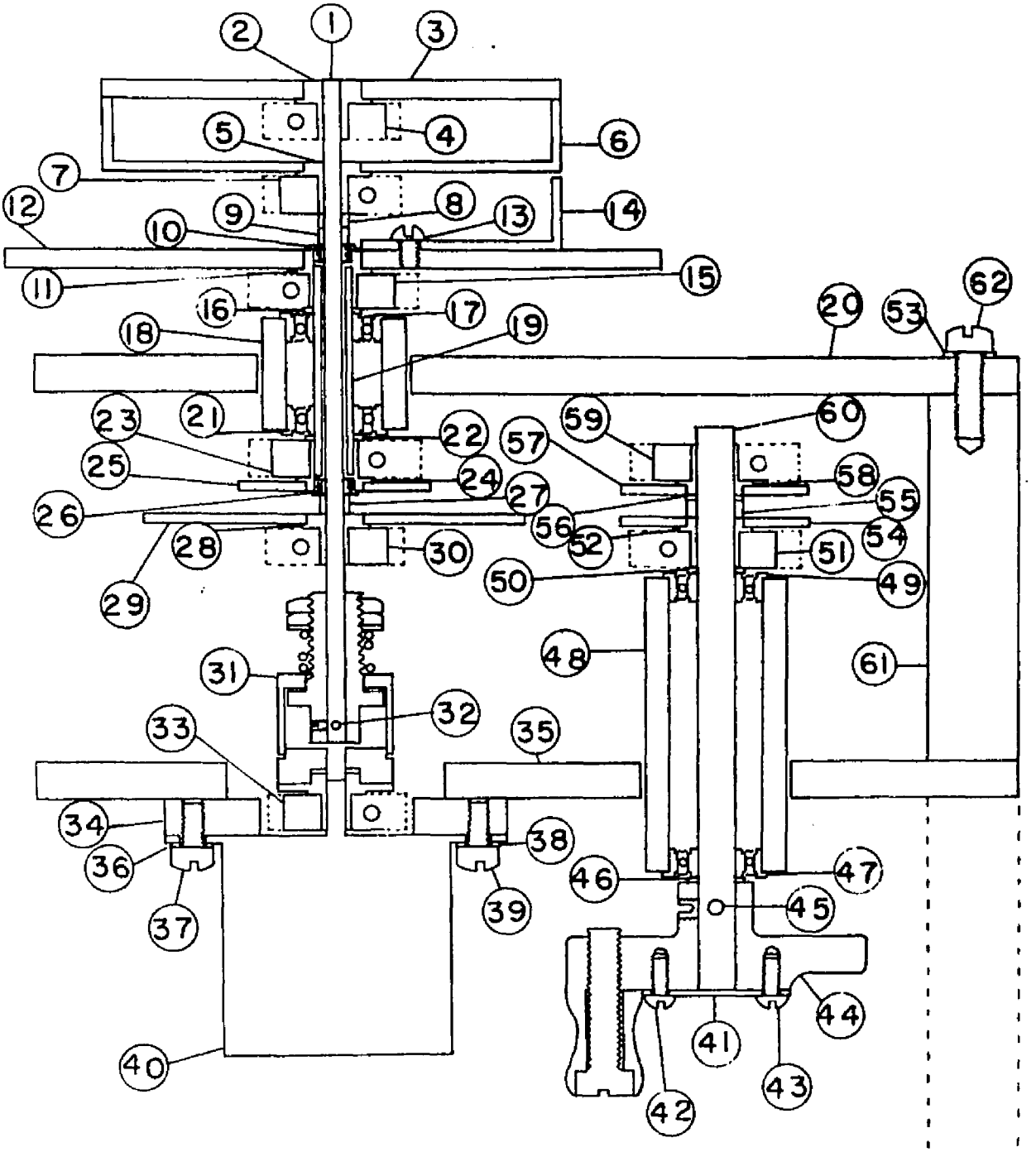

FIGURE 2. Longitudinal section of theta, two-theta goniometer through drive and coupler shafts (adjustable centers). The location of this section is shown as AA' in Figure 4.

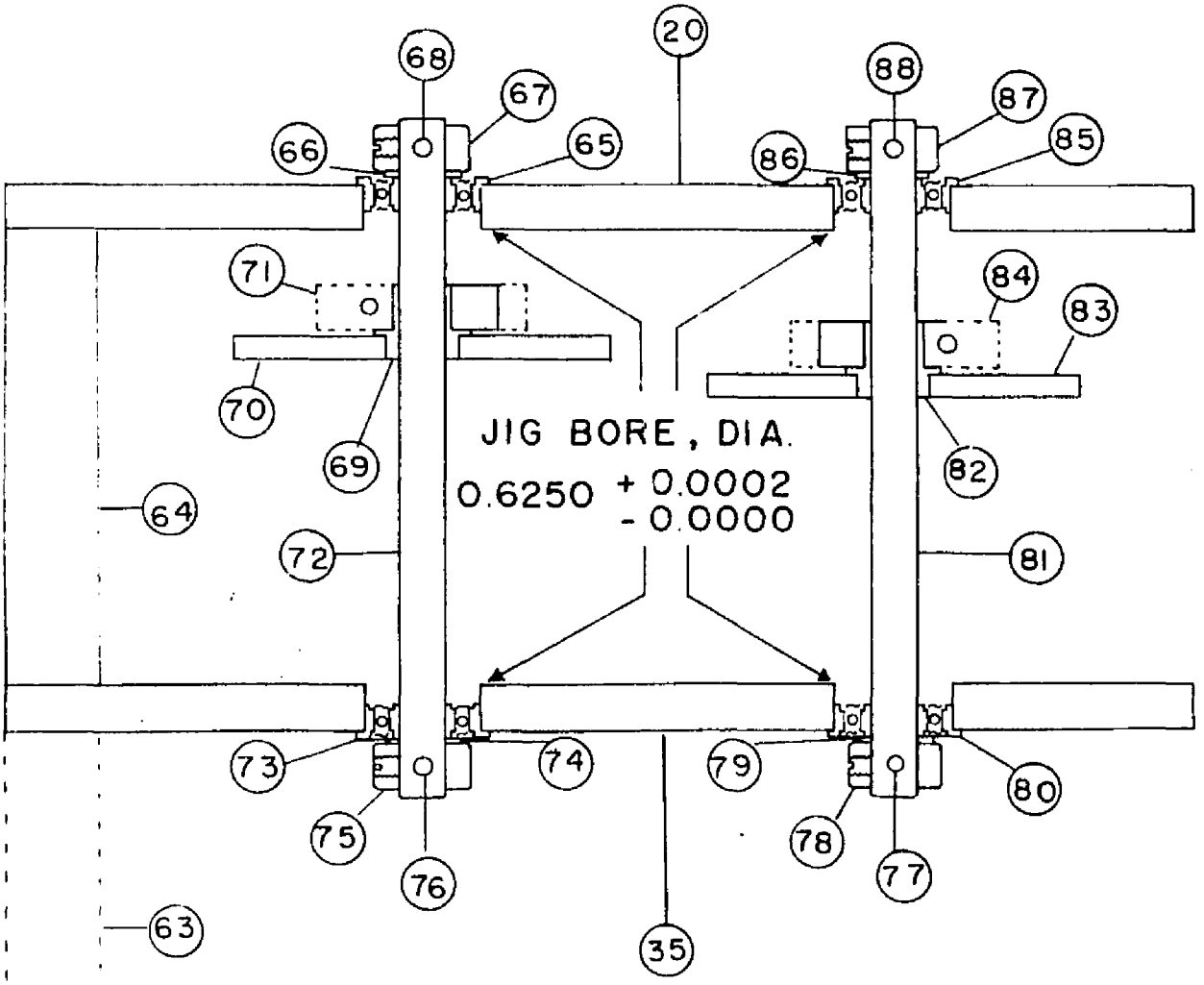

FIGURE 3. Longitudinal section of theta, two-theta goniometer, through idler shafts (fixed centers). The location of this section is shown as BB′ in Chapter 4.

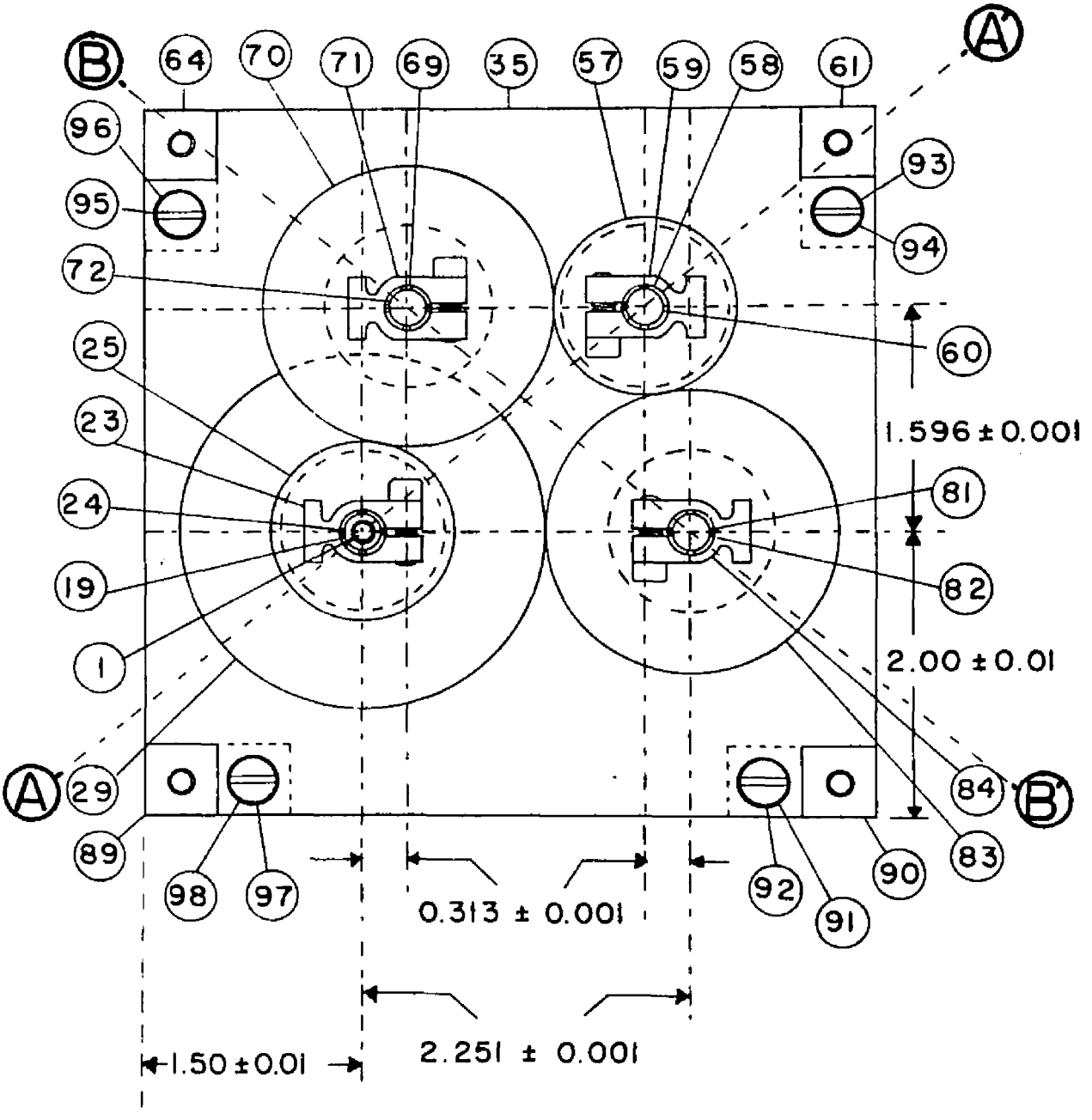

FIGURE 4. Top view of theta, two-theta goniometer, with upper bearing plate removed, showing shafts and spacer posts in cross-section, plus gears (teeth not shown) and lower bearing plate. Logitudinal sections AA' and BB' are shown in Figures 2 and 3, respectively.

the diameter of the V_R drive gear. The drive gears for the S and V_R shafts are coupled by means of a pair of gears of equal diameter, [54] and [57], fastened to a 6.35 mm shaft [60] supported by ball bearings [47] and [49] mounted on another turret [48].

A pair of idler gears [70] and [83] on separate 6.35 mm diameter shafts [72] and [81] are located on either side of the line joining the drive shafts and the coupler shafts. These gears separate the drive and coupler shafts to provide clearance for the drive and coupler gears.

The ball bearings [65], [73], [80] and [85] which support the idler shafts are mounted directly to the upper and lower bearing plates [20] and [35] thus fixing the location of the centers of these shafts. The alternation of fixed and adjustable centers permits some small adjustment to be made of the location of the drive and coupler shafts with respect to the intervening idler shafts, enabling the appropriate clearance of the meshing gears to be achieved during the assembly process. After adjustment, the turrets are pinned permanently in position through their mounting flanges into the bearing plate.

The gear train is driven by means of a Synchron 610 electric motor [40] mounted on the lower bearing plate, and coupled in-line to the lower extremity of the S shaft by means of an Oldham coupling [31]. The motor is timed to the 60 Hz ac power line and geared internally to produce one rotation of the external shaft in half an hour. The V_T table tracks the S table with sufficient accuracy so that the entire reflected beam is intercepted by the aperature of V_R

at all angles. The fine teeth on these gears may be crushed should the gear train become jammed, because of the rather high torque (0.212 N-m) of the driving motor. To prevent this the Oldham coupling is fitted with a cork-faced slip-clutch. The slipping torque on the clutch is adjustable up to a maximum of only 0.071 N-m, which is too low to crush the gear teeth. In addition to providing protection, the slip-clutch enables the motor to be overridden by a hand-crank [44] mounted onto the bottom of the coupler shaft. The hand crank can be used to rapidly reset the proper initial orientation of the S and V_R platforms with respect to the incident beam following a run. The upper (S) platform consists of a drum dial [6] topped with a gear blank [3]: the lower (V_R) platform consists of a gear blank [12] to which a vernier [14] has been fastened. The relative orientation of the two platforms can be read by means of the dial-vernier system to about $\pm \frac{1}{4}^{\circ}$.

The samples are supported on the S platform by means of an adjustable clamp fastened to the gear blank (see Figure 5). Proper alignment is achieved when the rotation axis of the shaft is tangent to the center of the entrance face of the sample. The centering is not critical, but the tangency is. If the rotation axis is not parallel to the entrance face, the reflected beam will nutate about the median plane of the detector as the sample is rotated. If the rotation axis is parallel to, but displaced from, the entrance face, the beam will first lead and then lag the position of V_R in the median plane by a distance equal to the displacement. Both the in-plane and out-of-plane tracking errors, when present, have a period of 360°.

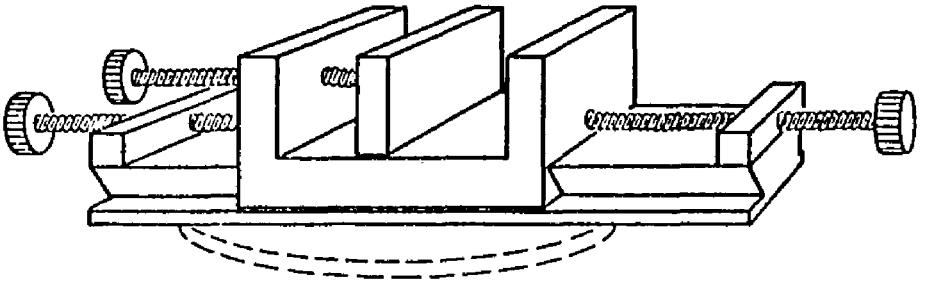

FIGURE 5. Adjustable clamp for samples fastened to upper (θ) platform of the theta, two-theta goniometer. Length of clamp is 108 mm.

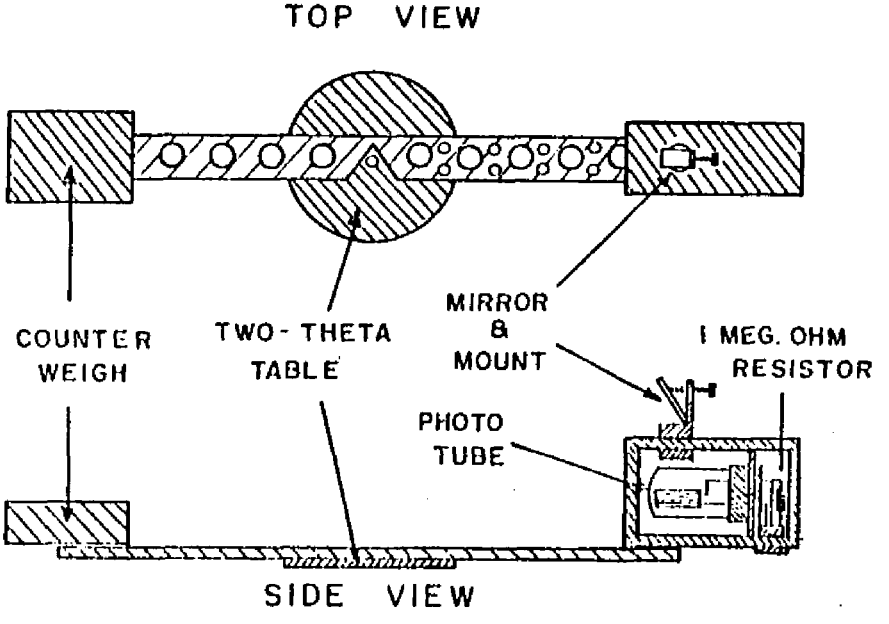

FIGURE 6. Reflectance detector mounted on the counterweighted mounting bar which is fastened to the lower (2θ) platform of the theta, two-theta goniometer. Total length of this subassembly is 465 mm. The detector head is shown in a cut-away view.

The reflectance transducer is supported on the V_R platform by a counter-weighted mounting bar, drilled to reduce its moment of inertia, and long enough to make the distance between the photosensitive surface and the rotation axis 168 mm. To prevent the detector from blocking out portions of the incident and transmitted beams at angles of incidence near 0° and 90°, V_R is mounted on its back, and a tiny (10 mm x 25 mm) "trap door" mirror is placed over the aperature. The blockage, then, is reduced from the angle subtended by V_R itself to the angle subtended by the mirror (about 3°). As a precaution against clutch slippage, we begin our scans at about -10°. We have not seen any effects attributable to slippage from $+2^\circ$ to 90°.

3. The Detection System

The photoelectric transducers V_I, V_R, and V_T, consist of vacuum photodiode tubes (1P39) mounted in small cast-aluminum boxes (Pomona, Model No. 3301). V_I and V_T are fitted with cylindrical aperatures; V_R contains a "trap door" mirror described previously. In each of the V boxes the tube socket is fastened to an aluminum septum which divides the box into two compartments. The upper compartment contains the tube; the lower compartment, a thin-film low-noise anode resistor (see Figure 6). A panel-mounted three-prong microphone connector is fastened to the wall of the box. These parts are wired to supply power to the photodiode and transmit the signal developed across the anode resistor to the analog computer, C, through a shielded three-conductor cable.

For samples of a few millimeters thick or less, the displacement of the transmitted beam by refraction through the sample is small enough so that the beam also remains on the photocathode of V_T. However, as the sample rotates, the beam traverses the photocathode surface, and as it passes across the center, the anode blocks part of the beam. For this reason, we have mounted a small piece of ground glass in front of each phototube to diffuse the incident light. The shadow effect then is very nearly independent of the orientation of the sample.

The wiring diagram of the signal processor is given in Figure 7. The first stage of each of the input channels (one for each detector head) consists of a Burr-Brown FET amplifier used in the non-inverting mode, which served as an impedance converter for the subsequent stages. Independent gain controls allow us to balance the system -- the procedure will be described later in this paper. The characteristics of those amplifiers are: 106 dB dc open circuit gain, 6V/μs slow rate, 100 GΩ input impedance, and 1.5 kΩ output impedance. Part of the output of each of these three amplifiers is tapped off to supply input to the summing amplifier, A4. Six precision (± 0.02%) resistors from Julie Research Corporation (R1-R6) assure the accuracy of the calculation of the absorbed pwer, P_A, by means of the Law of Conservation of Energy:

$$P_A = P_I - [P_R + P_T]. \qquad (1)$$

The output of the summing amplifier, together with the remaining output of the R and T amplifiers are fed to the numerator input leads

FIGURE 7. Schematic wiring diagram for the detection system of the RAT measurement assembly, including detector heads and signal processor. All resistors are rated for 2 watts and $\pm$ 5% R unless specified.

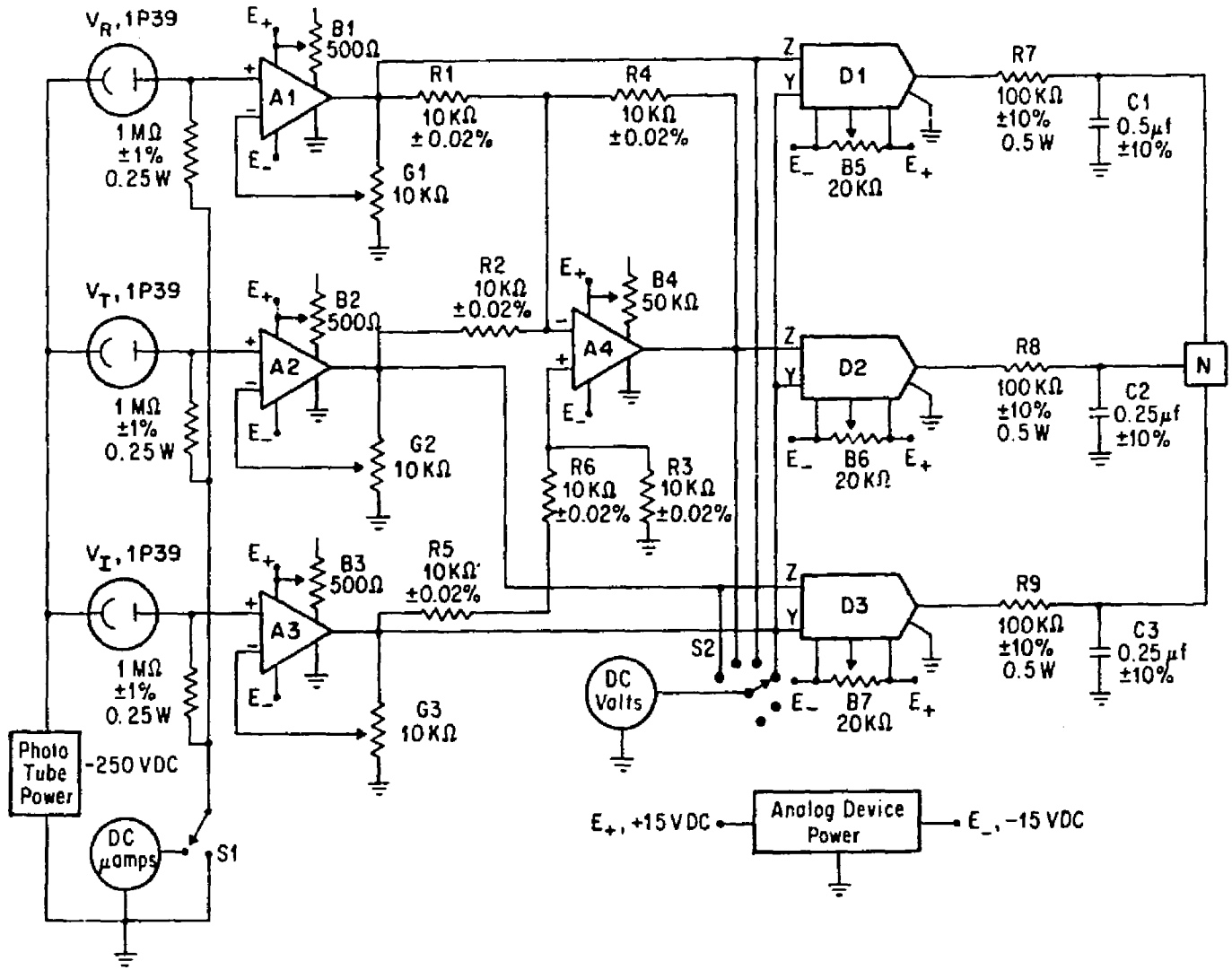
V_R, 1P39
V_T, 1P39
V_I, 1P39
1 MΩ ±1% 0.25 W
B1 500Ω
B2 500Ω
B3 500Ω
B4 50 KΩ
A1
A2
A3
A4
R1 10 KΩ ±0.02%
R2 10 KΩ ±0.02%
R3 10 KΩ ±0.02%
R4 10 KΩ ±0.02%
R5 10 KΩ ±0.02%
R6 10 KΩ ±0.02%
G1 10 KΩ
G2 10 KΩ
G3 10 KΩ
D1
D2
D3
B5 20 KΩ
B6 20 KΩ
B7 20 KΩ
R7 100 KΩ ±10% 0.5 W
R8 100 KΩ ±10% 0.5 W
R9 100 KΩ ±10% 0.5 W
C1 0.5 μf ±10%
C2 0.25 μf ±10%
C3 0.25 μf ±10%
N
S1
S2
Photo Tube Power
-250 VDC
DC μamps
DC Volts
E_+, +15 VDC
Analog Device Power
E_-, -15 VDC

of 3 precision ($\pm$ 0.1%) analog dividers, D1-D3 (supplied by Hybrid Systems Corporation). The remaining output of the I amplifier A3 is distributed among the three corresponding denominator inputs.

The three dividers, then, safeguard the measurements against instabilities in the light source. This is because these instabilities will be present in the outputs of the R, A, and T amplifiers as well, and should therefore cancel out. Our data confirm this expectation. Also, the dividers yield directly the optical properties of interest for the sample:

$$R \equiv P_R/P_I \tag{2}$$

$$A \equiv P_A/P_I \tag{3}$$

$$T \equiv P_T/P_I \tag{4}$$

All of the analog modules require input and output voltages in the -10V to +10V range, and are powered by a Burr-Brown dual power supply, Model 524 ($\pm$15 V dc) [characteristics: 200 mA output with $\leq$ 1.0 mV (rms) noise and ripple]. The same chassis which houses the processor also contains the power supply for the photodiodes. We used a small slot-range solid state 250 V dc supply (Deltron Inc., Cat. No. C-250-0-026) with $\pm$5% voltage adjustment, 0.26 ma output, 0.003% regulation (against fluctuations in line and load), and 5 mV ptp ripple. To reduce 60 Hz ripple, ac filters (R7-R9, C1-C3) were placed at the divider outputs.

The output devices, N, used in this study were of two types. A 3-pen mini-recorder (Leeds and Northrup Speedomax M, Cat. No. 803-29-29-29-000-000-000-0725-0725-0725-6-B1) with an inaccuracy in recording voltages (pen displacements) of about $\pm 0.5\%$, was the standard output device. For testing the accuracy of the overall performance of the RAT assembly, a Nova 1200 digital computer was used. The analog signal processor, C, was interfaced to the Nova through a 12 bit A/D converter. For a 10 V input the error ($\pm\frac{1}{2}$ bit) corresponds to 0.024%. The data is stored in 16 bit registers in the computer memory, and can be typed out on a teletype, displayed through a 10 bit D/A converter on a storage oscilloscope, or punched on paper tape. The paper tape can be converted to magnetic tape off-line and the magnetic tape can be used as input to an IBM 360 for further data manipulation.

C. OPERATION

1. Initialization

The signal processor, C, is initialized beginning with the signal from V_I, which is fed to A3. With the laser on and the room darkened, the gain of A3 is adjusted by adjusting G3 until the voltmeter reads nominally 9.5 volts. The laser beam is then blocked to prevent its reaching V_I, and the balance potentiometer B3 is adjusted until the output of A3 is zero volts. This effectively subtracts out the dark current of the phototube in V_I. With the laser beam again striking V_I, G3 is adjusted as before and the zeroing procedure repeated until no change in B3 is required.

Replacing the built-in voltmeter by a Keithly Model 150A Microvoltmeter permits one to achieve an accuracy of ± 1 mV in this zeroing process. The dividers D1-D3 are next balanced, with their numerator inputs shorted to ground and the denominator input to them from A3 at 9.5 V. Adjustments of B5-B7 should result in an output of 0.00 V at each channel. The use of the Keithly microvoltmeter now permits zeroing to ± 100 μV. A4, which has unit gain, is similarly zeroed with its input shorted to ground and balanced with B4.

Next, V_T is initialized, with the sample removed so that the beam exiting M impinges directly thereupon. The output of V_T is fed to A2; G2 is adjusted (using the recorder as the output device, N) until the output of D3 is 10 V. The beam is now blocked to prevent its striking V_T, and B2 is adjusted until the V_T output is zero. As in the case of the I detector, the gain and balance adjustments are repeated alternately until no further changes are required. A fine gain adjustment can now be made (utilizing the fact that the A4 and D2 outputs must be zero when either V_R or V_T receives 100% of the radiation) as follows. When the full beam entering V_T, G2 may be finely adjusted to make the D2 output (monitored by the Keithly 150A) $0(\pm 10)$ μV. The hand crank on the goniometer is then rotated until V_R eclipses V_T and the same procedure, just described for the adjustment of the gain of A2, is repeated for A1 by adjusting G1. Experience indicates that a two-hour warm-up period for the phototubes greatly improves the electronic stability of the system.

D. CALIBRATING THE ANGLES OF INCIDENCE

The sample is clamped in position on the S platform, and the goniometer is turned so that V_R is positioned a few degrees from the angle at which it would block the beam, on the side opposite the direction of rotation. When the goniometer motor is started, V_R will therefore pass through the incident beam, blocking V_R and V_T and causing the output of the R and T channels to become zero. As the rotation continues to an incident angle of 90°, V_T is again blocked and the output of the channel becomes zero. Thus, 0° and 90° angles of incidence are determined within $\pm 0.3^\circ$ and the R, T, or A of any inclusive angle of incidence is determined by a linear ($\pm 0.5\%$) interpolation between these two points.

E. MEASURING RAT OF A SLAB FROM 3° TO $\geq 75^\circ$

The sample chosen will yield results most nearly in accord with theory if it is of high optical quality, with opposite surfaces flat and parallel to a small fraction ($\sim 1/40$) of a wavelength over the illuminated area. The sample should have sufficient height so that the beam will not spill over the upper edge plus some extra length sufficient to permit its being held in the clamp. Probably 20 mm will suffice in every case. The sample should be as wide and as thin as possible so that data may be collected over a wide range of angles. No useful purpose can be served by increasing the width of thin samples beyond 100 mm, however, because at that point the limiting design parameter becomes the blockage of V_T due to

the width of the mirror on V_R used to collect the reflected beam. For thin samples, the rotation axis should very nearly bisect the entrance face; for thick ones, a slight improvement in the maximum angle of incidence can be achieved by shifting the sample ($\sim d/2$) in the direction of its trailing (e.g., "downstream" to the beam) edge.

The results of a typical run using a glass sample are displayed in Fig. 8. One can also see the effects of the calibration procedure described above. Similar measurements performed upon a Tiffen 0.3 Photar Neutral Density Filter are displayed in Fig. 9.

F. MEASURING THE OPTICAL PROPERTIES OF TRANSLUCENT MATERIALS

This apparatus can be used to measure the optical properties of diffuse reflectors and transmitters. In each case, the diffuse sample is supported on a horizontal metal rod at a fixed orientation directly over the S platform. The mounting clamp is therefore not used in these experiments. V_R, appropriately calibrated for the new arrangement, is then permitted to sweep through the range of angles of interest for each diffuser. When singly and doubly rough ground glass were tested as diffuse transmitters, the curves obtained agreed with those of previous studies[2] to within the experimental error of the latter. Tests were also made using a diffuse reflector (magnesium oxide powder on a glass plate). This sample was mounted at 45° to the incident beam and the R detector swept from -45° to 90° with respect to the sample normal. The resulting curve closely approximated that predicted by means of Lambert's Law, as expected for this type of diffuser.[3]

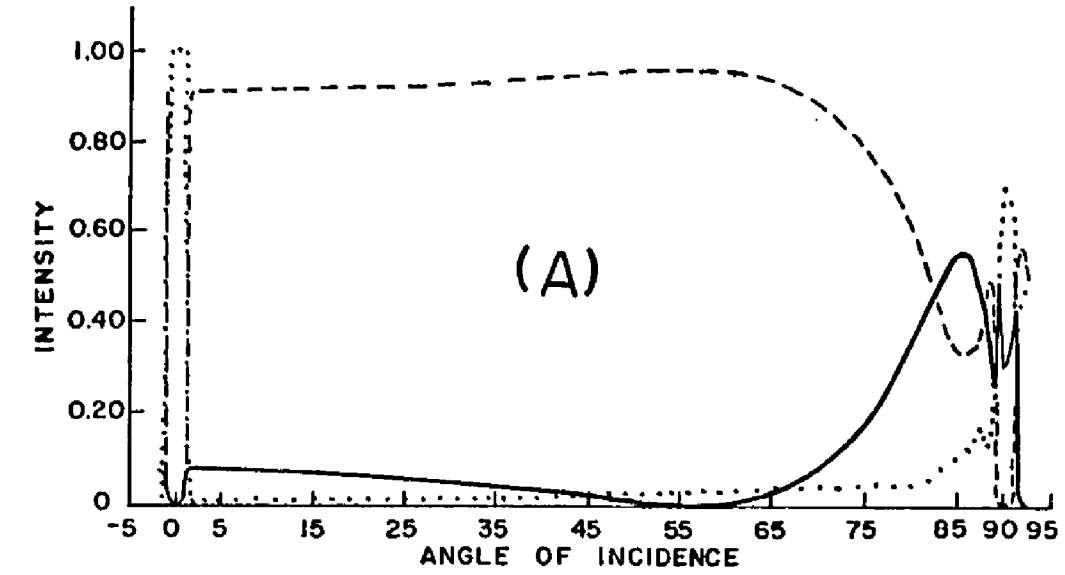

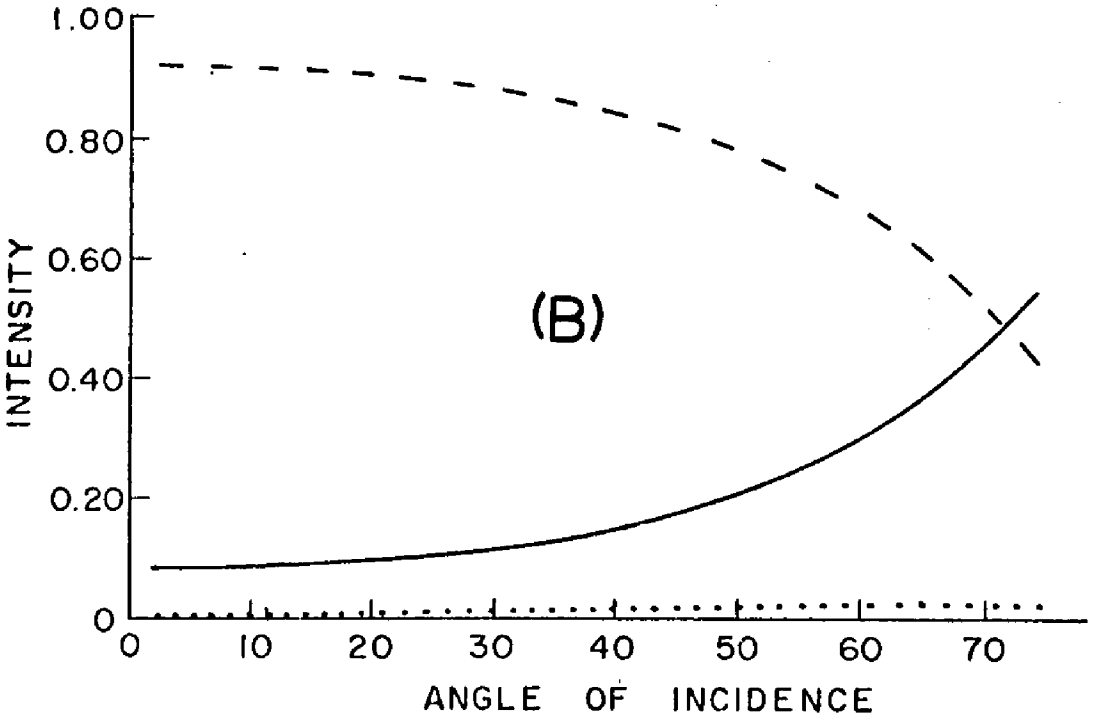

FIGURE 8. Experimentally determined reflectance (——), absorptance (•••), and transmittance (---) of 632.8 mm-wavelength by a glass flat 2.916 mm thick and 42.07 mm wide. A. angle of polarization, 2.8. Note oscillations near 0° and 90° due to eclipse of beam by reflectance detector.
B. Angle of polarization, 92.8°.

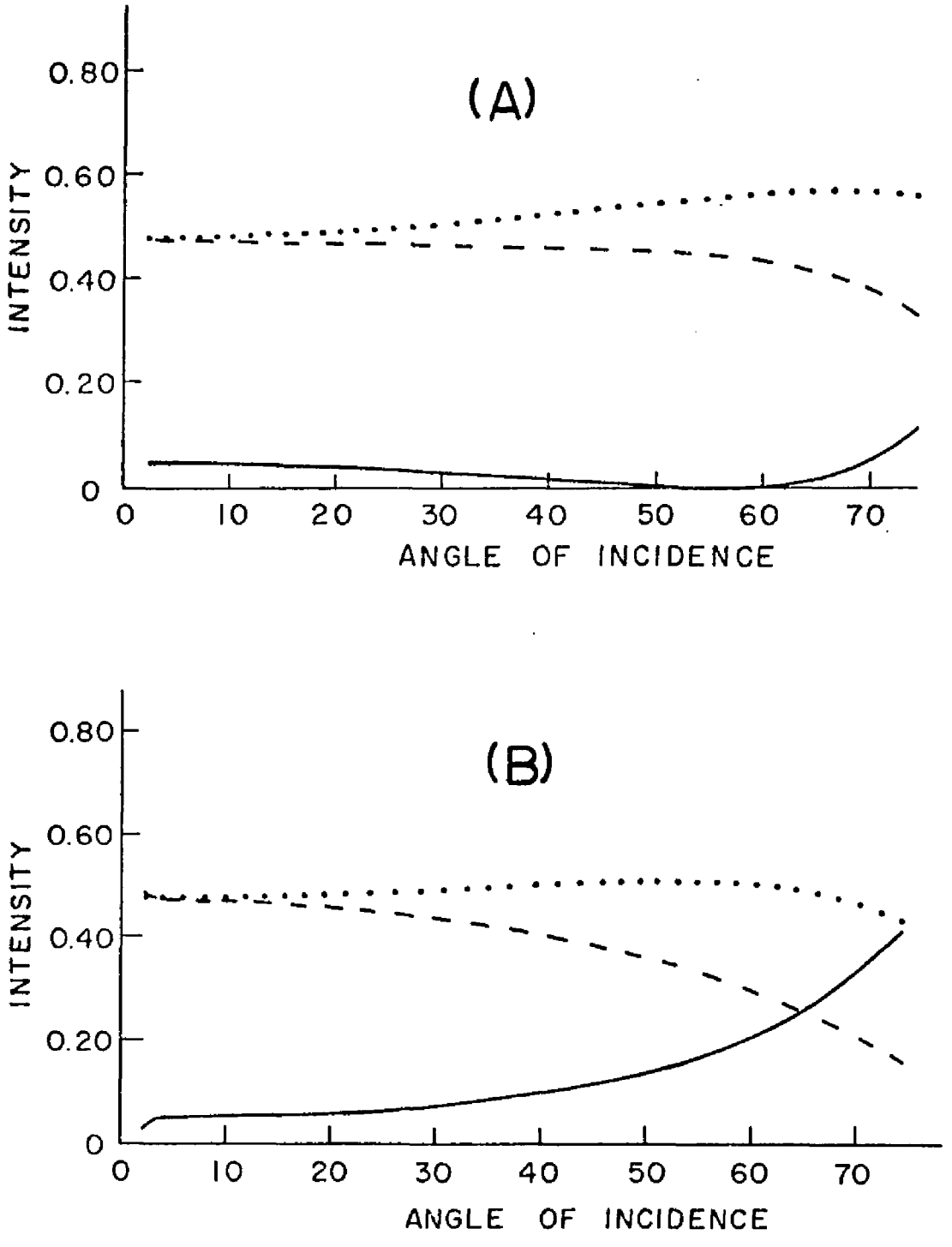

FIGURE 9. Experimentally determined reflectance (——), absorptance (•••), and transmittance (---) of 632.8 nm-wavelength light by a Tiffen 0.3 Photar Neutral Density Filter 2.340 mm thick and 48.43 mm in diameter. A. Angle of polarization, 1.3°. B. Angle of polarization, 91.3°.

G. MEASURING A LASER BEAM PROFILE

The divergence, diameter, and intensity profile of our laser beam were readily determined with only a slight modification in the experimental arrangement. A flat metal plate was mounted upon the V_R platform in front of the detector head. A pinhole (diameter of 500 μm) was located in this plate in such a way that the center of the laser beam could pass through it and strike the V_R aperature whenever the latter crossed the optic axis facing the laser. The beam was so narrow that the pinhole scanned through the beam very rapidly even when propelled by the relatively slow goniometer motor. Because of the large number of data points required for satisfactory resolution of the intensity profile, the data acquisition rate determined by the program in the Nova was exceeded. Consequently, the computer program had to be modified so that only the R channel was monitored; angular intervals of 0.0033° between data points was achieved thereby. After adjusting the zero and gain for the R channel to read 10 V for the peak signal, V_R, driven by the motor, was permitted to sweep across the beam. The calibration of the abscissa of the resulting curve can be determined from the sweep angle and sweep radius of V_R. The resulting beam profile is shown in Figure 10. In order to determine the beam divergence, these measurements were repeated at a smaller sweep radius. This was achieved by reversing the orientation of the aperature mirror of V_R and remounting the pinhole on the outboard side of the detector on the V_R platform.

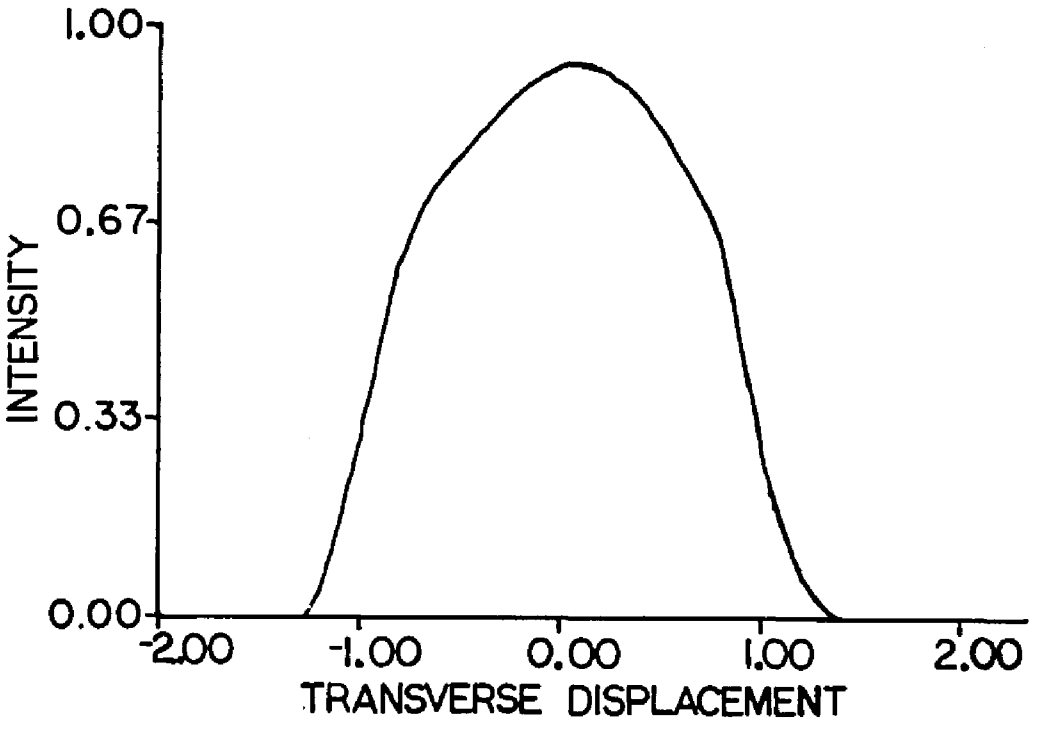

FIGURE 10. Transverse intensity profile of a Spectra-Physics Model 133 He-Ne Laser ($1/e^2$ beam radius at exit window, .70 mm: full angle between $1/e^2$ points, 5.76 milliradians). Measured by means of a scanning pin hole (radius 0.25 mm) 0.697 meters away.

Because of the low beam intensity, the diameter of the pinhole used to sweep the laser beam was necessarily an appreciable fraction of the total beam width. The detected signal was therefore the convolution of the transmittance function of the pinhole, f, with the actual beam profile, I.

$$\Sigma(\ell) = \int_{-\infty}^{\infty} dy' \int_{-\infty}^{\infty} dx' f(x'-\ell, y') I(x', y') \tag{5}$$

In Eq. (5), the beam is presumed to propagate along the z axis, passing through the origin of the coordinate system, and x and y are aligned parallel and perpendicular to the direction of scan, respectively. The displacement of the pinhole center from the optical axis is ℓ, and

$$f(x,y) = \begin{cases} 1, & x^2 + y^2 < u^2 \\ 0, & x^2 + y^2 \geq u^2 \end{cases} \tag{6}$$

Using the known value of u (pinhole radius), various functions were selected for I and trial functions for Σ were generated numerically for comparison with the experimental curves. For an ideal gas laser a Gaussian I is predicted, but we were unable to obtain a good fit past one halfwidth. This non-ideal behavior is caused by small irregular irregularities on the inside of the bore and the exit aperature of the laser which diffract a small percentage of the light off the principle axis and thus perturb the beam intensity

distribution within the near field of the laser aperature.[4] The following I produced a function of Σ which gave an excellent fit to the experimental Σ over 95% of the beam power when the best value of v was determined.

$$I(x,y) = I(0,0)\exp[-(x^2 + y^2)^2/v^4] \tag{7}$$

A mathematical investigation of the problem of finding I, given Σ and f led us to suspect a theorem: if I is "wider" than 2u, the widths of Σ and I will be very nearly the same. By "width" here is meant the distance between inflection points (values of x at which $[d^2\Sigma(x)/dx^2]y$ and $[\partial^2 I(x,y)/\partial x^2]_y$ equal zero). We were unable to prove this theorem in the general case, but numerical calculations based upon Eqs. (5)-(7), with various choices of u/v, established its validity in this instance. The inflection points of the experimental Σ can be determined numerically, and the parameters of the corresponding I(x,y) can then be determined from the relationships.

$$\rho^2 = x^2 + y^2 \tag{8}$$

and

$$v = \rho(1/e) = \rho(1/e^2)/2^{\frac{1}{4}} = (4/3)^{\frac{1}{4}}\,\rho(\text{infl}) \tag{9}$$

By determining ρ(inflection) of the laser beam at two different distances from the laser output mirror one can calculate the full angle beam divergence between the inflection points and the beam diameter at the laser output mirror.

H. THEORETICAL CALCULATIONS

1. RAT Formulae for Plane Waves

The angle of incidence, θ, is defined to be the angle between the direction of propagation of a ray and the normal to the surface it strikes. The angle of polarization, ϕ, is defined to be the angle between the plane of polarization and the plane of incidence. The plane of polarization is determined by the electric field vector associated with the light ray and its direction of propagation; the plane of incidence is determined by the latter and the normal to the surface of the sample. The reflectance, absorbtance, and transmittance, defined in Eqs. (2)-(4), may be computed from Eq. (3), plus the following:

$$R(\theta,\phi) = |r_{TM}(\theta)|^2 \cos^2\phi + |r_{TE}(\theta)|^2 \sin^2\phi \qquad (10)$$

$$T(\theta,\phi) = |t_{TM}(\theta)|^2 \cos^2\phi + |t_{TE}(\theta)|^2 \sin^2\phi \qquad (11)$$

In Eqs. (10) and (11), r and t are called the reflectance and transmittance coefficients, respectively, and the subscripts TE and TM stand for "transverse electric" and "transverse magnetic". The parameters r and t may be found in standard textbooks on optics.[5]

$$r_{TE} = i[(po/p) - (p/po)] \sin(\Gamma d)/\Delta_{TE} \qquad (12)$$

$$t_{TE} = 2/\Delta_{TE} \qquad (13)$$

$$\Delta_{TE} = 2\cos(\Gamma d) - i[(po/p) + (p/po)] \sin(\Gamma d) \qquad (14)$$

These definitions of r and t were derived by means of the characteristic matrix technique developed by Abelès. The corresponding equations for the amplitude properties of the TM wave differ from Eq. (12)-(14) only in the substitution of q for p. For a dielectric medium,

$$p = \omega\mu/\Gamma \tag{15}$$

$$q = \omega\epsilon/\Gamma \tag{16}$$

and

$$\Gamma = \omega(\mu\epsilon - \mu_o\epsilon_o \sin^2\theta)^{\frac{1}{2}} \tag{17}$$

The quantities p and q are called the slant impedance and admittance of the sample, respectively. The subscript zero refers to properties of the medium in which the sample is immersed (in our case, air).

$$p_o = (\mu_o/\epsilon_o)^{\frac{1}{2}}\sec\theta \tag{18}$$

$$q_o = (\epsilon_o/\mu_o)^{\frac{1}{2}}\sec\theta \tag{19}$$

The properties ϵ and μ, called respectively the permittivity and permeability, are related to η and χ (the complex electric and magnetic susceptibilities), respectively:

$$\epsilon = \epsilon_o\,(1 + \eta' + i\eta'') \tag{20}$$

$$\mu = \mu_o + \chi' + i\chi'' \tag{21}$$

The angular frequency of the light wave is ω, and i is the square root minus one. The symbols θ and d have been previously defined as

the angle of incidence and the thickness of the sample, respectively. The susceptibilities are related directly to tabulated optical properties of the sample. The magnetic susceptibility of non-magnetic materials is due primarily to magnetic-dipole-allowed quantum transitions in the atoms, ions, and molecules contained therein. Since these are not ordinarily important, χ can be neglected. In such cases, the index of refraction, n, is given by

$$n = [1 + \eta']^{\frac{1}{2}} \left[\frac{[1 + (\eta'')^2/(1 + \eta')^2]^{\frac{1}{2}} + 1}{2}\right]^{\frac{1}{2}} \qquad (22)$$

The absorbtion coefficient, β, is given by

$$\beta = 2\omega[\mu_o\epsilon_o(1 + \eta')]^{\frac{1}{2}} \left[\frac{[1 + (\eta'')^2/(1 + \eta')^2]^{\frac{1}{2}} - 1}{2}\right]^{\frac{1}{2}} \qquad (23)$$

If $$(\eta''/1 + \eta')^2 \ll 1,$$

$$n \cong (1 + \eta')^{\frac{1}{2}}. \qquad (24)$$

Equations (1) and (10) to (23) enable one to calculate the reflectance, absorbtance, and transmittance of any ray, incident at angle θ with polarization ϕ, upon dielectric nonmagnetic slab of thickness d, if one knows the index of refraction n and absorption coefficient β at the frequency ω. Conversely, if one measures R and T, one may calculate n and β with these formulae.

2. Intensity Corrections for a Non-Uniform Beam

Unfortunately, there is more than one ray in a laser beam. In general, each ray has a different incident intensity, and a different θ and ϕ. In Figure 11, we show two rays from a laser beam, originating from an effective common focus at O. One of these rays, $\underset{\sim}{A}$, is supposed to be the central ray of the beam, coinciding with the optical axis of the system. This ray lies upon the median plane, M; in the notation of Eqs. (5)-(8), M is the xz plane and $\underset{\sim}{A}$ is the -z axis. In addition to the axial ray, $\underset{\sim}{A}$, we show a general ray, $\underset{\sim}{G}$. In order to characterize $\underset{\sim}{G}$ we have constructed a reference half-plane, R, perpendicular to $\underset{\sim}{A}$ at the point P. This insures that R will also be perpendicular to M; their line of intersection is $\underset{\sim}{x}_1$. The general ray, $\underset{\sim}{G}$, intersects R and Q. We can identify $\underset{\sim}{G}$ by specifying its angle of divergence from $\underset{\sim}{A}$, $\langle$ QOP (which we call α), and the azimuthal angle in R between $\underset{\sim}{x}_1$ and $\underset{\sim}{B}$ -- the latter is a vector drawn from P through Q. This azimuthal angle is called Ψ.

We may, therefore, give the intensity of the ray $\underset{\sim}{G}$ in a beam with an intensity profile identical to the one previously determined:

$$I(\alpha,\Psi) = I(0,0)\ \exp[-(\tan\alpha/\tan\alpha_e)^4] \qquad (25)$$

By comparing Eqs. (25) and (7), with the help of Eqs. (8), (9), and Figure 11, we see that

$$\tan\alpha = \rho/\overline{OP} \qquad (26)$$

$$\tan\alpha_e = v/\overline{OP}$$

Note that the intensity is independent of Ψ (axial symmetry). (27)

FIGURE 11. Angular relationships among light rays in a conical beam obliquely incident upon a plane. The axial ray is $\underset{\sim}{A}$, with angles of incidence and polarization upon S of θ and ϕ, respectively. A general ray, $\underset{\sim}{G}$, located at an azimuth of ψ upon a cone with half-angle α, is incident upon S at the angle θ'. Although the electric vectors $\underset{\sim}{E_1}$ and $\underset{\sim}{E_2}$ associated with the two rays are parallel, the angles of polarization of $\underset{\sim}{G}$ is $\phi' \neq \phi$. M bisects the beam; R is a reference plane normal to $\underset{\sim}{A}$.

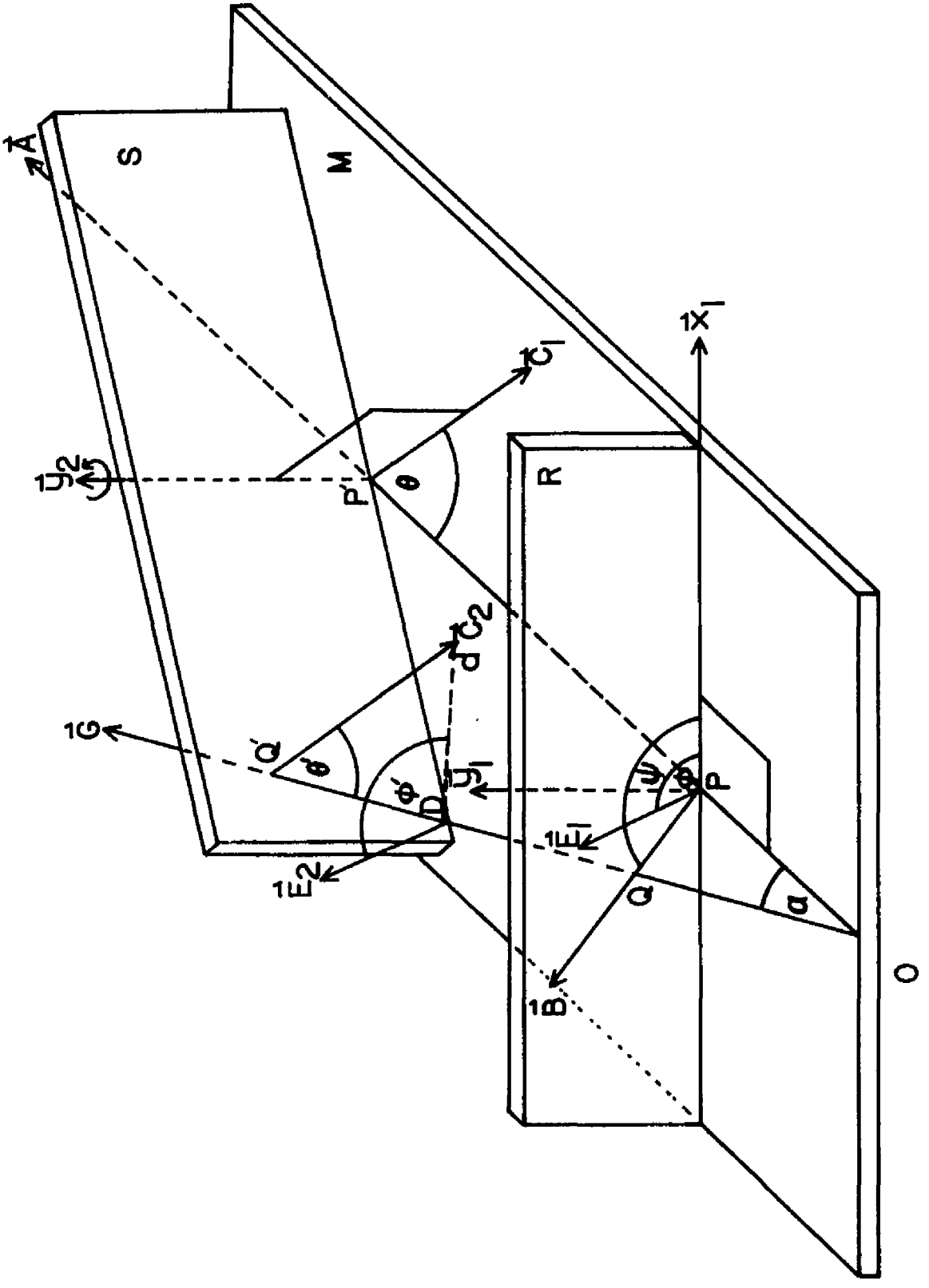
A
S
M
1X
1C
1J2
P
θ
R
dC2
1G
Q
θ
φ
dJ1
1J1
P
1E1
1E2
α
α
1B
O

3. Angular Formulae for a Diverging Beam

After the rays pass through the reference half-plane, R, they strike the sample half-plane, S (see Figure 11). S is perpendicular to M, and rotates about the axis $\underset{\sim}{y}_2$. The rays $\underset{\sim}{A}$ and $\underset{\sim}{G}$ intersect S at P′ and Q′; parallel normals to S have been constructed at these points and labelled $\underset{\sim}{C}_1$ and $\underset{\sim}{C}_2$, respectively. $\underset{\sim}{C}_1$ lies in M, and is perpendicular to $\underset{\sim}{y}_2$. This makes M the plane of incidence for the axial ray; the plane of incidence for the general ray is determined by $\underset{\sim}{C}_1$ and $\underset{\sim}{C}_2$. The angles of incidence are θ and θ', respectively. A little spherical trigonometry suffices to show that

$$\cos \theta' = \cos \alpha \cos \theta - \sin \alpha \sin \theta \cos \Psi \qquad (28)$$

The electric vectors of $\underset{\sim}{A}$ and $\underset{\sim}{G}$ are $\underset{\sim}{E}_1$ and $\underset{\sim}{E}_2$, respectively. Since $\underset{\sim}{E}_1$ represents the intersection of the plane of polarization of the axial ray with R, and since $\underset{\sim}{x}_1$ represents the intersection of the plane of incidence of the axial ray with R, the angle between $\underset{\sim}{x}_1$ and $\underset{\sim}{E}_1$ is the angle of polarization of the axial ray, ϕ. The vector $\underset{\sim}{E}_2$, presumed to be parallel to E_1, lies in the plane of incidence of the general ray, and is perpendicular to the intersection, $\underset{\sim}{G}$, of the planes of incidence and polarization. $\overline{Dd}$ lies in the plane of incidence of the general ray, and is also perpendicular to $\underset{\sim}{G}$. Therefore, the angle between $\underset{\sim}{E}_2$ and $\overline{Dd}$ is the angle of polarization of the general ray, ϕ'. After some effort, one can show

$$\cos \phi' = \frac{\sin \theta \cos \phi + \sin \alpha \cos \theta' \cos (\Psi - \phi)}{\sin \theta' \sin \{\cos^{-1}[\sin \alpha \cos (\Psi - \phi]\}} \qquad (29)$$

4. Computer Programs

A Fortran IV computer program was written for the IBM 360 computer based on Eqs. (25), (28), and (29). It is diagrammed in Fig. 12. Input to this program consists of characteristics of the sample (n, β, and d) and of the laser beam [v at the exit mirror, α_e, ϕ, and the total power, $\pi^{\beta/2}v^2 I(0,0)/2$]. Also, locations of the sample and the detector with respect to the laser beam are provided. The computer then generates a theoretical curve of the same form that one observes experimentally, as follows. The computer selects values of θ sequentially; for each θ, a series of α's are generated and the corresponding beam intensities are calculated by means of Eq. (25). For the first α, a series of Ψ's in a ring from 0° to 360° are generated. In each ray, specified by a particular choice of α and Ψ, θ' and ϕ' are computed by means of Eqs. (28) and (29). Finally, Eqs. (10)-(19) are used to compute the associated values of the reflectance, absorbtance, and transmittance. In this computation, θ' and ϕ' replace θ and ϕ, and the necessary physical parameters of the sample are called from storage, having been previously calculated from the input data by means of Eqs. (20)-(23). The results are summed over all Ψ's in the ring and multiplied by the appropriate intensity. Next, α is incremented and this process is repeated for each of the preselected values of α up to that which corresponds to the angle subtended by the aperature of the detector. Finally, the results for all the rings (α values) are added together and the result stored.

All of the operations described in the above paragraph are carried out for each value of θ; data thus produced can be subjected

FIGURE 12. Flow-sheet for Fortran IV Computer Program used to calculate theoretical values of the reflectance, absorptance, and transmittance of a dielectric slab of refractive index n, absorption coefficient β, and thickness d, illuminated by a laser beam of angular frequency ω, and divergence α_e (half-angle between rays 1/e times the intensity of the axial ray) at an angle of incidence θ and angle of polarization ϕ. The initial polarization is ϕ, and α_{max} is the angle subtended by the detector aperature.

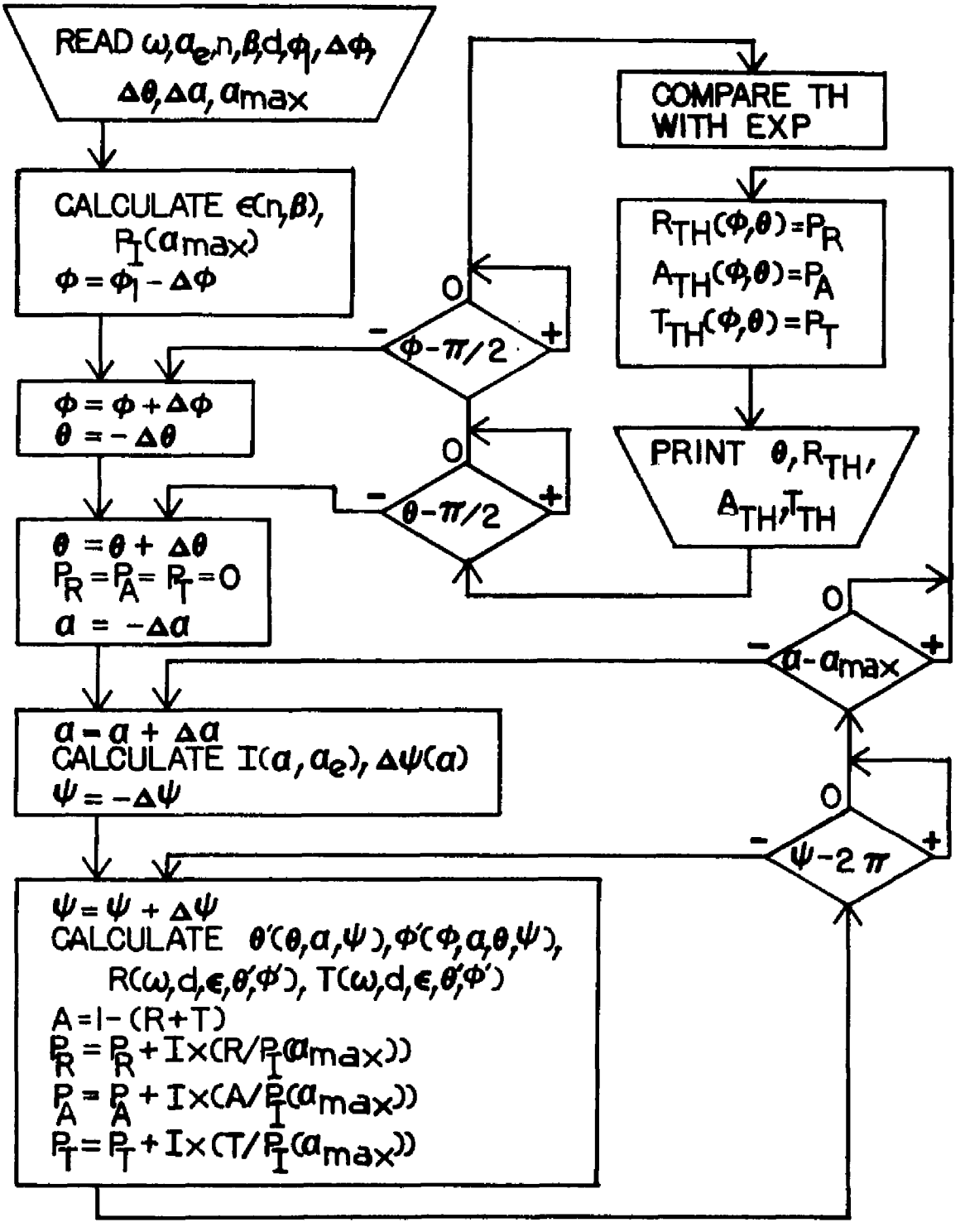
READ ω, a_e, n, β, d, φ_1, Δφ, Δθ, Δα, α_max
CALCULATE ε(n,β), P_I(α_max)
φ = φ_1 − Δφ
φ = φ + Δφ
θ = −Δθ
θ = θ + Δθ
P_R = P_A = P_T = 0
α = −Δα
α = α + Δα
CALCULATE I(α, a_e), Δψ(α)
ψ = −Δψ
ψ = ψ + Δψ
CALCULATE θ'(θ,α,ψ), φ'(φ,α,θ,ψ), R(ω,d,ε,θ',φ'), T(ω,d,ε,θ',φ')
A = 1 − (R+T)
P_R = P_R + I×(R/P_I(α_max))
P_A = P_A + I×(A/P_I(α_max))
P_T = P_T + I×(T/P_I(α_max))
φ − π/2
θ − π/2
α − α_max
ψ − 2π
0
−
+
R_TH(φ,θ) = P_R
A_TH(φ,θ) = P_A
T_TH(φ,θ) = P_T
PRINT θ, R_TH, A_TH, T_TH
COMPARE TH WITH EXP

to further analysis, tabulated by a printer, or fed to a plotter. Figure 13 displays the computer-calculated results for a sample with $n = 1.4970$, $\beta = 285.3$, m^{-1}, $d = 2.34$ mm; for the laser, $\phi = 1.3^{\circ}$, and $\alpha_e = 5.76/2(2)^{\frac{1}{4}}$ milliradians.

I. EXPERIMENTAL TESTS

1. Data-Collection Procedures

The Nova minicomputer, N, was programmed to read the three output signals with the analog-to-digital (A/D) converter, plot a visual display on a Textronix 611 storage oscilloscope, and store the R, T, and A values at $.1^{\circ}$ increments to be recalled as desired. Before each run the output signals from the analog computer were made individually to reach their maximum and minimum by blocking the aperatures of the appropriate detectors, and these values were read and recorded by the Nova. Due to the load on the analog dividers by the ac filters or perhaps the A/D converter, the maximum outputs of the three channels were always very near 9.95 V instead of the 10.00 V expected. Minimum readings were of the order of 5 mV or less due to improper zeroing or a drift in the dark current of the photo tubes. For this reason, the corresponding power readings for all work reported in this paper were normalized by means of the following equation

$$P(\text{corrected}) = \frac{P(\text{read}) - P(\text{min.})}{P(\text{max.}) - P(\text{min.})} . \qquad (30)$$

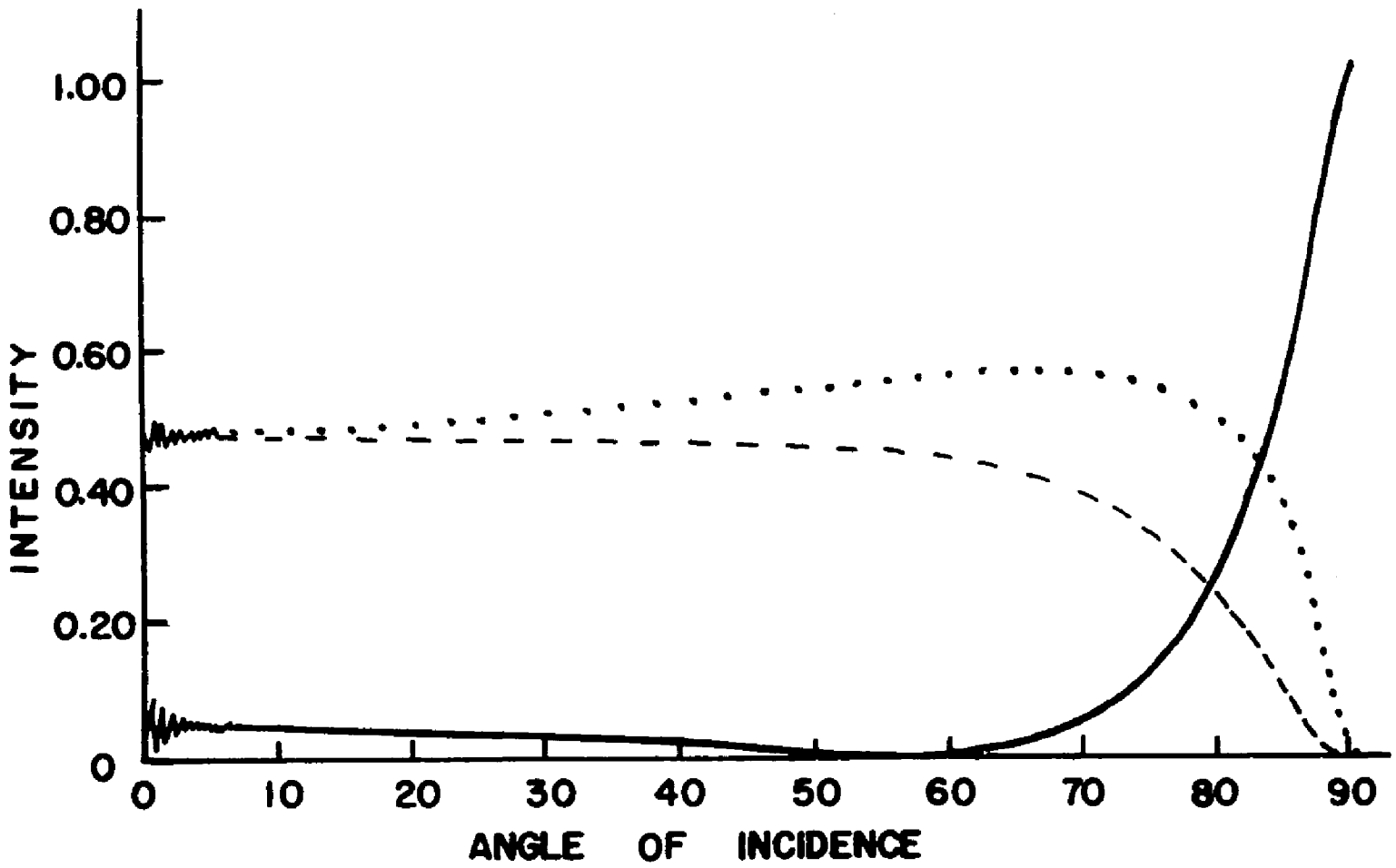

FIGURE 13. Theoretically calculated reflectance (——), absorptance (···), and transmittance (---) of 632.8 nm-wavelength light by a slab 2.34 mm thick, with refractive index 1.4974 and absorption coefficient 285.32 m^{-1}. Beam divergence, 5.76 milliradians (full angle between $1/e^2$ points); angle of polarization, 1.3°.

Because the error in the A/D after the above correction is only 0.024%, and the angular resolution is better than 0.1°, the overall accuracy of the RAT assembly is limited by the goniometer, G, and the signal processor, C.

2. Experimental Determination of Optical Parameters

In order to compare the theoretical calculations described in Section D with the experimental results, one must have a procedure for estimating the appropriate values of the parameters n, β, d, and ϕ. A good estimate of the refractive index, n, of the sample is calculated from Brewster's Angle (θ_B = arctan n) which is determined by the minimum of the R vs θ curve for TM polarization ($\phi = 0$). The absorption coefficient, β, is roughly calculated from the absorption at near normal incidence using Beer's law. The thickness, d, is easily measured with a micrometer. The polarizer setting, ϕ, for 0° polarization was determined by the setting that gave the minimum R when the sample was oriented in the vicinity of its Brewster's Angle. A small error in the 0° setting could result because of the flatness of the R curve near the Brewster's Angle.

3. Computer Optimization of Parameters

The computer program was modified for the comparison process as follows. First, the experimental RAT curves were entered as data, together with the trial values of n, β, d, and ϕ estimated in the manner just described. Theoretical curves were generated corresponding to each of the six experimental ones (R, A, and T at the

orthogonal directions of polarization). We then calculated the squares of the deviations of the experimental values for each of the six curves from their theoretical values for each of the ν angles at which measurements were made. The square root of the mean of these 6ν numbers served as our index for the goodness of fit. Then, each of the parameters n, β, and ϕ were varied, one at a time; each choice gave rise to a new σ. When σ was plotted as a function of the parameter being varied, it exhibited a minimum. Figure 14 illustrates this process for the index of refraction of the neutral density filter; the minimum occurs at n = 1.4070. The value of the parameter which produced the minimum replaced the initial trial value in subsequent calculations. This process was repeated until no further changes in the parameters occurred; the final values were assumed to be the optimum ones. The initial and final values of n, β, and ϕ obtained by this procedure for the two samples are listed in Table I. The reader might wonder why we assume that all six curves can be used to determine both values of ϕ. This is because there is really only one ϕ that we need to fix; the other is very accurately 90° different from the first due to the precision of the graduations on the polarizer mount.

4. Accuracy and Precision of Results

We may define an overall experimental error in the RAT measurement assembly, σ_o, as the value of σ computed using these optimum values. In Table II we present σ_o and the rms deviation

FIGURE 14. Total rms deviation, σ, as a function of the assumed refractive index for the neutral density filter. σ is computed from the deviations of the experimentally determined optical properties for each of the six curves from their theoretical values for each of the angles at which measurements were made. Wavelength of light source, 632.8 nm; angles of polarization, 1.3° and 91.3°; absorption coefficient, 285.32 m^{-1}.

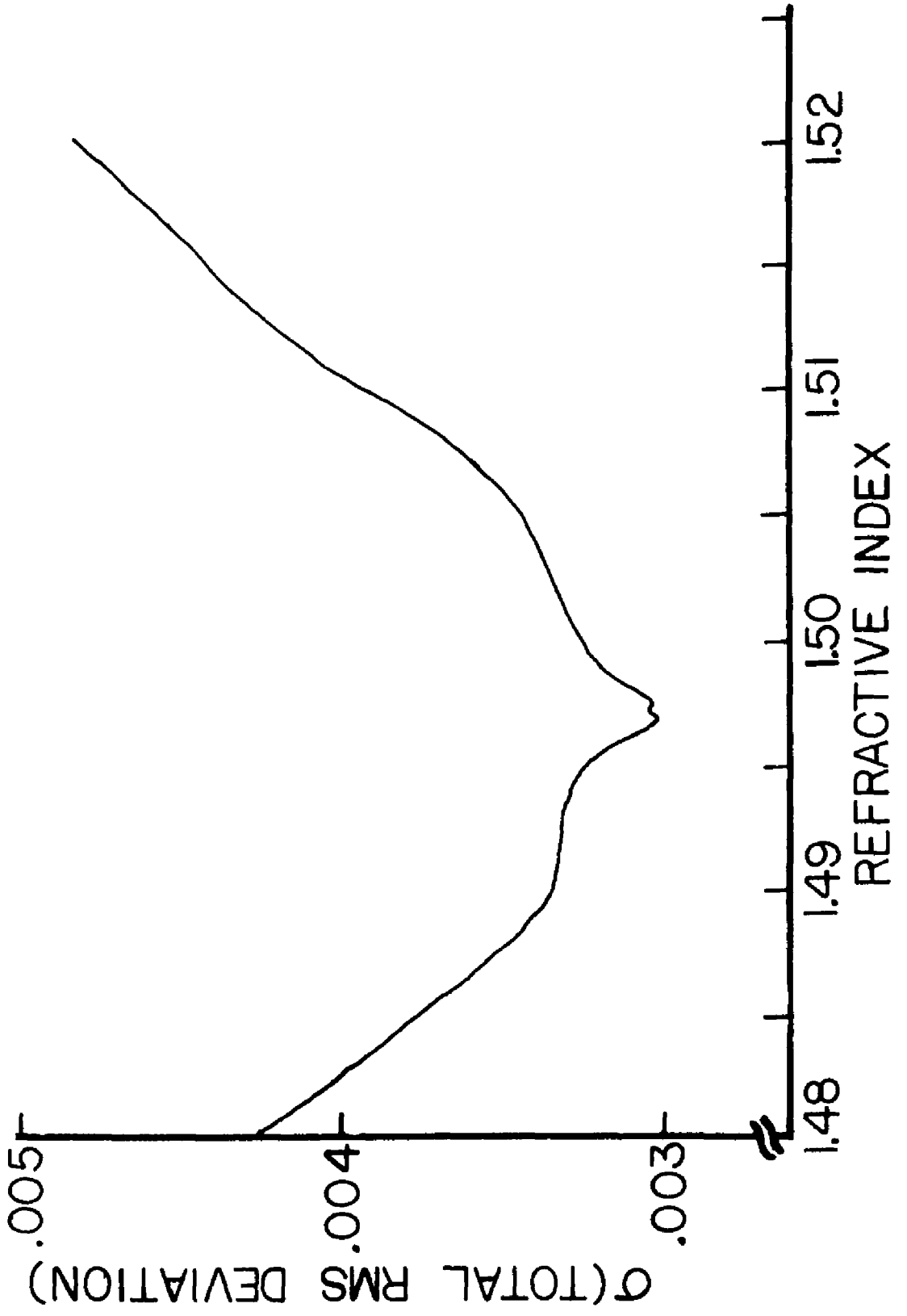
.005
.004
.003
σ (TOTAL RMS DEVIATION)
1.48
1.49
1.50
1.51
1.52
REFRACTIVE INDEX

TABLE I

COMPUTER-ASSISTED OPTIMUMIZATION OF OPTICAL PARAMETERS DETERMINED FROM DATA SUPPLIED BY THE RAT MEASUREMENT ASSEMBLY

SAMPLE	PARAMETER	INITIAL VALUE	OPTIMUM VALUE
Neutral	Refractive index, n	$1.50 \pm .02$	1.4970
Density	Absorption coefficient, β	$281 \pm 8\ m^{-1}$	$285.3\ m^{-1}$
Filter	Angles of polarization, ϕ	$0^\circ, 90^\circ \pm 3^\circ$	$1.3^\circ, 91.3^\circ$
Glass	Refractive index, n	$1.52 \pm .02$	1.517
Flat	Absorption coefficient, β	$2 \pm 1\ m^{-1}$	$5.5\ m^{-1}$
	Angles of polarization, ϕ	$0^\circ, 90^\circ \pm 3^\circ$	$2.8^\circ, 92.8^\circ$

TABLE II

ROOT-MEAN SQUARE DEVIATIONS OF EXPERIMENTALLY-DETERMINED OPTICAL PROPERTIES FROM THE CORRESPONDING THEORETICAL CURVES, THE LATTER DETERMINED FROM BEST-FIT PARAMETERS OF THE SAMPLE

PROPERTY (NOMINAL ANGLE OF POLARIZATION, ϕ)	RMS DEVIATION	
	NEUTRAL DENSITY FILTER	GLASS FLAT
R (0°)	0.00217	0.00417
T (0°)	0.00285	0.01080
A (0°)	0.00430	0.01070
R (90°)	0.00167	0.00756
T (90°)	0.00255	0.01112
A (90°)	0.00412	0.00810
σ_o, total rms of all curves	0.00310	0.00907

σ_{Total} (rms of both samples) 0.0068

for each of the six curves separately for the two samples used in the experiment. Note that the rms value of the two σ_o's is 0.68%, and that the results for the glass flat are nearly three times as bad as those for the neutral density filter. We have carefully reexamined our samples and have come to the conclusion that the optical quality of the neutral density filter is much greater than that of the glass flat. It seems likely, therefore, that the error in the determination of the optical properties of the former (0.31%) is much more likely to be representative of the inherent limitation of the equipment than is that of the latter, or of their average. In support of this contention, we may cite the fact that the irreproducibility of the system (based on runs at different times using the same sample under identical conditions of illumination) was found to be 0.324%.

REFERENCES

1. Most of the contents of this appendix were previously published: W. H. Thomason and J. D. Macomber, Rev. Sci. Instrum., 45, 264 (1974).
2. C. Tuttle, J. Opt. Soc. Am. 24, 272 (1934).
3. V. G. W. Harrison, Proc. Phys. Soc. (London) 58, 408 (1946).
4. A spatial filter may be used to obtain a smooth distribution in the near field. See Characteristics of Uniphase Radiation from a Gas Laser, Data Sheet on Stabilite Helium-Neon Gas Lasers (Spectra-Physics, Inc., Mountain View, California).
5. M. Born and E. Wolf, Principles of Optics, (Pergamon, Oxford, 1965), 3rd ed., pp. 60-62.

APPENDIX 2

COMPUTER PROGRAM - CHARACTERISTIC MATRIX TECHNIQUE APPLIED TO A SATURABLE ABSORBER.

The computer program presented in this appendix was developed to calculate the saturable optical properties of SF_6. The algorithm employed the theoretical procedure described in Chapter II and the special modifications described in Chapter V which were required to treat SF_6. The program was written in FORTRAN and consisted of the main program and nineteen subroutines. The execution of the program was performed by the IBM 360/65 computer of the LSU Computer Research Center. A brief description of the function of each subroutine (SR) will be given and a copy of the complete program will follow.

1. LASER computes the peak value of the electric fields of the incident laser beam and the angular frequency of the laser radiation.

2. GEOM divides the laser beam into a selected number of light rays, and computes for each ray the angle of incidence, the angle of polarization of the electric field, and the intensity.

3. OBLIKE computes the peak value of the fields associated with each light ray.

4. WAVE selects an initial phase for the oscillating fields of each light ray.

5. SAMPLE computes the temperature and the number density of the absorbing molecules, atoms, or ions of the absorber.

6. ELEMENT computes the electric susceptibility for each non-saturable optical element of the sample system.

7. ABSORB computes the number of absorption linewidths that separate the frequency of the exciting radiation and the center of the absorption band (δT_2). It also computes the transition dipole moment (m_e) and the small-signal susceptibility of the saturable absorber in the sample system.

8. DOPE incorporates the optical properties of the absorbing species with those of the matrix in which the absorbing species are contained.

9. PARM calculates the electric permittivity (ϵ) and magnetic permeability (μ) of each optical component of the sample system. It also calculates the slant impedance (p) and admittance (q) and the propagation vector for the $\hat{z}$ direction (Γ).

10. ABELES computes the elements of the characteristic matrix (CM) for each optical component of the sample system.

11. WRONSK checks the determinant of the CM to ensure that the CM was properly constructed.

12. MULMAT multiplies two CM together and the stores the product in the computer memory.

13. OPTICS computes the reflection coefficient (r) and the transmission coefficient (t) of each light ray. This SR also computes the intensity-weighted root-mean-square r and t of all the light rays which compose the light beam.

14. INITIAL computes the vector sum of the fields associated with the forward and backward-traveling electromagnetic (em) waves. This SR also propagates the em wave through an optical component by means of Eq. (3) of Chapter II.

15. SAT computes the electric susceptibility of the absorber as a function of the field strength of the em wave interacting with the absorbing centers.

16. DERIV computes the phase angle α defined by Eq. (10) of Chapter II.

17. TEST checks for convergence of the iteration procedure and computes the reflectance and transmittance from r and t.

18. BOLTZ computes the population distribution among the various vibrational energy levels of SF_6 as a function of the temperature of the gas.

19. COMPAR compares the experimental data with the results of the theoretical calculations.

```
//SA43IA2 JOB (095,1102,4,2,30,,,,60),'70950 THOMASON',MSGLEVEL=1          SAT 0010
// EXEC FOUTGCLG,PARM.FORT=(TERM,NOSOURCE,ID),PARM.LKED=NOXREF,           SAT 0020
// REGION.GO=95K,TIME=4                                                   SAT 0030
//FORT.SYSPRINT DD DUMMY                                                  SAT 0040
//FORT.SYSTERM DD SYSOUT=A                                                SAT 0050
//FORT.SYSIN DD *                                                         SAT 0060
      IMPLICITCOMPLEX*16(C),REAL*8(A-B,D-H,O-Z)                          SAT 0070
      REAL*8C,MU                                                         SAT 0080
      REAL*4 APROX,X(100),Y1(100),Y2(100)                                SAT 0090
      DIMENSIONCOIN(2,09),THICK(4),DIPOLE(2),SIGMA(2),CGAMMA(5),CDET(5,2SAT 0100
     *),B(2),CT(2),CP(2),CMNEW(2),CTNEW(2),CRN(2),CTB(2),CB(2),          SAT 0110
     3CSAVE1(09),CSAVE2(09),POWR(8),PSC(8,10),TSQ(8,10),DIPOL1(2)       SAT 0120
      COMMON/A1/CX(5,2,2),CD(5,2,2),CM(5,2,4)                            SAT 0130
      COMMON/A3/PI,ZNAT,C,Z,EP,MU,HEAR,BOLZ,AVAGAD                       SAT 0140
      COMMON/A4/FLUX(09),YYC(09)                                         SAT 0150
      COMMON/A5/PC(09),PS(09)                                            SAT 0160
      NAMELIST/MAIN/NEWS,ACURAT,NUE,LAVG                                 SAT 0170
      READ(5,MAIN)                                                       SAT 0180
      WRITE(6,MAIN)                                                      SAT 0190
      TOLD=301.5                                                         SAT 0200
      TCOR=TOLD                                                          SAT 0210
      APMAX=ACURAT/1.D2                                                  SAT 0220
      APROX=APMAX                                                        SAT 0230
      INPW= 1                                                            SAT 0240
      CALLLASER(E,H,OMEGA,WAVCTR,POWR)                                   SAT 0250
      CALL GECM(WAVCTR,KCONE)                                            SAT 0260
      KAL=1                                                              SAT 0270
      CALLOBLIKE(KAL,E,H,       EX,HX)                                   SAT 0280
      CALLWAVE(C,OMEGA       ,EX,HX,       YKC(KAL),COIN(1,KAL),COIN(2,KASAT 0290
     *L))                                                                SAT 0300
      CALLSAMPLE(TEMP,D,PR1)                                             SAT 0310
      DO 10 I=1,3                                                        SAT 0320
10    CALLELEMNT(WAVCTR,I,THICK(I))                                      SAT 0330
      CALLABSORB(TEMP,OMEGA,D,OFFSET,CSUSPT,DIPOLE,PR1,CSSL,QCCEF)       SAT 0340
      CALLDOPE(SIGMA)                                                    SAT 0350
      THICK(4)=THICK(2)                                                  SAT 0360
      DO 41 KAL=1,KCONE                                                  SAT 0370
      CALL WAVE3(YKC(KAL),COIN(1,KAL),COIN(2,KAL),E ,H )                 SAT 0380
      CALL DOPE2                                                         SAT 0390
      DO 11 L=1,5                                                        SAT 0400
   11 CALLPARAM(L,OMEGA,YKC(KAL),CGAMMA(L))                              SAT 0410
      CSAVE2(KAL)=CX(5,2,2)                                              SAT 0420
      CSAVE1(KAL) =CX(5,1,2)                                             SAT 0430
      DO 13 M=1,4                                                        SAT 0440
      CZETA=CGAMMA(M)*THICK(M)                                           SAT 0450
      DO 12 N=1,2                                                        SAT 0460
      CD(M,N,1)=(0.D0,0.D0)                                              SAT 0470
12    CD(M,N,2)=CX(M,N,2)                                                SAT 0480
      CSSB=CSSL                                                          SAT 0490
      CSSSPT=CSUSPT                                                      SAT 0500
      DIPOL1(1)=DIPOLE(1)                                                SAT 0510
      DIPOL1(2)=DIPOLE(2)                                                SAT 0520
      CALLABELES(M,CZETA)                                                SAT 0530
13    CALLWRONSK(M,APROX,CDET)                                           SAT 0540
      CALLMULMAT(4,1,5)                                                  SAT 0550
      CALLSOLMAT(3,5,5)                                                  SAT 0560
      CALLWRONSK(5,APROX,CDET)                                           SAT 0570
      CALLOPTICS(CDET,CB,CT,KAL,FLUX(KAL),KCONE)                         SAT 0580
  41  CONTINUE                                                           SAT 0590
      DXH=10.5910350-6/20.0                                              SAT 0600
      DTH=DXH*10.0/DFLOAT(LAVG)                                          SAT 0610
 101  CONTINUE                                                           SAT 0620
      DO 43 ITH=1,LAVG                                                   SAT 0630
      DCH=DFLOAT(ITH-1)*DTH                                              SAT 0640
      NCUT=NUE                                                           SAT 0650
 100  NSUM=NCUT*(NCUT+1)/2                                               SAT 0660
      NSUT=NCUT*11                                                       SAT 0670
      THT=THICK(4) -(DCH +DXH*DFLOAT(NSUT-NCUT))                         SAT 0680
      DI=THT/DFLOAT(NSUM)                                                SAT 0690
      DO 42 KAL=1,KCONE                                                  SAT 0700
      CALLINITAL(YKC(KAL),COIN(1,KAL),COIN(2,KAL),CR,1,5,KAL)            SAT 0710
      DO 40 N=1,NSUT                                                     SAT 0720
      IPX=MOD(N,11)                                                      SAT 0730
      CALL       SAT(OFFSET,CSSSPT,DIPOL1,IPX,CSSB)                      SAT 0740
      CALL DOPE1                                                         SAT 0750
      CALL PARAM(4,      OMEGA,YKC(KAL),CGAMMA(4))                       SAT 0760
      DZ=DXH                                                             SAT 0770
      IF(IPX.EQ.0) DZ=DI*DFLOAT(N/11)                                    SAT 0780
      CZETA =DZ*CGAMMA(4)                                                SAT 0790
```

```
      IF(N.GT.1)GO TO 15                                                SAT 0800
      DO 14 NI=1,2                                                      SAT 0810
      CD(4,NI,1)=(0.00,0.00)                                            SAT 0820
   14 CD(4,NI,2)=CX(4,NI,2)                                             SAT 0830
      GO TO 16                                                          SAT 0840
   15 CALL        DERIV(CZETA ,CP)                                     SAT 0850
   16 CALL APPLES(4,CZETA)                                              SAT 0860
      IF (N.GT.1)GO TO 18                                               SAT 0870
      DO 17 I=1,2                                                       SAT 0880
      DO 17 J=1,4                                                       SAT 0890
   17 CU(2,I,J)=CU(4,I,J)                                               SAT 0900
      GO TO 19                                                          SAT 0910
   18 CALL MULMAT(4,2,2)                                                SAT 0920
   19 CALL PROP(4,4)                                                    SAT 0930
      NX=N                                                              SAT 0940
   20 CONTINUE                                                          SAT 0950
      CALL WRONSK(2,APPCX,CDET)                                         SAT 0960
      CALL MULMAT(2,1,5)                                                SAT 0970
      CALL MULMAT(5,5,5)                                                SAT 0980
      CALL WRONSK(5,APBCX,CDET)                                         SAT 0990
      CX(5,1,2)=CSAVE1(KAL)                                             SAT 1000
      CX(5,2,2)=CSAVE2(KAL)                                             SAT 1010
      CALL OPTICS(CDET,CRNEW,CTNEW,KAL,FLUX(KAL),KCONE)                 SAT 1020
   42 CONTINUE                                                          SAT 1030
   72 KAL=1                                                             SAT 1040
      NX=NX/11                                                          SAT 1050
      CALL TEST(NX,CR,CT,CRNEW,CTNEW,APRAX,BSQ(ITH,INPW),TSQ(ITH,INPW), SAT 1060
     *621)                                                              SAT 1070
  917 CONTINUE                                                          SAT 1080
      A=1.0-BSQ(ITH,INPW) - TSQ(ITH, INPW)                              SAT 1090
      ABPW=POWR(INPW)*A*QCOEF                                           SAT 1100
      TCOR=TEMP + ABPW                                                  SAT 1110
      TCOR=(TCOR + TOLD)/2.0                                            SAT 1120
      TOLD=TCOR                                                         SAT 1130
      CALL BOLTZ(2,TCOR,PDIFF,FACT,FACT6)                               SAT 1140
C     DIPOLE & SQRT(T1),  I1 AS 1/VEL(SQRT(T))                          SAT 1150
      ABPW=DSQRT(300.0/TCOR)                                            SAT 1160
      PRINT 987,ABPW,ITH                                                SAT 1170
  987 FORMAT(25X,'ABPW= ',G20.6,40X,'ITH= ',I2)                         SAT 1180
      DIPOL1(1)=ABPW*DIPOLE(1)                                          SAT 1190
      DIPOL1(2)=ABPW*DIPOLE(2)                                          SAT 1200
      CSS6=FACT6*CSS1*PDIFF                                             SAT 1210
      CSSSPT=FACT*CSSSPT*PDIFF                                          SAT 1220
      TRATIO=TEMP/TCOR                                                  SAT 1230
      CSS6=CSS6*TRATIO                                                  SAT 1240
      CSSSPT=CSSSPT*TRATIO                                              SAT 1250
      NCUT=NCUT+NUP                                                     SAT 1260
      GO TO 100                                                         SAT 1270
   21 IF(NX.LT.6) GO TO 917                                             SAT 1280
   43 CONTINUE                                                          SAT 1290
      SFA=DSQRT(POWR(INPW + 1)/POWR(INPW))                              SAT 1300
      DO 22 I=1,KCONE                                                   SAT 1310
      CUIN(1,I)=CUIN(1,I)*SFA                                           SAT 1320
      CUIN(2,I)=CUIN(2,I)*SFA                                           SAT 1330
   22 CONTINUE                                                          SAT 1340
      TSUM=0.0                                                          SAT 1350
      RSUM=0.0                                                          SAT 1360
      DO 44 I=1,LAVG                                                    SAT 1370
      TSUM=TSUM + TSQ(I,INPW)                                           SAT 1380
      RSUM=RSUM + BSQ(I,INPW)                                           SAT 1390
   44 CONTINUE                                                          SAT 1400
      TSUM=TSUM/DFLOAT(LAVG)                                            SAT 1410
      RSUM=RSUM/DFLOAT(LAVG)                                            SAT 1420
      A=1.0-TSUM-RSUM                                                   SAT 1430
      PRINT 51,POWR(INPW),RSUM,TSUM,A,TCOR                              SAT 1440
   51 FORMAT('0','INCIDENT POWER=',G10.4,'WATTS/CMSQ',2X,'REFLECTANCE=',SAT 1450
     1G10.4,'TRANSMITTANCE=',G10.4, 'ABSORBTANCE=',G10.4,'TCOR=',F6.1,/)SAT 1460
      X(INPW)=DLOG10(POWR(INPW))                                        SAT 1470
      Y1(INPW)=TSUM                                                     SAT 1480
      Y2(INPW)=RSUM                                                     SAT 1490
      INPW=INPW + 1                                                     SAT 1500
      IF(INPW.GT. 8) GO TO 23                                           SAT 1510
      GO TO 101                                                         SAT 1520
   23 CONTINUE                                                          SAT 1530
      DO 24 INPW=1,8                                                    SAT 1540
      LV=LAVG                                                           SAT 1550
      PRINT 151,POWR(INPW),(BSQ(I,INPW),I=1,LV)                         SAT 1560
  151 FORMAT('0','POWER=',F10.6,'RS=',10F9.6)                           SAT 1570
      PRINT 152,(TSQ(I,INPW),I=1,LV)                                    SAT 1580
  152 FORMAT(10X,'TS=',10F9.6)                                          SAT 1590
```

```
      PRINT 153,Y2(INPW),Y1(INEW)                                        SAT 1600
  153 FORMAT(25X,'HAVG=',F9.6,5X,'HAVG=',F9.6)                           SAT 1610
   24 CONTINUE                                                           SAT 1620
      Y2(10)=0.01                                                        SAT 1630
      Y2(9)=0.15                                                         SAT 1640
      X(10)=-1.26                                                        SAT 1650
      X(09)=1.24                                                         SAT 1660
      Y1(09)=1.01                                                        SAT 1670
      Y1(10)=0.01                                                        SAT 1680
      CALL COMPAB(X,Y1,Y2)                                               SAT 1690
      CALL PLOT1(X,Y1,10,2,36HSATURATION DATA-TRANSMITTANCE              SAT 1700
     1,36HLOG STRONG BEAM INTENSITY                                      SAT 1710
     1,36HTRANSMITTANCE STRONG BEAM                          )           SAT 1720
      CALL PLOT1(X,Y2,10,2,36HSATURATION DATA-REFLECTANCE                SAT 1730
     2,36HLOG STRONG BEAM INTENSITY                                      SAT 1740
     1,36HREFLECTANCE STRONG BEAM                            )           SAT 1750
      STOP                                                               SAT 1760
      END                                                                SAT 1770
      BLOCK DATA                                                         SAT 1780
      IMPLICITREAL*8(A-H,M,O-Z)                                          SAT 1790
      COMMON/A2/SUB(19),NCALL(19)                                        SAT 1800
      COMMON/A3/PI,ENAT,C,Z,EP,MU,HBAR,BOLZ,AVAGAD                       SAT 1810
      DATA PI,ENAT,C,Z,EP,MU,HBAR,BOLZ,AVAGAD/3.1415926535898D0,2.718281SAT 1820
     1828459D0,2.99792501D8,1.76730367502,8.854185278D-12,1.256637C614SAT 1830
     2359D-6,1.05459193D-34,1.380546D-23,6.02216940D23/                  SAT 1840
      END                                                                SAT 1850
      SUBROUTINE LASER(E,H,OMEGA,WAVCTR,PW)                              SAT 1860
      IMPLICITREAL*8(A-H,M,O-Z)                                          SAT 1870
      DIMENSION PW(8)                                                    SAT 1880
      COMMON/A3/PI,ENAT,C,Z,EP,MU,HBAR,BOLZ,AVAGAD                       SAT 1890
      NAMELIST/LSR/POWR,DIAM,WAVE                                        SAT 1900
C     POWR IS PEAK FLUX IN WATTS/CMSQ, DIAM IS  1/E DIAM AT DETECTOR     SAT 1910
      READ(5,LSR)                                                        SAT 1920
      F=Z*2.004                                                          SAT 1930
      OMEGA=2.D9*PI*C/WAVE                                               SAT 1940
      WAVCTR=OMEGA/C                                                     SAT 1950
      WRITE(6,LSR)                                                       SAT 1960
      READ 1, (PW(I),I=1,8)                                              SAT 1970
    1 FORMAT(8F10.6)                                                     SAT 1980
      PRINT 2,(PW(I),I=1,8)                                              SAT 1990
    2 FORMAT(5X,8F10.6)                                                  SAT 2000
      POWR=PW(1)                                                         SAT 2010
      E=DSQRT(POWR*F)                                                    SAT 2020
      H=E/Z                                                              SAT 2030
      POW1=POWR                                                          SAT 2040
      RETURN                                                             SAT 2050
      END                                                                SAT 2060
      SUBROUTINE GEOM(WAVCTR,RAL)                                        SAT 2070
      IMPLICIT REAL*8(A-H,O-Z)                                           SAT 2080
      COMMON/A4/FLUX(09),XNC(09)                                         SAT 2090
      COMMON/A5/PC(09),PS(09)                                            SAT 2100
      NAMELIST/GM/RO,AO,B,DO,DS,B,T,NA                                   SAT 2110
      PI=3.1415926535898D0                                               SAT 2120
      HALFPI=PI/2.                                                       SAT 2130
      TWOPI=2.*PI                                                        SAT 2140
      READ (5,GM)                                                        SAT 2150
      WRITE (6,GM)                                                       SAT 2160
      RAD=PI/180.                                                        SAT 2170
      T=T*RAD                                                            SAT 2180
      B=B*RAD                                                            SAT 2190
      PO=1.0                                                             SAT 2200
      TAO=DSIN(AO)/DCOS(AO)                                              SAT 2210
      RAO=RO + (TAO*DO)                                                  SAT 2220
      C=DO*RO/TAO                                                        SAT 2230
      AMAX=B/C                                                           SAT 2240
      DS=RO/TAO + DS                                                     SAT 2250
      BS=DS/D                                                            SAT 2260
      AS=BS*BS                                                           SAT 2270
      C=R/DFLOAT(2*NA-1)                                                 SAT 2280
      XD=C/RAO                                                           SAT 2290
      DA=2.0*XD*TAO                                                      SAT 2300
      AB=AB*XB                                                           SAT 2310
      XJ=N/RAO                                                           SAT 2320
      EO=1.0-DEXP(-XJ*XJ)                                                SAT 2330
      CB=DCOS(B)                                                         SAT 2340
      CT=DCOS(T)                                                         SAT 2350
      ST=DSIN(T)                                                         SAT 2360
      STCB=ST*CB                                                         SAT 2370
      NY=0                                                               SAT 2380
      RAL=0                                                              SAT 2390
```

```
      Y=1.0                                                              SAT 2400
      DO 3 K=1,NA                                                        SAT 2410
      A=DFLOAT(K-1)                                                      SAT 2420
      A=DATAN(A*CA)                                                      SAT 2430
      CA=DCOS(A)                                                         SAT 2440
      SA=DSIN(A)                                                         SAT 2450
      CTCA=CT*CA                                                         SAT 2460
      STSA=ST*SA                                                         SAT 2470
      NZ=(2*K -1)                                                        SAT 2480
      NZ=NZ*NZ                                                           SAT 2490
      NP=NZ -NY                                                          SAT 2500
      DP=DFLOAT(NP)                                                      SAT 2510
      Z=DFLOAT(NZ)*XB                                                    SAT 2520
      Z=DEXP(-Z)                                                         SAT 2530
      P=(Y - Z)/DP                                                       SAT 2540
      DP=TWOPI/DP                                                        SAT 2550
      NY=NZ                                                              SAT 2560
      Y=Z                                                                SAT 2570
      P=P/PO                                                             SAT 2580
    1 P=-DP                                                              SAT 2590
      DO 2 L=1,NP                                                        SAT 2600
      P=P+DP                                                             SAT 2610
      CTP=CTCA - STSA*DCOS(P)                                            SAT 2620
      TP=DARCOS(CTP)                                                     SAT 2630
      CAP=SA*DCOS(P-B)                                                   SAT 2640
      AP=DABCOS(CAP)                                                     SAT 2650
      SNT=DSIN(TP)                                                       SAT 2660
      CS=1.                                                              SAT 2670
      IF(TP.NE.0.)CS=(STCP+(CAP*CTP))/(DSIN(AP)*SNT)                     SAT 2680
      S=DARCOS(CS)                                                       SAT 2690
      KAL=KAL+ 1                                                         SAT 2700
      SQ=DSIN(S)                                                         SAT 2710
      IF(SQ.LT.0.0)  SQ=-SQ                                              SAT 2720
      IF(CS.LT.0.0)  CS=-CS                                              SAT 2730
      PC(KAL)=CS                                                         SAT 2740
      PS(KAL)=SQ                                                         SAT 2750
      FLUX(KAL)=P                                                        SAT 2760
      YKC(KAL)=*AVCTB*SNT                                                SAT 2770
      PRINT 800,P,TP,S,KAL,YKC(KAL)                                      SAT 2780
    2 CONTINUE                                                           SAT 2790
    3 CONTINUE                                                           SAT 2800
  800 FORMAT(15X,'RAY AZIMUTH=',F9.6,',  ANGLE OF INCIDENCE=',F9.6,',   &SAT 2810
     *NGLE OF POLARIZATION=',F9.6,',  ',I3,',  YK= ',1PE13.6)           SAT 2820
      RETURN                                                             SAT 2830
      END                                                                SAT 2840
      SUBROUTINE OELIKE(KAL,E,H,EX,HX)                                   SAT 2850
      IMPLICITREAL*8(A-H,O-Z)                                            SAT 2860
      COMMON/A4/FLUX(09),YKC(09)                                         SAT 2870
      COMMON/A5/PC(09),PS(09)                                            SAT 2880
      EX=E*PS(KAL)                                                       SAT 2890
      HY=H*PS(KAL)                                                       SAT 2900
      EY=E*PC(KAL)                                                       SAT 2910
      HX=-H*PC(KAL)                                                      SAT 2920
      RETURN                                                             SAT 2930
      END                                                                SAT 2940
      SUBROUTINE WAVE(C,OMEGA       ,EX,HX,       YK,UIN1,UIN2)          SAT 2950
      IMPLICITREAL*8(A-H,O-Z)                                            SAT 2960
      COMPLEX*16 UIN1,UIN2,CPHASE,DCOPLX                                 SAT 2970
      NAMELIST/YANDT/Y,TIME                                              SAT 2980
      READ (5,YANDT)                                                     SAT 2990
      WRITE(6,YANDT)                                                     SAT 3000
      YY=Y/1.D2                                                          SAT 3010
      ENTRY WAVE3(YK,UIN1,UIN2,EX,HX)                                    SAT 3020
      ARG=(YK*YY)-(OMEGA*TIME*1.D-9)                                     SAT 3030
      ANGC=DCOS(ARG)                                                     SAT 3040
      ARGS=DSIN(ARG)                                                     SAT 3050
      CPHASE=DCMPLX(ANGC,ARGS)                                           SAT 3060
      UIN2  =EX*CPHASE                                                   SAT 3070
      UIN1  =HX*CPHASE                                                   SAT 3080
      RETURN                                                             SAT 3090
      END                                                                SAT 3100
      SUBROUTINE SAMPLE(T    ,D,PR1)                                     SAT 3110
      IMPLICITREAL*8(A-H,O-Z)                                            SAT 3120
      COMMON/A3/PI,ZMAT,C,Z,PP,NO,HBAR,BOLZ,AVAGAD                      SAT 3130
      NAMELIST/SMPL/TEMP,KIND                                            SAT 3140
      NAMELIST/GAS/PRESS                                                 SAT 3150
      READ(5, SMPL)                                                      SAT 3160
      WRITE(6,SMPL)                                                      SAT 3170
      T=TEMP + 273.15                                                    SAT 3180
      TEMP=T*BOLZ                                                        SAT 3190
```

```
    3 READ (5,GAS)                                                          SAT 3200
      WRITE(6,GAS)                                                          SAT 3210
      PR1=PRESS                                                             SAT 3220
      PRESS=PRESS*(1.013250+05)/7.602                                       SAT 3230
      D =PRESS/TEMP                                                         SAT 3240
   69 CONTINUE                                                              SAT 3250
      RETURN                                                                SAT 3260
      END                                                                   SAT 3270
      SUBROUTINE ELEMNT(WAVCTR,N,Z)                                         SAT 3280
      IMPLICITCOMPLEX*16(C),REAL*8(A-B,D-H,O-Z)                             SAT 3290
      COMPLEX*16DCMPLX                                                      SAT 3300
      COMMON/A1/CX(5,2,2),CD(5,2,2),CO(5,2,4)                               SAT 3310
      NAMELIST/PROPS/RINDEX,THICK,BETA                                      SAT 3320
      READ (5,PROPS)                                                        SAT 3330
      WRITE(6,PROPS)                                                        SAT 3340
      Z=THICK                                                               SAT 3350
      BETA=BETA*1.D2                                                        SAT 3360
      Z=Z/1.D2                                                              SAT 3370
      CX(N,2,1)=(0.D0,0.D0)                                                 SAT 3380
      CX(N,2,2)=(0.D0,0.D0)                                                 SAT 3390
      CX(N,1,1)=(0.D0,0.D0)                                                 SAT 3400
      BETA=BETA/(   RINDEX*WAVCTR*2.D0)                                     SAT 3410
      RINDEX=RINDEX*RINDEX                                                  SAT 3420
      ETA1=(RINDEX*(1.D0-(BETA*BETA)))-1.D0                                 SAT 3430
      ETA2=   RINDEX*BETA*2.D0                                              SAT 3440
      CX(N,1,2)=DCMPLX(ETA1,ETA2)                                           SAT 3450
      RETURN                                                                SAT 3460
      END                                                                   SAT 3470
      SUBROUTINE AESORB(TEMP,OMEGA,D,OFFSET,CSUSPT,DIPOLE,PR1,CSSL,Q)       SAT 3480
      IMPLICITCOMPLEX*16(C),REAL*8(A-B,D-H,O-Z)                             SAT 3490
      COMPLEX*16DCMPLX                                                      SAT 3500
      REAL*8C,MU,DIPOLE(2),F(2),PA(2)                                       SAT 3510
      COMMON/A1/CX(5,2,2),CD(5,2,2),CO(5,2,4)                               SAT 3520
      COMMON/A3/PI,ENAT,C,Z,EP,MU,HBAR,BOLZ,AVAGAD                          SAT 3530
      EQUIVALENCE(CX(2,1,2),F)                                              SAT 3540
      EQUIVALENCE(CX(2,2,2),PA)                                             SAT 3550
      NAMELIST/BAND/PEAK,DETX,FAG,T2,TIME,RINDEX,BUFFR                      SAT 3560
      READ (5,BAND)                                                         SAT 3570
      WRITE(6,BAND)                                                         SAT 3580
      DETX=DETX*PR1*100.0                                                   SAT 3590
      PR1=PR1 + BUFFR                                                       SAT 3600
      Q=3.42486 *DEXP(-0.28547 /(PR1**2))                                   SAT 3610
      CALL BOLTZ(1,300.,PDIFF,FACT,FACT6)                                   SAT 3620
      XSEC=DETX/(D*(FACT + FACT6))                                          SAT 3630
      PRINT 41,XSEC                                                         SAT 3640
   41 FORMAT(2X,'XSEC=',1PE13.6)                                            SAT 3650
      T2=T2/PR1                                                             SAT 3660
      TIME=TIME/PR1                                                         SAT 3670
      PEAK=2.D0*PI*C/(PEAK*1.D-9)                                           SAT 3680
      DELTA=(PEAK-OMEGA)*T2                                                 SAT 3690
      PRINT 49,DELTA                                                        SAT 3700
   49 FORMAT('0','DELTA= ',G14.6)                                           SAT 3710
      OFFSET=     (DELTA*DELTA)+1.D0                                        SAT 3720
      SUSCPT=C*DETX/PEAK                                                    SAT 3730
      DIPOL=HBAR/(D*PDIFF*T2)                                               SAT 3740
      CSUSPT=DCMPLX(DELTA,1.D0)                                             SAT 3750
      IF(MAG.NE.0)GO TO 2                                                   SAT 3760
      SUSCPT=(SUSCPT*RINDEX)-F(2)                                           SAT 3770
      DIPOLE(1)=DSQRT(DIPOL*SUSCPT*EP)                                      SAT 3780
      QR=DSQRT(FACT/(FACT + FACT6))                                         SAT 3790
      DIPOLE(1)=DIPOLE(1)*QR                                                SAT 3800
      DIPOLE(2)=0.D0                                                        SAT 3810
      CSUSPT=SUSCPT*CSUSPT                                                  SAT 3820
      CX(4,1,2)=CSUSPT/OFFSET                                               SAT 3830
      CX(4,2,2)=(0.D0,0.D0)                                                 SAT 3840
      GO TO 3                                                               SAT 3850
    2 SUSCPT=(SUSCPT/RINDEX)-PA(2)                                          SAT 3860
      DIPOLE(1)=0.D0                                                        SAT 3870
      DIPOLE(2)=DSQRT(DIFGL*SUSCPT)                                         SAT 3880
      CSUSPT=SUSCPT*CSUSPT                                                  SAT 3890
      CX(4,1,2)=(0.D0,0.D0)                                                 SAT 3900
      CX(4,2,2)=CSUSPT/OFFSET                                               SAT 3910
    3 CONTINUE                                                              SAT 3920
      IF(T2.GT.TIME)PRINT 5,TIME,T2                                         SAT 3930
    5 FORMAT('0ERROR IN SUBROUTINE AESORB,T1=',1PE13.6,',T2=',1PE13.6)      SAT 3940
      T=DSQRT(T2*TIME)/RDAM                                                 SAT 3950
      DIPOLE(1)=DIPOLE(1)*T                                                 SAT 3960
      DIPOLE(2)=DIPOLE(2)*T*RD                                              SAT 3970
      CSSL=CSUSPT*(FACT6/(FACT + FACT6))                                    SAT 3980
      CSUSPT=CSUSPT*(FACT/(FACT + FACT6))                                   SAT 3990
```

```
      RETURN                                                            SAT 4000
      END                                                               SAT 4010
      SUBROUTINE COPE(SIGMA)                                            SAT 4020
      IMPLICITCOMPLEX*16(C),REAL*8(A-B,D-H,O-Z)                         SAT 4030
      COMPLEX*16DCMPLX                                                  SAT 4040
      DIMENSION SIGMA(2),CSAVE(9)                                       SAT 4050
      COMMON/A1/CX(5,2,2),CD(5,2,2),CU(5,2,4)                           SAT 4060
      NAMELIST/CONDCT/SIGMAE,SIGMAM                                     SAT 4070
      READ (5,CONDCT)                                                   SAT 4080
      PRINT 1                                                           SAT 4090
    1 FORMAT(1X)                                                        SAT 4100
      WRITE(6,CONDCT)                                                   SAT 4110
      SIGMA(1)=SIGMAE                                                   SAT 4120
      SIGMA(2)=SIGMAM                                                   SAT 4130
      DO  6 N=1,3                                                       SAT 4140
    6 CSAVE(N)=CX(N,1,2)                                                SAT 4150
      CSAVE(5)=CX(4,1,2)                                                SAT 4160
      CSAVE(6)=CX(4,2,2)                                                SAT 4170
      GO TO 12                                                          SAT 4180
      ENTRY COPE2                                                       SAT 4190
      DO 5 N=1,3                                                        SAT 4200
      CX(N,1,1)=(0.D0,0.D0)                                             SAT 4210
      CX(N,2,1)=(0.D0,0.D0)                                             SAT 4220
      CX(N,2,2)=(0.D0,0.D0)                                             SAT 4230
    5 CX(N,1,2)=CSAVE(N)                                                SAT 4240
      CX(4,1,2)=CSAVE(5)                                                SAT 4250
      CX(4,2,2)=CSAVE(6)                                                SAT 4260
   12 CONTINUE                                                          SAT 4270
      DO 11 J=1,2                                                       SAT 4280
      DO11 K=1,2                                                        SAT 4290
      CD(5,J,K)=CX(2,J,K)                                               SAT 4300
   11 CX(5,J,K)=(0.D0,0.D0)                                             SAT 4310
      ENTRY COPE1                                                       SAT 4320
      DO 2 J=1,2                                                        SAT 4330
      CX(4,J,2)=CD(5,J,2)*CX(4,J,2)                                     SAT 4340
    2 CX(4,J,1)=DCMPLX(0.D0,SIGMA(J))                                   SAT 4350
      RETURN                                                            SAT 4360
      END                                                               SAT 4370
      SUBROUTINE PARAM(L,OMEGA,YR,CGAMMA)                               SAT 4380
      IMPLICITCOMPLEX*16(C),REAL*8(A-B,D-H,O-Z)                         SAT 4390
      COMPLEX*16DCMPLX                                                  SAT 4400
      REAL*8C,MU                                                        SAT 4410
      COMMON/A1/CX(5,2,2),CD(5,2,2),CU(5,2,4)                           SAT 4420
      COMMON/A3/PI,ENAT,C,Z,EP,MU,HBAR,BOLZ,AVAGAD                      SAT 4430
      FREQ=OMEGA                                                        SAT 4440
      CFREQ=DCMPLX(FREQ,0.D0)                                           SAT 4450
      DO  1 I=1,2                                                       SAT 4460
    1 CX(L,I,2)=1.*CX(L,I,2)                                            SAT 4470
      CX(L,1,2)=CX(L,1,2)*EP                                            SAT 4480
      CX(L,2,2)=CX(L,2,2)*MU                                            SAT 4490
      DO 2 J=1,2                                                        SAT 4500
    2 CX(L,J,1)=CX(L,J,1)+(CFREQ*CX(L,J,2))                             SAT 4510
      YRSQ=YR*YR                                                        SAT 4520
      CGAMMA=DCMPLX(YRSQ,0.D0)                                          SAT 4530
      CGAMMA=(CX(L,1,1)*CX(L,2,1))-CGAMMA                               SAT 4540
      CGAMMA=CDSQRT(CGAMMA)                                             SAT 4550
      DO 4 K=1,2                                                        SAT 4560
    4 CX(L,K,2)=CX(L,K,1)/CGAMMA                                        SAT 4570
      RETURN                                                            SAT 4580
      END                                                               SAT 4590
      SUBROUTINE AEELES(N,CZETA)                                        SAT 4600
      IMPLICITCOMPLEX*16(C),REAL*8(A-B,D-H,O-Z)                         SAT 4610
      COMPLEX*16DCMPLX                                                  SAT 4620
      COMMON/A1/CX(5,2,2),CD(5,2,2),CU(5,2,4)                           SAT 4630
      CI=(.0D0,1.D0)                                                    SAT 4640
      CSZETA=CI*CDSIN(CZETA)                                            SAT 4650
      CCZETA=CDCOS(CZETA)                                               SAT 4660
      DO 1 K=1,2                                                        SAT 4670
      CAPP=CDSQRT(CX(N,K,2)*CD(N,K,2))                                  SAT 4680
      CU(N,K,2)=CSZETA*CAPP                                             SAT 4690
      CU(N,K,3)=CSZETA/CAPP                                             SAT 4700
      CAPQ=CAPP/CD(N,K,2)                                               SAT 4710
      CTZETA=-CI*CSZETA*CD(N,K,1)                                       SAT 4720
      CU(N,K,4)=  (CCZETA+CTZETA)/CAPQ                                  SAT 4730
    1 CU(N,K,1)=  (CCZETA-CTZETA)*CAPQ                                  SAT 4740
      RETURN                                                            SAT 4750
      END                                                               SAT 4760
      SUBROUTINE WBONSK(N,AFRCX,CDET)                                   SAT 4770
      IMPLICITCOMPLEX*16(C),REAL*8(D-H,O-Q,S-Z)                         SAT 4780
      COMPLEX*8 CDET(5,2)                                               SAT 4790
```

```
      DIMENSION CDET(5,2)                                                SAT 4800
      COMMON/A1/CX(5,2,2),CO(5,2,2),CU(5,2,4)                            SAT 4810
      DO 6 M=1,2                                                         SAT 4820
      CDET(M,M)=(CU(M,M,1)*CU(M,M,4))-(CU(M,M,2)*CU(M,M,3))              SAT 4830
      CDET(M,M)=CDET(M,M)                                                SAT 4840
      KTEST=AIMAG(CDET(M,M))/APROX                                       SAT 4850
      IF(KTEST.NE.0) GO TO 1                                             SAT 4860
      KTEST=(REAL(CDET(M,M))-1.D0)/APROX                                 SAT 4870
      IF(KTEST.NE.0) GO TO 1                                             SAT 4880
    6 CONTINUE                                                           SAT 4890
      RETURN                                                             SAT 4900
    1 PRINT 2,M,M                                                        SAT 4910
    2 FORMAT('0ERROR IN SUBROUTINE MRCHSK,M=',I1,',M=',I1)               SAT 4920
      PRINT 5,CDET(M,M)                                                  SAT 4930
    5 FORMAT(' DETERMINANT OF CHARACTERISTIC MATRIX, REAL PART=',1PE13.6SAT 4940
     1,', IMAGINARY PART=',1PE13.6)                                      SAT 4950
      STOP                                                               SAT 4960
      END                                                                SAT 4970
      SUBROUTINE MULMAT(I,J,K)                                           SAT 4980
      IMPLICITCOMPLEX*16(A-E,U,X)                                        SAT 4990
      REAL*8 SUB(19)                                                     SAT 5000
      COMMON/A1/ X(5,2,2), D(5,2,2), U(5,2,4)                            SAT 5010
      DO 1 L=1,2                                                         SAT 5020
      A=(U(I,L,1)*U(J,L,1))+(U(I,L,2)*U(J,L,3))                          SAT 5030
      B=(U(I,L,1)*U(J,L,2))+(U(I,L,2)*U(J,L,4))                          SAT 5040
      C=(U(I,L,3)*U(J,L,1))+(U(I,L,4)*U(J,L,3))                          SAT 5050
      E=(U(I,L,3)*U(J,L,2))+(U(I,L,4)*U(J,L,4))                          SAT 5060
      U(K,L,1)=A                                                         SAT 5070
      U(K,L,2)=B                                                         SAT 5080
      U(K,L,3)=C                                                         SAT 5090
      U(K,L,4)=E                                                         SAT 5100
    1 CONTINUE                                                           SAT 5110
      RETURN                                                             SAT 5120
      END                                                                SAT 5130
      SUBROUTINE GETICS(DET,RO,TO,KAL,P,KCONE)                           SAT 5140
      IMPLICITCOMPLEX*16(D,R,T,U,X,C),REAL*8(P)                          SAT 5150
      REAL*8 SUB(19),P,PP(2),CDABS,ER(4),ET(4),RX(4),TX(4),DSQRT         SAT 5160
      DIMENSION DET(5,2),R(2),T(2),RO(2),TO(2),PRX(2),PTX(2)             SAT 5170
      COMMON/A1/ X(5,2,2), D(5,2,2), U(5,2,4)                            SAT 5180
      COMMON/A5/PC(C9),PS(C9)                                            SAT 5190
      EQUIVALENCE(R,ER)                                                  SAT 5200
      EQUIVALENCE(T,ET)                                                  SAT 5210
      IF(KAL.NE.1) GO TO 6                                               SAT 5220
      CONE=(0.D0,1.D0)                                                   SAT 5230
      TWO=(2.D0,0.D0)                                                    SAT 5240
      DO 8 I=1,4                                                         SAT 5250
      RX(I)=(0.D0,0.D0)                                                  SAT 5260
    8 TX(I)=(0.D0,0.D0)                                                  SAT 5270
    6 CONTINUE                                                           SAT 5280
      PP(1)=PC(KAL)                                                      SAT 5290
      PP(2)=PS(KAL)                                                      SAT 5300
      DO 1 I=1,2                                                         SAT 5310
      DENOM=(U(5,I,2)-(U(5,I,1)*X(5,I,2)))-(U(5,I,4)-(U(5,I,3)*X(5,I,2))SAT 5320
     1)*X(5,I,2)                                                         SAT 5330
      R(I)=((U(5,I,2)+(U(5,I,1)*X(5,I,2)))-(U(5,I,4)+(U(5,I,3)*X(5,I,2))SAT 5340
     1)*X(5,I,2))/DENOM                                                  SAT 5350
      T(I)=-TWO*DET(5,I)*X(5,I,2)/DENOM                                  SAT 5360
      T(I)=T(I)*PP(I)                                                    SAT 5370
      R(I)=R(I)*PP(I)                                                    SAT 5380
      PTX(I)=CDABS(T(I))                                                 SAT 5390
      PRX(I)=CDABS(R(I))                                                 SAT 5400
      RO(I)=R(I)                                                         SAT 5410
      TO(I)=T(I)                                                         SAT 5420
    1 CONTINUE                                                           SAT 5430
      IF(KCONE.EQ.1) GO TO 9                                             SAT 5440
      DO 7 I=1,4                                                         SAT 5450
      TX(I)=TX(I) +ET(I)*P*ET(I)                                         SAT 5460
      RX(I)=RX(I) +ER(I)*P*ER(I)                                         SAT 5470
    7 CONTINUE                                                           SAT 5480
      RO(1)=DSQRT(RX(1))-CONE*DSQRT(RX(2))                               SAT 5490
      RO(2)=-DSQRT(RX(3))+ CONE*DSQRT(RX(4))                             SAT 5500
      TO(1)=DSQRT(TX(1))*CONE*DSQRT(TX(2))                               SAT 5510
      TO(2)=DSQRT(TX(3))*CONE*DSQRT(TX(4))                               SAT 5520
    9 CONTINUE                                                           SAT 5530
      PTT=PTX(1)*PTX(1) + PTX(2)*PTX(2)                                  SAT 5540
      PRR=PRX(1)*PRX(1) + PRX(2)*PRX(2)                                  SAT 5550
      PRINT 11,KAL,PRR,PTT                                               SAT 5560
   11 FORMAT(10X,'KAL=',I3,5X,'R=',1PE13.6,5X,'T=',1PE13.6)              SAT 5570
      RETURN                                                             SAT 5580
      END                                                                SAT 5590
```

```
      SUBROUTINE INITAL(YK,UIN1,UIN2,R,B,M,KAL)                          SAT 5600
      IMPLICITCOMPLEX*16(C,E,H,U,V,X)                                    SAT 5610
      REAL*8 SUB(19),YK,PC,PS,ENP                                        SAT 5620
      DIMENSION UIN(2),R(2),UO(2),VO(2),PNP(2)                           SAT 5630
      COMMON/A1/ X(5,2,2), E(5,2,2), U(5,2,4)                            SAT 5640
      COMMON/A5/PC(09),PS(09)                                            SAT 5650
      PNP(1)=PC(KAL)                                                     SAT 5660
      PNP(2)=PS(KAL)                                                     SAT 5670
      UIN(1)=UIN1                                                        SAT 5680
      UIN(2)=UIN2                                                        SAT 5690
      DO 1 I=1,2                                                         SAT 5700
      VO(I)=UIN(I)*PNP(I) - UIN(I)*R(I)                                  SAT 5710
      VO(I)=VO(I)/X(5,I,2)                                               SAT 5720
      UO(I)=UIN(I)*PNP(I) + UIN(I)*R(I)                                  SAT 5730
    1 CONTINUE                                                           SAT 5740
      ENTRY PROP(B,R)                                                    SAT 5750
      DO 2 I=1,2                                                         SAT 5760
      U(5,I,1)=(UO(I)    *U(M,I,1))+(VO(I)    *U(M,I,2))                SAT 5770
      U(5,I,2)=(UO(I)    *U(M,I,3))+(VO(I)    *U(M,I,4))                SAT 5780
      U(5,I,3)=-YK*U(5,I,1)/X(M,I,1)                                     SAT 5790
      U(5,I,4)=(U(5,I,2)*U(5,I,2))+(U(5,I,3)*U(5,I,3))                   SAT 5800
      U(5,I,4)=CDSQRT(U(5,I,4))                                          SAT 5810
      UO(I)    =U(5,I,1)                                                 SAT 5820
      VO(I)    =U(5,I,2)                                                 SAT 5830
    2 CONTINUE                                                           SAT 5840
      RETURN                                                             SAT 5850
      END                                                                SAT 5860
      SUBROUTINE SAT(OFFSET,CSUSPT,DIPOLE,IFX,CSS6)                      SAT 5870
      IMPLICITCOMPLEX*16(C),REAL*8(A-B,D-H,O-Z)                          SAT 5880
      REAL*8LAMBDA,CDABS                                                 SAT 5890
      DIMENSION DIPOLE(2)                                                SAT 5900
      COMMON/A1/CX(5,2,2),CD(5,2,2),CU(5,2,4)                            SAT 5910
      IF(IFX.NE.1) GO TO 5                                               SAT 5920
      C1=CX(4,1,2)                                                       SAT 5930
      C2=CX(4,2,2)                                                       SAT 5940
      AVG=0.0                                                            SAT 5950
    5 CONTINUE                                                           SAT 5960
      CI=(.000,1.00)                                                     SAT 5970
      E=                                                                 SAT 5980
    1 CDABS(CU(5,2,1)-CI*CU(5,1,4))                                      SAT 5990
      R=                                                                 SAT 6000
    2 CDABS(CU(5,1,1)-CI*CU(5,2,4))                                      SAT 6010
      LAMBDA=(DIPOLE(1)*E)+(DIPOLE(2)*R)                                 SAT 6020
      LAMBDA=OFFSET+(LAMEDA*LAMBDA)                                      SAT 6030
      CD(4,1,2)=CX(4,1,2)                                                SAT 6040
      CD(4,2,2)=CX(4,2,2)                                                SAT 6050
      IF(IFX.NE.0) GO TO 6                                               SAT 6060
      LAMBDA=AVG/10.0                                                    SAT 6070
      CD(4,1,2)=C1                                                       SAT 6080
      CD(4,2,2)=C2                                                       SAT 6090
    6 CONTINUE                                                           SAT 6100
      AVG=AVG + LAMBDA                                                   SAT 6110
      CBLOCH=CSUSPT/LAMBDA  + CSS6                                       SAT 6120
      IF(DIPOLE(1)-DIPOLE(2)) 1,3,2                                      SAT 6130
    1 CX(4,1,2)=(0.00,0.00)                                              SAT 6140
      CX(4,2,2)=CBLOCH                                                   SAT 6150
      GO TO 4                                                            SAT 6160
    2 CX(4,1,2)=CBLOCH                                                   SAT 6170
      CX(4,2,2)=(0.00,0.00)                                              SAT 6180
      GO TO 4                                                            SAT 6190
    3 CX(4,1,2)=CBLOCH/2.00                                              SAT 6200
      CX(4,2,2)=CBLOCH/2.00                                              SAT 6210
    4 CONTINUE                                                           SAT 6220
      RETURN                                                             SAT 6230
      END                                                                SAT 6240
      SUBROUTINE DERIV(CDZETA,CP)                                        SAT 6250
      IMPLICITCOMPLEX*16(C),REAL*8(A-B,D-H,O-Z)                          SAT 6260
      DIMENSION CP(2)                                                    SAT 6270
      COMMON/A1/CX(5,2,2),CD(5,2,2),CU(5,2,4)                            SAT 6280
      CONE=(1.00,0.00)                                                   SAT 6290
      CTWO=(2.00,0.00)                                                   SAT 6300
      DO 1 I=1,2                                                         SAT 6310
      CD(4,1,1)=((CX(4,I,2)/CD(4,I,2))-CONE)/(CTWO*CDZETA)               SAT 6320
    1 CONTINUE                                                           SAT 6330
      RETURN                                                             SAT 6340
      END                                                                SAT 6350
      SUBROUTINE TEST(N,R,T,RNEW,TNEW,APROX,BSQ,TSQ,*)                   SAT 6360
      COMPLEX*16      TNEW(2),R(2),T(2),RNEW(2)                          SAT 6370
      REAL*8 APROX,BSQ,TSQ,CDABS,AVR(2),AVT(2)                           SAT 6380
      DO 9 I=1,2                                                         SAT 6390
```

```
      AVR(I)=CDABS(RNEW(I))                                              SAT 6400
    9 AVT(I)=CDABS(TNEW(I))                                              SAT 6410
      RSQ=AVR(1)*AVR(1) + AVR(2)*AVR(2)                                  SAT 6420
      TSQ=AVT(1)*AVT(1) + AVT(2)*AVT(2)                                  SAT 6430
      DO 2 I=1,2                                                         SAT 6440
      KTEST=                                                             SAT 6450
     1      CDABS(RNEW(I)-R(I))/APROX                                    SAT 6460
      IF(KTEST.NE.0)GO TO 7                                              SAT 6470
      KTEST=(CDABS(TNEW(I)) -CDABS(T(I)))/APROX                          SAT 6480
      IF(KTEST.NE.0)GO TO 7                                              SAT 6490
    2 CONTINUE                                                           SAT 6500
      PRINT 3,N                                                          SAT 6510
    3 FORMAT('0CONVERGENCE ACHIEVED WITH  ',I6,' INTERVALS.')            SAT 6520
      PRINT 42,RSQ,TSQ                                                   SAT 6530
   42 FORMAT(' INTENSITY REFLECTANCE=',G14.7,',INTENSITY TRANSMITTANCE='SAT 6540
     1,G14.7)                                                            SAT 6550
      RETURN 1                                                           SAT 6560
    7 DO 8 K=1,2                                                         SAT 6570
      R(K)=RNEW(K)                                                       SAT 6580
      T(K)=TNEW(K)                                                       SAT 6590
    8 CONTINUE                                                           SAT 6600
      PRINT 43,KTEST,N                                                   SAT 6610
   43 FORMAT(10X,'KTEST= ',I5,5X,'ITERATION= ',I3,/)                     SAT 6620
      RETURN                                                             SAT 6630
      END                                                                SAT 6640
      SUBROUTINE BOLTZ(K,TCOR,PDIFF,FACT,FACT6)                          SAT 6650
      IMPLICIT REAL*8(A-H,O-Z)                                           SAT 6660
      DIMENSION FREQ(6),IDEG(6),ZO(6)                                    SAT 6670
      DATA FREQ,IDEG,HCGK/770.,640.,548.,614.,522.,350.,1,2,3,3,3,3,     SAT 6680
     *1.439/                                                             SAT 6690
      HCOT=HCGK/TCOR                                                     SAT 6700
      Z=1.D0                                                             SAT 6710
      DO 1 I=1,6                                                         SAT 6720
      ZO(I)=DEXP(-HCOT*FREQ(I))                                          SAT 6730
      Q=1.D0/(1.D0-ZO(I))                                                SAT 6740
      C=Q**IDEG(I)                                                       SAT 6750
      ZO(I)=ZO(I)*DFLOAT(IDEG(I))                                        SAT 6760
    1 Z=Z*Q                                                              SAT 6770
      DO 3 I=1,6                                                         SAT 6780
      ZO(I)=ZO(I)/Z                                                      SAT 6790
    3 CONTINUE                                                           SAT 6800
      ZGR=1.0/Z                                                          SAT 6810
      PRINT 4,ZGR,(ZO(I),I=1,6)                                          SAT 6820
    4 FORMAT(10X,7(F9.6,3X))                                             SAT 6830
      FACT=ZGR                                                           SAT 6840
      PDIFF=ZGR - ZO(3)                                                  SAT 6850
      FACT6=ZO(6)                                                        SAT 6860
      IF(K.EQ.1) GO TO 2                                                 SAT 6870
      FACT=FACT/FAC1                                                     SAT 6880
      PDIF1=ZGR + ZO(3)                                                  SAT 6890
      PDIFF=PDIFF/PDIF1                                                  SAT 6900
      FACT6=FACT6/FAC6                                                   SAT 6910
      PRINT 782,TCOR,FACT,PDIFF ,FACT6                                   SAT 6920
      RETURN                                                             SAT 6930
    2 FAC1=FACT                                                          SAT 6940
      FAC6=FACT6                                                         SAT 6950
      PRINT 782,TCOR,FACT,PDIFF ,FACT6                                   SAT 6960
  782 FORMAT(10X,'TCOR=',G14.6,'  FACT=',G14.6,'  PDIFF=',G14.6,' FACT6=SAT 6970
     1',G14.6)                                                           SAT 6980
      RETURN                                                             SAT 6990
      END                                                                SAT 7000
      SUBROUTINE COMPAR(X,Y1,Y2)                                         SAT 7010
      DIMENSIONX(100),Y1(100),AS(10),DATE(10) ,Y2(100)                   SAT 7020
      READ 110,(DATE(I),I=1,10)                                          SAT 7030
  110 FORMAT(10A4)                                                       SAT 7040
      PRINT 204,(DATE(I),I=1,10)                                         SAT 7050
  204 FORMAT('1',35X,'TRANSMITTANCE DATA FOR SATURATION OF SF6 WITH A COSAT 7060
     12 LASER',///,45X,10A4,///)                                         SAT 7070
      SDIF=0.0                                                           SAT 7080
      SDIFR=0.0                                                          SAT 7090
      PRINT 5                                                            SAT 7100
    5 FORMAT('0',6X,'LOG PW TEXP     YCAL      DIF       REXO          RCAL SAT 7110
     *    RDIF */)                                                       SAT 7120
      DO 2 I=1,8                                                         SAT 7130
      IP=I + 10                                                          SAT 7140
      READ 1,Y1(IP),Y2(IP)                                               SAT 7150
    1 FORMAT(10X,2F10.6)                                                 SAT 7160
      X(IP)=X(I)                                                         SAT 7170
      DIF=Y1(IP)-Y1(I)                                                   SAT 7180
      DIFR=Y2(IP) - Y2(I)                                                SAT 7190
```

```
      SDIP=SDIF + DIF*DIF                                                    SAT 7200
      SDIPB=SDIPB + DIFB*DIFB                                                SAT 7210
      PRINT 4,X(I),Y1(IP),Y1(I),DIF,Y2(IP),Y2(I),DIFB                        SAT 7220
    4 FORMAT(5X,7F10.6)                                                      SAT 7230
      J=I                                                                    SAT 7240
      PUNCH 777,X(J),Y1(J),Y2(J),PB1                                         SAT 7250
  777 FORMAT(4F10.6)                                                         SAT 7260
    2 CONTINUE                                                               SAT 7270
      SDIP=SQRT(SDIP/8.0)                                                    SAT 7280
      SDIPB=SQRT(SDIPB/8.0)                                                  SAT 7290
      PRINT 6,SDIP,SDIPB                                                     SAT 7300
    6 FORMAT('0',25X,'ROOT MEAN SQUARE DEVIATION=',2G14.6)                   SAT 7310
      RETURN                                                                 SAT 7320
      END                                                                    SAT 7330
//GO.SYSIN DD *                                                            SAT 7340
 &MAIN NE=S=0, ACURAT=0.2,  NOP=5, LAVG= 8, &END                           SAT 7350
 &LSR FOKH=10.0, DIAM=6.0,  WAVE=10.5910350+3, &END                        SAT 7360
0.0906    0.164     0.33      0.615     01.66      2.56      5.3       1SAT 7370
 &GM BO=1.78E-3,  AO=7.90-4,   B=1.00E-3,  DO=2.03,  DS=1.76,  E=90.0,   SAT 7380
  T=0.001, NA=1,&ESC                                                       SAT 7390
 &YANDT Y=3.0,  TIME=1.0, &END                                             SAT 7400
 &SMEL TEMP=40.C,  KIND=3, &END                                            SAT 7410
 &GAS PRESS=0.430, &END                                                    SAT 7420
 &PROPS RINDEX=1.454462,THICK=0.6498090, BETA=0.0,&END                     SAT 7430
 &ERCPS RINDEX=1.0000,  THICK=10.C00C6,  BETA=0.00    ,&END               SAT 7440
 &PRCPS RINDEX=1.454462,THICK=0.6498090, BETA=0.0,&END                     SAT 7450
 &BAND PEAK=10.5910350D3,BETE=0.46   ,  MAG=0,  T2=20.D-9,  TIME=122.D-6,SAT 7460
  RINDEX=1.0CC0, BUFPR=0.0,   &END                                         SAT 7470
 &CONDCT SIGMAE=0.0,  SIGMAM=0.0, &END                                     SAT 7480
  RUN 5  26 APRIL 75                                                       SAT 7490
 7.        .149301   .0627665                                             SAT 7500
 6.        .156865   .0656625                                             SAT 7510
 5.        .173141   .07C5795                                             SAT 7520
 4.        .195994   .0682916                                             SAT 7530
 3.        .266894   .07C753                                              SAT 7540
 2.        .308768   .0743358                                             SAT 7550
 1.        .373077   .0787341                                             SAT 7560
 0.        .450082   .0849651                                             SAT 7570
```

757 CARDS READ

APPENDIX 3
FREQUENCY STABILIZATION OF THE CO_2 LASER[1]

A. INTRODUCTION

This appendix describes an inexpensive modification to a Model 948 CO_2 laser that greatly improves the long and short term frequency stability. This modification does not require prisms, gratings, an infrared detector, or an expensive lock-in-amplifier. Also, accurate tuning and locking of the frequency over the Doppler gain profile for each available laser transition is made possible thereby.

One of several possible laser transitions is selected by changing the cavity length: the rear laser cavity reflector is mounted upon a piezoelectric transducer for that purpose. The manufacturer acheived some frequency stability by stabilizing the dc voltage applied to the piezoelectric transducer and by designing a laser cavity which resists changes in length due to thermal and mechanical fluctuations. The manufacturer claims a long term (hours) frequency deviation less than 2 MHz after a 1/2 hour warm-up when an auxiliary heat exchanger is used to obtain greater-thermal stability. On some occasions the laser did acheive this frequency stability; however, in most cases the frequency drift was sufficient to cause a jump from one laser transition to another in less than one hour.

The modification is a servo system which modulates the cavity length of the laser and uses the effects of this modulation upon the impedance of the laser plasma tube to produce a frequency correction. The cavity length is modulated by adding an ac voltage to the piezoelectric transducer described above. Since the resonance frequency of the laser cavity is inversely proportional to this length, a frequency modulation is obtained thereby. The bandwidth of the cavity resonance frequency is very much narrower than that of the gain curve for any one laser transition. With proper selection of the amplitude of the ac voltage, the modulation impressed upon the cavity resonance will be large in comparison with the bandwidth of the cavity resonance, but small in comparison with the gain width. Therefore the output power of the laser is caused to oscillate by a few percent of its maximum at the same frequency as that of the ac voltage. A typical laser gain vs frequency curve, which is shown in Fig. 1, illustrates that the amplitude and phase relationship between the frequency modulation signal and laser gain modulation signal will be unique for any portion of the laser gain profile above the threshold level.[2] The modulation of the output power of the laser, in turn, produces an oscillation in the impedance of the plasma tube because the impedance decreases as the power output increases.[3,4] Synchronous detection of the impedance modulation, using the ac piezoelectric signal as a reference, gives a voltage that is proportional in magnitude and sign to the peak-seeking correction signal. This latter is defined as the frequency correction needed to cause the cavity resonance frequency to coincide with the

Figure 1: Gain vs frequency curve above the threshold level for a typical laser transition. ΔL is the cavity length (frequency) modulation that produces a modulation in the gain and also in the impedance (ΔZ) of the plasma tube. (a) Laser frequency operation far from the center frequency. (b) Laser operation near the center frequency.

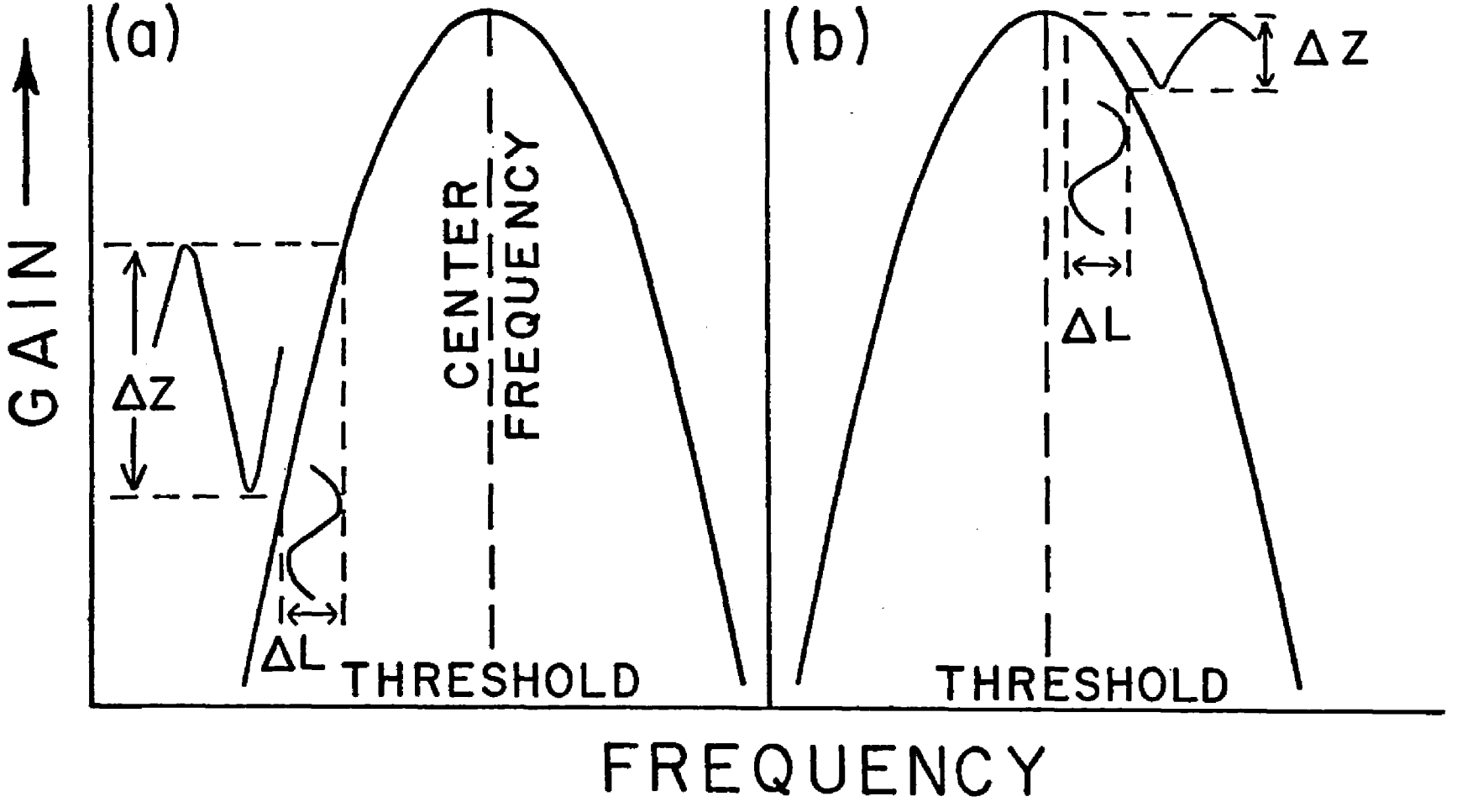
(a)
(b)
GAIN
ΔZ
ΔL
CENTER FREQUENCY
THRESHOLD
THRESHOLD
ΔZ
ΔL
FREQUENCY

peak of the laser gain profile for a particular laser transition. The peak-seeking correction signal is integrated and the resulting dc voltage is added to the other voltages being applied to the piezoelectric transducer. This integration causes the output frequency of the laser to be changed until the synchronously detected signal becomes zero. The frequency at which this occurs corresponds to the peak of the gain profile as intended. To operate at a frequency within this gain curve other than that of its peak, a dc voltage is added to the synchronously detected signal. The integration now causes the frequency output of the laser to be changed until this sum becomes zero. Thus variation in magnitude and sign of this added dc voltage permits frequency tuning over the entire laser gain profile.

The technique of modulating the laser frequency and utilizing the resulting perturbation of the impedance of the laser plasma tube to produce an error signal was first reported by Skolnick.[4] His laser cavity, however, contained dispersive elements (4 Brewster-angle prisms) which insured laser operation at a single transition. He used his system to stabilize the frequency of the laser radiation at the peak of the laser gain vs frequency curve and acheived a drift rate of less than 50 kHz/h. The system described herein may be able to acheive the same stability for accessible laser transitions without the use of the dispersive elements.

B. DESCRIPTION OF MODIFICATION

The heart of the frequency stabilization system is the electronic device which synchronously detects the perturbations in the impedance of the laser plasma tube and generates a voltage which can be used to correct any changes in the laser cavity length. It may be built for less than $150 assuming an oscilloscope and audio oscillator are available. A circuit schematic of this device and its connections to the laser electronics is given in Fig. 2.

Additionally, two modifications of the electronics of the laser are required. The first alteration is necessary to obtain a voltage signal that indicates the plasma tube impedance. A resistor R1 is placed in series with the plasma tube and R2. The high voltage dc power supply is current regulated but has a slow response compared to the modulation frequency (650 Hz) we used. Thus a rapid modulation in the plasma tube impedance produces a modulation in the current which is measured as a voltage modulation across R1. This voltage is then ac coupled to the electronic device which uses this voltage signal to regulate the length of the laser cavity. The capacator C1 which is in parallel with R1 damps out high frequency oscillations of the power supply. The second alteration involves the low voltage side of the piezoelectric transducer which was originally grounded at point A. In the original configuration tuning the cavity length over its ~ 6 micron adjustment range was accomplished by varying R3 which caused 0-400 V dc to be applied to the piezoelectric transducer. Because it was convenient, both the modulation

Figure 2: Schematic of Modification. Resistances (ohms) and capacitances (microfarads) are within 10% of nominal values, and resistors are power rated at ½-watts, unless otherwise stated. (*) Items mounted on front panel. HP designates Motorola products; SK designates RCA products.

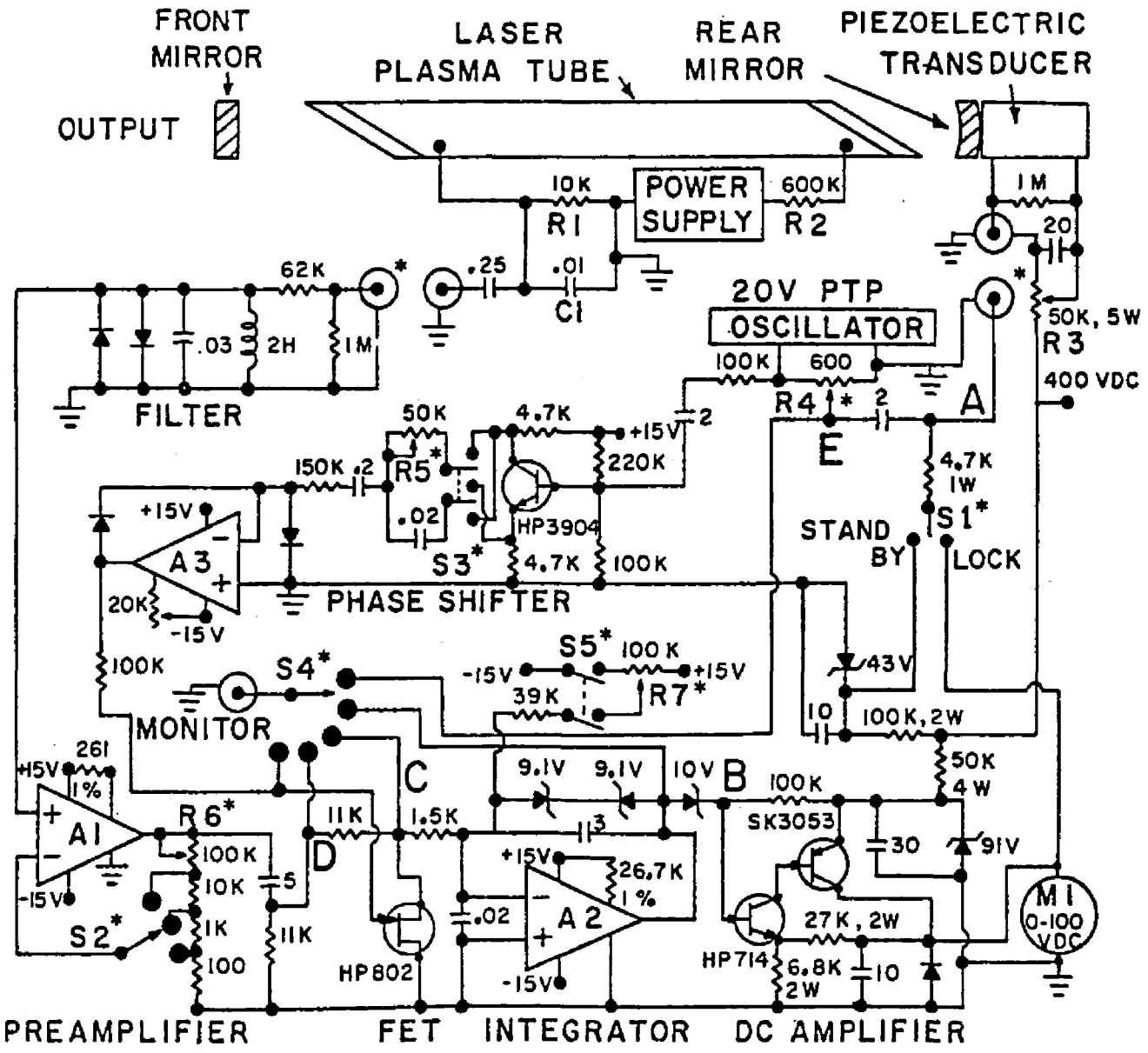
FRONT MIRROR
OUTPUT
LASER PLASMA TUBE
REAR MIRROR
PIEZOELECTRIC TRANSDUCER
10K
R1
POWER SUPPLY
600K
R2
1M
20
62K
.25
.01
C1
20V PTP OSCILLATOR
50K, 5W
R3
400 VDC
100K
600
R4*
2
A
E
.03
2H
1M
FILTER
50K
4.7K
+15V
2
150K
.2
R5*
220K
4.7K
1W
S1*
STAND BY
LOCK
.02
HP3904
S3*
4.7K
100K
+15V
A3
20K
-15V
PHASE SHIFTER
100K
S4*
MONITOR
S5*
100K
-15V
+15V
39K
R7*
43V
10
100K, 2W
50K
4W
261
1%
+15V
A1
R6*
11K
1.5K
C
9.1V
9.1V
10V
B
100K
SK3053
30
91V
D
100K
10K
5
1K
100
S2*
11K
HP802
.02
+15V
26.7K
1%
A2
-15V
27K, 2W
HP714
6.8K
2W
10
M1
0-100 VDC
PREAMPLIFIER
FET INTEGRATOR
DC AMPLIFIER

signal and the error correction signal are applied to the low voltage side of the piezoelectric transducer. This leaves the original cavity tuning method unchanged. Also for convenience we use a positive (0-86 V) dc amplifier to produce the final error correction voltage. Since frequency errors may be either positive or negative, the electronics are designed to generate 43 V dc at A for a zero frequency error when S1 is switched to "lock". While varying R3 to find a particular frequency S1 is switched to "stand-by" position. This applies a constant 43 V dc at point A. The 86 V range of the dc amplifier permits the position of the mirror mounted on the piezoelectric transducer to be automatically regulated over $\pm$ 11% of its full range when S1 is in the "lock" position.

The frequency-regulating electronics receive an input signal from the voltage modulation across R1. The signal is first passed through a tank circuit used as a band-pass filter.[5] The audio oscillator was tuned to match the resonance frequency of the filter (650 Hz). The signal (a few millivolts) is then amplified with a Burr Brown Model 3308 operational amplifier in the non-inverting mode. This amplified signal is next ac coupled to an integrator constructed with a Burr Brown Model 3267 operational amplifier. Synchronous detection is realized by connecting the source and drain of a field effect transitor (FET) across the inputs of the integrator. When 0.4 V dc is applied to the gate of the FET it has a low resistance and effectively shorts the inputs of the integrator. When -15 V dc is applied to the gate of the FET it has a very large resistance and the amplified signal from the preamplifier (A1) is effectively integrated. The phase shifting network produces a two level (0.4 or

-15 V) voltage output that is used as the reference signal in this method of synchronous detection. The integrator continuously sums the voltages produced by each cycle of synchronous detection. When the laser cavity length error is corrected, synchronous detection gives a zero voltage for center frequency operation, but the integrator still maintains the voltage sum which produced the desired voltage correction on the piezoelectric transducer. The integrator will continue to hold this voltage sum (time constant for decay $\sim$ 100 s) until a change in the laser cavity length causes the synchronous detector to produce a non-zero voltage. To operate at a frequency other than the center frequency of the gain curve, S5 is closed and an adjustable voltage is added to the synchronously detected signal at the integrator input. The system will now strive to adjust the cavity length until this sum is zero. The integrator output is fed to the anode of a 10 V Zener diode. The cathode of the Zener diode is maintained at 10 V greater than the anode. Since the integrator output may range from -10 V to +10 V, the input to the dc amplifier (point B) then ranges from 0 to 20 V dc. This dc signal is amplified by a factor of 4.3. The output from the dc amplifier goes to S1 and the low voltage side of the piezoelectric transducer. Thus when the integrator output is zero volts, point B is at 10 V dc and the dc amplifier output is 43 V.

The phase shifting network is ac coupled to the same audio oscillator which drives the piezoelectric transducer. The phase of this voltage may be shifted up to 180 degrees by varying R5. Switching S3 permits a 180 degree phase variation. This phase shifted

signal is next coupled to a Fairchild # 741 operational amplifier (A3) in the inverting configuration with a diode permitting only positive feedback. When the input to A3 is negative, A3 has a low gain and outputs a maximum positive voltage equal to the threshold of the feedback diode. When the input is positive A3, cannot drive its inputs equal and saturates to -15 V dc at the output. Thus a sine wave input will produce a two level (0.4 or -15 V) square wave at the output of A3. This square wave is fed to the synchronous detector.

The circuit elements of the frequency regulating electronics are totally enclosed in an aluminum housing. The dc voltmeter, input and output terminals, and all designated switches and variable resistors are mounted on the front panel. Power to operate the electronics is obtained externally from a Burr-Brown dual power supply, model 524 ($\pm$ 15 V dc) [$\leq$ 1.0 mV (rms) noise and ripple] and from the 400 V dc power supply integral to the laser. The driving oscillator is also external and is connected through the rear panel. A Hewlett Packard Model 200 I audio oscillator with 600 ohm output impedance is used in this work, and it is operated at 20 V peak to peak. If a low impedance audio oscillator is not available one could be easily constructed following available oscillator circuits.[6]

C. OPERATION

To bring the frequency stabilizing system into operation S1 is initially switched to "stand-by", S5 is opened, and the gain of the preamplifier (A1) is set to a minimum with S2. An oscilloscope

is connected to the monitor output in order to observe the voltage signals at various test points. The audio oscillator is set at the proper frequency and then R4 is adjusted so that a 2 V peak to peak modulation is applied to point E and the piezoelectric transducer. This will produce less than one MHz modulation in the frequency of the output radiation. Next, power is supplied to the frequency-regulating electronics and the CO_2 laser is started. The frequency selector R3, is adjusted to set the laser cavity length so that the output frequency of the laser is near the center frequency of the desired laser transition. The gain of A1 is now increased to 60 dB or until the ac signal at the output of A1 (point D) is about 4 V peak to peak.

The peak of the available laser transitions can be accurately located by simply observing when the voltage amplitude at point D goes through a minimum. To find the center frequency while monitoring point D, R3 is finely adjusted until the oscillating voltage produced by the plasma tube impedance modulation goes to a minimum amplitude and changes phase by 180° with continued adjustment of R3. To complete the tuning, the integrator input (point C) is monitored and the phase of the reference signal is adjusted to center the $\frac{1}{2}$-cycle window on a peak of the oscillating voltage. The voltmeter should be reading about 43 V. When S1 is switched to "lock", the stabilizing system will automatically track the peak of the frequency vs gain curve for this laser transition. If the error correction voltage swings to either extreme, the phase of the reference signal must be shifted 180 degrees with S3.

After acheiving a lock at the center frequency the lock is firmed and tested. To firm the lock, the gain of A1 is increased to 60 dB or until the voltmeter starts to oscillate. When oscillations occur the gain is then decreased until the voltmeter oscillations cease. This firming will insure a maximum correction speed to any perturbations which might cause the laser cavity length to change. A good test of the lock is to vary R3: with a true lock the voltmeter reading will change to exactly compensate the voltage change that is applied to the high voltage side of the piezoelectric transducer.

To operate at frequencies other than the center frequency of a laser transition, the system is first locked at the center frequency. The variable resistor R7 is set to its middle setting and S5 is closed. While monitoring point D, R7 is varied to achieve laser operation at the desired frequency. If the peak to peak amplitude at D reaches 16 V, further tuning is acheived by decreasing the gain of A1 with R6. During the off center frequency tuning R3 may require adjustment to maintain the correction voltage in its middle range.

Since the regulating capability extends only over $\pm$ 11% of the laser cavity length adjustment range, a large perturbation may cause the cavity length to drift out of the regulation range. When this occurs the initial lock is temporarily lost. It is a good practice to adjust R3 to bring the error correction signal back to its middle range of 43 V whenever it approaches the limit of the regulating range. This adjustment is usually needed only during the first half hour of operation.

Facilities to accurately test the ultimate frequency stability of this modified laser were not available. The response time (required for the correction to reach 90% of its final magnitude) of this present system was measured for both center frequency and off center frequency operation. When voltage perturbations of 1.0 to 20 V were applied to the piezoelectric transducer, the correction response times ranged from 1.0 to 1.4 seconds and were equivalent for both modes of operation. Faster responses could be obtained by increasing the gain of the integrator and constructing a more responsive synchronous detector.[7] Since the 1.0 V perturbation corresponds to a 0.5 MHz frequency change and this system readily responded to this perturbation, the frequency stabilizing system described herein must considerably exceed a frequency of 0.5 MHz for perturbations slower than 1 Hz. Unfortunately, operation in the off-center frequency mode may not acheive this high stability over long term operation. In this mode, frequency corrections rely on the stability of the laser output power, the amplitude of the audio oscillator, and the gain of the servo electronics. A 2% total change in these quantities would cause a 1 MHz frequency drift when operating far from the center frequency. Since there is a greater variation in the slope of the gain vs frequency curve near the center frequency, a much greater change in the above quantities would be necessary to produce a 1 MHz drift when operating near the center frequency. After a 30 minute warm-up time, a 2% stability in these quantities was readily obtainable. Fortunately, operation in the center frequency mode is not subject to these instabilities.

REFERENCES

1. The frequency stabilizing system described in this appendix was built in collaboration with Don C. Elbers. The contents herein were presented in part by the author at the annual meeting of the Optical Society of America, Houston, October 1974. These contents were later published in their entirety, W. H. Thomason and Don C. Elbers, Rev. Sci. Instrum., 46 409 (1975).
2. An inflection point in the laser gain profile was not observed. This suggests that the gain at threshold for our laser is above the inflection point of a Doppler-broadened gain profile. Another posibility is that the gain profile of our laser has the shape of a parabola such as that reported by Schiffner for a similar laser. (Parabolas have no inflection points.) G. Schiffner, IEEE J. Quantum Electron. 8, 877 (1972).
3. H. Kindl, W. Leeb, and G. Schiffner, Proc. IEEE, 56, 781 (1968).
4. M. L. Skólnick, IEEE J. Quantum Electron., 6, 139 (1970).
5. The 2 H inductor and 0.03μf capacitor are integral components of a General Radio Type 1231-P5 Adjustable Filter.
6. M. K. V. Kooi, Ed., "Linear Applications" (National Semiconductor Corp., Santa Clara, Ca., 1973) pp. AN20-9, AN51-8.
7. L. C. Caplan and R. Stern, Rev. Sci. Instrum., 42, 689 (1971).

APPENDIX 4

ELECTRONICS AND PROCEDURE - TRANSMITTANCE EXPERIMENT

The various electronic devices which were used to conduct the transmittance experiments and the procedure followed in their employment are discussed in this appendix. Figure 1 is a block diagram which shows these electronic devices and their wiring connections. The outputs of both pyroelectric detectors (D1 and D2) were applied to preamplifiers PA1 and PA2. The output of PA1 was applied to an absolute value determining circuit (ADCV); the output of which was applied to the I input of the analog computer (AC) described in Appendix 1. The output of PA2 was applied to a dual-channel lock-in amplifier (DCL) which required three synchronous signals. The synchronous signals were supplied by pulse generators (PG) which were ultimately synchronized with the mechanical light chopper. The oscilliscope (O) was used to monitor the detector outputs and set the synchronous signals. The DCL had two outputs which were applied to the inputs of the R and T channels of the analog computer. The AC processed these three signals and applied the resulting voltage signals (0-10 V) to the inputs of the three-channel strip-chart recorder (R) described in Appendix 1.

Operational amplifiers (OA) were used extensively in this work as the active electronic components of the various circuits described in Appendices 1,3,4, and 5. They are easy to employ and have a wide variety of applications. The OA has two input

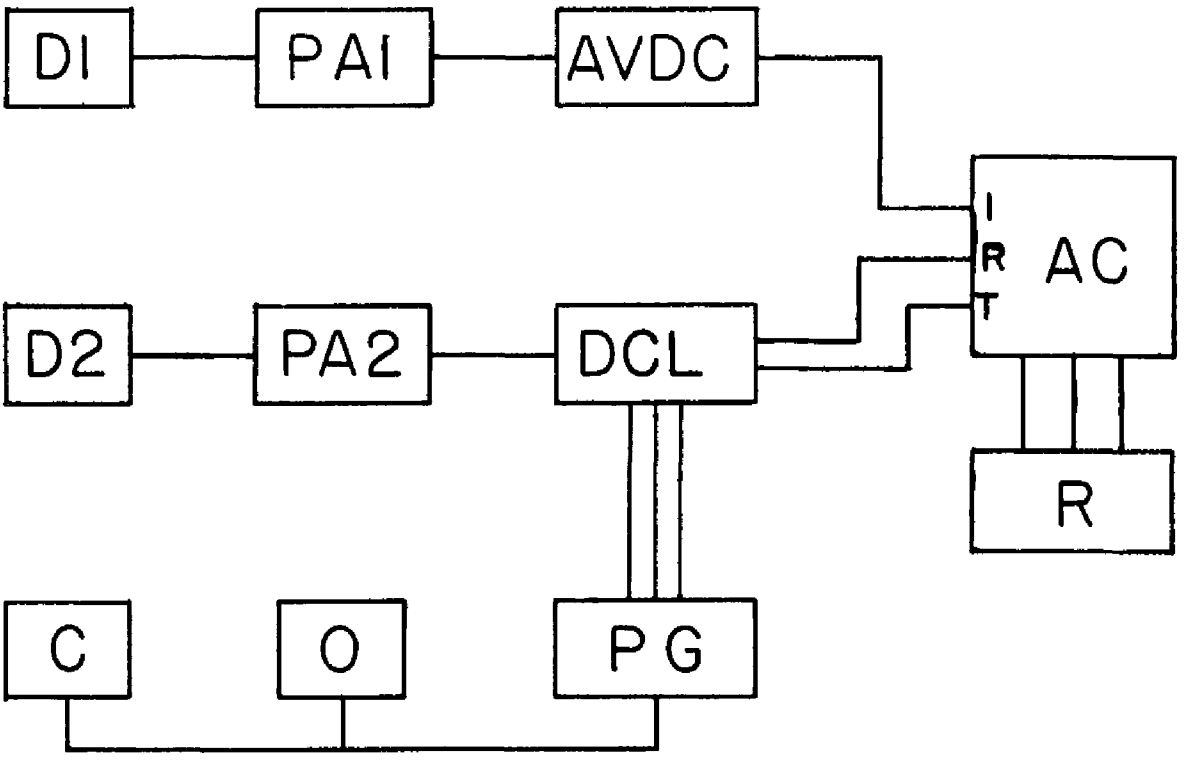

FIGURE 1. Block diagram of electronic devices used in the transmittance experiment with detectors (D1 and D2), preamplifiers (PA1 and PA2), mechanical light chopper (C), oscilliscope (O), absolute value determining circuit (AVDC), dual-channel lock-in (DCL), pulse generators (PG), analog computer (AC), and recorder (R).

channels and one output channel. The inverting input is signified by a (-) and the non-inverting input by a (+). The usual circuit configuration provides for a current feedback from the output to the (-) input. The OA will produce a voltage at the output so as to supply sufficient current to the (-) input that the potential of the (-) input will be the same as the (+) input. This feedback feature enables the OA to act as a linear electronic device. The most common application of an OA is to amplify and change the polarity of a voltage signal. This application requires that the OA be used in an inverting mode which is shown in Fig. 2. The

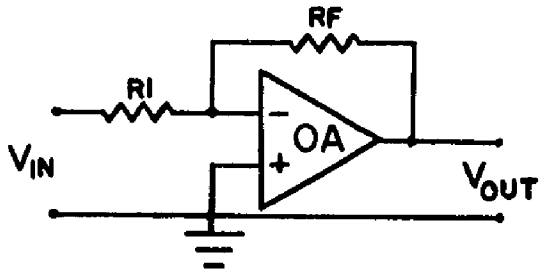

FIGURE 2. Operational Amplifier in the Inverting Mode

voltage gain of the circuit shown in Fig. 2 is -RF/RI. One disadvantage of this inverting circuit is that the input impedance is RI which limits the ability of this circuit to receive an input from a high impedance voltage source. When a high input impedance is desired, the OA is used in the non-inverting mode which is illustrated in Fig. 3. In this non-inverting circuit the input impedance is typically several million ohms (Ω) and can be increased to 10^8 Ω when the OA has an FET input. The gain of the

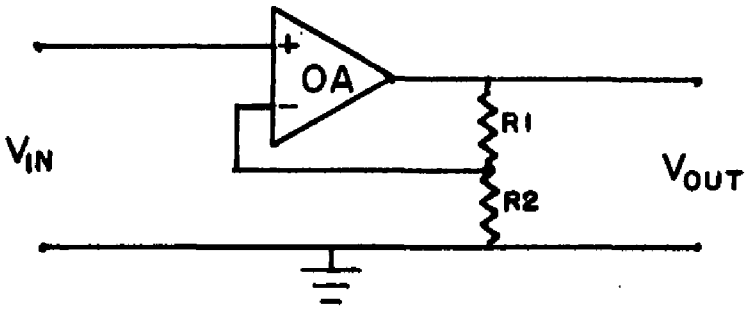

FIGURE 3. Operational Amplifier in the Non-inverting Mode

non-inverting configuration is (R1 + R2)/R2. These two OA configurations are the most common applications, but this simple feedback principle can be used to acheive a large variety of voltage and current treatments with an OA. Some of these treatments of input voltages are addition, substraction, integration, differentiation, multiplication, division, and logrithmic extraction. These treatments are accomplished by using appropriate resistors, capicators, diodes, or transistors in the input and feedback positions of the OA circuit. All of the OAs used in this work required input and output voltages to be in the range of $\pm$ 10 V. The OAs required $\pm$ 15 V for operational power and this was supplied by a Burr Brown dual power supply, model 524 ($\pm$ 15 V dc, $\leq$ 1.0 mV rms noise and ripple). The electronic circuits of PA1, PA2, the AVDC, and the dual-channel lock-in amplifier were each housed in an aluminum box which was fitted with appropriate electrical receptacles for the dc power inputs and the signal inputs and outputs.

A. PREAMPLIFIERS

Two preamplifier circuits were required to amplify the voltage outputs of the two pyroelectric detectors used in the optical saturation experiments. Each detector was equipped with a low gain FET amplifier which provided a low impedance output which consisted of a series of pulses produced by the intermittent laser radiation which struck the detectors. The magnitude of these pulses were typically a few millivolts and they were superimposed upon a +1 V dc signal. These signals were the inputs for the preamplifiers PA1 and PA2 which serviced detectors D1 and D2 respectively.

The following description of PA1 and PA2 refers to the circuit schematic which is presented in Fig. 4. A high pass filter removed the dc voltage component and only the ac signal generated by the detector was applied to the non-inverting input of the Burr Brown model 3308 OA. In this configuration the gain of the OA was varied by means of resistor RG. The gain of the circuit could be rapidly changed by a factor of 10 by means of switch S. When S was in the up position the gain was continuously variable from 1 to 100. With S in the down position, the gain could be variated from 10 to 1000. The output of PA1 was applied to the absolute value determining circuit, and the output of PA2 was applied to the input of the dual-channel lock-in amplifier. Before the initial use of these amplifiers, the dc offset voltage was set to zero volts. This was accomplished by shorting the inputs of the OAs and varying resistor B until the output voltage was zero.

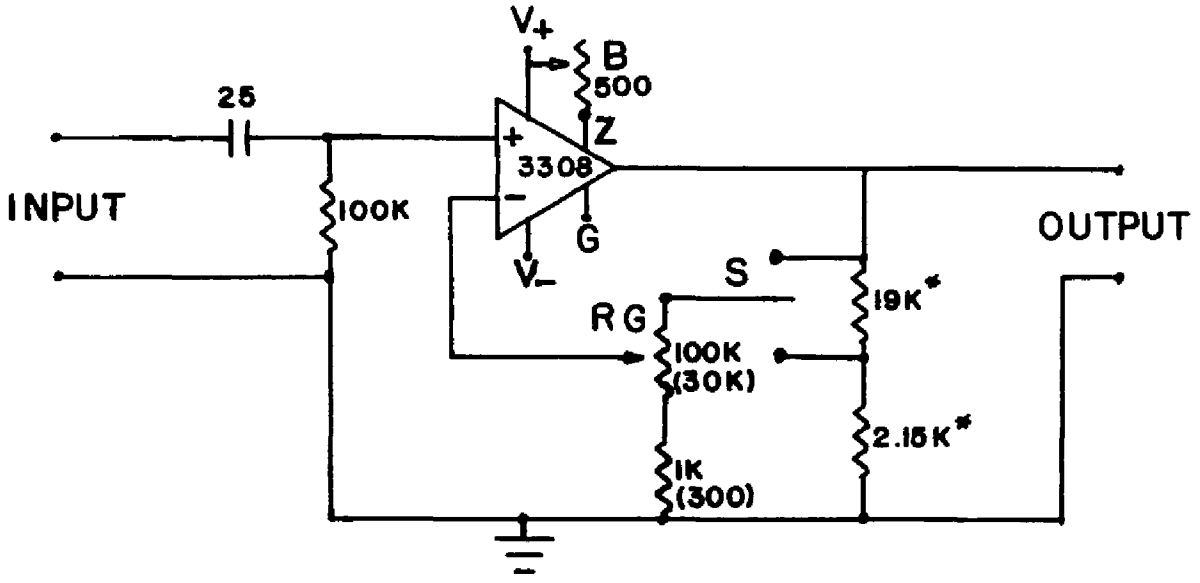

FIGURE 4. Schematic of preamplifier circuits. Resistances (ohms) and capacitances (microfarads) are within 10% of nominal values, and resistors are power rated at ½ W. Precision resistors (1%) are designated by (*) and PA2 variations from PA1 by parenthesis.

B. ABSOLUTE VALUE DETERMINING CIRCUIT

The absolute value determining circuit was designed to output a dc voltage which was proportional to the average of the absolute value of the input signal. A schematic of this circuit is presented in Fig. 5. A high pass filter was used to reject any dc voltage component which might have been introduced by the preamplifier. This circuit used two Burr Brown model 3267 OAs. The first OA (A1) was used in the inverting mode with a diode feedback. A negative input produced a positive output at H of equal magnitude. A positive input produced an output at H of zero volts. The second OA (A2) added the input signal to twice the output of A1. This sum was a full wave rectification of the input voltage. The second stage further provided a gain of minus five and the capacitor in parallel with the feedback resistor RF smoothed the dc output of A2. A RC filter provided additional filtering to give a peak-to-peak ripple of less than 0.1% of the dc voltage when the input signal was series of pulses at 40 Hz.

The rms average of the input voltage to the AVDC had to be less than 2 V. The output voltage was 0 to -10 V. This output voltage was applied to the input of the I channel of the analog computer described in Appendix 1.

C. DUAL-CHANNEL LOCK-IN AMPLIFIER

The voltage output of detector D2 and PA2 consisted of two alternating pulses of different amplitude. The large pulse

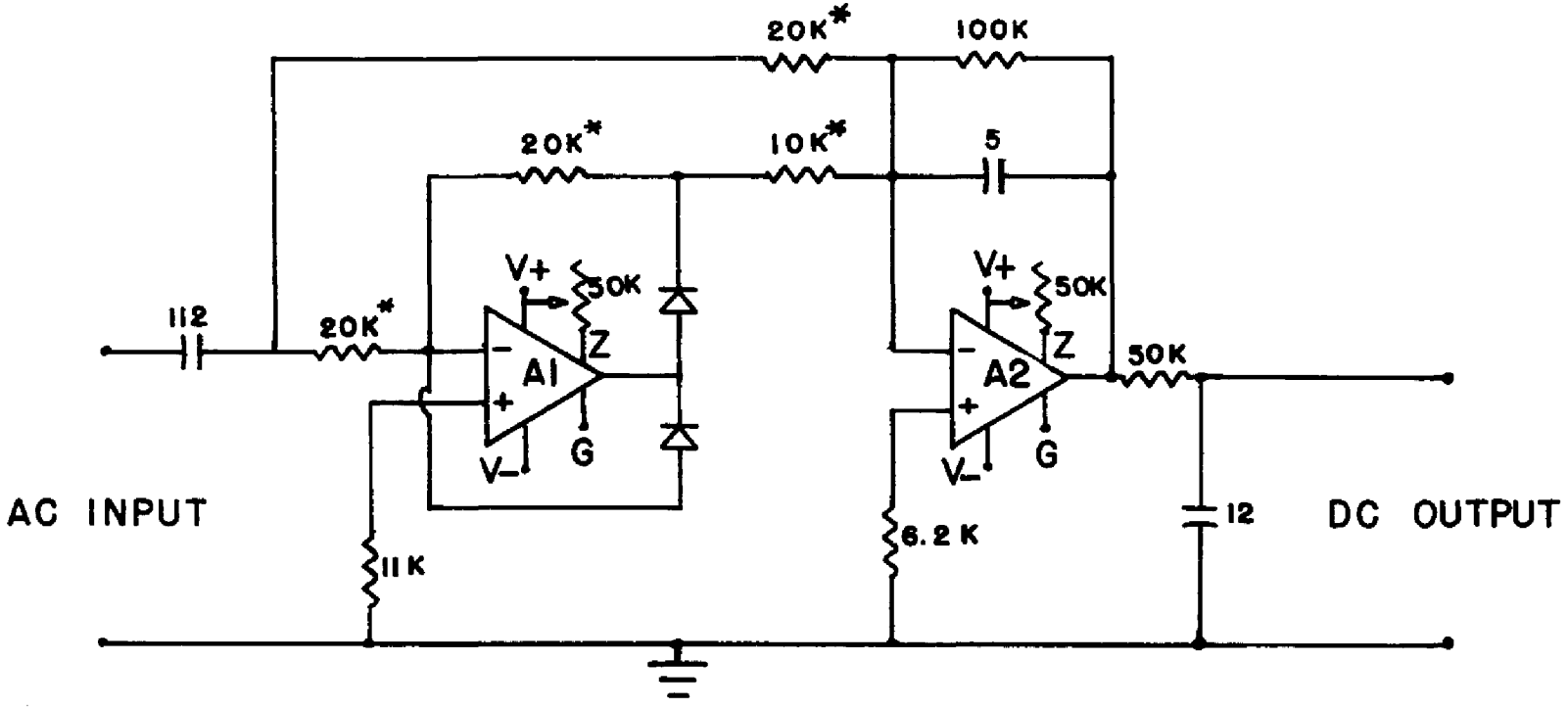

FIGURE 5. Schematic of absolute value determining circuit. Resistances (ohms) and capacitances (microfarads) are within 10% of nominal values, and resistors are rated at ½ W. Precision resistors are designated by (*)., and are within 1% of nominal values.

of different amplitude. The large pulse occurred when the chopper slit with no attenuator was open to the laser beam. The smaller pulse occurred when the chopper slit covered with a 0.36 attenuator was open to the beam. To resolve the magnitudes of these two pulses when the electronic noise level was significant in comparison with the pulse, a lock-in amplifier (synchronous detector) with two channels was required. Commercial lock-in amplifiers were not available to us and could not be purchased because of the prohibitive cost. Therefore a lock-in amplifier was designed and constructed by us. A schematic of the electrical circuit is shown in Fig. 6.

The feature of the voltage signal from the detector and pre-amplifier that was proportional to the intensity of the radiation that struck the detector was the height of the voltage pulse with respect to the voltage base line. Unfortunately the baseline voltage was negative and the peak of the pulse was a positive voltage. The procedure employed by the dual-channel lock-in was to sample and hold the baseline voltage and also the voltage at the peak of each pulse. The negative baseline voltage was then electronically substracted from the peak voltage and this difference was the output of the DCL.

Two dual 741 OAs which were purchased from Radio Shack were employed in the DCL. The input voltage was applied to a sample and hold circuit which contained A1. The n-channel FET (F1) was used as an electronic switch to permit sampling of the voltage at some desired time. Normally -15 V dc were applied to the gate of F1 which caused the resistance of F1 to be very great and prevent

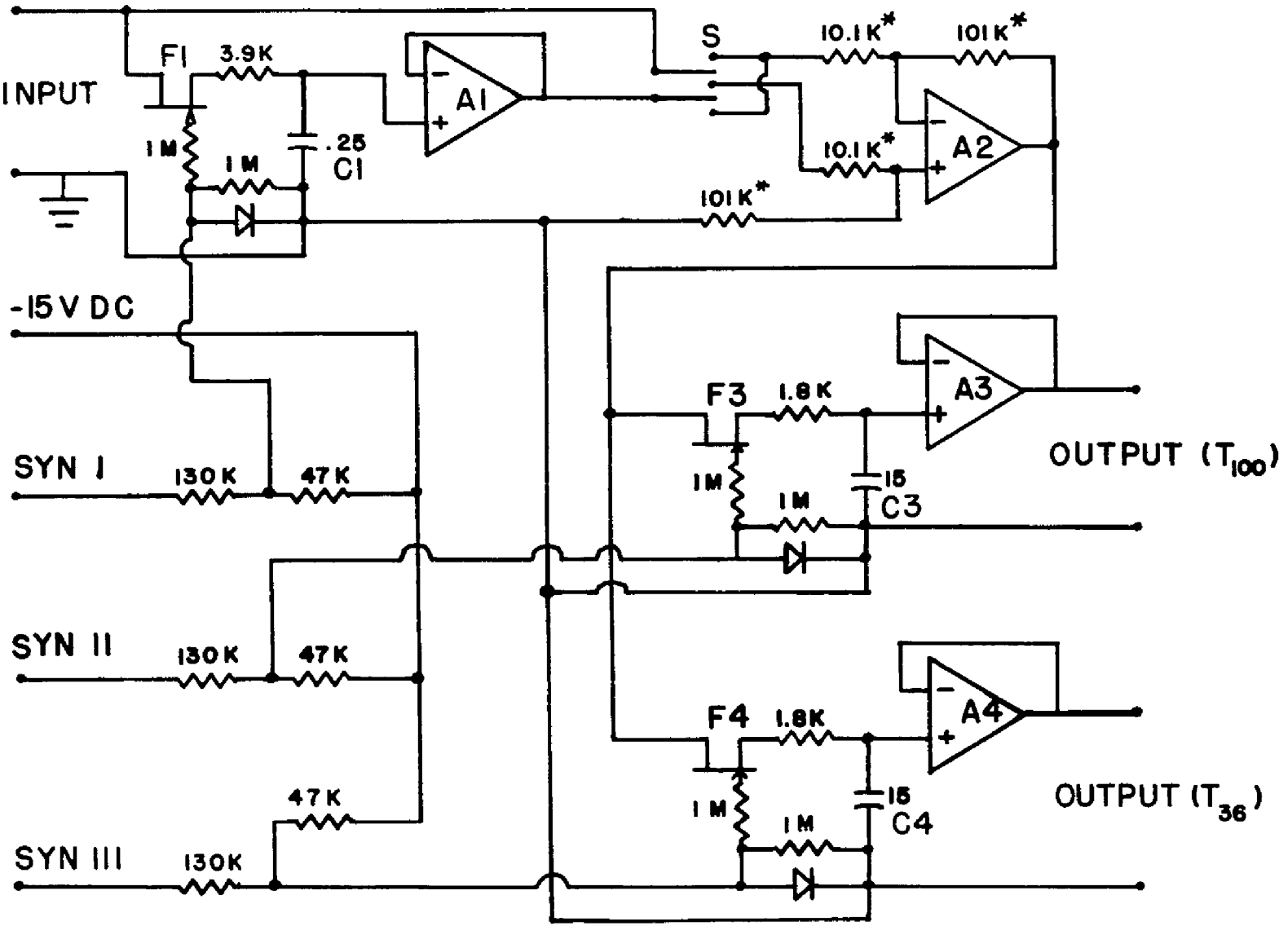

FIGURE 6. Dual-channel lock-in amplifier, schematic. Resistances (ohms) and capacitances (microfarads) are within 10% of nominal values, and resistors are rated at ½ W. Precision resistors (1%) are designated by (*).

current flow through C1. When 50 V were applied to syn. III, the potential at the gate of F1 was positive and F1 had only a small resistance. While the resistance of F1 was small, current flowed through C1 charging it to the input voltage occurring at that time. The OA A1 which was in the non-inverting mode with unity gain had nearly infinite input impedance, so that C1 would not discharge when F1 was closed. The output of A1 was then equal to the voltage potential held by C1. Thus a sample of the voltage input to the DCL could be taken whenever a 50 V pulse was applied at the syn. III input. The sampling would last through the duration of the 50 V pulse and C1 would continue to hold the voltage which was occurring in the input signal when the 50 V pulse ceased. This circuit associated with A1 was used to sample and hold the baseline voltage of the pulse train. The input signal to the DCL was substracted from the output of A1 by means of A2 used in the differential mode. The output of A2 was the same waveform as the input signal, but the baseline was now at zero potential and the polarity was reversed. In order for the DCL to be compatable with the AC, the output of A2 had to be negative. If the input voltage were of a negative polarity, switch S facilitated the reversing of the polarity. The OA A2 also amplified this voltage difference by a factor of 10. The output of A2 was now a series of pulses whose absolute peak heights were proportional to the intensity of the radiation striking the detector.

The output of A2 was applied to two other sample and hold circuits. One of these was controlled by syn. II and sampled the

voltage of the peak which occurred when the 100% transmitting slit of the chopper was open to the laser beam. The other was controlled by syn. I and sampled the voltage of the peak which occurred when the 36% slit was open. An additional feature of the sample and hold circuits which used A3 and A4 permitted a voltage integration similar to that used by a Boxcar Integrator. The FET switches (F3 and F4) were followed by resistors which increased the charging time of C3 and C4. The sampling time was typically 5 msec; however, the RC charging constant associated with these two capacitors was 30 msec. This meant that 60 msec were required for the capacitors to change their potential by 86% of the difference between their original potential and that of the input being sampled. Thus each sampling would contribute approximately 1/12 to the potential held by C3 and C4. The instaneous outputs of A3 and A4 were the average of the voltages of several previous peaks which were sampled by each circuit. By decreasing the sampling time the absolute charging time of C3 and C4 would be further increased and an average over a greater number of pulses could be obtained. Averaging over more pulses, however, decreases the response time of the synchronous detecting system. The outputs of A3 and A4 were smoothed with an RC filter network (not shown in Fig. 6) to remove any ripple in the voltage outputs. The total response time (90% realization of any input voltage change) of this system was about one second. The filtered outputs of A3 and A4 were applied to the R and T inputs of the analog computer.

The three synchronous pulses which operated the FET switches in the sample and hold circuits were supplied by three Tektronix Type 163 pulse generators. A voltage signal which was synchronous with the intermittent laser pulses was obtained from the photocell circuit in the chopper housing and used to trigger a Tektronix Type 162 Waveform Generator. The waveform generator produced a negative going voltage ramp called a sawtooth each time it was triggered. The sawtooth signal was applied to the input of the pulse generators. The triggering level of the pulse generators could be varied so that they would output a pulse only when a selected voltage input was received. Thus the output of the pulse generators would be delayed until the sawtooth waveform had reached a selected voltage. This procedure permitted the pulse generators to be triggered at a selected delay time after the beginning of the sawtooth waveform and also after the chopper synchronizing signal. The pulse generators were then set to output a pulse of the desired time width at times corresponding to the opening of the 100% and the 36% slits and at a time just before the opening of the 100% slit. A typical pulse train and the timing of the synchronous pulses are shown in Fig. 7.

D. PROCEDURE

The procedure which was followed to collect data in the transmittance experiments is described by the following steps.

(1) All of the electronic equipment shown in Fig. 1 and

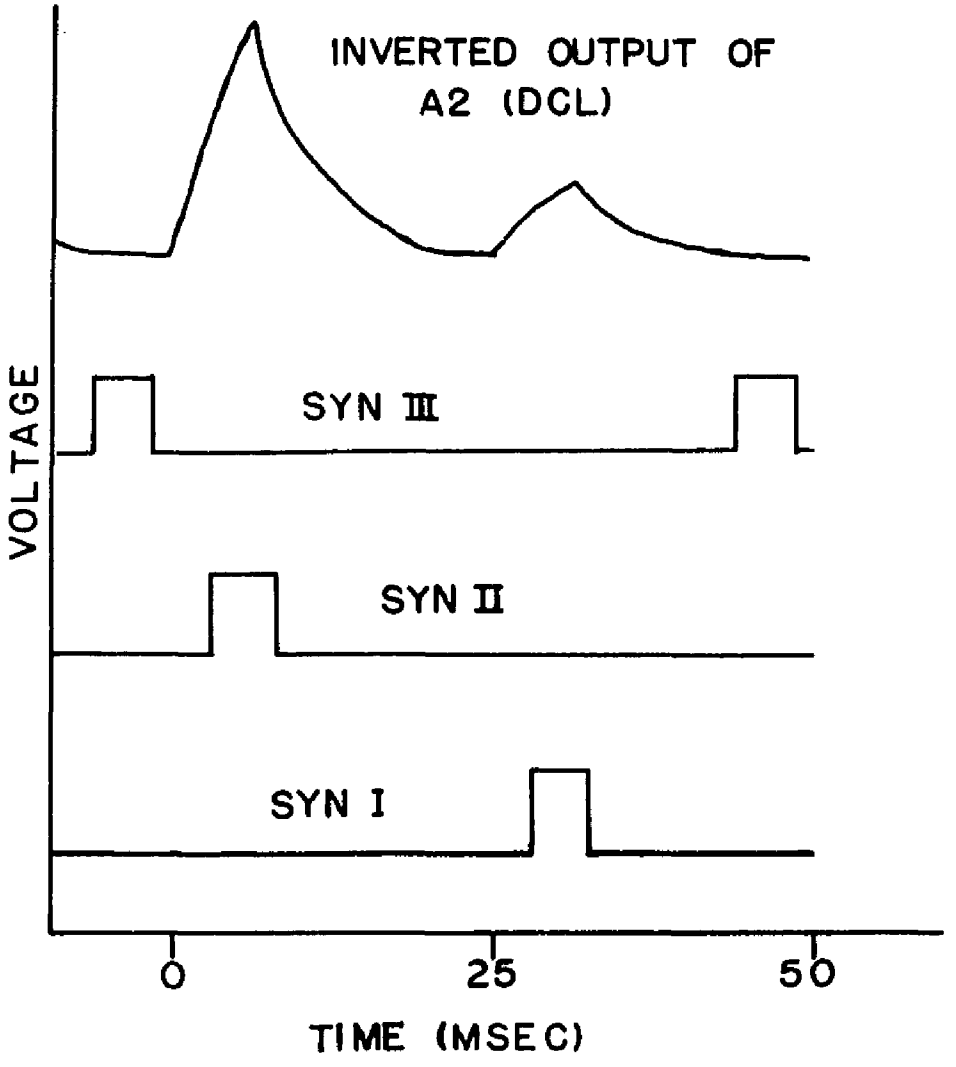

FIGURE 7. Typical waveform produced by the pyroelectric detector and the optimum temporal relationships of the three synchronous signals.

the chopper motor were started. The gain switches of PA1 and PA2 were set to the x1 position.

(2) The laser was started and tuned to the P(20) line at 10.59-μm. A thirty-minute warm-up period significantly improved the power and frequency stability of the laser.

(3) The KBr attenuators were placed on detectors D1 and D2 and the detectors were aligned to receive the maximum radiation intensity.

(4) The gain of PA1 was adjusted until the output of the AVDC was about -1 V. This voltage was applied to the I input of the analog computer which was also an amplifier whose output was applied to the three-channel recorder. The gain of the I channel was increased until the recorder read about 90% of full scale.

(5) With the sample cell evacuated, the gain of PA2 was adjusted until the peak-to-peak output voltage was about 0.5 V, or the maximum of the variable gain control was reached.

(6) The delay times for the synchronous signals which were applied to the DCL were adjusted to achieve the proper synchronization with the waveform produced by detector D2. This was accomplished by means of a Dumont model 304-A oscilloscope. The output of A2 of the DCL was applied to the y input of the oscilloscope. The internal time base unit of the oscilliscope applied a ramp voltage to the x input which was synchronized with the chopping wheel. The syn. signal to be checked was applied to the z input of the oscilloscope after the voltage level of the signal was temporarily set

to about +20 V. Since the z input of the scope determines the intensity of the trace, the waveform displayed on the screen of the scope was brightened throughout the duration of the syn. pulse. Thus the delay time and width of the particular syn. pulse being observed could be set so that the syn. pulse would occur at the desired time relative to the signal waveform of D2. A pulse width of 5 msec was normally used and the delays were adjusted to correspond to the relative positions of the syn. pulses and signal waveform that are shown in Fig. 7.

(7) The attenuator cell was filled with a helium-ethylene mixture until the recorder reading of the I channel was decreased by 20. The KBr attenuators were removed from the two detectors.

(8) With the laser beam blocked from D2, the R and T channels of the analog computer were set to zero by means of the voltage offset capability of the analog computer. The laser beam was then permitted to strike D2 and the gain of the T channel (100% pulse) was adjusted until the recorder pen of that channel reached full scale. The gain of the R channel (36% pulse) was adjusted until the recorder pen associated with the R output read 36% full scale. The zero settings were then checked and reset if necessary. The 100% and 36% settings were reset if the zero settings required adjustment.

(9) The attenuator cell was further filled with the helium-ethylene mixture until the intensity of the laser beam was reduced by a factor of 1000. The gains of PA1 and PA2 were set

to the x10 positions and the zero setting of the R and T channels were checked and reset if necessary. The gains of the R and T channels were not changed.

(10) The sample cell was filled with the desired pressure of SF_6.

(11) The helium-ethylene mixture was slowly pumped from the attenuator cell so that a gradual increase in the intensity of the radiation incident upon the sample occurred. When the recorder reading of the I channel had changed from 10% to 90% full scale the pumping was stopped.

(12) The gain of PA1 and PA2 were switched to the x1 position. This caused the I recorder output to return to 10% of full scale and the R and T recorder outputs to remain unchanged if the zero settings were still valid. The zero settings of the R and T channels were checked and reset if necessary.

(13) The removal of the helium-ethylene mixture from the attenuator cell was continued until the I output of the recorder again reached 90% of full scale. At this time the head of the Cintra radiometer was placed directly in front of the sample cell and the intensity of the laser beam was determined. The true intensity was the intensity read by the radiometer divided by the duty cycle of the chopper which was 0.174. By knowing the absolute intensity of the beam the recorder output of the I channel could be normalized with respect to its present reading and calibrated in absolute intensity. The radiometer head was removed and the KBr attenuators were placed on the two pyroelectric

detectors. The attenuators reduced the outputs of the detectors by approximately a factor of 10 which once again reduced the recorder reading of the I channel to 10% full scale.

(14) The removal of the helium-ethylene mixture from the attenuator cell was continued until it was evacuated and the full intensity of the laser beam struck the sample cell.

(15) The sample cell was evacuated and the D2 detector was swept through the center of the laser beam by means of a synchronous motor which operated the traversing mount on which D2 was mounted. An intensity profile of the laser beam was obtained by this procedure. The speed of the synchronous motor, the gearing of the traversing mount, and the speed of the motor which advanced the chart paper were such that a one-to-one ratio existed between the distance swept by the detector and the advancement of the chart paper. The peak intensity of laser beam could then be calculated by means of Eq (1) of Chapter III and the beam dimensions obtained from the intensity profile of the laser beam. These 14 steps were required for a data run which measured the transmittance of SF_6 gas as a function of the intensity of the laser radiation striking the sample cell. To conduct another run this procedure would have to be repeated from step 3. Usually only fine adjustments were required for the second run. An additional option was made possible by a modification to the analog computer which enabled the operator to obtain either the transmittance of the 36% pulses (T_{36}) or the ratio of the 36% pulses to the 100% pulses (T_R) as the output of the R channel. This option was exercised with a switch located on

the rear of the AC chasis. Of course the T_{38} option had to be used for setting the zero and the maximum of the R channel. The laser was <u>always</u> turned off before the chopper motor in the shut down of the experiment.

APPENDIX 5

ELECTRONICS AND PROCEDURE - NOVA EXPERIMENT

The electronics devices employed in the Nova experiments were less complicated than those used in the transmittance experiments. More importantly, the devices used in the Nova experiment were also much easier to operate and were subject to less error by the operator. A block diagram of the electronic devices of the Nova experiment is presented in Fig. 1. The outputs from the two pyroelectric detectors were amplified by preamplifiers PA1 and PA2 which were described in Appendix 4. As before PA1 and PA2 eliminated the dc voltage component from the output of the detectors and the resulting ac waveform was a series of eight pulses which decreased in amplitude from the first to the eighth pulse. The outputs of PA1 and PA2 were applied to a signal processor (SP) which automatically added the appropriate voltage to the train of eight pulses so that the baseline voltage was at zero potential. The signal processor further amplified the last three pulses of the two waveforms by factors of 23 and 21. The outputs from the signal processor which consisted of two separate channels were applied to the multiplexer unit of the Nova system. The function of the multiplexer was to apply the voltage received by one of eight input channels to the analog-to-digital (A/D) converter. A pulse-shaping network (PSN) received two synchronous signals from the mechanical light chopper. The PSN used these input signals to generate two series of pulses- one synchronous with the slit

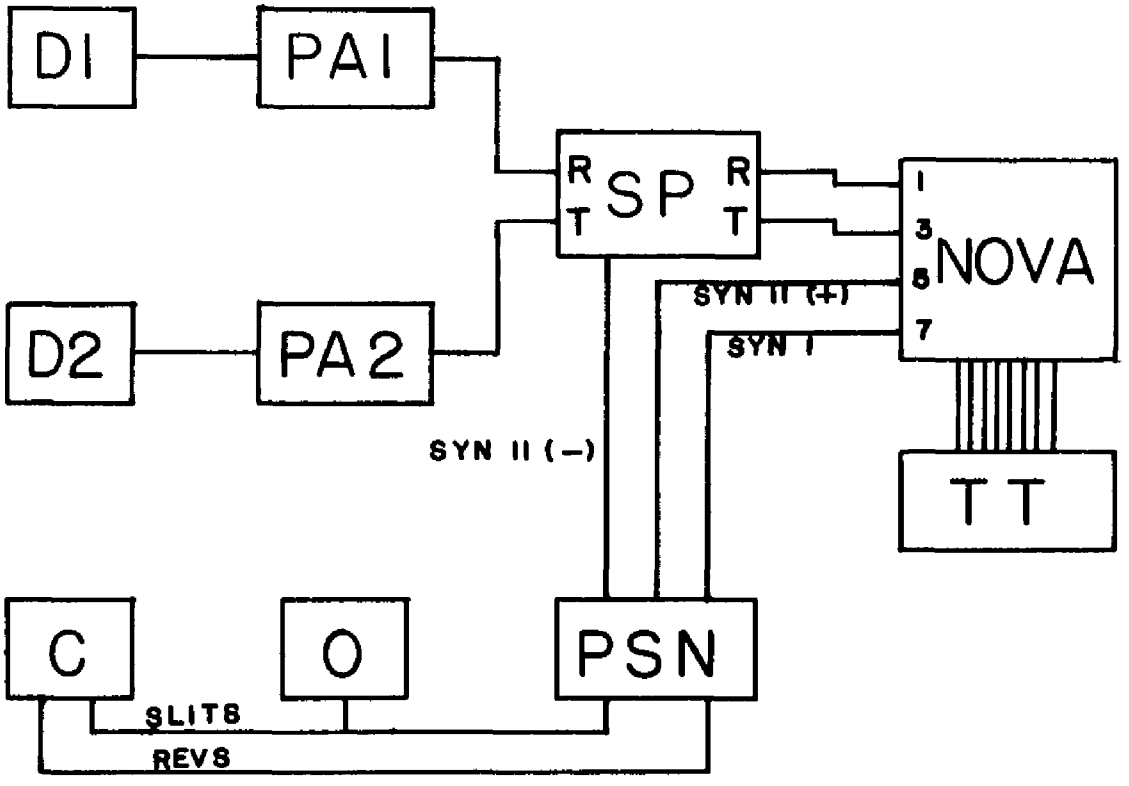

FIGURE 1. Block diagram and cable connections for electronic components used in the Nova experiments with detectors (D1 and D2), preamplifiers (PA1 and PA2), mechanical light chopper (C), oscilliscope (O), signal processor (SP), pulse-shaping network (PSN), Nova minicomputer, and teletype (TT).

openings in the chopping wheel and the other synchronous with the revolutions of the chopping wheel. The oscilliscope (O) was used to monitor the various voltage signals and to set the proper synchronization of the pulses from the PSN. The signal processor, the pulse-shaping network, and the procedure followed in their employment will be discussed in this appendix.

A. SIGNAL PROCESSOR

The signal processor was designed with two separate channels which were used to treat the voltage signals orginating from the reflected and transmitted radiation. Each channel was designed to convert the amplified ac voltage outputs of the pyroelectric detectors to a form which would be compatible with the A/D converter which was a part of the Nova system. The A/D converter required that the input voltage be within a 0-10 V range. Since the voltage signals which would be converted by the A/D were often quite noisy, it was necessary to insure that any voltage spikes caused by the noise would also be within this range, if signal-averaging was to be effective. The minimum resolution of the 12-bit A/D converter was 2.5 mV. The 2.5 mV resolution required that voltage signals which were to be accurately read have a magnitude of at least 25 mV. The amplitudes of the eight voltage pulses in the waveform obtained from the preamplifiers for this experiment ranged from 5 V to 35 mV when the sample cell was evacuated. When the cell was filled with a saturable absorber this range was

nominally 3 V to 3.5 mV. In order to accurately convert each of the eight voltage pulses to a digital number with the A/D converter, it was necessary to amplify the weaker pulses but not the stronger ones. To amplify the weaker pulses by a factor of 20, however, the baseline of the pulse train must be very nearly zero volts since any voltage offset would also be amplified. A schematic of an electronic circuit which performed the proper signal processing for the input to the A/D converter is shown in Fig. 2.

The signal processor was constructed from three dual 741 operation amplifiers identical to those used in the dual-channel lock-in amplifier described in Appendix 4. Since the function of both channels are the same, only the reflectance channel will be discussed. The input to the SP was a high pass filter which eliminated any dc component from the output of PA1. The first two operational amplifiers (OA) automatically set the dc level of the pulse train so that the most negative position of the input waveform was at zero potential. Further, A1 provided a gain of -10 in the magnitude of all eight pulses of the waveform. (A4 had a gain of -1 for the transmittance waveform.) The output of A1 was applied to the inverting input of A2 through a 4.7K Ω resistor. This caused the output of A2 to have an opposite polarity from A1. The output of A2 was applied to a diode which permitted only a negative current to charge C1. A negative current could only be produced by A2, however, when its (-) input and the output of A1 were positive. The voltage potential held by C1 was also applied to the (+) input of A1. Whenever C1 was at a negative potential, the output of

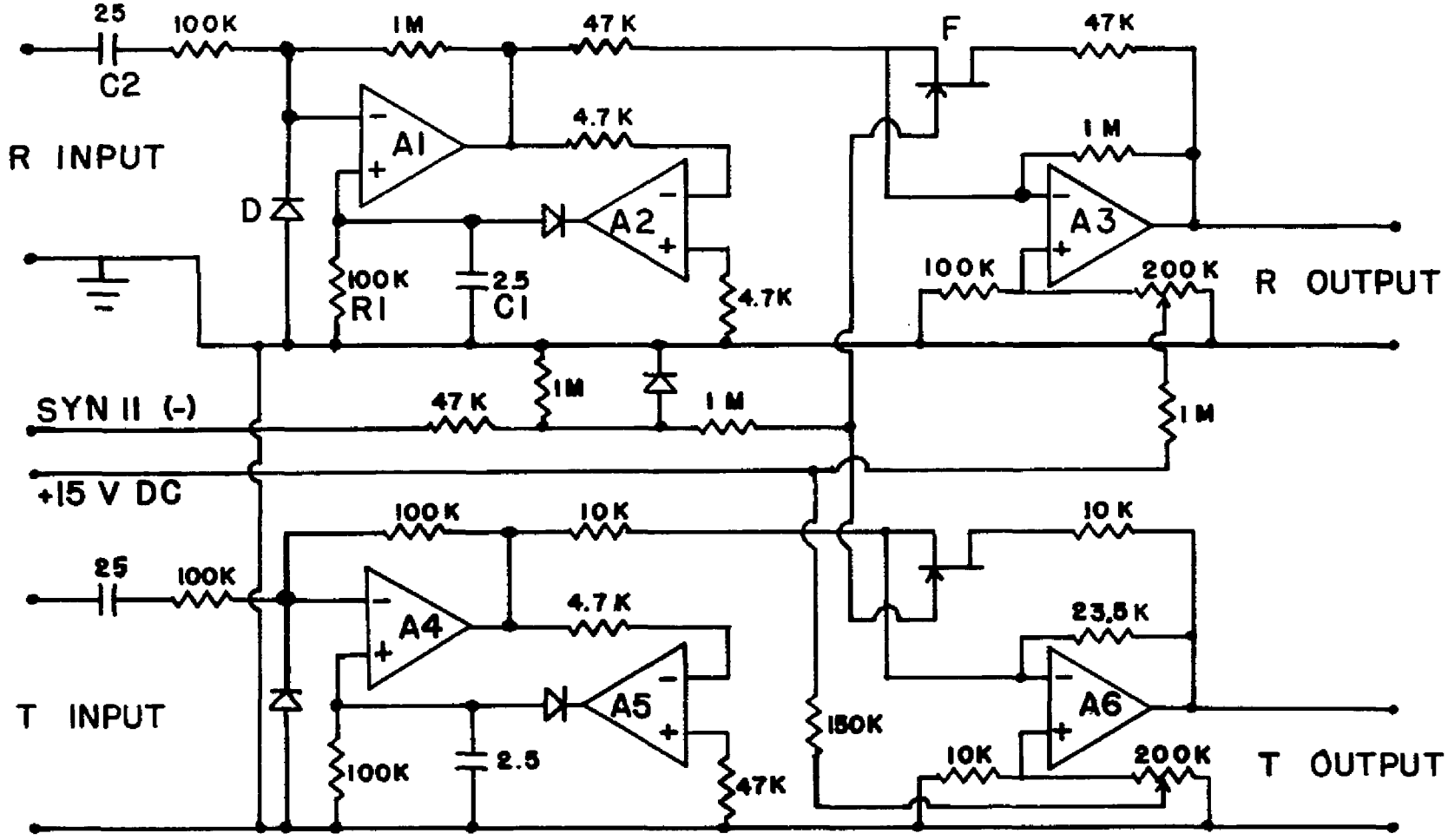

FIGURE 2. Electrical schematic of the signal processor. Resistances (ohms) and capacitances (microfarads are within 10% of nominal values, and resistors are power rated at ½ W.

A1 became more negative by 10 times the magnitude of the voltage on C1. Any charge held by C1 would slowly be conducted to ground potential through the resistor R1. The net effect of A1 and A2 was that whenever the output of A1 became positive, A2 charged C1 to a negative potential which drove the (+) input of A1 more negative until the output of A1 was no longer positive. The purpose of C1 was to hold the (+) input of A1 at the proper offset voltage through the duration of one pulse in the input waveform. If C1 were not employed, any negative input to A1 (-) would be negated by the feedback through A2. The diode D was required to prevent charge build-up on C2. Finally, the output of A2, which was a waveform of eight negative pulses with a baseline at exactly zero volts, was applied to A3 (-) through a 47K Ω resistor.

This final operational amplifier, A3, was used as an amplifier in the inverting mode. Thus the negative output of A2 was inverted by A3 before being applied to the input of the A/D converter. Two feedback paths were used from the output of A3 to A3 (-). One path contained a n-channel FET and a 47K Ω resistor. The other contained only a 1M Ω resistor. When the gate of the FET was at ground potential, the resistance between the drain and source of the FET was about 200 Ω. Thus the effective feedback resistance was a little less than 47K Ω. When -15V was applied to the gate of the FET (F), the drain to source resistance was very great compared to 1M Ω which was now the effective feedback resistance of the circuit involving A3. The gain of an operational amplifier in the inverting mode is the negative of the ratio of the feedback

resistance (47K Ω or 1M Ω in this case) to the input resistance (47K Ω). The gain of A3 was about -1 when zero volts were applied to the gate of F and -21 when -15 V were applied to the gate of F. If a pulse with a -15 V amplitude was commensurate in time with the three weaker pulses of the signal waveform, it could be applied to the gate of F to cause the weaker pulses to be amplified by -21 while the remaining 5 pulses were amplified by -1. Finally, a small positive dc voltage was applied to A3 (+) to produce a positive voltage offset of about 0.3 V. The dc offset insured that even the noise of the signal waveform would not reach a negative voltage.

B. PULSE-SHAPING NETWORK

The pulse-shaping network produced two sets of synchronous pulses. One (syn. I) was synchronous with the openings of the slits of the chopping wheel, and the other (syn. II) with the revolutions of the chopping wheel. The syn. II pulses were used to switch the gains of A3 and A6 in the signal processor. Both sets of synchronous pulses were applied to the multiplexer unit of the Nova system. The computer program employed in the Nova minicomputer directed the digital conversion of these pulsed signals to determine specific temporal positions on the signal waveform as illustrated by Fig. 6 of Chapter III. A block diagram and circuit schematic of the PSN is presented in Fig. 3.

For the syn. I pulses the PSN used a Tektronix Type 162 Waveform Generator (WG) and a Type 163 Pulse Generator (PG1). The output from the chopper which was synchronous with the slit

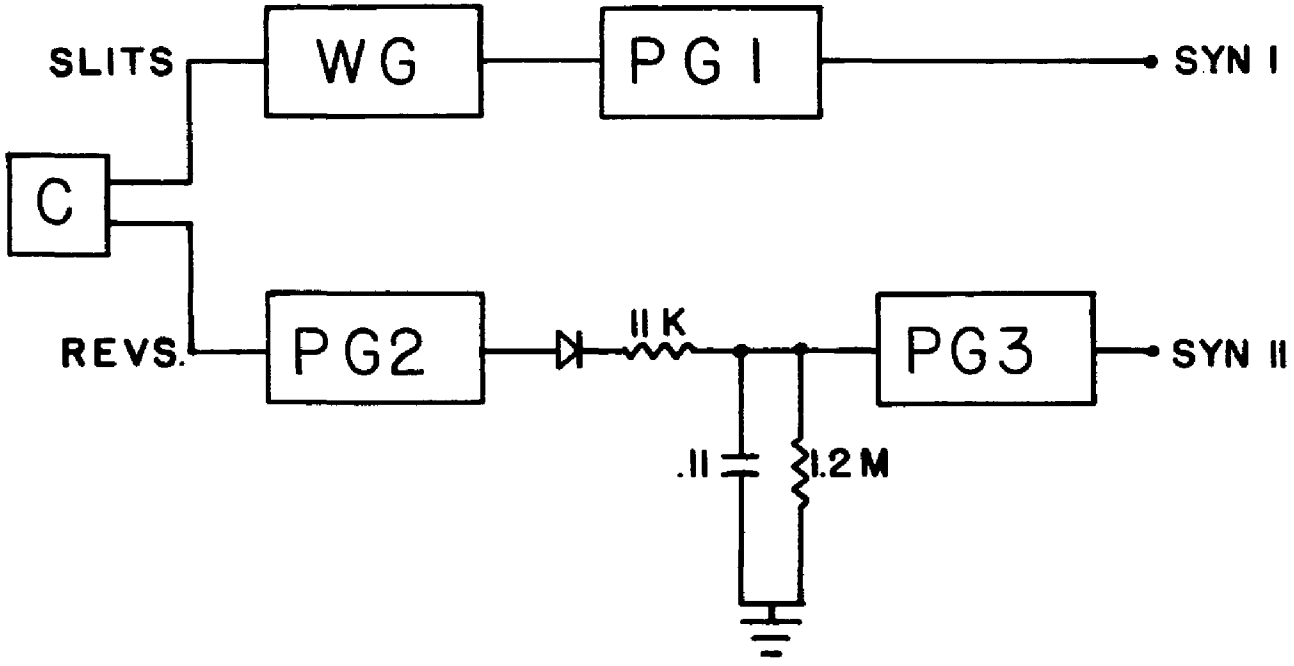

FIGURE 3. Block diagram and electrical schematic of the pulse-shaping network with mechanical light chopper (C), waveform generator (WG), pulse generators (PG1, PG2, and PG3), and synchronous signals (syn. I and syn. II).

openings was used to trigger the waveform generator which produced a negative going sawtooth waveform each time it was triggered. The duration of the sawtooth was selected to be less than the time interval between the slit openings which was about 5.7 msec. The output of the waveform generator was used to trigger PG1 which had an adjustable triggering level. By selecting the proper triggering level the pulse produced by PG1 could be delayed to occur simultaneously with any temporal position on the sawtooth waveform. The appropriate delay was selected with the use of a Dumont model 304-A oscilloscope. The output of the SP was applied to the y input and the x input was driven by a time-base unit which was synchronized with the slit openings of the chopping wheel. The output of the pulse generator (syn. I) was applied to the z input of the scope. The oscilloscope trace of the signal waveform was brightened throughout the duration of the positive pulse produced by PG1. Thus the location of the syn. I pulse was easily determined and the delay of the pulse was conveniently set by adjusting the triggering level of the pulse generator. A width of 0.7 msec was selected for the output pulses of PG1.

The syn. II pulses could have been produced and adjusted by the same procedure, but only one waveform generator was available. Therefore, a negative going voltage ramp was produced by using another Tektronix Type 163 Pulse Generator (PG2) and a RC circuit. The output from the chopper which was synchronous with the revolutions of the chopping wheel was used to trigger PG2. A pulse of 50 V amplitude was generated by PG2 and applied to the

RC circuit shown in Fig. 3. The diode permitted PG2 to positively charge the capacitor C but prevented the capacitor from discharging into PG2. The capacitor had to discharge through the 1.2M Ω resistor and the input resistor (1M Ω) of PG3 which received this negative going voltage. This third PG was identical to PG1 and PG2. The waveform generated by the discharging of C was used to trigger PG3. The adjustable triggering level of PG3 permitted the selection of the appropriate delay time so that the syn. II pulses would begin just after the completion of the 5th pulse in the signal waveform outputed by the SP. The width of the syn. II pulses was selected by means of that adjustment on PG3 so that the syn. II pulses persisted until the eighth pulse of the waveform output of the SP was completed. As for syn. I the proper delay time was determined by means of the Dumont oscilloscope. The PGs had both positive and negative outputs. The amplitude of the positive output of PG3 was set to about 8 V, and the pulses were applied to the multiplexer unit of the Nova system. The amplitude of the negative output was set to -15 V and these pulses were applied to the SP.

C. PROCEDURE

Once the initial start-up and calibration were complete the procedure required for the performance of the Nova experiment was fairly routine for the operator. The following steps describe the procedure which was employed.

(1) The Nova minicomputer and the teletype were started and the various paper tapes on which the programs and BASIC compiler were recorded were read into the memory of the computer via the paper tape reader of the teletype. The exact procedure for the reading of these tapes was described in the instructions supplied with the "Call" BASIC compiler.

(2) All of the electronic systems shown in Fig. 1 were started and the sample cell was evacuated. The temperature control unit for the sample cell was adjusted to acheive a sample cell temperature of about 39° C. All of the cable connections shown in Fig. 1 were made. The amplitude of the negative syn. II pulses was temporarily set to 0 V.

(3) The CO_2 laser was started and the frequency tuned to the P(20) line of the 10.59-μm transition. The Cintra radiometer which was used in the tuning procedure was positioned afterwards so as to receive the radiation reflected from the salt wedge.

(4) The laser beam was directed to strike the center of the iris of the adjustable pinhole.

(5) The sample cell was aligned so that the windows were exactly normal to the laser beam.

(6) The output of PA2 was monitored with the oscilloscope and D2 was aligned to acheive a maximum output of PA2. The gain of PA2 was adjusted so that the peak-to-peak (ptp) voltage of the output was about 5 V.

(7) Step #6 was repeated for PA1 and D1 except that the gain of PA1 was adjusted to acheive a 0.5 ptp output voltage.

(8) The appropriate delay times and pulse widths were set for syn. I and syn. II by using the Dumont oscilloscope.

(9) The optical alignment was rechecked and adjusted if necessary.

(10) The average intensity of the laser beam was determined with the Cintra radiometer which received a portion of the laser radiation which was incident upon the sample cell.

(11) The execution of the computer program in the Nova memory was begun and it interrogated the operator as to the parameters and options desired for the experiment via the teletype. There were two options available concerning the treatment of the data which would be obtained. One option (calibration) instructed the program to store the collected data as calibration constants and the other (data) option instructed the program to normalize the collected data with the previously obtained normalization constants. The "calibration" option was selected, but the execution of the data collection procedure of the program was not started.

(12) The temperature control unit for the sample cell was set to the maximum temperature to produce heating of the sample cell. Switch #0 on the console of the computer was turned on. (These two operations will be refered to as "OT turned on" in the future. Returning the temperature setting so as to acheive a temperature of 39°C and turning switch #0 off will be referenced as "OT off".) The execution of the data collection procedure of the Nova program was started immediately after OT was turned on.

(13) The modulation in the data clusters collected for the reflected radiation of the strongest pulse was observed on the screen of the storage oscilliscope. When three complete cycles were completed OT was turned off. This stopped the data collection when the present data cluster being obtained was completed.

(14) When the teletype had completed typing the values of the calibration constants obtained, three options were given to the operator. These options were to print the values of the individual data clusters obtained, to execute the second type of calibration, or to return the program execution to the beginning of the program so that another data collection could be performed. The third was selected.

(15) The "data" option was selected for this second run and polystyrene attenuators of 0.25 and 0.5 were placed in front of D1 and D2 respectively.

(16) When the temperature of the sample cell had reached 39°C, OT was turned on and the execution of the data collection procedure was begun.

(17) When three cycles of the modulation of the reflectance data clusters were completed OT was turned off. After the eight transmittances and reflectances were typed by the teletype, the second type of calibration option was selected. This option improved the values of the calibration constants and returned the program execution to the start of the program.

(18) The calibration was complete and the sample cell was filled with the desired pressure of SF_6 or SF_6-He mixture.

(19) Since the "data" option was still in effect, OT was turned on and the execution of the data collection procedure was begun immediately thereafter.

(20) When exactly two or three cycles in the modulation of the reflectance were observed, OT was turned off. When the teletype had completed typing the eight reflectance and transmittance averages, the "data dump" option could be selected if desired. If not, the option which returned the program execution to the beginning of the program for another run was selected. When the "data dump" option was selected the program execution automatically returned to the beginning of the program when the typing of all of the data clusters was complete.

(21) Steps #18-20 were repeated for each sample to be studied. If the calibration was invalidated for some reason, the procedure would have to be repeated from step #10.

(22) A profile of the intensity of the laser beam was taken at the end of a series of data runs because this procedure destroyed the calibration of the experiment. The detector D2 was traversed by manually turning the traversing adjustment of the mount which held D2 until the ptp amplitude of the SP output for the T channel had decreased by 99%. With the temperature of the sample cell held constant, switch #0 on the computer console was turned on and a data run was begun with the sample cell evacuated. When a data cluster was obtained the translating adjustment of the D2 mount was turned $\frac{1}{2}$ turn so that D2 would move 0.64 mm across the laser beam perpendicularly to the direction of the beam. The

computer program caused the bell on the teletype to ring upon the completion of each data cluster, thus permitting the operator to synchronize the movement of D2 with the data collection. When the output of the T channel of the SP had passed through a maximum and decreased to a few percent, switch #0 was turned off. The "data dump" option was selected to obtain the data clusters which represented the intensity profile of the laser beam. The appropriate beam dimensions were obtained from the beam profile so that the peak intensity of the laser beam could be computed from the average beam intensity measured earlier with the Cintra radiometer.

(23) To terminate the experiment the laser was turned off first and then the other equipment.

APPENDIX 6

COMPUTER PROGRAMS - NOVA EXPERIMENT

Two types of computer programs are presented in this appendix. The first type used a computer language called BASIC which required that a "Call" BASIC compiler supplied by Data General Corporation be stored in the computer memory to compile and execute the BASIC program. The "Call" BASIC compiler permitted machine language subroutines to be used by the BASIC program. The second type of program used assembly-language which was subsequently converted to machine language by an assembler routine also supplied by Data General Corporation.

The master program was written in BASIC, which could temporarily pass control to the previously compiled subroutines when speed and auxiliary devices were required. Data manipulation and input and output with the teletype were relatively easy to program using BASIC, but BASIC had two weaknesses for conducting an experiment. One was that the execution of an operation by the BASIC compiler system was usually much slower than the same operation when it was programed in assembly-language. The other weakness was that the BASIC language had no provision for interacting with the analog-to-digital (A/D) converter, the digital-to-analog (D/A) converter, or the oscilliscope. Assembly-language was difficult to employ for data input and output, but it was fast and could interact with any of the auxiliary devices of the Nova system.

Therefore, subroutines that would output data to the oscilliscope by means of the D/A converter and rapidly collect a set of data clusters by means of the A/D converter were written in assembly-language. These subroutines were assembled into machine language and stored in the computer memory so that they could be called by the BASIC program. All of the remaining input, output, and data manipulations were handled by the BASIC program.

The"Call"BASIC system greatly simplified the computer programing. First, BASIC computer language was much easier to use and to learn than assembly-language. And second, the BASIC program could be modified at any time directly from the teletype. Modifications of a precompiled assembly-language program were not as simple.

A listing of the BASIC program and the assembly subroutines compose the remainder of this appendix.

A. BASIC PROGRAM

DATA COLLECTION

```
100  DIM R[7,50],T[7,50],S[7],W[7],U[7],Z[7],D[20],C[7],B[7]
103  LET P1=1
110  PRINT "ARE CURRENT  INPUTS CORRECT? YES-COLLECT DATA(1)"
111  PRINT "NO(2),  PRINT CURRENT PARAMETERS(3)"
120  INPUT X
130  IF X=3 GOTO  200
140  IF X=1 GOTO  300
145  PRINT
150  PRINT "ENTER # OF THE INPUT AND THE CORRECT VALUE.(0,0-ENDS)"
160  INPUT N,V
165  PRINT
170  IF N= 0 GOTO  200
180  LET D[N]=V
190  GOTO  160
200  PRINT
210  PRINT
220  PRINT "JULIAN DATE(1)=";D[1];" 1975"
230  PRINT "RUN TYPE(2)=";D[2];"(CALIBRATION=1,DATA=2)"
235  PRINT "   RUN NUMBER(3)=";D[3]
240  PRINT "PSF6(4)=";D[4];"TORR   PHE?(5)=";D[5];"TORR"
250  PRINT "LASER POWER(6)=";D[6];"WATTS/SQCM"
251  PRINT "BEAM DIAMETER AT HALF HEIGHT(7)=";D[7];"CM"
260  PRINT "TRAN. FACTOR(8)=";D[8];"REF. FACTOR(9)=";D[9]
261  LET F1=D[9]*P1/D[6]
262  LET F2=D[8]*P1/D[6]
270  PRINT "WILL SCOPE BE USED(10)?";D[10];"(YES=0,NO=1)"
271  PRINT "WILL TELETYPE BE USED CONCURRENTLY(11)?";D[11]
280  PRINT "MAX # POINTS(12)=";D[12];"  READINGS PER POINT(13)=";D[13]

281  PRINT "(MUST BE 2?1)"
285  PRINT
290  GOTO  110
300  CALL 4,D[13]
303  PRINT
304  LET M2=6.71088E+7
305  GOSUB  950
307  LET M6=100/M2
310  FOR J= 0 TO 7
320    LET S[J]= 0
330    LET W[J]= 0
340  NEXT J
350  LET N2=D[12]-1
360  FOR I= 0 TO N2
370    CALL 1,X
380    IF X= 0 GOTO  620
390    FOR K= 0 TO 7
400      CALL 2,T[K,I]
402      CALL 2,R[K,I]
407      GOTO  420
```

```
420       IF D[2]=1 GOTO  450
430       LET R[K,I]=R[K,I]+F1/U[K]
440       LET T[K,I]=T[K,I]+F2/Z[K]
450       LET S[K]=S[K]+R[K,I]
460       LET W[K]=W[K]+T[K,I]
470     NEXT K
480     LET I1=I+1
490     IF D[10]=1 GOTO  590
500     IF D[2]=1 GOTO  520
510     LET I2=M2/I1
515     GOTO  525
520     LET I2=1/I1
525     FOR K= 0 TO 2
530       LET K1=3*K+1
540       LET X=S[K]*I2
545       LET X1=I1*10
550       CALL 3,X,X1
560       LET X=W[K]*I2
569       LET X1=I1*10+507
570       CALL 3,X,X1
580     NEXT K
582     LET X=R[ 0,I]*I2*I1+M3
584     CALL 3,X,X1-507
586     LET X=T[ 0,I]*I2*I1+M4
588     CALL 3,X,X1
590     IF D[11]=1 GOTO  610
600     GOSUB  891
610   NEXT I
620   PRINT
630   LET X=D[13]*I1
640   PRINT  TAB (15);"DATA ACQUISITION COMPLETE"
650   PRINT  TAB (5);"EACH AVERAGE BASES ON";X;"MEASUREMENTS"
660   PRINT
670   FOR K= 0 TO 7
680     LET S[K]=S[K]/I1
690     LET W[K]=W[K]/I1
700     PRINT "AVERAGES FOR POWER";K;"ARE R=";S[K];"    T=";W[K]
710     IF D[2]=2 GOTO  740
720     LET U[K]=S[K]
730     LET Z[K]=W[K]
734     LET P1=D[6]
740   NEXT K
760   PRINT
770   PRINT
780   IF D[11]= 0 GOTO  110
790   PRINT "IS DATA DUMP DESIRED (Y=0,N=1),CALIBRATION(5)"
800   INPUT X
810   IF X=1 GOTO  110
813   IF X<>5 GOTO  820
815   GOSUB  1100
817   GOTO  110
820   LET N2=I1-1
830   FOR I= 0 TO N2
840     LET I1=I+1
850     GOSUB  891
```

```
860  NEXT I
870  GOTO  110
880  STOP
890  REM        SUB START
891  IF D[2]=2 GOTO  900
892  FOR K= 0 TO 7
894    LET R[K,I]=R[K,I]*M6
896    LET T[K,I]=T[K,I]*M6
898  NEXT K
900  IF I> 0 GOTO  908
902  PRINT
904  PRINT "   DATA TABLE GIVES POINT NUMBER,8 R'S, AND 8 T'S"
906  PRINT
908  PRINT "**";I1
910  PRINT R[ 0,I];R[1,I];R[2,I];R[3,I];R[4,I];R[5,I];R[6,I];R[7,I]
920  PRINT T[ 0,I];T[1,I];T[2,I];T[3,I];T[4,I];T[5,I];T[6,I];T[7,I]
930  RETURN
940  REM    BEGIN GRAPH SUBROUTINE
950  LET G=M2/1023
955  LET Y=-G
960  FOR M= 0 TO 1023
970    LET Y=Y+G
980    CALL 3,Y, 0
985    CALL 3,Y,507
990    CALL 3,Y,1013
1000 NEXT M
1006 LET M3=M2/2
1007 LET M4=M3/2
1008 LET M5=M3+M4
1010 FOR M= 0 TO 102
1020   LET M1=M*10
1030    CALL 3, 0,M1
1040    CALL 3,M2,M1
1050    CALL 3,M3,M1
1060    CALL 3,M4,M1
1070    CALL 3,M5,M1
1080 NEXT M
1090 RETURN
1100 LET X1= 0
1102 LET X= 0
1104 FOR L=1 TO 4
1106   LET X=X+S[L]/4
1108   LET X1=X1+W[L]/4
1110 NEXT L
1112 PRINT
1114 PRINT "R AVG=";X;"  T AVG=";X1
1116 FOR L= 0 TO 7
1118   LET U[L]=U[L]*S[L]/X
1119   PRINT
1120   LET Z[L]=Z[L]*W[L]/X1
1122 NEXT L
1124 RETURN
1127 PRINT
1170 STOP
1180 END
```

B. SUBROUTINES (ASSEMBLY-LANGUAGE)

```
7/02/75                                    .MAIN

 LOC    CODE    STMT     SOURCE STATEMENT

00010                1                .LOC    10
00010 017000         2        LOC10:  17000           ; TELL BASIC LOC OF SUB/R
17000                3                .LOC    17000   ; LOAD S/R HERE
17000 000530         4        INTER:  530
17001 000001         5                1               ;BT S/R
17002 017021         6                SUB1            ;ENTRY POINT
      000004         7                .BDX 4          ;TO BASE 4
17003 140000         8                30000000        ;DATA FROM SR
17004 000002         9                2
17005 017270        10                SUB2
17006 140000        11                30000000        ;DATA FROM SR
17007 000003        12                3
17010 017320        13                SUB3
17011 120000        14        22000000                ;DATA TO SR
17012 000004        15                10              ;10=4 BASE 4
17013 017354        16                SUB4
17014 100000        17                20000000        ;DATA TO SR
      000010        18                .BDX 8          ;TO BASE 8
17015 177777        19                -1
17016 063077        20                HALT
17017 063077        21                HALT
17020 000200        22        BASO:   200
17021 020777        23        SUB1:   LDA     0,BASO
17022 062077        24                DOB     0,CPU
17023 000401        25                JMP     .+1
17024 054573        26                STA     3, SAVR ;STORE RETURN
17025 060477        27                DIA     0, CPU  ;READ SWITCHES
17026 101223        28                MOVZR   0,0,SNC ;CHECK BIT 15
17027 000500        29                JMP     QIT     ;QUIT IF 0 IN 15
17030 024565        30                LDA     1,NPTS
17031 044571        31                STA     1,CNT3  ;SET CNT3
17032 030571        32                LDA     2,ARRY
17033 050571        33                STA     2,CNT2  ;SET CNT2
17034 004501        34                JSR     ZERO    ;GO ZERO ARRAYS
17035 000401        35                JMP     .+1
17036 000401        36                JMP     .+1
17037 024566        37        NXT1:   LDA     1,NCHN
17040 044566        38                STA     1,CNT1  ;SET CNT1
17041 020557        39                LDA     0,FIVE  ;SET CHN0 TO BE READ
17042 004527        40                JSR     SYNDN   ; GO WAIT FOR SYN
17043 020564        41        NXT2:   LDA     0,SYN   ; SET CHN.TO BE READ
17044 004500        42                JSR     SYNUP
17045 101220        43                MOVZR   0,0     ; GET 3 IN AC0
17046 004571        44                JSR     READ    ; GO READ AD3
17047 050562        45                STA     2,PLT
17050 102520        46                SUBZL   0,0     ; PUT 1 IN AC0
17051 004566        47                JSR     READ    ; GO READ AD1
17052 050556        48                STA     2,BLR
17053 020554        49                LDA     0,SYN   ;LDA CH0 OF SYN
17054 004515        50                JSR     SYNDN
17055 101220        51                MOVZR   0,0     ; GET 3 IN AC0
17056 004561        52                JSR     READ
17057 050553        53                STA     2,PKT
17060 102520        54                SUBZL   0,0
```

7/02/75 .MAIN

```
 LOC   CODE   STMT    SOURCE STATEMENT

17061 004556    55              JSR     @READ
17062 024546    56              LDA     1,@LB
17063 034541    57              LDA     3,CNT2
17064 132423    58              SUBZ    1,2,SNC ;PERVENTS NEG ERROR
17065 015401    59              DSZ     1,3
17066 000401    60              JMP     .+1
17067 021400    61              LDA     0,0,3
17070 143022    62              ADDZ    2,0,SZC ; SUM R DATA
17071 011401    63              ISZ     1,3
17072 000401    64              JMP     .+1
17073 041400    65              STA     0,0,3
17074 024535    66              LDA     1,@LT
17075 000401    67              JMP     .+1     ;PATCH
17076 000401    68              JMP     .+1     ;PATCH
17077 030533    69              LDA     2,PRT
17100 132423    70              SUBZ    1,2,SNC ;PERVENTS NEG ERROR
17101 015403    71              DSZ     3,3
17102 000401    72              JMP     .+1
17103 021402    73              LDA     0,2,3
17104 143022    74              ADDZ    2,0,SZC ; SUM T DATA
17105 011403    75              ISZ     3,3
17106 000401    76              JMP     .+1
17107 041402    77              STA     0,2,3
17110 010514    78              ISZ     CNT2
17111 010513    79              ISZ     CNT2
17112 010512    80              ISZ     CNT2
17113 010511    81              ISZ     CNT2
17114 014512    82              DSZ     CNT1    ; PTS PER CYCLE
17115 000726    83              JMP     NXT2
17116 000401    84              JMP     .+1     ;PATCH
17117 165000    85              MOV     3,1
17120 034503    86              LDA     3,ARRY
17121 054503    87              STA     3,CNT2  ; PREPARE FOR SR2
17122 014500    88              DSZ     CNT3    ; # PTS PER LOOP
17123 000714    89              JMP     NXT1
17124 004537    90              JSR     @ELL
17125 034472    91              LDA     3,SAVR
17126 000402    92              JMP     .+2
17127 126440    93      QIT:    SUBO    1,1
17130 102440    94              SUBO    0,0
17131 031400    95              LDA     2,0,3
17132 041000    96              STA     0,0,2
17133 045001    97              STA     1,1,2
17134 001401    98              JMP     1,3
17135 102440    99      ZERO:   SUBO    0,0     ; SET AC0 TO 0
17136 024460   100              LDA     1,NFWY  ; SET ARRAY AREA TO ZERO
17137 041000   101              STA     0,0,2
17140 151400   102              INC     2,2
17141 125404   103              INC     1,1,SZR
17142 000775   104              JMP     .-3
17143 001400   105              JMP     0,3
17144 061121   106      SYNUP:  DOAS    0,ADCV
17145 063621   107              SKPDN   ADCV
17146 000777   108              JMP     .-1
```

```
 7/02/75                                        .MAIN

 LOC   CODE   STMT     SOURCE STATEMENT

17147 061121   109                DOAS    0,ADCV
17150 054463   110                STA     3,RTAD
17151 034450   111                LDA     3,LTST
17152 063621   112                SKPDN   ADCV
17153 000777   113                JMP     .-1
17154 072421   114                DIC     2,ADCV
17155 061121   115                DOAS    0,ADCV
17156 063621   116          RPTO: SKPDN   ADCV
17157 000777   117                JMP     .-1
17160 066421   118                DIC     1,ADCV
17161 061121   119                DOAS    0,ADCV
17162 146423   120                SUBZ    2,1,SNC ;SKP IF 2 LE 1
17163 000403   121                JMP     .+3
17164 136033   122                ADCZ#   1,3 SNC ;SKP WHEN 1 LT 3
17165 002446   123                JMP     @ RTAD
17166 133000   124                ADD     1,2
17167 000767   125                JMP     RPTO
17170 063077   126                HALT
17171 061121   127          SYNDN: DOAS    0,ADCV
17172 063621   128                SKPDN   ADCV
17173 000777   129                JMP     .-1
17174 061121   130                DOAS    0,ADCV
17175 054436   131                STA     3,RTAD
17176 034423   132                LDA     3,LTST
17177 063621   133                SKPDN   ADCV
17200 000777   134                JMP     .-1
17201 072421   135                DIC     2,ADCV
17202 061121   136                DOAS    0,ADCV
17203 063621   137          RPTD: SKPDN   ADCV
17204 000777   138                JMP     .-1
17205 066421   139                DIC     1,ADCV
17206 061121   140                DOAS    0,ADCV
17207 132423   141                SUBZ    1,2,SNC ; SKP IF AC1 LE AC2
17210 000403   142                JMP     .+3
17211 156033   143                ADCZ#   2,3 SNC ;SKP WHEN 3 GT 2
17212 002421   144                JMP     @ RTAD
17213 131000   145                MOV     1,2
17214 000767   146                JMP     RPTD
17215 000200   147          NPTS: 200
17216 177740   148          NFWI: -40
17217 000000   149          SAVR: 0
17220 000005   150          FIVE: 5
17221 001400   151          LTST: 1400
17222 000000   152          CNT3: 0
17223 017430   153          ARRY: 17430
17224 000000   154          CNT2: 0
17225 000010   155          NCHN: 10
17226 000000   156          CNT1: 0
17227 000007   157          SVN:  7
17230 000000   158          BLR:  0
17231 000000   159          BLT:  0
17232 000000   160          PKT:  0
17233 000000   161          RTAD: 0
17234 000401   162                JMP     .+1     ;PATCH
```

7/02/75 .MAIN

```
 LOC   CODE   STMT    SOURCE STATEMENT

17235 063077   163              HALT            ;PATCH
17236 063077   164              HALT
17237 061121   165      READ:   DOAS    0,ADCV
17240 024421   166              LDA     1,AVN
17241 044421   167              STA     1,CNT4
17242 152440   168              SUBO    2,2     ;ZERO AC2 AND CARRY
17243 063621   169              SKPDN   ADCV
17244 000777   170              JMP     .-1
17245 061121   171              DOAS    0,ADCV
17246 063621   172              SKPDN   ADCV
17247 000777   173              JMP     .-1
17250 066421   174              DIC     1,ADCV
17251 061121   175              DOAS    0,ADCV
17252 133000   176              ADD     1,2
17253 014407   177              DSZ     CNT4
17254 000772   178              JMP     .-6
17255 001400   179              JMP     0,3
17256 063077   180              HALT            ;PATCH
17257 063077   181              HALT
17260 063077   182              HALT            ;PATCH
17261 000004   183      AVN:    4
17262 000000   184      CNT4:   0
17263 020744   185      BELL:   LDA     0,SVN
17264 063511   186              SKPBZ   TTO
17265 000777   187              JMP     .-1
17266 061111   188              DOAS    0, TTO
17267 001400   189              JMP     0,3
17270 054727   190      SUB2:   STA     3,SAVR
17271 034421   191              LDA     3,MFV   ; LDA REQUIRED  # TO SHIFT
17272 030732   192              LDA     2,CNT2  ; GET ARRY ADD
17273 025000   193              LDA     1,0,2   ; LOAD WORK RG IN AC1
17274 021001   194              LDA     0,1,2   ; LOAD OVERFLOW RG IN AC0
17275 175405   195              INC     3,3,SNR ; CONV TO  BIT #  16
17276 000404   196              JMP     .+4     ; CONV. TO 16 BIT #
17277 125120   197              MOVZL   1,1     ;MOVE LOW REG LEFT,SAVE CARRY
17300 101100   198              MOVL    0,0     ;MOVE OVERFLOW REG LEFT AFIX CARRY AT RT
17301 000774   199              JMP     .-4
17302 006132   200              JSR     @.FIOT
17303 034714   201              LDA     3,SAVR  ; GET RT ADD
17304 031400   202              LDA     2,0,3   ; GET ADD-PARM AREA
17305 041000   203              STA     0,0,2   ; STORE # TO RET TO BASIC
17306 045001   204              STA     1,1,2   ; STA # TO RET TO BASIC
17307 010715   205              ISZ     CNT2
17310 010714   206              ISZ     CNT2
17311 001401   207              JMP     1,3     ; RT TO ADD 1>SAVE ADD
17312 177773   208      MFV:    -5
      000132   209       .FIOT= 132
17313 063077   210              HALT
17314 063077   211              HALT
17315 063077   212              HALT
17316 063077   213              HALT
17317 063077   214              HALT
17320 054427   215      SUB3:   STA     3,SAVR1
17321 035400   216              LDA     3,0,3   ; GET ADD OF X
```

7/02/75 .MAIN

```
 LOC   CODE   STMT     SOURCE STATEMENT

17322 021400   217              LDA     0,0,3   ; LOAD  X
17323 025401   218              LDA     1,1,3   ; LOAD  X
17324 006130   219              JSR     @.FIX   ; CNV TO INT
17325 034422   220              LDA     3,SAVR1
17326 126520   221              SUBZL   1,1     ; GET 1 IN AC1
17327 066023   222              DOB     1,DACV  ; SET FOR Y
17330 061023   223              DOA     0,DACV  ; GIVE Y VALUE
17331 035401   224              LDA     3,1,3
17332 021400   225              LDA     0,0,3
17333 025401   226              LDA     1,1,3
17334 006130   227              JSR     @.FIX
17335 062023   228              DOB     0,DACV
17336 034407   229              LDA     3,HW
17337 065123   230              DOAS    1,DACV
17340 125400   231              INC     1,1
17341 175224   232              MOVZR   3,3,SZR
17342 000775   233              JMP     .-3
17343 034404   234              LDA     3,SAVR1
17344 001402   235              JMP     2,3
      000130   236      .FIX=   130
17345 001000   237      HW:     1000
17346 000000   238      CNTX:   0
17347 000000   239      SAVR1:  0
17350 063077   240              HALT
17351 063077   241              HALT
17352 063077   242              HALT
17353 063077   243              HALT
17354 054773   244      SUB4:   STA     3,SAVR1
17355 031400   245              LDA     2,0,3   ; GET ADD Y #1
17356 021000   246              LDA     0,0,2
17357 025001   247              LDA     1,1,2
17360 006130   248              JSR     @.FIX
17361 044634   249              STA     1,NPTS
17362 152440   250              SUBO    2,2
17363 125222   251              MOVZR   1,1,SZC ; SHIFT TO DETERMINE SHIFT #
17364 000403   252              JMP     .+3
17365 151400   253              INC     2,2
17366 000775   254              JMP     .-3
17367 024431   255              LDA     1,TWL
17370 146400   256              SUB     2,1
17371 130400   257              NEG     1,2
17372 050720   258              STA     2,NPV
17373 102440   259              SUBO    0,0
17374 040752   260              STA     0,CNTX  ; SET CNTX AT ZERO
17375 126400   261              SUB     1,1
17376 000401   262              JMP     .+1
17377 067323   263              DOCP    1,DACV  ; SET MODE AND ERASE
17400 101404   264              INC     0,0,SZR ; WAIT FOR SCOPE TO ERASE
17401 000777   265              JMP     .-1
17402 125523   266              INCZL   1,1,SNC
17403 000775   267              JMP     .-3
17404 062023   268              DOB     0,DACV  ; SET FOR X
17405 030740   269              LDA     2,HW
17406 071023   270              DOA     2, DACV ; GIVE X = 512
```

VITA

William Hugh Thomason was born on April 4, 1945 in Hampton, Arkansas. His parents were Jack Thomason and Nelle Stuart Thomason. He received his elementary and high school education at Hampton High School in Hampton, from which he graduated in May, 1963.

He entered Hendrix College, Conway, Arkansas, in the fall of 1963, and graduated from this institution cum laude with a B. A. degree in chemistry in June, 1967. In the fall of 1967 he entered the graduate school of LSU-BR as a candidate for the degree of Doctor of Philosophy in physical chemistry.

In October of 1968 he was drafted into the US Army. He graduated from Infantry Office Candidate School in September 1969, and received a commission in the US Army Chemical Corps. After serving two years with the US Army Technical Escort Center, he reentered the graduate school of LSU-BR in September 1971, to continue his candidacy for the degree of Doctor of Philosophy.

He is married to the former Sarah Jane Moseley of Warren, Arkansas, and they have one child, Arthur Hugh Thomason. His wife is a pediatrician and is currently on the pediatric staff of the LSU Medical School.

EXAMINATION AND THESIS REPORT

Candidate: William H. Thomason

Major Field: Chemistry

Title of Thesis: Saturable Optical Behavior of Sulfur Hexafluoride.

Approved:

James Dale Warnock
Major Professor and Chairman

James D. Graybeal
Dean of the Graduate School

EXAMINING COMMITTEE:

Joel Selbin

Robert V. Hanman

R G Goodrich

Neil R. Keating

Date of Examination:

August 4, 1975